Climatological analysis of planetary wave propagation in Northern Hemisphere winter

Qian Li

Climatological analysis of
planetary wave propagation
in Northern Hemisphere winter

Dissertation zur Erlangung des Doktorgrades der Naturwissenschaften
im Departement Geowissenschaften der Universität Hamburg
vorgelegt von

Qian Li
aus Xinjiang, China

Hamburg 2006

Qian Li
Max-Planck-Institut für Meteorologie
Bundesstrasse 53
20146 Hamburg
Germany

Als Dissertation angenommen
vom Departement Geowissenschaften der Universität Hamburg

auf Grund der Gutachten von
Prof. Dr. Guy Brasseur
und
Prof. Dr. Hans-F. Graf

Hamburg, den 8. Dezember 2006
Prof. Dr. Kay-Christian Emeis
Leiter des Departements für Geowissenschaften

Climatological analysis of planetary wave propagation in Northern Hemisphere winter
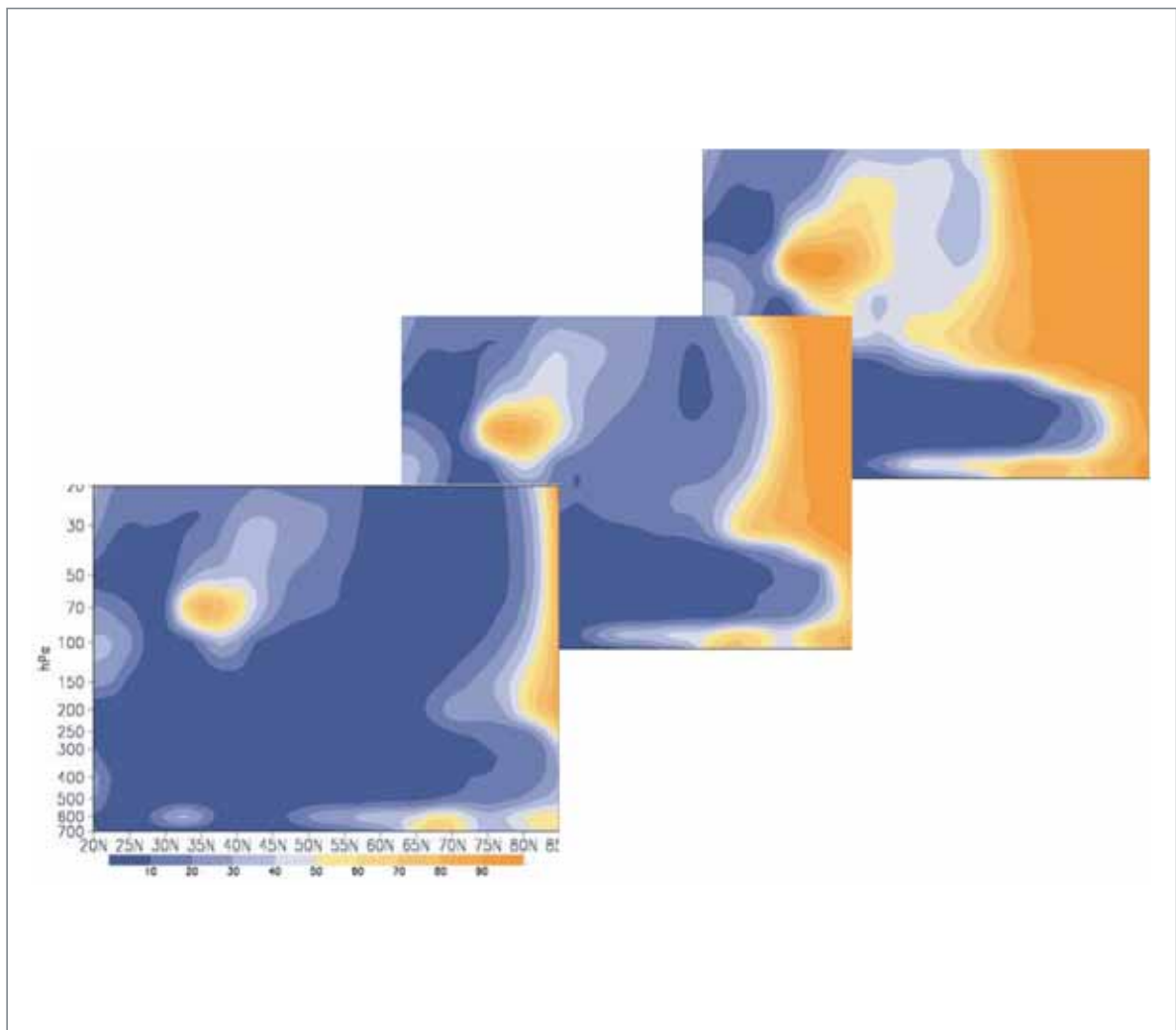
Qian Li

Hamburg 2006

Contents

Abstract:

The atmospheric control on planetary wave propagation, and planetary wave activities and eddy forcing on mean flow in the troposphere and stratosphere in Northern Hemisphere (NH) winter, has been investigated by the new introduced analysis - frequency of negative refractive index squared ($f(n_k^2 < 0)$), and E-P flux and its divergence by using the NCEP/NCAR reanalysis data from 1958 to 2002. It was found that the atmospheric zonal mean zonal wind (ZMZW), vertical shear of ZMZW and atmospheric stability can control the planetary wave propagation. On the other hand, the planetary waves can also affect atmospheric circulation by wave–mean flow interactions. The interannual and intraseasonal anomalies of the polar and subpolar stratospheric circulation, which can be defined as the strong polar vortex regime (SVR) and weak polar vortex regime (WVR) by applying the zonal wind at 50hPa, 65°N as a diagnostic, have been explored. It was found that the planetary waves contribute significantly on the constructing and maintaining of the stratospheric polar vortex regimes. On the other hand, the regime itself also has effects on the planetary wave propagation. Furthermore, the different contributions of stationary waves and transient waves on atmospheric mean flow have been investigated, respectively.

The violent tropical volcanic eruptions can induce impacts on climate system by injecting a huge amount of aerosols into the lower stratosphere, which can spread to globe and disturb the radiative balance. The stronger polar vertex, weaker tropical jet, tropical stratospheric warming and polar stratospheric cooling in NH winter can be observed after the violent tropical volcanic eruptions. By choosing three cases (Agung 1963 eruption, El Chichon 1982 eruption, and Pinatubo 1991 eruption), the impacts of volcanic eruptions on atmosphere and their influences on planetary wave propagation have been studied. The "dipole" structures of anomalies of ZMZW and zonal mean temperature were found in both volcanic winters and SVR. Moreover, it was found in volcanic winters, the stationary planetary waves can propagate more from the troposphere to the stratosphere and, these waves can continuously transport more eddy heat fluxes upward from the lower stratosphere to the middle and higher stratosphere than in other winters.

The general circulation models' (GCMs) performance on atmospheric circulation and planetary wave propagation has also been studied. The bias of a stronger stratospheric polar vortex was found in the simulation of the GCM (ECHAM5_AMIP2) possibly due to the low upper boundary level (10hPa). The bias can be modified in the simulation of the middle atmospheric GCM (MAECHAM5_AMIP2) with higher upper boundary level (0.01hPa), although the stratospheric polar vortex is becoming too weak. The influences of ocean on planetary wave propagation have also been investigated by analyzing the simulation of atmosphere-ocean coupled GCM (MAECHAM5_MPIOM). The stratospheric polar vortex is still too weak in MAECHAM5_MPIOM. In the simulations of all these three GCMs, the wave activities and zonal easterly momentum forcing are weaker for stationary waves in both the troposphere and stratosphere but stronger for transient waves in the troposphere compared with observations. The major differences between MAECHAM5_AMIP2 and MAECHAM5_MPIOM were mainly located in the

troposphere, which implies that the influences of ocean on planetary wave propagation cannot reach up to the stratosphere.

Chapter 1

Introduction

The climatological zonally asymmetric structure of geopotential surface in the northern stratosphere, exposing the Aleutian high over the Pacific and a low centered over the Scandinavian region, is generally considered as a superposition of stationary planetary-scale waves which can propagate vertically from the troposphere to the stratosphere (Charney and Drazin, 1961). The planetary waves, which are generated by the topography and diabatic heating in the troposphere, are disturbances having zonal wavelengths of the scale of the Earth's radius. The vertically propagating planetary waves are dynamically important in the stratosphere because they provide a large part of the total eddy momentum and heat fluxes, and they explain large deviations between the observed wintertime temperature in the northern polar stratosphere and radiative equilibrium temperatures. The propagation and temporal variation of planetary waves in the atmosphere are fundamental problems in observational and theoretical studies of dynamical meteorology. The main mechanism of the role of planetary waves in atmospheric general circulation is that the propagation of planetary waves is controlled by atmospheric mean flow, and the background zonal mean flow may be changed through deposition of zonal momentum by planetary waves.

The first study on vertical planetary wave propagation was done by Charney and Drazin (1961), based on the linear wave theory, and it was concluded that vertical propagation of stationary waves happens only when the zonal winds are westerly and not exceeding the critical Rossby velocity. This effect of zonal wind on planetary wave propagation has been addressed as Charney Drazin Theorom (Andrew et al., 1987; Appendix A.1). Lin (1982) found that the latitudinal location of the polar night jet, and therefore the vertical shear of zonal wind, also has a significant influence on the wave propagation. The planetary wave propagation can possibly be enhanced by vertical shear of zonal wind (Hu and Tung, 2002), and controlled by atmospheric stability near the tropopause in the extratropics (Chen and Robinson, 1992).

On the other hand, planetary waves also have a strong influence on the zonal mean zonal wind based on the wave-mean flow interaction theorem (Eliassen and Palm, 1961; Andrews, 1985). Planetary waves propagated upward to the stratosphere, can change stratospheric circulation when they break and get absorbed. When zonal mean zonal winds exceed the critical Rossby velocity (Charney and Drazin, 1961), planetary waves, which propagate upward from the troposphere to the stratosphere, will be refracted downward or in meridional direction (Matsuno, 1970). These refracted waves may in turn influence the planetary waves in the troposphere and could also induce changes in zonal mean flow in the troposphere. The critical Rossby velocity depends on wave number and latitude, implying that only ultra-long waves have the possibility to propagate from the troposphere to the stratosphere in middle and high latitudes (Charney and Drazin, 1961; Matsuno, 1970). In the Southern Hemisphere, in the polar vortex zonal winds exceed the

critical Rossby velocity during high winter, thus excluding planetary wave forcing for most of the southern winter time.

As indicated above, the tropospheric and stratospheric circulations play a key role in controlling planetary wave propagation. In Northern Hemisphere winter, the lower to middle stratosphere is characterized by strong and almost zonally symmetric westerly flows in subpolar latitudes, whereas weaker easterly winds prevail in summer. The westerly flow pattern is referred to as the stratospheric polar vortex. It is mainly thermally driven due to the cooling of the northern polar region, which is associated with a substantial reduction of incoming solar radiation in winter. The vortex thus usually forms in early winter, whereas it normally decays in late winter to early spring when circulation changes back to the summer situation. However, the vortex may also be subject to disturbances during high winter. Such events are associated with warming of the polar stratosphere, i.e. with a reducation of the meridional temperature gradient, but do not always lead to a change towards easterly winds in the stratosphere, i.e. to a breakdown of the vortex. The center of the polar vortex is often observed around 65°N. The strength of the stratospheric polar vortex is characterized by an interannual and intraseasonal regime-like behavior. By examining the probability density distribution, Christiansen (2003) showed that the first Principal Component timeseries of winter mean geopotential heights in the middle and lower stratosphere – describing variations in the strength of the polar vortex – has a bimodal probability density distribution. This indicates that the strength of stratospheric polar vortex is characterized by two regimes in which the vortex is either primarily strong or weak. By studying zonal mean zonal wind at 50hPa and 65°N, Walter (2003) found that the strength of the stratospheric polar vortex shows 30-days persistence. This implies monthly persistence time-scale, which exceeds the time-scales of radiatively driven changes, implies a need for a dynamical maintenance mechanism. In the study of Walter (2003), all calendar months in which the monthly mean zonal wind at 50hPa and 65°N is stronger than 20m/s, those months are considered to be part of the strong polar vortex regime (SVR) and those months in which the zonal mean zonal wind is westerly but weaker than 10m/s are considered as a weak vortex regime (WVR). This threshold has also been applied in Castanheira and Graf (2003) but based on daily mean data. However, as addressed in Christiansen (2003), when unsorted monthly data are used, the probability density distributions are unimodal since the presence of higher frequencies can obscure the existence of bimodality (Palmer, 1993).

It is well known that not only the stationary planetary waves but also the transient planetary waves play an important role in the wave-mean flow interaction (Andrews et al., 1987). By using a dynamical model, Matsuno (1971) investigated the mechanism of the stratospheric sudden warming phenomenon and he found that propagating transient planetary waves from the troposphere to the stratosphere can decelerate the polar jet and induce a rapid warming of the polar atmosphere. Meanwhile, Palmer (1981) and O'Neill and Youngblut (1982) studied the stratospheric sudden warming phenomenon by applying Eliassen-Palm flux (E-P flux) and its divergence as diagnostics. Afterwards, Salby and Garcia (1987) studied the interference of stationary and traveling (transient) planetary waves. Straus and Shukla (1988) also investigated the patterns of stationary waves and transient fluctuations, respectively. However, in these studies, although it was

well agreed that both stationary and transient waves play key roles in the wave-mean flow interaction, the different contributions to the stratospheric circulation between stationary and transient waves were still unclear. Only recently, Limpasuva and Hartmann (2000) investigated the separate effects of stationary and transient waves on the mean flow, respectively. They found that the high-frequency (synoptic) transient waves contribute most to the total eddy forcing in the Southern Hemisphere while in the Northern Hemisphere (NH) the stationary waves dominate the eddy momentum fluxes although the high-frequency transient waves still have important contributions. This finding sheds light on the study of the transient waves and raised the needs of further investigations.

1.1 Planetary wave-mean flow interaction

1.1.1 Atmospheric state control on stationary planetary wave propagation: refractive index

The atmospheric control on planetary wave propagation can mainly be reflected by the analysis of the so-called refractive index, which was firstly introduced by Matsuno (1970). The refractive index of stationary planetary waves has been frequently applied by many researchers (Lin, 1982; Huang and Gambo, 1982; Hu and Tung, 2002; Mukougawa and Hirootka, 2004; etc.) to investigate stationary planetary wave propagation. The effective index of refraction of vertically propagating planetary waves of a given zonal wave number at a specific latitude depends primarily on the vertical structure of the atmosphere (Charney and Drazin, 1961; Matsuno, 1970). An important parameter is the vertical and meridional distribution of zonal mean zonal wind. Theoretically planetary waves tend to avoid regions where zonal winds are easterly or westerly and exceeding the critical Rossby velocity. They are attracted towards regions where the value of refractive index squared is the maximum. This theory provides an important paradigm for our thinking about the dynamic forcing of the stratosphere by the troposphere.

In this study, the form of refractive index developed by Andrews et al. (1987) and furthermore extended by Hu and Tung (2002) is applied:

$$n_k^2(y,z) = \frac{\overline{q}_\varphi}{\overline{u}} - \left(\frac{k}{a\cos\varphi}\right)^2 - \left(\frac{f}{2NH}\right)^2 \qquad (1.1.1)$$

where

$$\overline{q}_\varphi = \frac{2\Omega}{a}\cos\varphi - \frac{1}{a^2}\left[\frac{(\overline{u}\cos\varphi)_\varphi}{\cos\varphi}\right]_\varphi - \frac{f^2}{\rho_0}\left(\rho_0\frac{\overline{u}_z}{N^2}\right)_z \qquad (1.1.2)$$

is the meridional gradient of the zonal mean potential vorticity (PV). $\rho_0 = \rho_s \exp(-z/H)$ is the background air density. Here k, N, H, $f = 2\Omega\sin\varphi$, a, Ω and φ denote the zonal wave number, buoyancy frequency, scale height, Coriolis

parameter, the Earth's radius, the Earth's rotation frequency and latitude respectively. Expansion of the third term on the right-hand side of Equation 1.1.2 yields

$$-\frac{f^2}{\rho_0}\left(\rho_0\frac{\overline{u}_z}{N^2}\right)_z = \left(\frac{f^2}{HN^2}+\frac{f^2}{N^4}\frac{dN^2}{dz}\right)\overline{u}_z - \frac{f^2}{N^2}\overline{u}_{zz} \qquad (1.1.3)$$

It is expected that planetary waves of zonal wave number k are able to propagate in regions where $n_k^2 > 0$ and are refracted from regions where $n_k^2 < 0$ and that the larger the n_k^2 in a region, the easier it is for planetary waves to propagate (Matsuno 1970).

Equation 1.1.1, 1.1.2 and 1.1.3 show that zonal mean zonal wind, vertical shear of zonal mean zonal wind, and atmospheric stability have control on planetary wave propagation. However, in most of the studies, the buoyancy frequency, which represents the atmospheric stability, was treated approximately as a constant (Matsuno, 1970; Huang and Gambo, 1982; Andrews et al., 1987), or a variable of altitude only (Chen and Robinson, 1992; Limpasuvan and Harmann, 2000; Hu and Tung, 2002). The variation of buoyancy frequency with latitudes was considered negligible. However, Chen and Robinson (1992) also found that the variation of buoyancy frequency is not as negligible as it has been hypothesized in other applications. They concluded that the propagation of planetary waves from the troposphere to the stratosphere is sensitive to the distribution of atmospheric stability especially near the subtropical tropopause. Therefore, a simplistic treatment of buoyancy frequency could induce errors in the analysis of refractive index.

The refractive index is a useful diagnostic for vertical and meridional planetary wave propagation. However, as it is shown from the equation of the refractive index, although it is highly simplified, the high degree of freedom, introduced by a number of parameters used to compute the refractive index, still sometimes gives unsatisfying results (e.g. Mukougawa and Hirooka, 2004). Another problem with the traditional analysis of the refractive index is that it generally lacks the ability to illustrate the climatological state of the atmosphere for the propagation of planetary waves due to the overlapping of positive and negative refractive index squared. This often makes a mean refractive index squared hard to interpret.

1.1.2 Planetary wave activities and eddy forcing on mean flow: Eliassen-Palm flux and its divergence

Planetary waves can also induce forcing on the mean flow. The Eliassen-Palm flux (E-P flux hereafter) and its divergence (Eliassen and Palm, 1961; Andrew et al., 1987), which represent the wave activities and the eddy forcing, respectively, were applied to analyze the planetary wave propagation in many previous studies (Muench, 1965; Hirota and Sato, 1969; O'Neill and Taylor, 1979; Quiroz, 1979; Boville, 1986; Randel 1987; Huang and Zou, 1987; Chen and Robinson, 1991; Christianson, 2001; Chen and Huang, 2002, Chen and Graf, 2002; Hu and Tung, 2002; Hitoshi and Hirooka, 2004).

To study planetary wave-mean flow interaction in the troposphere and the stratosphere in Northern Hemisphere winter, the quasi-geostrophic version of E-P flux vector $\vec{F}$ in spherical geometry (Andrew et al., 1987), is an appropriate choice and shown here,

$$\vec{F} = \left[0, -\rho_0 a(\cos\varphi)\overline{v'u'}, \rho_0 a(\cos\varphi)f\overline{v'\theta'}/\theta_{0_z} \right] \qquad (1.1.4)$$

$\rho_0 = \rho_s \exp(-z/H)$ is the background air density.

Then meridional and vertical components of the E-P flux are

$$F_y = -\rho_0 a(\cos\varphi)\overline{v'u'} \qquad (1.1.5)$$

$$F_z = \rho_0 a(\cos\varphi)f\overline{v'\theta'}/\theta_{0_z} \qquad (1.1.6)$$

and the divergence of E-P flux is

$$D_F = \frac{\nabla \bullet \vec{F}}{\rho_0 a \cos\varphi} \qquad (1.1.7)$$

Using the following approximate geostrophic formulas in spherical coordinates (Andrew et al., 1987):

$$u' = -(fa)^{-1}\Phi'_\varphi, \ v' = (fa\cos\varphi)^{-1}\Phi'_\lambda \qquad (1.1.8)$$

together with (1.1.4), gives

$$\vec{F} = \rho_0 \left[0, \overline{\Phi'_\varphi \Phi'_\lambda}/f^2 a, \overline{\Phi'_z \Phi'_\lambda}/N^2 \right] \qquad (1.1.9)$$

where Φ' represents the departure of the climatological mean geopotential from its zonal mean value. (Equation 1.1.8 and 1.1.9 will not be valid near the equator where f is small.)

From Equation 1.1.5, 1.1.6, it can be seen that the meridional and vertical E-P flux components correspond with eddy momentum flux ($\overline{v'u'}$) and eddy heat flux ($\overline{v'\theta'}$), respectively. The divergence of the E-P flux (Equation 1.1.7) represents the eddy momentum forcing on mean flow. It should be indicated that the convergence of the E-P flux implies the zonal easterly forcing induced by waves on mean flow (Andrew et al., 1987) that decelerates a westerly zonal mean flow.

1.2 External forcing of volcanic eruptions

Variations in strength of the stratospheric polar vortex are mainly caused by the interaction of upward propagating planetary waves from the troposphere with the mean flow in the stratosphere (Matsuno, 1970). However, several external forcings also have the potential to influence the intensity of the stratospheric polar vortex. Labitzke and van Loon (1988) detected a 10-12 year oscillation in the lower stratospheric temperature and in geopotential height. This oscillation reveals to be in phase with the 11-year solar cycle. Holton and Tan (1980) showed an effect of the quasi-biennial oscillation (QBO) on the strength of the vortex, and Labitzke (1987) reported an influence of the QBO on the probability for a breakdown of the vortex. For a review of the QBO and related effects see Baldwin et al. (2001). It has been observed that during the past 2 to 3 decades, the polar vortex has been significantly strengthened (Graf et al., 1995; Perlwitz and Graf,

1995; Kodera and Koide, 1997; Thompson and Wallace, 1998). This can at least in part be explained by the increasing anthropogenic emission of greenhouse gases: Sensitivity experiments with comprehensive climate models show that the polar vortex continuously intensifies with increasing concentration of greenhouse gases (Graf et al., 1995; Shindell et al., 1999; Dameris et al., 2005).

Moreover, violent volcanic eruptions in the tropics may lead to a strengthened meridional temperature gradient and, thus to a stronger vortex (Labitzke and van Loon, 1996). Violent volcanic eruptions inject huge amounts of sulfate aerosols into the atmosphere, which can modulate the radiation balance (Angell, 1993; Robock, 2001). The aerosols injected into the stratosphere by violent volcanic eruptions result in warming of the layer where the aerosol resides due to absorption of solar and terrestrial radiation by volcanic aerosols (Lacis et al., 1992; Angell, 1993). The stratospheric tropical warming begins 1 to 3 months after eruptions and lasts 1 to 2 years (Robock, 2001). By a nonlinear response through atmospheric dynamics, warmer winters over the Northern Hemisphere continents following a large tropical eruption are also observed. This will happen few months after the eruptions and last 1 to 3 years (Robock, 2001).

The stratospheric warming by natural external forcing, especially violent volcanic eruptions, has been found by Ramaswamy et al. (2006). By applying a coupled atmosphere-ocean model, they studied the stratospheric temperature trend from 1979 to 2003 and tried to demonstrate that the complex space-time pattern of the lower stratospheric temperature anomalies is a consequence of combined temporal changes in natural forcing and anthropogenic forcing. The obvious stratospheric warmings, which are caused by El Chichon eruption (1982) and by Pinatubo eruption (1991), were found for both observation and the model experiments with the natural forcing (Ramaswamy et al., 2006). By using a longer dataset (1958 – 1999), Cordero and Forster (2006) found another case of Agung eruption (1963).

However, following violent tropical volcanic eruptions, especially during the Northern Hemisphere winter, a major stratospheric cooling around the northern polar area has also been observed. For the single case of Pinatubo eruption (1991), the stratospheric winter cooling at the Northern Hemisphere pole during the following winter (1991-1992) was observed (Kodera and Yamazaki, 1994). Stenchikov et al. (2004) found that the polar stratospheric cooling occurred for following two winters after the eruption. The cooling for other violent volcanic eruption cases has also been noticed by Oman et al. (2005) and Stenchikov et al. (2006).

The lower stratospheric warming at tropical and middle latitudes during boreal winter after violent tropical volcanic eruptions increases the meridional temperature gradient. This may initiate a geostrophically driven strengthening of the polar vortex in early winter. The strengthened stratospheric polar vortex and stronger zonal mean zonal winds extend down into the troposphere (Graf et al. 1993; Graf et al. 1994; Kodera, 1994; Kodera and Yamazaki, 1994; Robock, 2001). This dynamic feedback mechanism provides a very important contribution to the resulting climate anomaly (Robock and Mao, 1992; Graf et al., 1993; Kirchner and Graf, 1995; Mao and Robock, 1998).

Based on the Charney Drazin Theorem, the anomalies of the stratosphere induced by violent tropical volcanic eruptions can have potential influences on planetary wave propagation. It will help to improve our understanding of influences of external forcing on the atmospheric climate system, to investigate the mechanism of dynamical feedback of planetary wave to external forcing of the volcanic eruptions.

1.3 GCM simulations of planetary wave propagation

Combined with observational studies, the general circulation models (GCMs) are tools, which help us to study the climate system. If all relevant physical processes are correctly represented, then a GCM should provide a faithful simulation of the three-dimensional circulation. There are various experiments of atmospheric general circulation models (AGCMs) or Atmosphere-Ocean couple general circulation models (AOGCMs) being performed to solve varied scientific problems. One of the main purposes to apply GCMs to simulate different regimes is to help to improve our understanding of the climate system and the mechanisms of climate change. In this study, we are interested in the planetary wave propagation and its influence on mean flow in the troposphere and stratosphere. Validated by observational analysis, it will help our understanding to investigate the simulations of GCMs on atmospheric circulation and planetary wave propagation.

However, many current climate GCMs show a bias of a stronger stratospheric polar vortex in Northern Hemisphere winter (Pawson et al., 2000; Perlwitz, 2000) than known from observations. The strength of the polar vortex might be better simulated in GCMs with higher upper boundary levels (Shindell, 1999). The appropriate representation of the stratospheric polar vortex in GCMs is essential for planetary wave propagation from the troposphere to the stratosphere. It is crucially important for modelling studies of the troposphere-stratosphere dynamical coupling that, the strength of the polar vortex and related propagation and refraction of planetary waves are properly represented in the simulations of atmospheric climate system. It is interesting to study the properties of planetary wave propagation in the simulations of GCMs with different upper boundary levels since previous studies showed that the altitudes of the upper boundary in GCMs have influences on the simulations of the NH stratospheric polar vortex (Pawson, 2000). In this thesis, numerical simulations with the ECHAM5 GCM of the Max Planck Institute (MPI) for Meteorology (Rockner et al., 2003) and its middle atmospheric version – MAECHAM5 (Manzini et al., 2006) are analyzed.

In GCMs, the atmospheric circulation is represented by primitive equations discretized at finite horizontal and vertical resolution and parameterization schemes representing processes which cannot be resolved. Because of limitations in the representation of the atmosphere in numerical models, biases in model climatologies in comparison with observations, which have their own uncertainties, must be expected. Many compromises are necessary for scientific reasons and computational efficiency reasons for modelling studies. Therefore, an appropriate attempt to compare the observed climate with a

modeled climate is to run a GCM experiment with boundary conditions as realistic as possible.

Moreover, it has been demonstrated that the variations of polar vortex can be influenced by the changes of SST (van Loon and Labitzke, 1987; Hamilton 1993a; Baldwin and O'Sullivan, 1995; Kodera et al., 1996; Garcia-Herrera et al., 2006; Manzini et al., 2006). The interaction between ocean and atmosphere is of particular interest to understand the climate system dynamics. For this purpose coupled atmosphere-ocean general circulation models (AOGCMs) have been developed. In this thesis, the simulation of MAECHAM5 coupled with MPIOM (MPI Ocean Model) (Jungclaus et al., 2006) – MAECHAM5_MPIOM – is also analyzed to investigate the influence of ocean on planetary wave propagation.

1.4 Structure of the thesis

In this thesis, there are three major chapters based on the objectives of the study.

In Chapter 2, the climatology of planetary wave propagation, planetary wave activities and eddy forcing on mean flow, in Northern Hemisphere winter is investigated. A new analysis of the refractive index of planetary wave propagation, which can avoid the problems in traditional analysis and more clearly illustrate the atmospheric control on planetary wave propagation, is introduced. Furthermore, the analysis of E-P flux and its divergence show the major properties of planetary wave activities and eddy forcing in relationship to the new statistics. The stratospheric polar vortex regimes and the contributions of planetary waves to maintain the polar vortex regimes will also be analyzed. Furthermore, both stationary and transient planetary waves are investigated in the general Northern Hemisphere winter and under the stratospheric polar vortex regimes.

In Chapter 3, the anomalies of stratospheric zonal wind and temperature in the Northern Hemisphere winter, induced by violent tropical volcanic eruptions, are discussed. Moreover, the influence of volcanic eruptions on planetary wave propagation is studied.

Biases in the polar vortex and in the wave-mean flow interaction, as represented in GCMs, are investigated in Chapter 4, associated with the analysis of observations. This chapter compares two experiments with different altitudes of the model top layer, and two experiments with prescribed observed ocean boundary conditions and with a coupled OGCM, respectively.

Finally, the overview of the conclusions and the outlook are given in Chapter 5.

* Two papers have been produced based on this thesis. (Li et al., 2006)

Chapter 2

Climatological analysis of planetary propagation in Northern Hemisphere winter

2.1 Introduction

Planetary waves, generated by the topography and diabatic heating in the troposphere, are disturbances having zonal wavelengths of the scale of the Earth's radius. The propagation and temporal variation of planetary waves in the atmosphere are fundamental problems in observational and theoretical studies of dynamical meteorology. The propagation of planetary waves is controlled by the zonal wind profile and atmospheric stability, and in turn, the background zonal mean flow may be changed through the deposition of zonal momentum of planetary waves (Charney and Drazin, 1961).

Charney and Drazin (1961) firstly investigated the vertical propagation of planetary waves based on the linear wave theory and concluded that the vertical propagation of stationary waves only happens when the zonal wind are westerly and not too strong by calculating the effective index of refraction which mainly depends on the distribution of zonal mean wind. This effect of zonal wind on planetary wave propagation has been addressed in Charney Drazin Theorom (Andrew et al., 1987; Appendix A.1). Afterwards, Dickinson (1968) found presence of the "polar wave guide", created by the westerly jet of the winter upper stratosphere, will refract the propagating planetary waves, while the "equatorial wave guide", formed by the zero wind line in tropics, will absorb rather than refract the planetary waves. Supposing the planetary waves in the stratosphere are propagating from the troposphere, Matsuno (1970) simulated the observed vertical structure and horizontal pattern of stationary planetary waves in the winter stratosphere by using a quasi-geostrophic model and he found that the results agree well with observation. In the discussion of the properties of planetary wave propagation, Lin (1982) found that the latitudinal location of the polar night jet, and therefore the vertical shear of zonal wind, also has a significant influence on the wave propagation. Chen and Robinson (1992) concluded that the key parameters controlling the vertical wave propagation include not only the zonal winds, the vertical shear of zonal winds, but also the vertical gradient of buoyancy frequency. Limpasuvan & Hartmann (2000) and Hartmann et al. (2000) concluded that a large positive vertical shear of zonal wind impedes the upward propagation of planetary wave. However, Hu and Tung (2002) found that rather than impeding, the large positive vertical shear of zonal wind tends to enhance wave propagation, which was also found in this study. The finding of Hu and Tung (2002) is also assumed in this thesis.

Controlled mainly by the structure of zonal mean wind, as well as its vertical shear (Charney and Drazin, 1961; Lin, 1982; Chen and Robinso, 1992; Hu and Tung, 2002), planetary waves also have strong influences on mean flow based on the wave-mean flow

interaction theorem (Eliassen and Palm, 1961; Andrews, 1985). To be more detailed, planetary waves which are generated in the troposphere by the topography and diabatic heating will propagate upward to the stratosphere when zonal mean zonal winds are westerly and not exceeding the critical Rossby velocity (Charney and Drazin, 1961; Appendix A.1). These waves can modify the stratospheric circulation when they break and get absorbed. On the other hand, when the zonal winds exceed the critical Rossby velocity, planetary waves, which propagate upward from the troposphere to the stratosphere, will be refracted downward or in meridional direction (Matsuno, 1970). These refracted waves may in turn influence the planetary wave pattern in the troposphere and could also induce changes in the mean flow and the transient eddies of the troposphere. Boville (1984), by applying a general circulation model, showed that (unrealistically) large changes in the zonal mean wind distribution of the upper troposphere and lower stratosphere could produce dramatic alterations in the mid-tropospheric wave field and these changes affect not only the stationary planetary wave structure but also the transient cyclone-scale waves as well. The critical Rossby velocity depends on the wave number and latitude, implying that only ultra-long waves have the possibility to propagate to the stratosphere in mid- and high latitudes (Charney and Drazin, 1961; Matsuno, 1970).

After the theoretical study of Charney and Drazin (1961), the refractive index was firstly introduced as a diagnostic by Matsuno (1970) and has frequently been used by a number of researchers thereafter (Lin, 1982; Huang and Gambo, 1982; Hu and Tung, 2002; Mukougawa and Hirootka, 2004; etc.) to study planetary wave propagation. The effective index of refraction of vertically propagating planetary waves of a given zonal wave number at a specific latitude depends primarily on the vertical structure of the atmosphere (Charney and Drazin, 1961; Matsuno, 1970). An important parameter is the vertical and meridional distribution of the zonal mean zonal wind. Planetary waves tend to avoid regions where the zonal winds are easterly or are westerly but exceed a critical, wave number dependent velocity. They are attracted towards regions where the value of refractive index squared is a maximum. This theory provides an important paradigm of our thinking about the dynamic forcing of the stratosphere by the troposphere and is a useful diagnostic for vertical and meridional planetary wave propagation. However, as it is shown from the equations of refractive index (Matsuno, 1970; Equation 1.1, 1.2 and 1.3), although they are highly simplified, the high degree of freedom, which is introduced by the number of parameters used to compute the refractive index, still sometimes gives unsatisfying results (e.g. Mukougawa and Hirooka, 2004). Another problem with the traditional analysis of refractive index is that it generally lacks the ability to illustrate the climatological state of atmosphere for propagation of planetary waves due to the overlapping of the positive and negative values of refractive index squared, which often makes the mean of refractive index squared hard to interpret. In order to improve this, the seasonal frequency distribution of days with negative refractive index squared ($f(n_k^2<0)$) is introduced in this thesis. This allows estimating the probability that the atmospheric state permits propagation of planetary waves in specific periods at different latitudes and heights and avoids the overlapping problem. This new analysis may help to enhance our understanding about the influence of the zonal mean zonal wind on planetary wave vertical propagation from the troposphere to the stratosphere.

Another popular diagnostic to investigate the planetary wave-mean flow interaction is the so-called Eliassen-Palm flux and its divergence (Eliassen and Palm, 1961; Andrews et al., 1987). Contrasting with the refractive index, the Eliassen-Palm flux (E-P flux hereafter) is a measure of wave activities and its divergence shows the eddy momentum forcing on the zonal mean flow (Andrews et al., 1987). Moreover, it is well known that not only stationary planetary waves but also the transient planetary waves play a key role in wave-mean flow interaction (Andrews et al., 1987).

This chapter aims 1) to reveal the climatology of planetary wave propagation and refraction between the troposphere and the stratosphere; and 2) to improve our understanding of the dynamics of planetary wave-mean flow interaction. The following of this chapter is arranged such that: in section 2, the data sets and the methodology are introduced; in section 3, the new analysis of $f(n_k^2<0)$ is introduced, furthermore, combing the analysis of E-P flux and its divergence, the climatologies of stationary planetary wave propagation and wave activities and momentum forcing on mean flow are investigated; recently it was suggested that there are two different circulation regimes describing the Northern Hemisphere stratospheric interannual variability (Christiansen, 2003) and, it was found that the variations of the stratospheric polar vortex have effects on the planetary wave propagation (Castanheira and Graf, 2003; Walter, 2003), therefore, in section 4, the stratospheric polar vortex regimes and their influences on planetary wave propagation are discussed; as another key role in wave-mean flow interaction, the transient planetary waves are also analyzed in section 5; finally, a brief summary is given in section 6.

2.2 Data and methods

In this thesis, we have used 45 years (1958-2002) of dataset from the National Centers for Environmental Prediction – National Center for Atmospheric Research (NCEP/NCAR) reanalysis project (Kalnay et al., 1996; Kistler et al., 2001). The dataset contains daily averages of geopotential height, wind, and temperature on $2.5^o \times 2.5^o$ grid at 17 vertical pressure levels extending from 1000 to 10 hPa with six levels in the stratosphere (100 hPa, 70 hPa, 50 hPa, 30 hPa, 20 hPa and 10 hPa). This thesis focuses on the climatology of planetary wave propagation in Northern Hemisphere winter, therefore only the daily average data of Northern Hemisphere extended winter season (November, December, January, February, March and April) were applied.

It is well known that there were two major changes in the observing system, which had effect on the NCEP/NCAR reanalysis dataset (Kistler et al., 2001). The first happened from 1948 to the International Geophysical Year (IGY) in 1957, when the upper-air observations network was established. And the second took place in 1979 when the global operational use of satellite sounding was introduced. By comparing 50 hPa geopotential height and 100 hPa temperature of two datasets: the NCEP/NCAR reanalysis dataset, and an independent long-term dataset from the Free University of Berlin (FUB) (Pawson et al., 1993), Perlwitz (2000) concluded that the reanalyses of stratospheric geopotential height and temperature data in the Southern Hemisphere (SH) and in the Northern Hemisphere (NH) lower latitudes should not be used for long-term

climate change. However, after the IGY mid- and high latitude data in the boreal winter and high latitude data in the boreal summer are reliable for the statistical analysis of climate trends. She also found that stratospheric NCEP/NCAR reanalysis from the NH extratropics after 1958 can quite reliably be used for studying coupled interannual tropospheric-stratospheric variability in winter, whereas upper-level data before 1958 should be handled with care. This finding is supported by Kistler et al. (2001) who also found that the reanalysis illustrates rather accurate initial conditions for forecasts in lower levels even before 1958 in the Northern Hemisphere.

In this thesis, planetary waves are separated into stationary waves and transient waves based on time series analysis (Andrews et al., 1987). Firstly, the climatology is first calculated by time mean of 44 (1958-2002) Northern Hemisphere winter – December, January and February (DJF hereafter). After computing the climatological mean, stationary waves are defined as zonally varying anomalies from the zonal mean (Andrews et al., 1987) (Appendix A.2) and can be further separated into zonal Fourier components with different zonal wave number (ZWN hereafter) (Appendix A.3). Since increasing ZWN corresponds to decreasing critical Rossby velocity, at which vertically propagating waves are selectively reflected/refracted (Charney and Drazin, 1961), separate treatment of single wave fields with different ZWNs is a proper approach to study planetary wave propagation and to illustrate the dynamical interaction between the troposphere and stratosphere (Perlwitz, 2000).

It is well know that the mid- latitudinal atmospheric circulation is characterized not only by stationary waves but also by transient eddies of varied frequencies and their interaction with the mean flow. In order to isolate transient eddies from different frequencies domains, the 21-point filters introduced by Blanckmon and Lau (1980) are applied here (Appendix A.4). The filtering procedures are applied to the October-to-April data. The months October and April are discarded afterwards to omit spurious fluctuations resulting from jumps in the data between two winters. Before doing the filtering, the annual mean, annual and semi-annual Fourier harmonics corresponding to 1 and 0.5 years were removed from the time series of all relevant variables for all grid points (Straus and Shukla, 1988; Walter, 2003).

It should be mentioned that as indicated before, only the ultra-long waves can propagate from the troposphere vertically to the stratosphere since the increasing ZWNs correspond to decreasing critical Rossby velocities (Charney and Drazin). Therefore, in this thesis, only ZWN1, 2 and 3 stationary planetary waves are studied.

2.3 Frequency of negative refractive index squared of stationary planetary wave propagation

As a powerful diagnostic, the quasi-geostrophic refractive index of stationary planetary waves was introduced by Matsuno (1970) and has been frequently applied. Matsuno (1970) concentrated on the hypothesis that the stationary waves in the Northern

Hemisphere winter stratosphere are forced from the troposphere and a linearized quasi-geostrophic potential vorticity equation in spherical coordinates was used in his study. In order to understand the wave-mean flow interaction dynamics of sudden warmings, Palmer (1981a, b), O'Neill and Youngblut (1982), Kanzawa (1982, 1984) also performed a refractive index and Eliassen-Palm (E-P hereafter) flux diagnostic during observed sudden stratospheric warmings. In Butchart et al. (1982) and Mukougawa and Hirooka (2004), the refractive index and E-P flux diagnostic were performed on the stratospheric sudden warming phenomenon not only for the observed regimes but also for model simulations. Mainly concentrating on the analysis of E-P flux, Shiotani (1986) used the refractive index as a subsidiary diagnostic to study the planetary wave activities in Northern Hemisphere winter. By using a linearized quasi-geostrophic model, Huang and Gambo (1982) concluded that on the meridional distribution of refractive index squared, there are two "wave guides" for ZWN1 stationary planetary waves in Northern Hemisphere winter. But in case of in Northern Hemisphere summer, Huang (1984) found that the locations of these "wave guides" have been changed. Lin (1982) applied a primitive equation linear model and he found that the role of the polar night jet in channeling planetary waves as they propagate vertically is very important and the latitudinal location of the polar night jet has a significant influence on the wave propagation. By use of the refractive index and the E-P flux, Boville (1986) studied the wave-mean flow interactions in the General Circulation Model (GCM) of troposphere and stratosphere. He also concluded that a strong lower stratospheric jet tends to favor weak wave forcing of the jet, while a weak jet favors stronger wave forcing. Limpasuvan and Hartmann (2000) and Hu and Tung (2002) found that the vertical shear of zonal wind plays an important role in some region for channeling the waves.

As it was mentioned before, based on the Charney-Drazin theorem, the effective index of refraction of vertically propagating planetary waves of a given zonal wave number at specific latitude depends primarily on the atmospheric state. An important parameter is the vertical distribution of the zonal mean zonal wind. Stationary planetary waves tend to avoid regions where the zonal winds are easterly or are westerly but exceed a critical wave number dependent Rossby velocity (Charney and Drazin, 1961). They are attracted to regions where the value of refractive index squared is a positive maximum (Matsuno, 1970). However, as mentioned above, the traditional analysis of refractive index lacks the ability to illustrate the climatology of the atmospheric state supportive of vertical propagation of planetary waves due to the overlapping of positive and negative value of n_k^2. Figure 2.1 shows the mean of n_k^2 of 44 boreal winters (1958-2002), single winter (1958-1959 and 1978-1979), and single days (1959/01/01 and 1979/01/01) for ZWN1, 2 and 3 planetary waves, respectively. It can be seen for the ZWN1 planetary wave, that there are differences between the means of n_1^2 for 44 winters (Fig.2.1a) and for single winters (Fig.2.1d) for the negative value of n_1^2 near the northern pole. Differences can also be found between the mean of 44 winters (Fig.2.1a) and single day (Fig.2.1j) not only at the pole but also in mid-latitudes. On the other hand, the mean of n_1^2 is distributed differently for each single winter (Fig.2.1d, g). Clear differences can also be observed between single days from different winters (Fig.2.1j, m). Similar conclusions can also be drawn for ZWN2 and 3 waves.
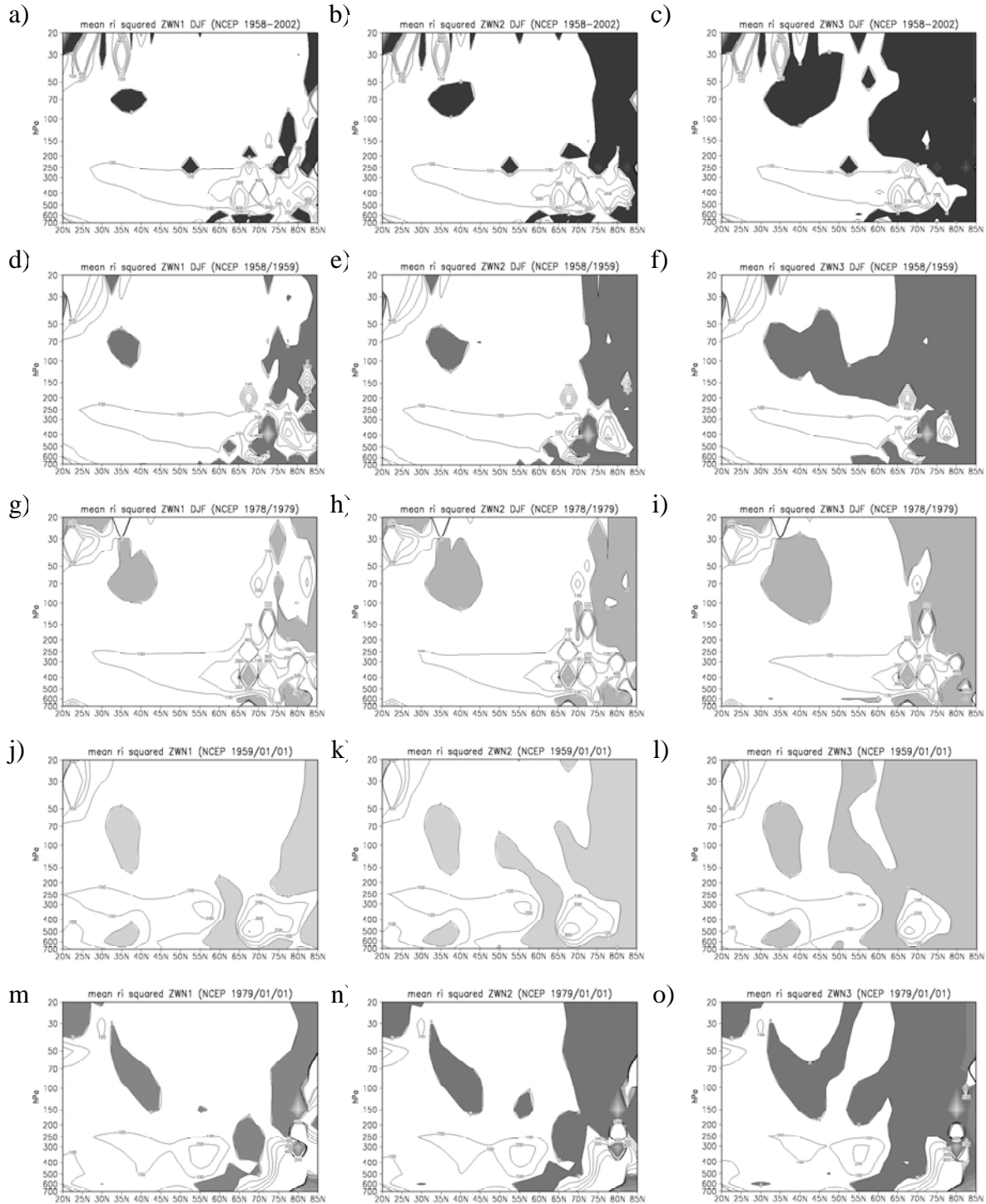
Figure 2.1. Refractive index squared ($a^2 n^2$) for ZWN1 (first column) ZWN2 (second column) and ZWN3 (third column) stationary waves (NCEP/NCAR RA, 1958-2002) for mean of 44 boreal winters (December, January and February)(first row), mean of 1958-1959 DJF (second row), mean of 1978-1979 DJF (third row), 1959/01/01 (fourth row) and 1979/01/01 (last row). In the plot, contours range from 0 to 400 with an interval of 100, regions with negative values are shaded.

a)

b)

c)

Figure 2.2. f (n_k^2<0) for stationary planetary waves in DJF (NCEP/NCAR RA 1958-2002): a) ZWN1 wave; b) ZWN2 wave; c) ZWN3 wave. Unit of f (n_k^2<0) is %.

In Fig.2.1, n_k^2 shows different patterns when the time mean is calculated. The calculation of the time mean of n_k^2 induces a reduction of information, which makes it is hard to interpret the r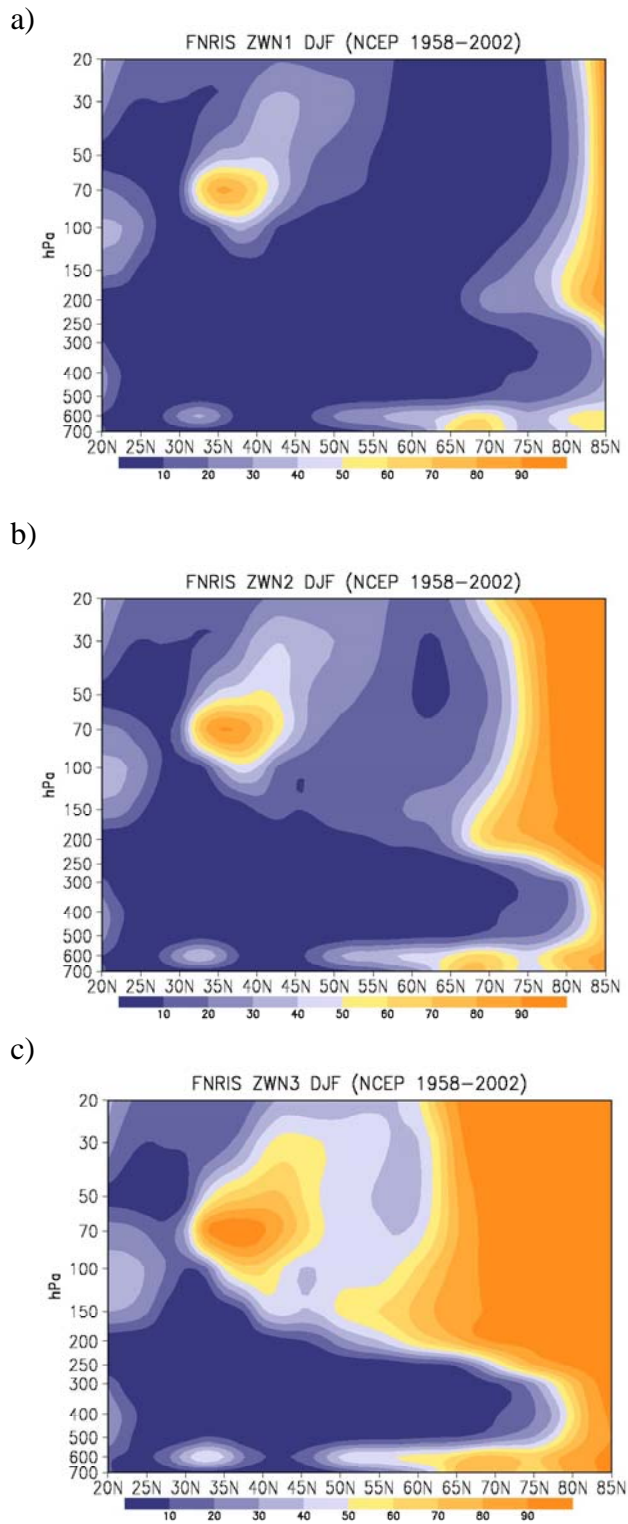esults. In order to avoid the problem caused by overlapping of positive and negative n_k^2 when the time mean is of interest, the seasonal frequency distribution of days with negative n_k^2 (f (n_k^2<0) hereafter) is introduced in this section.

The f (n_k^2<0) is produced from the daily mean data by counting the number of days in whole dataset with negative n_k^2. Dividing it by the total number of days, this is done on the meridional plane. Thus a two-dimensional probability distribution of refraction of planetary waves is obtained. At places where the probability of negative n_k^2 is small, planetary waves have a good chance to propagate, while large probabilities indicate that very seldom planetary waves are allowed to propagate across these places. This analysis does not provide any indication of the direction and total energy flux of planetary waves, but it turns out that it clearly provides a picture of probable wave propagation by 'channels' of low probability of negative n_k^2. This statistical analysis also implies the control of the mean flow on waves. The data for ZWN1, 2 and 3 stationary planetary waves in Northern Hemisphere winter in December, January and February (DJF) were analyzed, respectively.

Figure 2.2 shows the distribution of f (n_k^2<0) for stationary planetary waves in Northern Hemisphere winter (DJF) of 1958-2002 on the meridional plane for ZWN1, 2 and 3 waves, respectively. Since this analysis was performed based on the quasi-geostrophic theory, which is not appropriate near the tropics, all figures are drawn only north of 20^oN. In order to enhance the clearness of the atmospheric state for planetary wave propagation in both troposphere and stratosphere, and to avoid the boundary effects of datasets, patterns are shown only between 700hPa and 20hPa in figures.

There are common characteristics for all ZWN1, 2 and 3 waves. It is clear that the planetary waves have rather big chances to propagate upward in the troposphere for all ZWN1, 2 and 3 (Fig.2.1a, b and c). This corresponds with the general thinking that the ultra-long waves can propagate from the troposphere vertically to the stratosphere (Charney and Drazin, 1961; Matsuno, 1970). But the waves initiated from the lower troposphere (below 500 hPa) have less probability to propagate at higher latitudes (north of 50^oN). This can be explained that one of the initiations of stationary planetary waves in troposphere is the topography which distribute ideally mostly in the extratropics (Huang and Gambo, 1982). However, the great potential of vertical propagation from the troposphere to the stratosphere does not distribute on the most part of the meridional plane. This opposes to the general distribution of mean refractive index squared, which showed positive value of n_k^2 for ZWN1 on almost whole meridional plane (Huang and Gambo, 1982, Fig.7; Limpasuvan and Hartmann, 2000, Fig.8). It is noted that there is a small area above the subtropical tropopause where the value of f (n_k^2<0) is rather higher for all ZWN1, 2 and 3 waves.
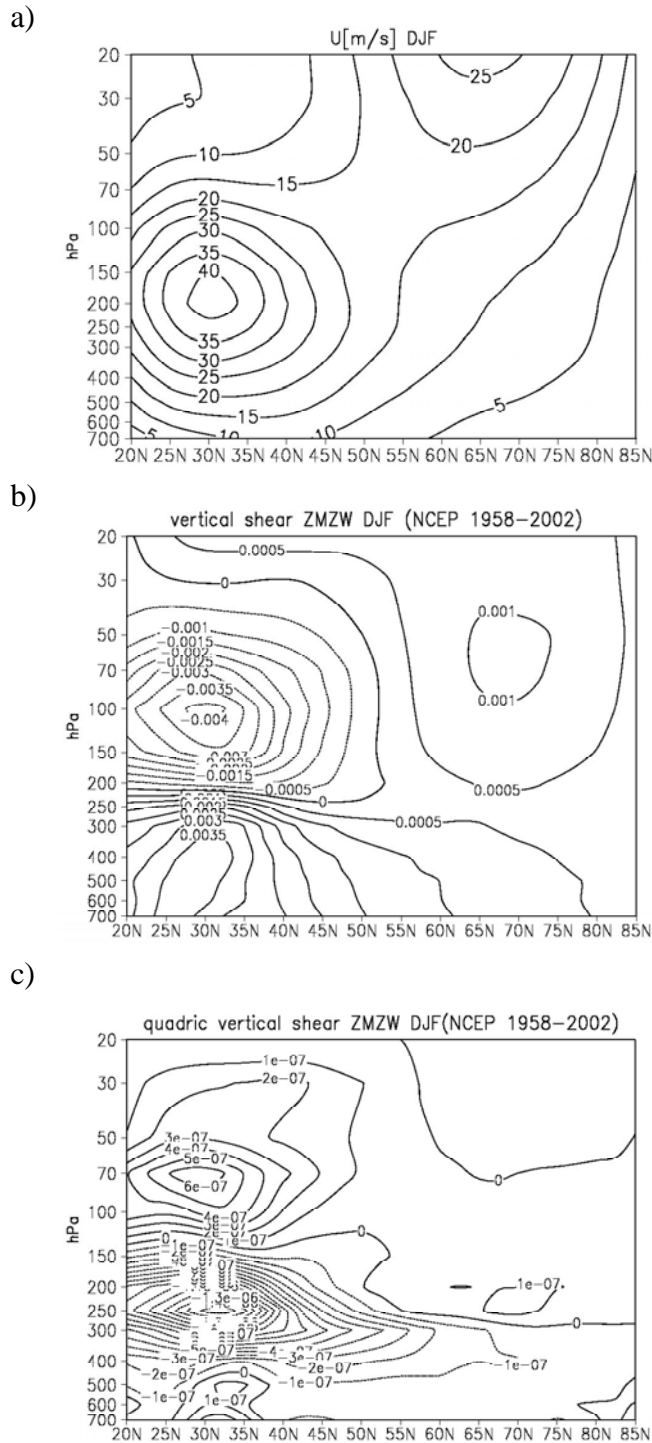
a)

b)

c)

Figure 2.3. a) Zonal mean zonal wind $\bar{u}$ (m/s); b) vertical shear of zonal mean zonal wind $\frac{\partial \bar{u}}{\partial z}$ (s^{-1}); and c) vertical shear of $\frac{\partial \bar{u}}{\partial z}$ (m^{-1}s^{-1}) on meridional plane in DJF (NCEP/NCAR RA 1958-2002).

This small area is also found in Hu and Tung's (2002, Fig.5 c and d) for ZWN1 wave. The location of this small area can be related to another small area above the subtropical jet (Fig.2.3a) where the negative vertical shear of the zonal mean zonal wind centers (Fig.2.3b). This corresponds to Chen and Robinson's (1992) conclusion, that larger negative vertical wind shear impedes wave propagation across the tropopause. While the distribution of quadratic vertical shear of zonal wind $\dfrac{\partial^2 \overline{u}}{\partial z^2}$ (Fig.2.3c) on the meridional plane does not show clear connection with the impeded wave propagation across the subtropical tropopause. This point has also been indicated by Hu and Tung (2002). Another common characteristic is the existence of a "channel" from the troposphere to the stratosphere at middle latitudes between the existence of high values of $f(n_k^2<0)$ at rather higher latitudes and the small area indicated above. The presence of this "channel" corresponds to the "wave guide" indicated by Huang and Gambo (1982, Fig.7) from the lower troposphere at 40°N to the stratosphere at high latitudes.

There are also obvious differences between ZWN1, 2 and 3 waves on the distribution of $f(n_k^2<0)$. First of all, Fig.2.2a, b and c plotting $f(n_k^2<0)$ for ZWN1, 2 and 3, respectively, the values of $f(n_k^2<0)$ on the whole meridional plane increase with increased ZWNs, which implies that the probability of wave propagation decreases with the increasing ZWNs. This obviously agrees well with the ZWN-depending critical Rossby velocity theorem (Charney and Drazin, 1961). To be more detailed, the small area above the subtropical tropopause with rather higher values of $f(n_k^2<0)$ strengthens with the increasing ZWNs, but the general location does not move. The width of narrow column at the north pole with higher $f(n_k^2<0)$ for ZWN1 wave (Fig.1a) increases strongly equatorward with increasing ZWNs (Fig.2.2b and Fig.2.2c). These two enhanced patterns, finally narrow the "channel" indicated above for wave propagation from the troposphere to the stratosphere. This represents the reduction of the probability of propagation of ZWN3 wave from the troposphere to the stratosphere.

It should be mentioned here that in this thesis in the calculation of the refractive index the buoyancy frequency squared N^2 is treated as variable of both latitude and altitude ($N^2(\varphi,z)$). The buoyancy frequency represents the stability of atmosphere. In some previous studies, the buoyancy frequency was treated as a constant (Matsuno, 1970; Huang and Gambo, 1982; Andrews et al., 1987), or as a variable of altitude only (Chen and Robinson, 1992; Limpasuvan, 2000; Hu and Tung, 2002). Chen and Robinson (1992) found the variation of N^2 is not negligible as it has been hypothesized in other applications (Matsuno, 1970; Andrews et al., 1987). They found that the propagation of planetary waves from the troposphere to the stratosphere is sensitive to the distribution of $N^2(z)$ especially near the subtropical tropopause. While in this thesis the buoyancy frequency N^2 is considered as a variable of not only altitude but also latitude (Fig.2.4a). The comparisons of $N^2(z)$ with $N^2(\varphi,z)$ on different latitudes, are shown on Fig.4b. It is found that the values of N^2 are not homogenously distributed with altitude and latitude

(Fig.2.4a). The values of N^2 near the subtropical and extratropical tropopauses have fairly strong vertical and meridional gradients. This can also be found in the comparision of $N^2(z)$ and $N^2(\varphi, z)$ (Fig.2.4b). These gradients of N^2 have influence on distribution of planetary wave propagation. The distribution of f ($n_k^2 < 0$), considering the N^2 as variable of only latitude, is presented in Fig.2.5 for ZWN1, 2 and 3 waves, respectively. Comparing Fig.2.5 with Fig.2.2, it is obvious that the vertical gradient near the extratropical tropopause has effect on the probability of planetary wave propagation for all ZWN1, 2 and 3 waves at the same region. It can be concluded that the strong vertical gradient of N^2 reduces the probability of waves propagation (Fig.2.5). This is consistent with the conclusion of Chen and Robinson (1992). On the other hand, since the distribution of buoyancy frequency N^2 is not constant on meridional plane, the meridional distribution of N^2 has also influence on propagation of planetary waves. Therefore, it is a proper way to treat the buoyancy frequency $N^2(\varphi, z)$ as in real atmosphere instead of the simplified $N^2(z)$. This treatment will be applied in this thesis.
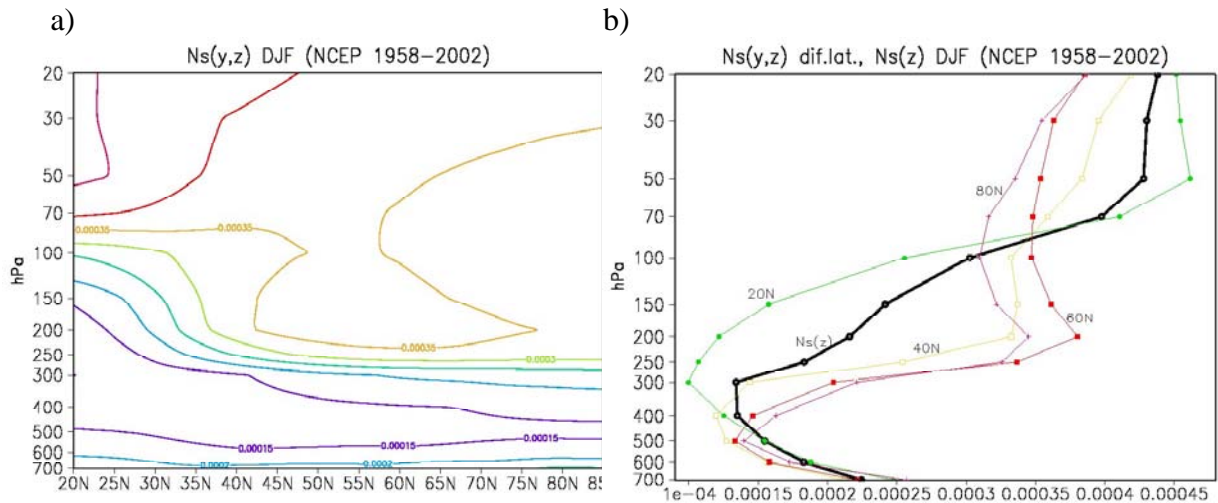
Figure 2.4. Buoyancy frequency of Northern Hemisphere winter (DJF) (NCEP RA 1958-2002): a) $N^2(\varphi, z)$ on meridonal plane; b) $N^2(z)$ profile (black line) and $N^2(\phi, z)$ profiles on different latitudes. Unit of N^2 is s^{-2}.
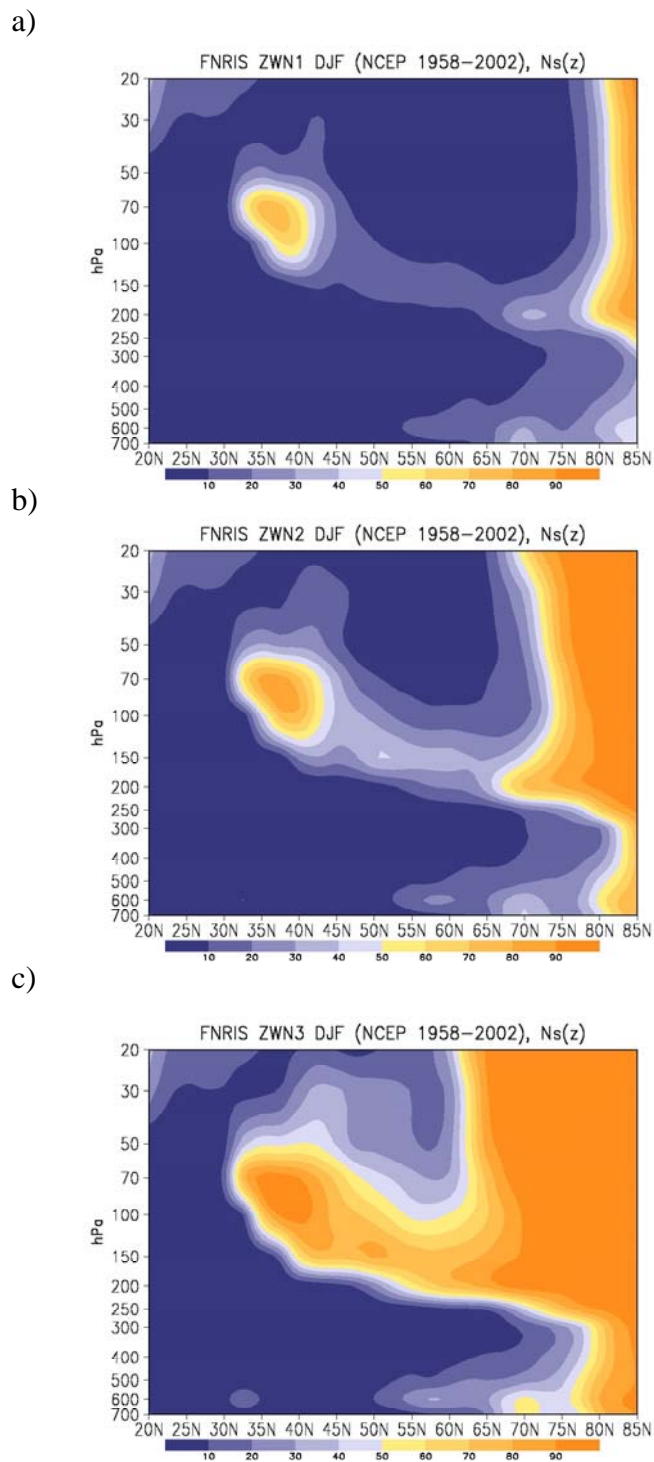
a)

b)

c)

Figure 2.5. f (n_k^2<0)for stationary planetary waves in DJF (NCEP/NCAR reanalysis data 1958-2002), considering N^2(z): a) ZWN1 wave; b) ZWN2 wave; c) ZWN3 wave. Unit of f (n_k^2<0) is %.

As discussed above, the analysis of f (n_k^2<0) only gives the information of the state of the atmospheric zonal mean flow for the probability of propagation of stationary planetary waves. The refractive index implies that it is useful in determining the influence of the mean flow on the waves. On the other hand, the Eliassen-Palm (E-P) flux and its divergence are of fundamental importance in determining the wave activities and forcing on the zonal mean flow. As a powerful analysis, the E-P flux (Eliassen and Palm, 1961; Andrew et al., 1987) was applied as a momentum flux associated with planetary wave activities in many studies (Muench, 1965; Shiotani, 1987; Randel 1987; Chen and Robinson, 1992; Chen and Graf, 2002; Hu and Tung, 2002; Hitoshi and Hirooka, 2004, etc).The analysis of the E-P flux and its divergence will help to understand the dynamics of planetary waves – mean flow interaction between the troposphere and the stratosphere. Based on this purpose, E-P flux and its divergence for planetary waves are also applied to study the climatology of planetary wave propagation in this thesis.

Fig.2.6 shows the cross section of E-P flux and its divergence on the meridional plane in Northern Hemisphere boreal winter (DJF) for ZWN1, 2, 3, ZWN1+2+3 and all ZWNs waves, respectively. It is observed that there are two branches of the vectors of E-P flux for all ZWNs stationary waves and they start in the extratropics, which corresponds to the "channel" showed in the frequency of negative refractive index squared f (n_k^2<0) (Fig.2.2). One branch of the verctors starts from the lower troposphere and points upward across the tropopause to the lower and middle stratosphere (Fig.2.6e). This implies that in Northern Hemisphere winter, the eddy heat flux (baroclinic forcing, Hartmann & Lo, 1998) dominates the wave activities between the troposphere and the lower and mid-stratosphere, and therefore the baroclinic energy prevails there. The branch of upward E-P flux vectors also correspond with the "channel" showed by f (n_k^2<0) (Fig.2.2). Another branch of vectors starts also from the lower troposphere but turns equatorward in the upper troposphere. This implies the importance of the eddy momentum flux (barotropic forcing, Hartmann & Lo, 1998) in the subtropical upper troposphere. There are two major regions where the divergence of E-P flux is negative, which means an easterly zonal momentum force exerted by planetary waves on the atmosphere. One is located in the extratropical upper troposphere and another in the subpolar mid-stratosphere. The latter one is relatively weaker.

Considering the contribution of different ZWNs waves, E-P flux and its divergence of ZWN1 wave (Fig.2.6a) show the same pattern as in the all ZWNs waves (Fig.2.6e) with two major branches of vectors and two major convergences. But the amplitudes are much smaller for ZWN1 wave. However, there is only one branch of vectors left for ZWN2 wave and ZWN3 wave. For ZWN2 wave (Fig.2.6b) only the upward branch is left and the amplitudes of the vectors become smaller especially in the subpolar lower and mid-stratosphere compared with ZWN1 wave (Fig.2.6a). In contrast, for ZWN3 wave (Fig.2.6c) only the equatorward branch in troposphere still exists. About the two major convergent regions, same as in ZWN1 wave, they are also reduced for ZWN2 wave (Fig.2.6b). However the one in the subpolar lower and middle stratosphere disappears for ZWN3 wave (Fig.2.6c), although there is potential possibility for wave propagation (Fig.2.2c).
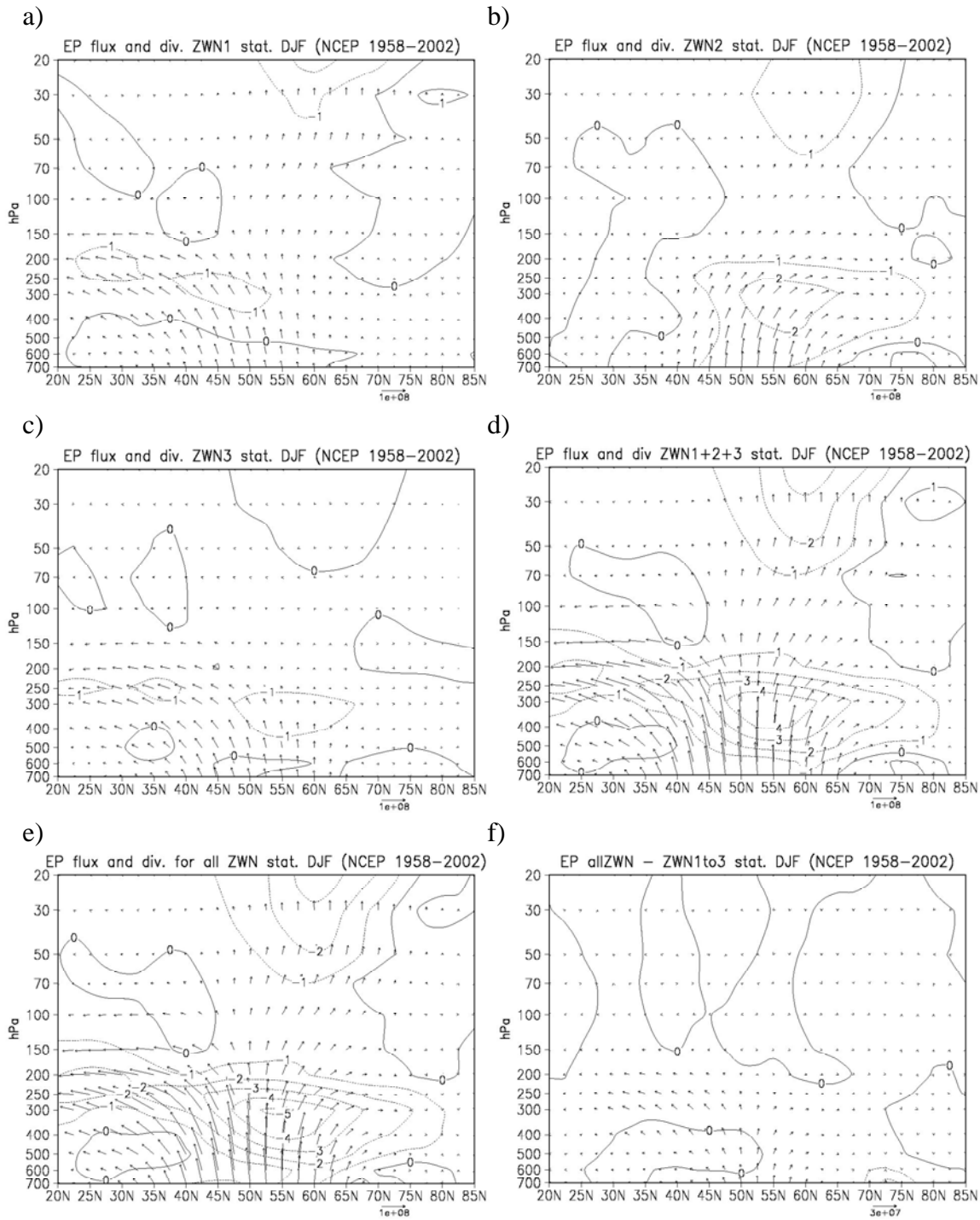
a)

b)

c)

d)

e)

f)

Figure 2.6. Cross section of E-P flux for stationary planetary waves in DJF (NCEP/NCAR RA 1958-2002); a) ZWN1 wave; b) ZWN2 wave; c) ZWN3 wave; d) ZWN1+2+3 waves; e) all ZWNs waves; f) difference between all ZWNs waves and ZWN1+2+3 waves. Divergence contour interval is 1 ms^{-1}day^{-1}, the unit of vector is kg s^{-2}.

To briefly summarize, stationary planetary waves can transfer eddy heat energy (baroclinic forcing) from the troposphere to the stratosphere and eddy momentum energy (barotropic forcing) to the subtropical upper troposphere. They exert easterly zonal momentum forcing on the atmospheric mean flow at the extratropical upper troposphere and the subpolar lower and middle stratosphere. The ZWN1 wave contributes mostly on the wave propagation from the troposphere to the stratosphere, compared with ZWN2 and 3 waves, which refers to the ZWN-depending critical Rossby velocity theorem (Charney and Drazin, 1961).

Fig.2.6d shows the E-P flux and its divergence for ZWN1, 2 and 3 waves together. It is very similar with the patterns showed for all ZWNs waves (Fig.2.6e). To be clearer, Fig.2.6f gives the differences between these two (all ZWNs waves minus ZWN1+2+3) and it is apparent that the difference is negligible. This implies that only the ultra-long (ZWN1, 2 and 3) waves can propagate from the troposphere to the stratosphere (Charney and Drazin, 1961; Matsuno, 1970).

2.4 Stratospheric polar vortex regimes

In the discussion of planetary wave propagation, the wave-mean flow interaction should be considered with caution since the distribution of zonal mean zonal wind (Charney and Drazin, 1961; Matsuno, 1970) and vertical shear of zonal wind (Lin, 1982; Chen and Robinson, 1992; Hu and Tung, 2002) plays a key role on the planetary wave propagation in both the troposphere and the stratosphere. The stratospheric circulation is characterized by strong westerly flows at high latitudes (Fig.2.2a) in Northern Hemisphere winter. This so-called stratospheric polar vortex usually forms in early winter as a consequence of the cooling of the northern polar region due to the strong radiative cooling above the winter pole. It is well known that the stratospheric polar vortex undergoes annual anomalies (Baldwin and Dunkerton, 1999, 2001; Perlwitz and Graf, 1995, 2000, 2001a, b; Castanheira and Graf, 2003; Christiansen, 2003), which generally can be observed by the zonal wind distribution and are separated into strong polar vortex regime and weak polar vortex regime. In the Northern Hemisphere, the linkage between the stratosphere and troposphere appears most obvious when the stratospheric polar vortex undergoes unusually strong variation in wind strength and temperature (Limpasuvan, et al., 2005).

Christiansen (2003) presented evidence that the existence of two different circulation regimes in the Northern Hemisphere stratospheric interannual variability. The regimes correspond to the strong stratospheric polar vortex and weak stratospheric polar vortex. By studying the PDFs of the leading PC of the geopotential height over Northern Hemisphere average of winter half-year (from October to March), he found that the existence of a bimodal probability density distribution in middle and lower Northern stratosphere. Similar results are found, if averages are taken over three winter months (December, January and February) (Christiansen, 2003). However, if monthly means are used, Christiansen (2003) found that the PDFs are unimodal as in Gillet et al. (2002) reported for daily data of temperature. As indicated by Palmer (1993), the presence of higher frequencies can obscure the existence of bimodality. On the other hand, in Perlwitz and Graf (2001a, b), the bimodality in the distribution of anomaly correlations of

the geopotential height (2001a) and zonal wind (2001b) at 50hPa over monthly means has been found. However, recently Christiansen (2005) found that the bimodality in the distribution of anomaly correlations is not evident for a system with multiple atmospheric regimes but only for a system with few degrees of freedom.

By analyzing the zonal mean zonal wind at 50hPa and 65°N, Walter (2003) found that the strength of stratospheric polar vortex shows 30-days persistence. Then she counted all months in which the monthly mean zonal wind at 50hPa and 65°N is stronger than 20 m/s to the strong polar vortex regime and those months in which the monthly mean zonal wind at 50hPa and 65°N is weaker than 10 m/s were counted to the weak vortex regime. This threshold has been discussed in Castanheira and Graf (2003) but based on daily mean data. They concluded that this regime threshold is somehow arbitrary for the real atmosphere but it reflects critical Rossby velocity (20m/s) for ZWN 1 planetary wave near the polar circle for a climatological Northern Hemisphere zonal wind profile.

In this thesis, in order to increase the clearness of the results and to avoid the unimodal problem when the monthly mean is used, the definition of strong and weak polar vortex regimes is based on daily means, which was also applied in Castanheira and Graf (2003). Considering the daily means of zonal mean zonal wind at 50 hPa and 65°N ($\overline{u}_{50}(65^o N)$ of Northern Hemisphere winter (November to March), the strong polar vortex regime (SVR hereafter) consists of all days in which $\overline{u}_{50}(65^o N) > 20$ m/s for at least 30 days. The weak polar vortex regime (WVR hereafter) is defined as the regime including all days in which $0 < \overline{u}_{50}(65^o N) < 10$ m/s and also is lasting at least 30 days. Based on this, the data are subdivided into the two polar vortex regimes. The strong polar vortex regime (SVR) and weak polar vortex regime (WVR) therefore will be discussed separately.

Table 2.1 shows the periods of SVR (Table 2.1a) and WVR (Table 2.1b) in all winter seasons from 1958 to 2002 based on the zonal mean zonal wind data from NCEP/NCAR Reanalysis daily mean data. There are 11 SVR cases and 12 WVR cases. Including all days, SVR covers 777 days and WVR 529 days. The shortest period of SVR includes 45 (1959-01-22 to 1959-03-07, Table 2.1a) days, which are longer than the one of WVR 33 days (1981-02-26 to 1981-03-30, Table 2.1b). This corresponds to the general knowledge that the stratospheric circulation in Northern Hemisphere winter prefers to stay stronger westerly. It is obvious that there is no single winter in which both SVR and WVR happened and this corresponds to the understanding that the anomalies of stratospheric polar vortex in Northern Hemisphere winter should be considered as interannual phenomenons (Baldwin and Dunkerton, 1999, 2001; Limpasuvan and Hartmann, 2000).

The distribution of zonal mean zonal wind and vertical shear for SVR and WVR is shown in Fig.2.7, respectively. Both zonal mean zonal wind (Fig.2.7a) and wind shear (Fig.2.7b) of SVR are similar with patterns in DJF (Fig.2.3a, b) except that the strength of wind at subpolar is much stronger in SVR. It should be indicated that there exists a positive wind shear at the subpolar lower stratosphere for both DJF (Fig.2.3b) and SVR (Fig.2.7b) but the value is bigger in SVR. On the other hand, both the strong westerly and the positive wind shear at the subpolar stratosphere have been reduced in WVR (Fig.2.7c, d). In order

a)

Starting dates	Ending dates
1959/01/22	1959/03/07
1963/12/24	1964/02/28
1967/01/03	1967/03/31
1975/12/01	1976/03/24
1987/11/20	1987/01/14
1988/12/16	1989/02/17
1989/12/17	1990/03/31
1990/11/02	1990/12/29
1991/11/24	1992/01/18
1992/12/05	1993/02/11
1994/11/26	1995/01/18

b)

Starting dates	Ending dates
1958/01/26	1958/03/31
1960/11/01	1960/12/27
1963/02/08	1963/03/13
1965/11/12	1965/12/25
1968/12/20	1969/01/27
1981/02/26	1981/03/30
1984/12/28	1985/02/13
1987/11/24	1987/12/28
1996/11/14	1996/12/22
1998/12/09	1999/01/11
2000/11/08	2000/12/22
2001/02/04	2001/03/31

Table 2.1. Lasting periods of polar vortex regimes; a) strong polar vortex regime (SVR) and b) weak polar vortex regime (WVR) (NCEP/NCAR RA 1958 to 2002).

to clarify the mean flow anomalies, the difference of zonal mean zonal wind and wind shear between SVR and WVR is drawn in Fig.2.7e and Fig.2.7f.

The f ($n_k^2 < 0$) is also analyzed in SVR and WVR for ZWN1, 2 and 3 stationary planetary waves, respectively (Fig.2.8). Comparing with DJF, similar general patterns also exist in SVR and WVR except for the variation of the "channel" at middle latitudes between the troposphere and stratosphere with increased ZWNs. For ZWN1 wave, the "channel" which represents the high probability of wave propagation is narrower in SVR (Fig.2.8a) than in WVR (Fig.2.8b), even than in DJF (Fig.2.2a). This means that the ZWN1 stationary planetary wave has less chance to disturb the stratospheric circulation in SVR than in WVR (Castanheira and Graf, 2003) and in DJF. On the other hand, the probability of wave propagation from the troposphere to the stratosphere in WVR is bigger. This point has been addressed by several other previous studies (Perlwitz and Graf, 2001a; Castanheira and Graf, 2003; Walter, 2003). This finding can also be observed for ZWN2 wave (Fig.2.8c, d). However, for ZWN3 wave, the "channel" in which wave has chance to propagate from the troposphere to the stratosphere is almost totally "blocked" in SVR (Fig.2.8e). This is different with in DJF (Fig.2.2c) and in WVR (Fig.2.8f). Based on the analysis of f ($n_k^2 < 0$), it can be concluded that the anomalies of atmospheric mean flow have influences on the probability of stationary planetary wave propagation, which corresponds to the zonal wind-dependent theorem for planetary wave propagation (Charney and Drazin, 1961; Matsuno, 1970).
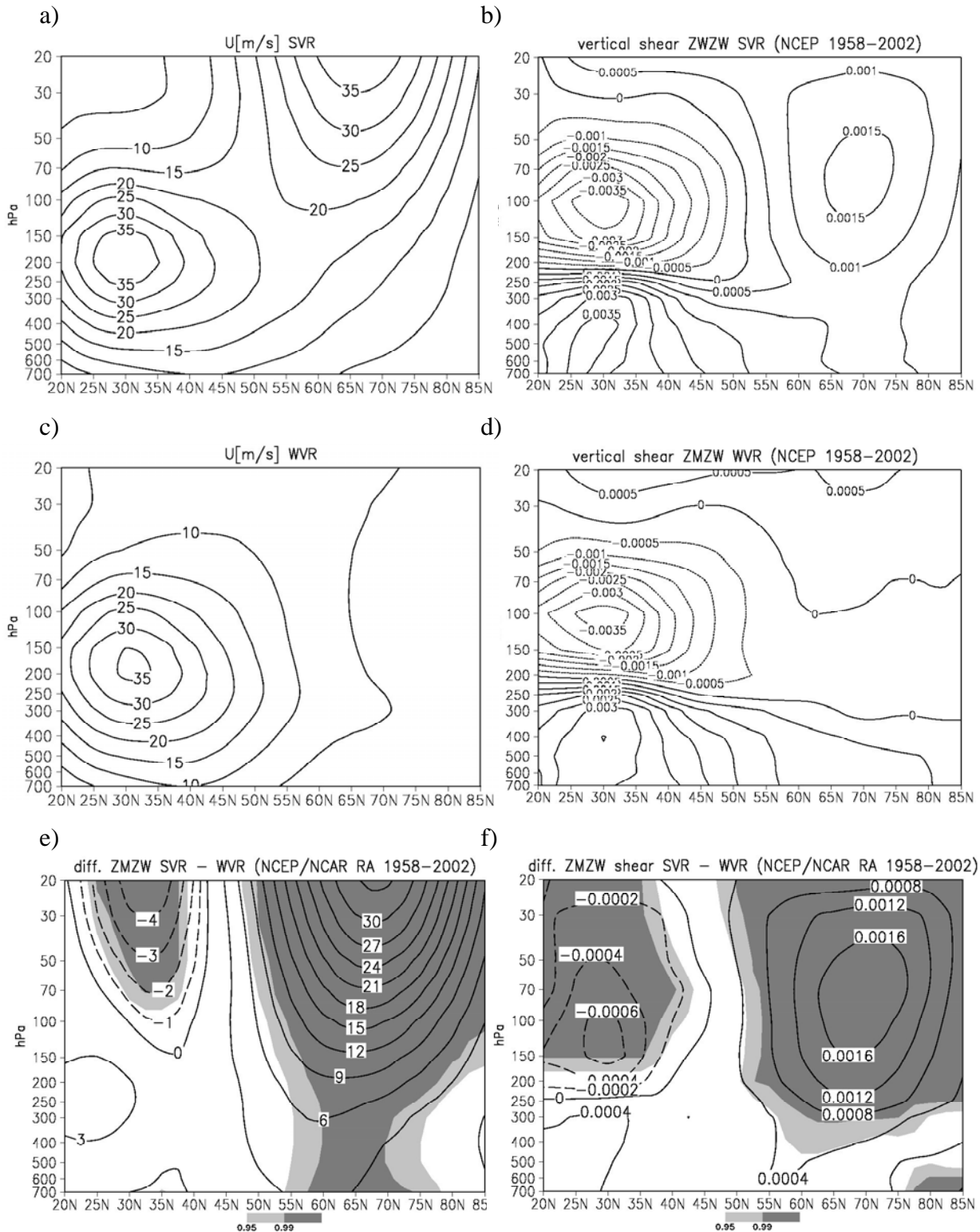
a)

b)

c)

d)

e)

f)

Figure 2.7. Zonal mean zonal wind (m/s) (left column) and its vertical shear (s^{-1}) (right column) on meridional plane for SVR (first row), WVR (second row) and difference between SVR and WVR (bottom row) (NCEP/NCAR RA 1958-2002). Area with significant level above 99% is heavily shaded.

a)

FNRIS ZWN1 SVR (NCEP 1958-2002)

b)

FNRIS ZWN1 WVR (NCEP 1958-2002)

c)

FNRIS ZWN2 SVR (NCEP 1958-2002)

d)

FNRIS ZWN2 WVR (NCEP 1958-2002)

e)

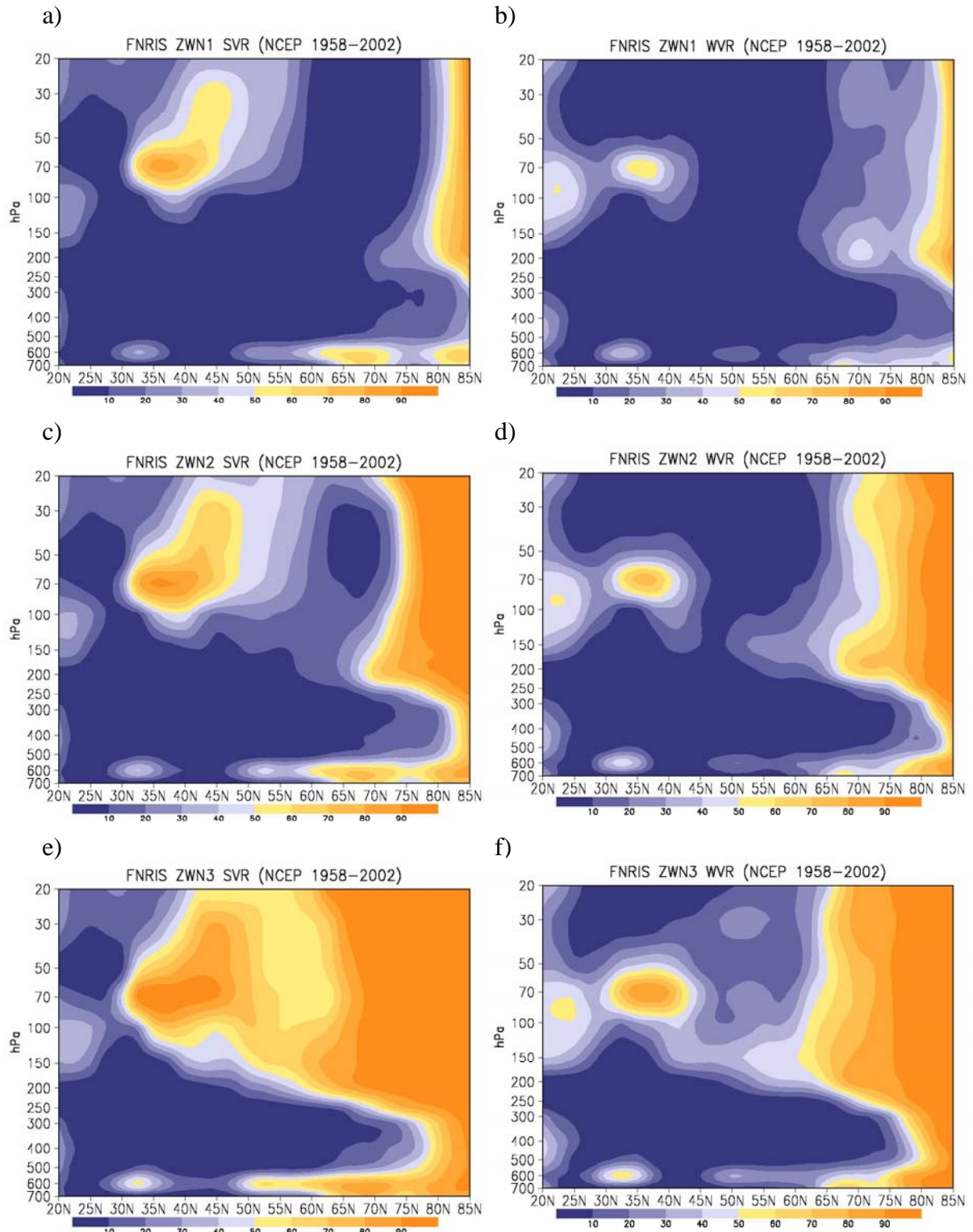FNRIS ZWN3 SVR (NCEP 1958-2002)

f)

FNRIS ZWN3 WVR (NCEP 1958-2002)

Figure 2.8. f (n_k^2<0) for stationary planetary waves in SVR (left column and WVR (right column separately for ZWN 1 wave (first row), ZWN 2 wave (second row) and ZWN 3 wave (bottom row). Unit of f (n_k^2<0) is %.

In order to enhance our understanding of wave-mean flow interaction, the E-P flux and its divergence are also analyzed in SVR and WVR like in the general winter seasons (DJF). Fig.2.9 shows the cross section on the meridional plane for E-P flux and divergence in SVR and WVR, for ZWN1, 2, 3 and 1+2+3 waves. As it has been indicated, the difference between all ZWNs and ZWN1+2+3 stationary waves is negligible (Fig.2.6f), therefore in this section all ZWNs waves will not be discussed further.

The major patterns of E-P flux and its divergence as shown in DJF (Fig.2.6) have been well illuminated in both SVR and WVR (Fig.2.9). For ZWN1+2+3, in both SVR and WVR, there exist the two major branches of vectors, as well as the two major convergent areas. However, there is also obvious difference between these two stratospheric polar vortex regimes. The convergent area in the subpolar stratosphere has been strengthened both on amplitude and area in WVR (Fig.2.9h). In fact, almost the whole extratropical and subpolar stratosphere is covered by the convergence of E-P flux in WVR, which means the wave-exerted easterly zonal momentum forcing on mean flow is dominating in stratosphere. The similar variation in WVR is shown for ZWN1 and 2 waves with less intensity. However, there is intensified divergence in the polar stratosphere in SVR, which can induce westerly momentum forcing on mean flow in the polar lower and mid-stratosphere. Limpasuvan and Hartmann (2000) also indicate that the baroclinic contribution can lead to strong westerly forcing in the high-latitude middle stratosphere.

In order to clarify the potential influence of wave activities on the anomalies of mean flow, the differences of E-P flux and divergence between in SVR and in DJF, and between SVR and in WVR, are shown in Fig.2.10. The major patterns of these two sets of differences are similar for ZWN1+2+3 waves (Fig.2.10g and h). The equatorward vectors and the divergence of E-P flux in the extratropical upper troposphere are stronger in SVR, while the upward vectors and divergence in the polar lower and mid-stratosphere are stronger in WVR (Fig.2.10h). Therefore, stationary waves prefer to reduce the westerly in the subtropical troposphere (Fig.2.7a) in SVR. In WVR waves also tend to reduce the westerlies, but in the polar stratosphere. The difference of E-P flux and its divergence of ZWN1 wave shows similar patterns (Fig.2.10a, b). For ZWN3 wave, only the stronger equatorward vectors in the extratropical upper troposphere in SVR can be observed. However, for ZWN2 wave, in WVR there exits stronger equatorward and upward vectors in the subtropical troposphere.

Finally, it should be mentioned that the positive vertical zonal wind shear is also intensified in SVR (Fig.2.7f) in the subpolar lower stratosphere. However, a significant influence of this positive wind shear on stationary planetary waves is not observed (Fig.2.8). From the difference of f (n_k^2<0) between SVR and WVR (not shown), although the slightly bigger chance around 65^oN – 70^oN for ZWN1 and 2 waves in SVR, which probably corresponds to the bigger values of the vertical shear of zonal mean zonal wind, can be observed, the much more possibilities of planetary wave propagation from the troposphere to the stratosphere at mid latitudes in WVR can also be found. This implies that the intensified vertical shear of ZMZW in SVR can probably enhance the permission of the stationary wave propagation in the lower stratosphere at high latitudes.
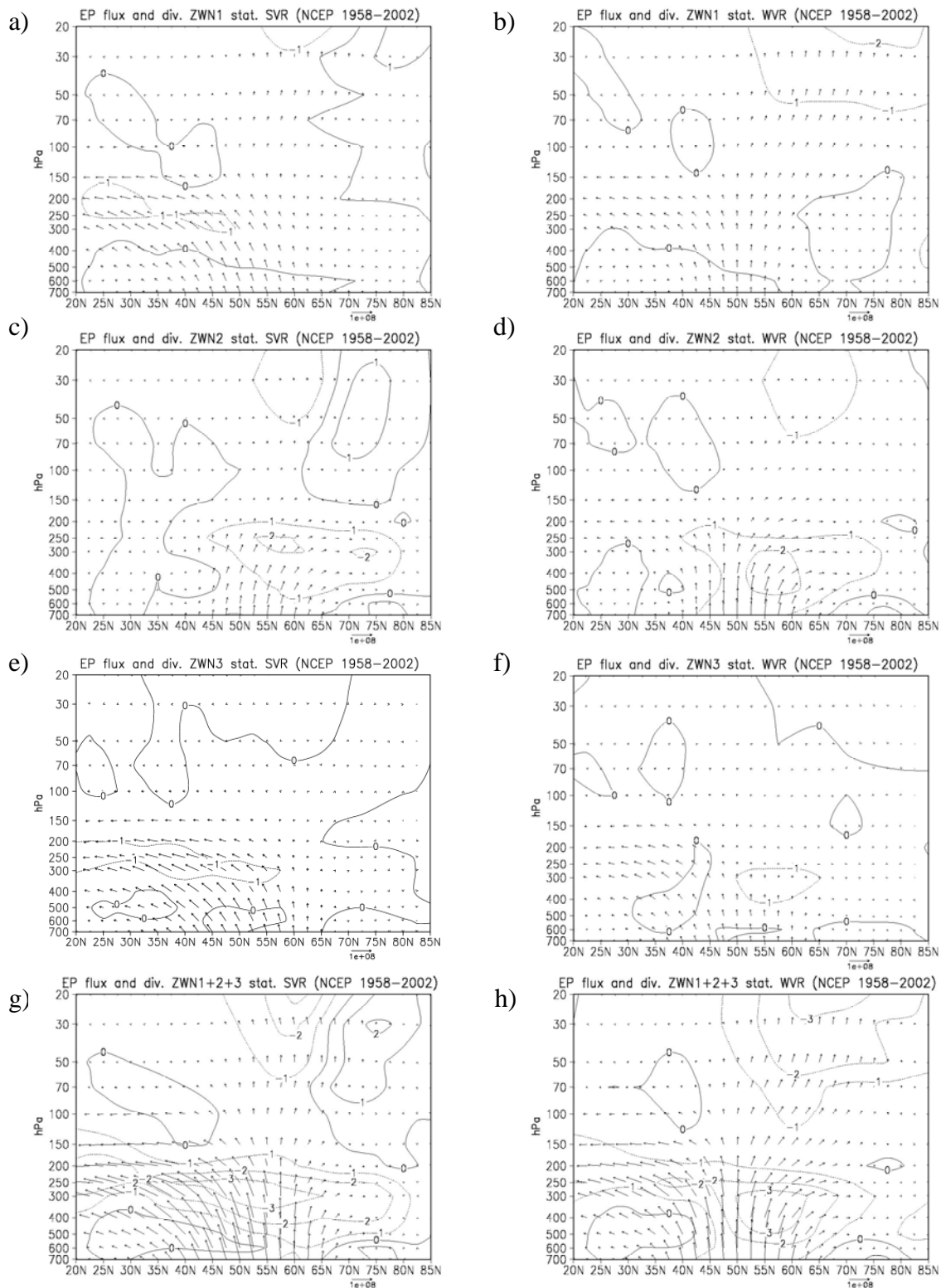
Figure 2.9. Cross section of E-P flux and divergence for stationary planetary waves in SVR (left column) and WVR (right column) for ZWN1 wave (first row), ZWN2 wave (second row), ZWN3 wave (third row) and ZWN1to3 waves (bottom row). Divergence contour interval is $1ms^{-1}day^{-1}$, the unit of vector is $kg\ s^{-2}$.

a) EP flux and div. ZWN1 stat. WVR−DJF (NCEP 1958−2002)

b) EP flux and div. ZWN1 stat. WVR−SVR (NCEP 1958−2002)

c) EP flux and div. ZWN2 stat. WVR−DJF (NCEP 1958−2002)

d) EP flux and div. ZWN2 stat. WVR−SVR (NCEP 1958−2002)

e) EP flux and div. ZWN3 stat. WVR−DJF (NCEP 1958−2002)

f) EP flux and div. ZWN3 stat. WVR−SVR (NCEP 1958−2002)

g) EP flux and div. ZWN1+2+3 stat. WVR−DJF (NCEP 1958−2002)

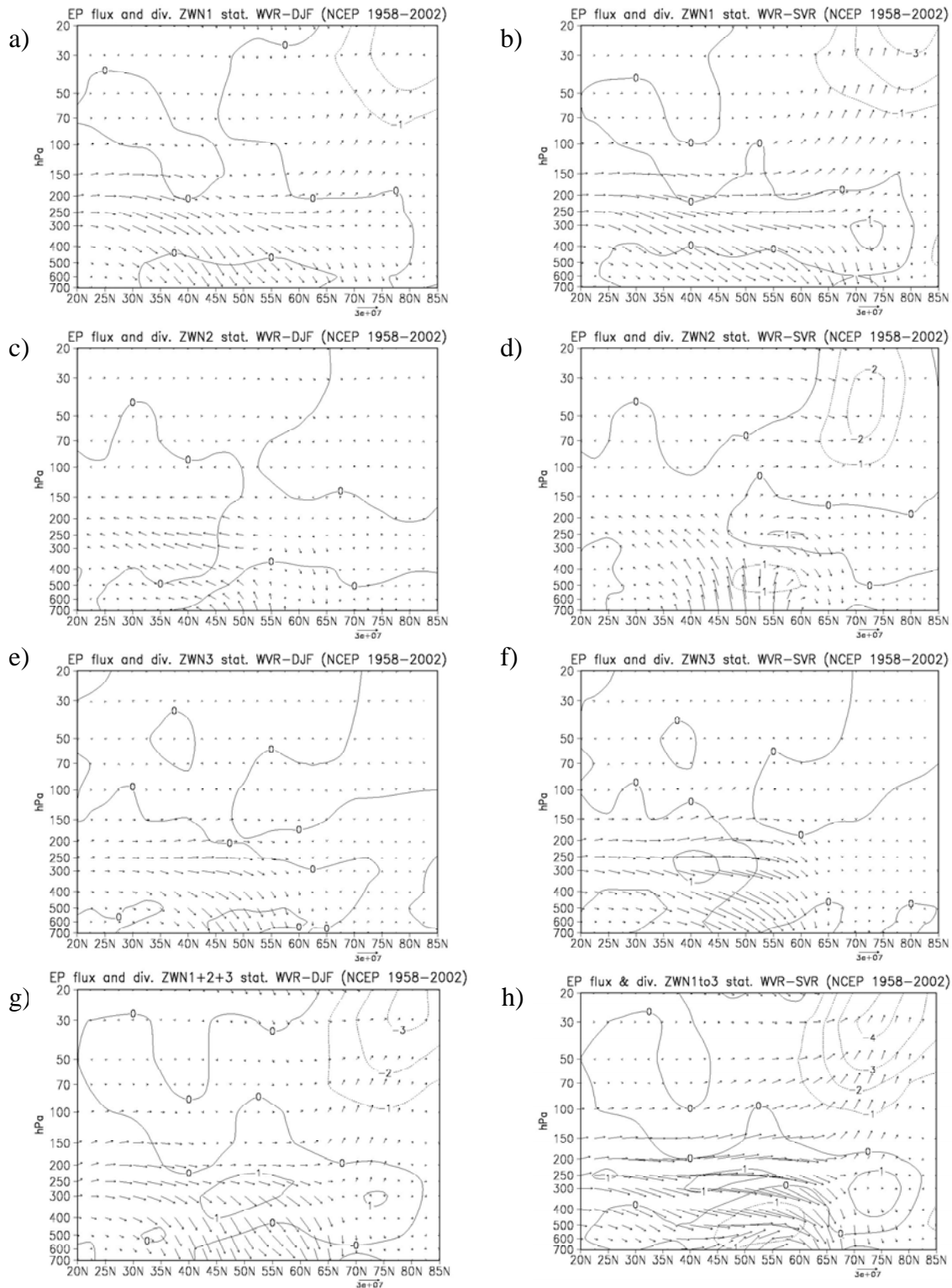h) EP flux & div. ZWN1to3 stat. WVR−SVR (NCEP 1958−2002)

Figure 2.10. Cross section of difference of E-P flux and divergence for stationary planetary waves between WVR and DJF (left column) and between SVR and DJF (right column) for ZWN1 wave (first row), ZWN2 wave (second row), ZWN3 wave (third row), ZWN1to3 waves (bottom row). Divergence contour interval is $1 \text{ms}^{-1}\text{day}^{-1}$, the unit of vector is kg s^{-2}.

However, the amplitudes of the differences $f(n_k^2<0)$ between SVR and WVR (not shown) in the lower stratosphere at high latitudes are much smaller than those at middle latitudes. This implies that the enhanced vertical shear of ZMZW in the lower stratosphere at high latitudes probably does not play such an important role for planetary wave propagation. This point has also been indicated by Chen and Robinson (1992) who concluded that the wave propagation is sensitive to the wind shear at the subtropical tropopause, but not so in the stratosphere.

2.5 Correlations between $f(n_k^2<0)$ and E-P flux

In order to improve our understanding of the atmospheric control on propagation of stationary planetary waves from the troposphere to the stratosphere and wave activities, the correlation between the vertical component of E-P flux (F_z hereafter) and $f(n_k^2<0)$ at 70hPa, $35^o – 80^oN$ is analyzed in Figure 2.11 and 2.12.

Fig.2.11 shows the scatters of F_z and $f(n_k^2<0)$ in DJF for ZWN1 (Fig.10a), ZWN2 (Fig.2.11b) and ZWN3 (Fig.2.11c) waves, respectively. In Fig.10a, the distribution shows that there is an assembly of scatters with high value (up to 100000 kg s^{-2}) of F_z and small value (less than 50%) of $f(n_1^2<0)$, which presents that the connection of strong vertical E-P flux entering the stratosphere and high chances of wave propagation at 70hPa, $35^o – 80^oN$ for ZWN1 wave. For ZWN2 wave (Fig.2.11b), this assembly has a similar shape as for ZWN1, but the values of F_z is smaller (up to 60000 kg s^{-2}), which indicates that although the ZWN2 wave still has big chance to propagate from the troposphere to the stratosphere, the actual wave activities are not as strong as ZWN1 wave. For ZWN3 wave (Fig.2.11c), the assembly at low values of $f(n_3^2<0)$ almost disappeared, and most scatters locate at $f(n_3^2<0) > 50\%$ having values of $F_z \sim 0$, which means for ZWN3 wave, there is rare wave activity and small chance for planetary wave to propagate from the troposphere to the stratosphere. In order to clarify the difference between ZWN1, 2 and 3 waves, the average of F_z with fixed values of $f(n_k^2<0)$ was analyzed (Fig.2.11d). The average of all F_z at each value of $f(n_k^2<0)$ was computed and 3-point running mean was performed afterwards. Figure 10.d shows that, for ZWN1 and 2 waves, when $f(n_k^2<0) < 50\%$, the values of F_z decrease with increased values of $f(n_k^2<0)$. The values of F_z for ZWN1 wave are relatively bigger than ZWN2 wave at specific value of $f(n_k^2<0)$. However, when $f(n_k^2<0) > 50\%$, F_z are negligible for both ZWN1 and 2 waves. For ZWN3 wave, the values of F_z are mostly around 0 and only small values are observed when $f(n_k^2<0) < 30\%$.

The same analysis was also performed for SVR and WVR (Fig.2.12). It can be observed that the scatters distribute more frequently around the area with high values of F_z and
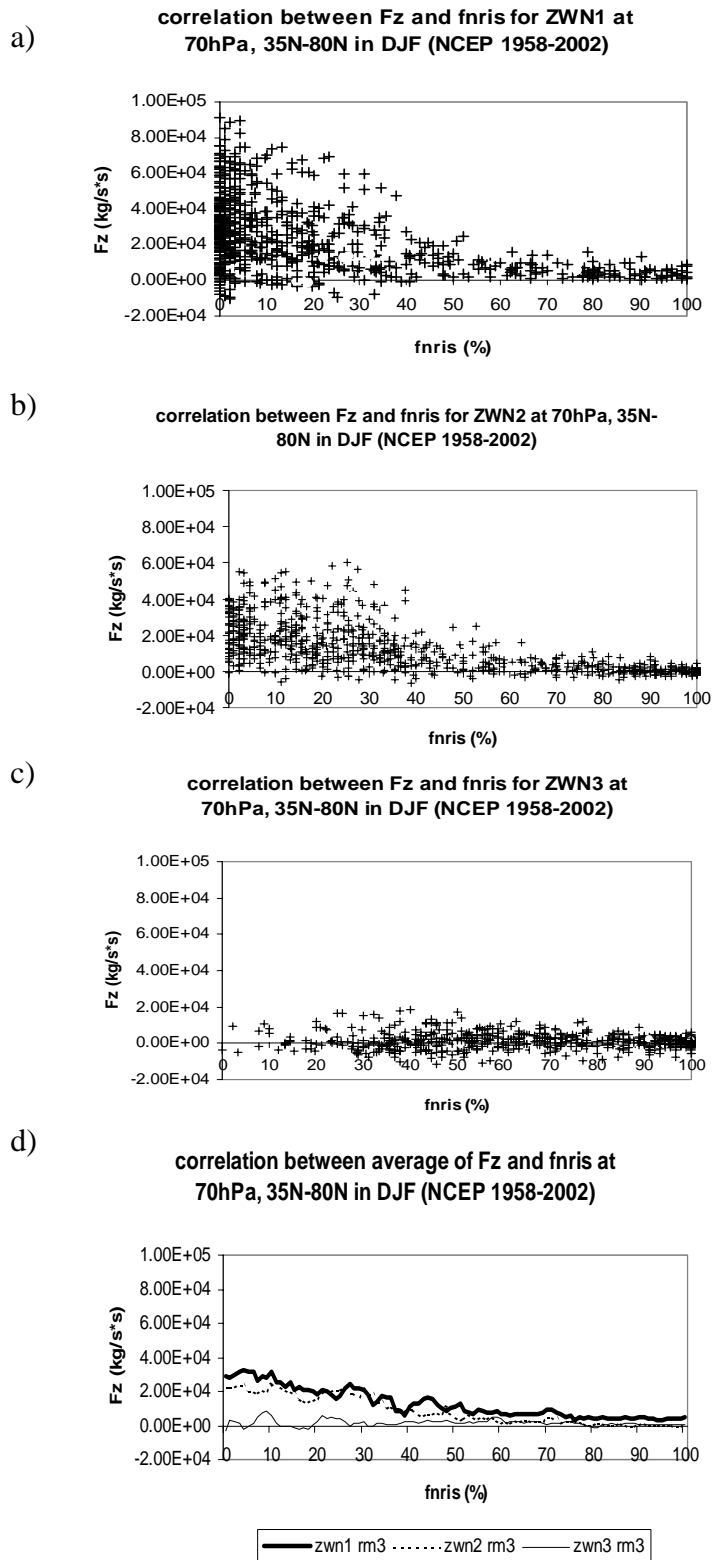
a)

correlation between Fz and fnris for ZWN1 at 70hPa, 35N-80N in DJF (NCEP 1958-2002)

b)

correlation between Fz and fnris for ZWN2 at 70hPa, 35N-80N in DJF (NCEP 1958-2002)

c)

correlation between Fz and fnris for ZWN3 at 70hPa, 35N-80N in DJF (NCEP 1958-2002)

d)

correlation between average of Fz and fnris at 70hPa, 35N-80N in DJF (NCEP 1958-2002)

Figure 2.11. Correlation between vertical component of E-P flux and f ($n_k^2 < 0$) at 70hPa, $35^o – 80^oN$ for stationary planetary waves in DJF (NCEP/NCAR RA 1958 to 2002) for ZWN 1 wave (first row), ZWN 2 wave (second row), ZWN 3 wave (third row), and the average of F_z with f ($n_k^2 < 0$) for ZWN1, 2 and 3 (bottom row).
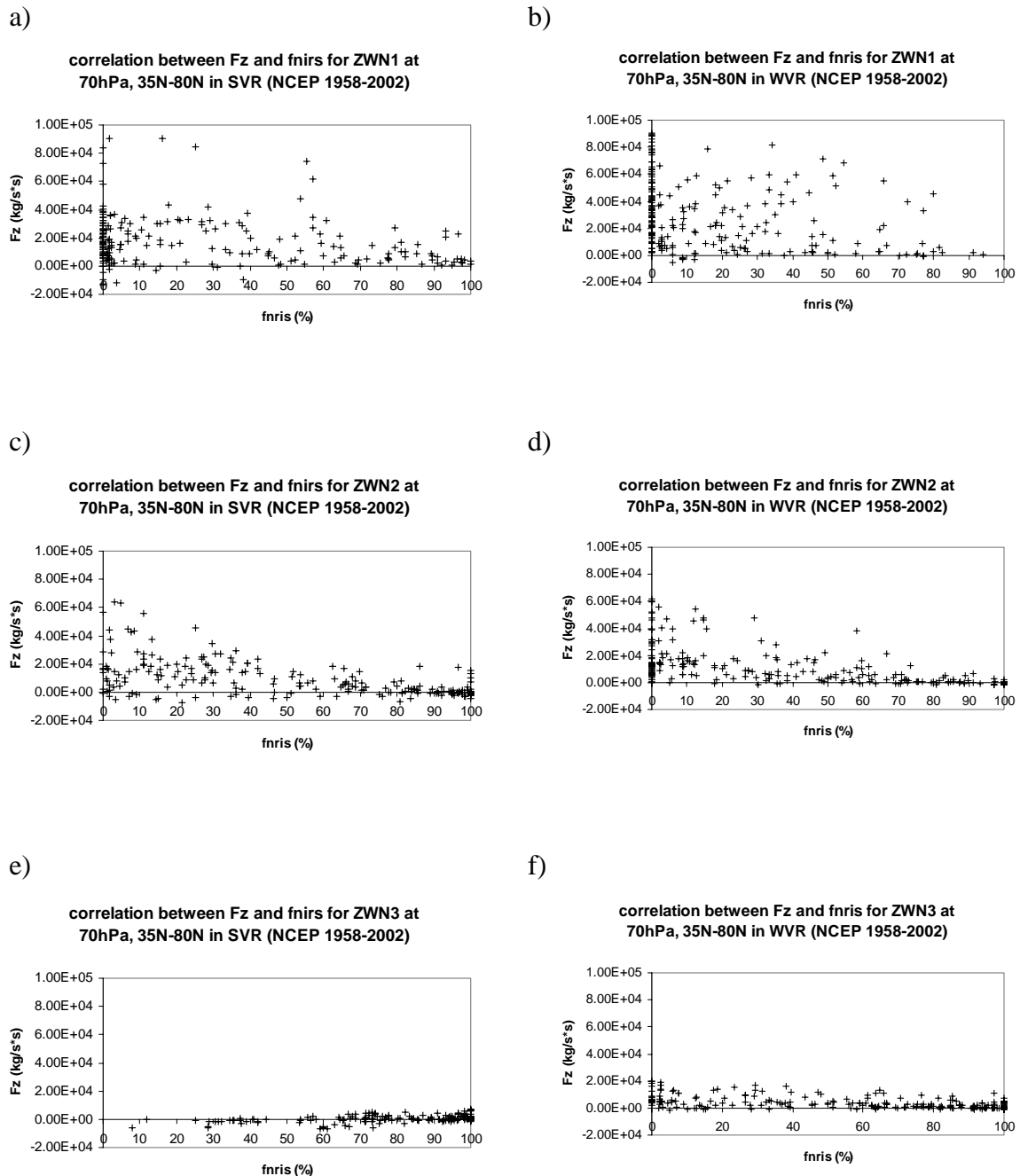
a)

**correlation between Fz and fnirs for ZWN1 at
70hPa, 35N-80N in SVR (NCEP 1958-2002)**

b)

**correlation between Fz and fnris for ZWN1 at
70hPa, 35N-80N in WVR (NCEP 1958-2002)**

c)

**correlation between Fz and fnirs for ZWN2 at
70hPa, 35N-80N in SVR (NCEP 1958-2002)**

d)

**correlation between Fz and fnris for ZWN2 at
70hPa, 35N-80N in WVR (NCEP 1958-2002)**

e)

**correlation between Fz and fnirs for ZWN3 at
70hPa, 35N-80N in SVR (NCEP 1958-2002)**

f)

**correlation between Fz and fnris for ZWN3 at
70hPa, 35N-80N in WVR (NCEP 1958-2002)**

Figure 2.12. Correlation between vertical component of E-P flux and f ($n_k^2<0$) at 70hPa, $35^o – 80^o$N for stationary planetary waves in SVR (left column) and WVR (right column) (NCEP/NCAR RA 1958 to 2002) for ZWN 1 wave (first row), ZWN 2 wave (second row), ZWN 3 wave (third row), and the average of F_z with f ($n_k^2<0$) for ZWN1, 2 and 3 (bottom row).

.

small values of $f(n_1^2<0)$ in WVR (Fig.2.12b, d, f) than in SVR (Fig.2.12a, c, e) for all ZWN1, 2 and 3 waves. Therefore, it can be concluded that there is a high correlation between the strong wave activities and the better chance of wave propagation from the troposphere to the stratosphere in WVR. Based on this correlation analysis, the strong connection between wave activities indicated by extratropic upward E-P flux at 70hPa and probability of stationary planetary wave propagation represented by $f(n_k^2<0)$, is addressed.

2.6 Transient planetary waves in Northern Hemisphere winter

It is well known that not only stationary planetary waves but also the transient planetary waves play a key role in wave-mean flow interaction (Andrews et al., 1987). The dynamical properties and transports of transient waves have been studied by a lot of scholars (Matsuno, 1971; O'Neill and Youngblut, 1982; Straus and Shukla, 1987; Chen and Robinson, 1992; Limpasuvan and Hartmann, 2000; etc.). The influence on the time-mean flow, including the stationary waves, of transient waves has also been analyzed (Blackmon, 1976; Sasamori and Chen, 1982; Salby, Garcia, 1987; Walter, 2003).

Theoretically, planetary waves can be divided into stationary waves and transient waves. The climatological mean flow patterns tend to take a wavy form in the Northern Hemisphere winter. These patterns can be furthermore separated into zonal mean and deviations from zonal mean. The zonal deviations are known as "stationary waves" and can be further separated into zonal Fourier components, while the time-dependent departures from the climatological average are often known as "transient waves" (Andrews et al., 1987).

To be more precise, the stationary waves can be defined as the departures from the zonal mean, averaged over season. The seasonal averages of the eddy component were further averaged over the number of equivalent seasons to obtain the final seasonal mean stationary eddy field. Zonally averaged eddy variances and covariances are calculated directly from the final seasonal mean stationary eddy field (Straus and Shukla, 1988). On the other hand, the transient waves are computed by obtaining the seasonal time series of all relevant variables at all grid points, then removing the annual mean and, the annual and semi-annual harmonics. Furthermore, time-filtering of the time series with an appropriate filter is applied on the time series of the variables. Finally calculating the variances from both the filtered and unfiltered series for each season and averaging over equivalent seasons in each data set will be performed (Straus & Shukla, 1988). The 21-point filters introduced by Blackmon and Lau (1980) are applied to isolate the fluctuations with low frequency (10days< period <90days) and medium (2.5days< period <6days), which correspond to low frequency eddies and synoptic eddies, respectively (Appendix A.4).

Fig.2.13 shows the cross section of E-P flux and its divergence for transient waves in Northern Hemisphere winter (DJF). Fig.2.13a illustrates the distribution of E-P flux and its divergence for unfiltered transient waves (with all frequencies). Similar to the stationary waves (Fig.6e), there are also two major branches of vectors for transient waves – one equatorward in the subtropical upper troposphere, and one upward in the subpolar lower and mid- stratosphere. But only one major convergent area dominates for the transient waves (Fig.2.13a). Instead of the rather stronger convergence in the subpolar stratosphere which is observed for stationary waves (Fig.2.6e), there is a very weak convergent area located in the extratropical stratosphere for transient waves. The amplitudes of equatorward vectors of E-P flux for unfiltered transient waves are larger than those for stationary waves, while those of the upward vectors are rather smaller. Unlike the stationary waves that are excited mostly from the extratropical troposphere, the distribution of sources of the transient waves are generated, is fairly reaching from the subtropics to the subpolar latitudes. This implies that the transient waves can be exited at higher latitudes than stationary waves in the troposphere (Andrews et al., 1987). The stronger equatorward fluxes of transient waves can lead to more barotropic forcing on the westerlies in the subtropical troposphere. On the other hand, the weaker upward vectors of transient waves show their diminished ability to bring baroclinic forcing from the troposphere to the stratosphere in comparison to stationary waves. At the same time, the convergence of stationary waves E-P flux is located in the subpolar stratosphere, which shows an easterly zonal momentum forcing on the mean flow. This cannot be observed for transient wave propagation.

Therefore, it can be concluded that although transient waves are generated widely and strongly in troposphere, they have less impact on the stratospheric mean flow compared with stationary waves.

The low-pass filtered transient waves (Fig.2.13b) show similar propagating characteristics as unfiltered transient waves but with smaller amplitudes. As mentioned above, the low-pass filtered waves are those fluctuations with periods longer than 10 days but less than 90 days. On the other hand, magnitudes of E-P flux and divergence for band-pass filtered transient waves (Fig.2.13c) with period from 2.5 to 6 days are much smaller especially for the upward vectors in stratosphere. This means that the eddy forcing of transient waves mainly is due to the low frequency waves while the synoptic waves' contribution is negligible.

In order to enhance our understanding of dynamical interaction of transient waves with the anomalies of mean flow, the cross sections of E-P flux and its divergence of transient waves are also drawn in SVR and in WVR, respectively (Fig.2.14). Fig.2.14 shows the similarly wide source and the strong equatorward vectors of transient waves in the troposphere, which has been observed in DJF, in both SVR and WVR. In contrast from the stationary waves, stronger divergence of transient waves dominates in the polar stratosphere in WVR (Fig.2.14b). As indicated before, the transient wave activities also mainly relate to the low frequency waves in both SVR (Fig.2.14a) and WVR (Fig.2.14b). The differences of E-P flux and divergence for transient waves between WVR and SVR are shown in Fig.2.15. The stronger equatorward fluxes as shown for stationary waves in
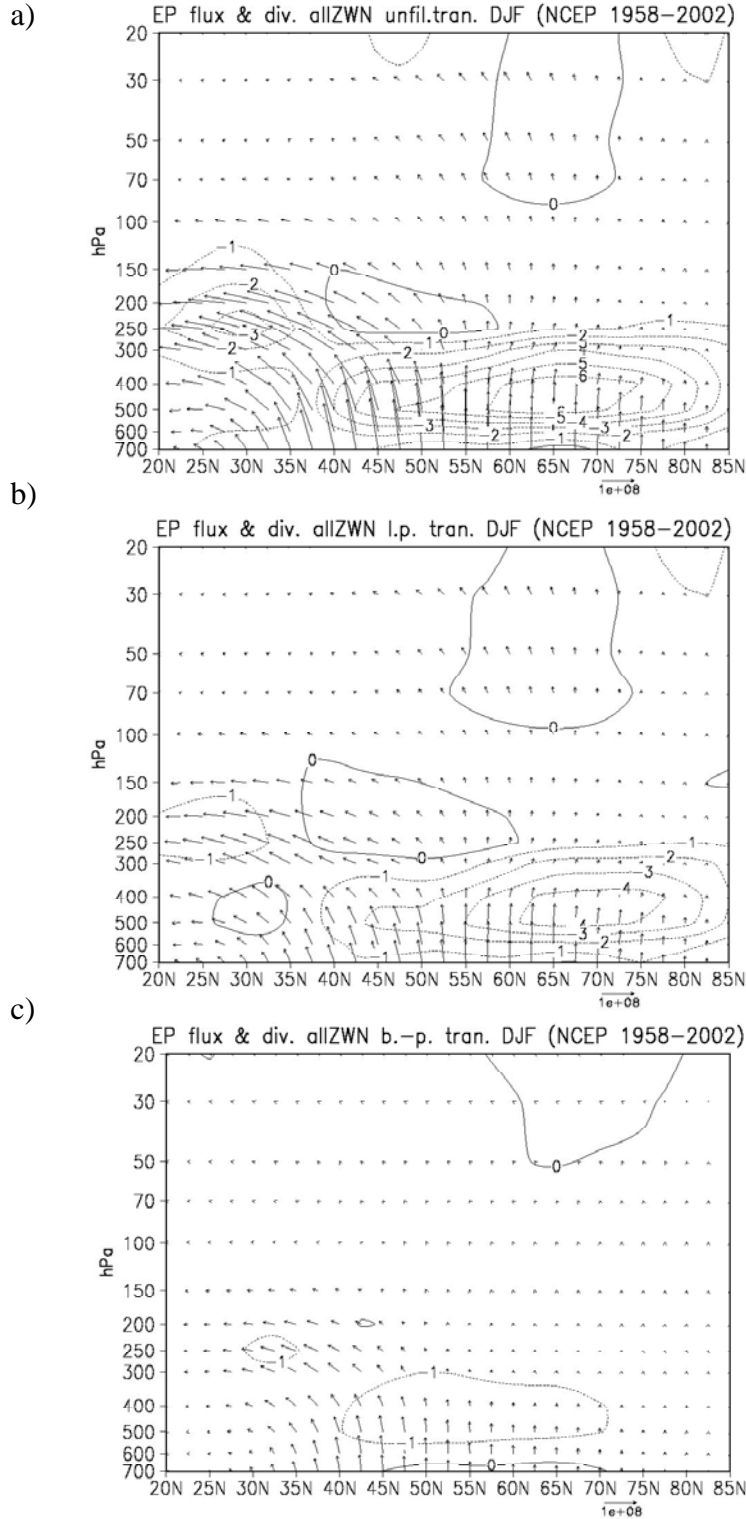
a)

b)

c)

Figure 2.13. Cross section of E-P flux and divergence for transient planetary waves in DJF (NCEP/NCAR RA 1958-2002); a) unfiltered transient waves; b) low-pass filtered transient waves; c) band-pass filtered transient waves. Divergence contour interval is $1 \text{ms}^{-1}\text{day}^{-1}$, the unit of vector is kg s^{-2}.
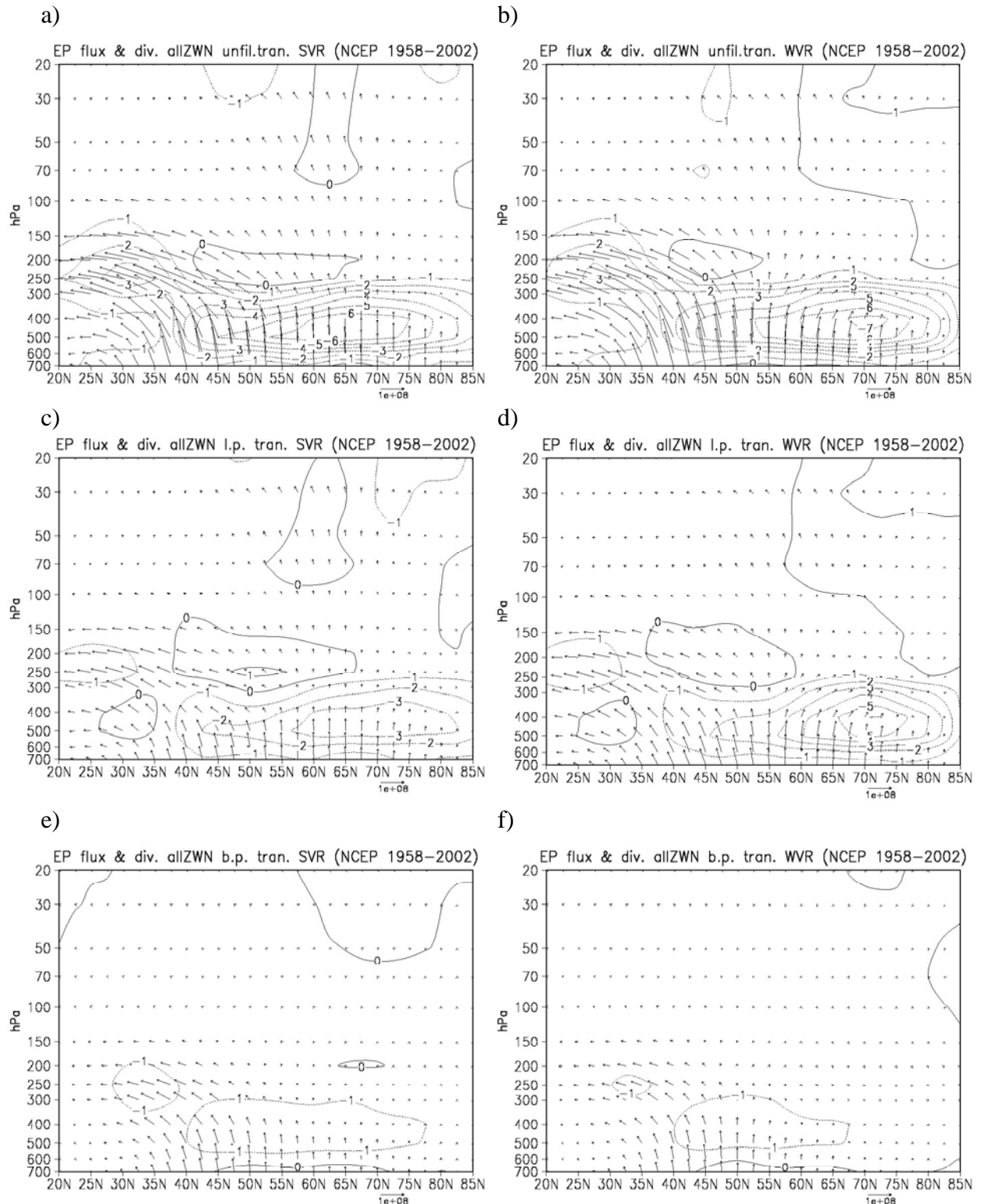
a)

EP flux & div. allZWN unfil.tran. SVR (NCEP 1958−2002)

b)

EP flux & div. allZWN unfil.tran. WVR (NCEP 1958−2002)

c)

EP flux & div. allZWN l.p. tran. SVR (NCEP 1958−2002)

d)

EP flux & div. allZWN l.p. tran. WVR (NCEP 1958−2002)

e)

EP flux & div. allZWN b.p. tran. SVR (NCEP 1958−2002)

f)

EP flux & div. allZWN b.p. tran. WVR (NCEP 1958−2002)

Figure 2.14. Cross section of E-P flux and divergence for transient planetary waves in SVR (left column) and WVR (right column) for unfiltered transient waves (first row), low-pass filtered transient waves (second row) and band-pass filtered transient waves (bottom row). Divergence contour interval is $1ms^{-1}day^{-1}$, the unit of vector is kg s^{-2}.

a)

EP allZWN unfil. tran. WVR-DJF (NCEP 1958-2002)

b)

EP allZWN unfil.tran. WVR-SVR (NCEP 1958-2002)

c)

EP allZWN l.p. tran. WVR-DJF (NCEP 1958-2002)

d)

EP allZWN l.p. tran. WVR-SVR (NCEP 1958-2002)

e)

EP allZWN b.p. tran. WVR-DJF (NCEP 1958-2002)
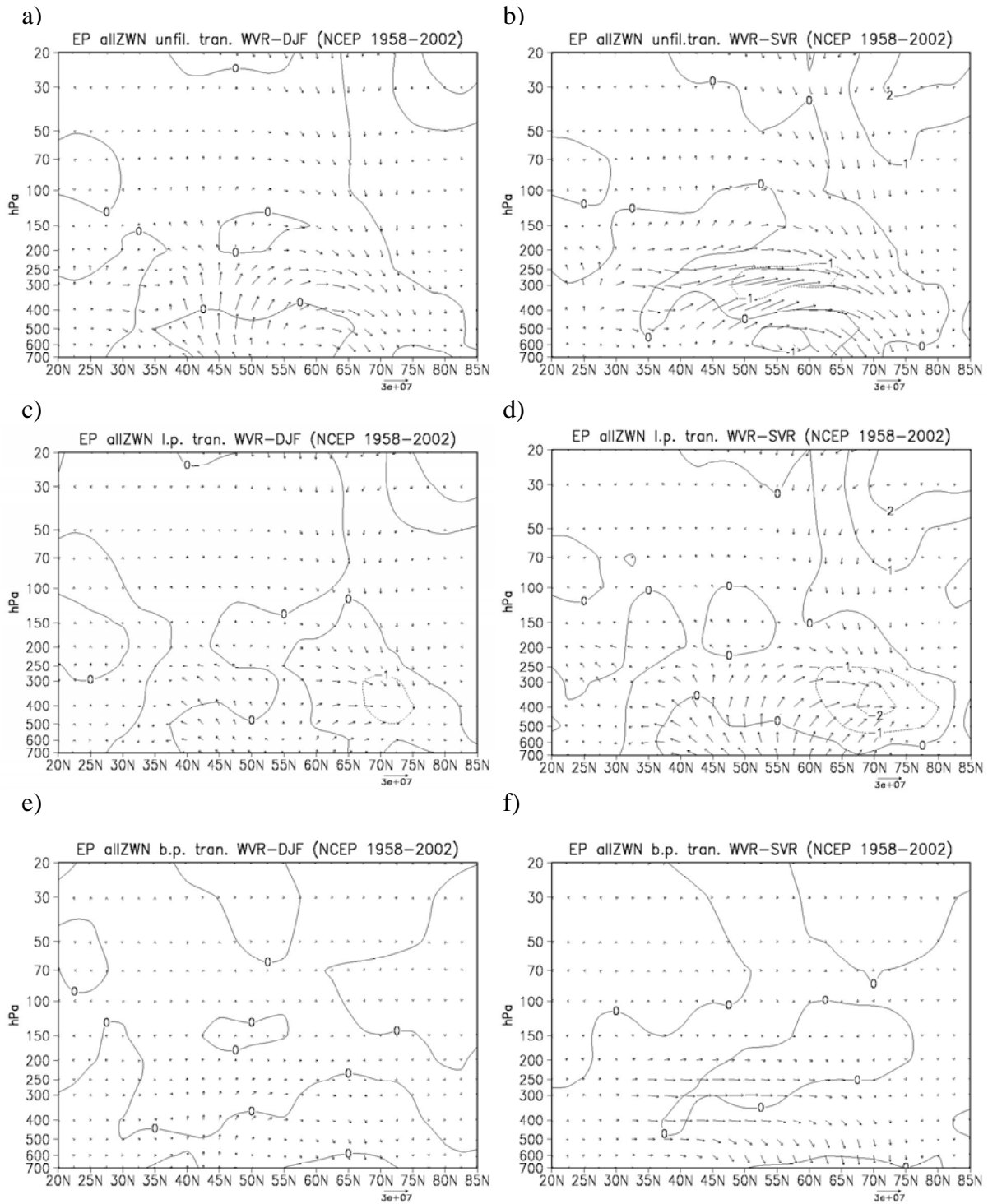
f)

EP allZWN b.p. tran. WVR-SVR (NCEP 1958-2002)

Figure 2.15. Cross section of difference of E-P flux and divergence for transient planetary waves between WVR and DJF (left column), WVR and SVR (right column) for unfiltered transient waves (first row), low-pass filtered transient waves (second row) and band-pass filtered transient waves (bottom row). Divergence contour interval is $1 ms^{-1} day^{-1}$, the unit of vector is $kg \, s^{-2}$.

SVR compared with in WVR (Fig.2.10) are also observed for unfiltered transient waves, low-pass transient waves and band-pass transient waves combined (Fig.2.15). This means that, in the troposphere transient waves also tend to reduce the westerlies in the subtropical troposphere in SVR. However, unlike for stationary waves, the transient waves have stronger upward vectors in the subpolar stratosphere in SVR, instead of weaker upward vectors in the subpolar stratosphere in WVR. This implies that transient waves also have influences on mean flow and anomalies in stratosphere but in different way compared with stationary waves.

2.6 Summary

The climatology of stationary planetary wave propagation in the Northern Hemisphere winter is analyzed based on the NCEP/NCAR reanalysis data 1958-2002. The so-called frequency of negative refractive index squared f ($n_k^2 < 0$) is introduced and applied to study the atmospheric state of planetary wave propagation from the troposphere to the stratosphere. This zonal wind-dependent refractive index shows the control of atmospheric zonal mean flow on planetary wave propagation. As it is observed, not only the zonal mean zonal wind but also the vertical shear of zonal wind affects the stationary planetary wave propagation. The zonal mean flow controls the propagation based on the ZWN-depended critical Rossby velocity theorem (Charney and Drazin, 1961). The vertial shear of zonal mean zonal wind above the subtropical tropopause also influences planetary wave propagation (Chen and Robinson, 1992; Hu and Tung, 2002). The effects of the atmospheric stability on wave propagation are also investigated by studying the influence of buoyancy frequency variations on f ($n_k^2 < 0$). It is found that the atmospheric stability can partly control the stationary planetary wave propagation, especially around the extratropical tropopause. On the other hand, the E-P flux and its divergence (Andrews et al., 1987) representing wave activities and eddy momentum forcing on the mean flow, is also analyzed. In Northern Hemisphere winter, the better chances of stationary planetary wave propagation from the troposphere to the stratosphere for ZWN1 and 2 waves, corresponds to the branch of upward E-P fluxes. In short, planetary waves are controlled by zonal mean zonal wind, vertical shear of zonal mean zonal wind and atmospheric stability. On the other hand, the planetary waves can also transfor wave activities and exert eddy momentum forcing on mean flow by two major branches of vectors and two major convergences.

The correlation between wave activity and probability of wave propagation is also analyzed at in this thesis. The strong connection between the stationary planetary wave activity and probability of propagation from the troposphere to the stratosphere is observed. Strong E-P fluxes to the NH stratosphere occur when and where the frequency of negative refractive index squared is smaller than 50%, for ZWN1 and 2. ZWN3 wave related E-P fluxes are not effective, even in the rare cases of low frequency of negative refractive indices squared.

The anomalies of mean flow in Northern Hemisphere winter can be isolated into two major regimes – strong polar vortex regime (SVR) and weak polar vortex regime (WVR) considering time series of the zonal mean zonal wind at 50hPa and 65°N ($\overline{u}_{50}(65^o N)$ as a diagnostic. It is found that the SVR will last longer than WVR and none of them has been observed occurring simultaneously in a single winter yet. Variation of the polar vortex regimes can be related with the different propagation structures of planetary waves (Limpasuvan and Hartmann, 2000; Perlwitz and Graf, 2000a; Walter, 2003). The analysis of f (n_k^2<0) shows that the anomalies of atmospheric mean flow have influences on the stationary planetary wave propagation. In WVR, planetary waves have more possibilities to propagate from the troposphere to the stratosphere than in SVR. The possibility decreases with the increasing ZWNs. Planetary waves have better chances to propagation from the troposphere to the stratosphere in WVR. In SVR, the planetary waves lead to strong westerly forcing in the polar stratosphere while in WVR the easterly forcing prevails in both the polar and sub-polar stratosphere. For planetary wave activities, the equatorward eddy momentum fluxes in the upper troposphere around subtropics are much stronger in SVR, while the eddy heat fluxes from the troposphere upward to the stratosphere around the northern pole are much stronger in WVR.

Like stationary planetary waves, transient waves also play a key role in wave-mean flow interaction in Northern Hemisphere winter, but with some differences. The transient waves propagate less from the troposphere to the stratosphere, while induced more wave activities to the subpolar upper troposphere, compared to stationary waves propagation. Propagation of transient waves especially the upward propagation mainly relates to the low-frequency transients. The synoptic waves are negligible. Unlike the stationary waves, the transient waves transport more heat fluxes upward from the troposphere to the subpolar stratosphere in SVR.

The mean flow and its anomalies can control or influence the wave activities for both stationary and transient waves (Charney and Drazin, 1961). Waves, on the other hand, modify the mean flow by exerting eddy momentum forcing (Andrews et al., 1987). This two-way interaction is supported by the analysis in this chapter.

Finally, it should be addressed that the influences of the external influence (e.g. super volcanic eruption, variation of solar radiation, and greenhouse gases etc.) on climate system and surely, the atmospheric circulation and planetary wave generation and propagation, have drawn attention recently. These potential external influences will be investigated further by analyzing the external forcing in Chapter 3.

Chapter 3

Influences of anomalies of wind and temperature induced by violent volcanic eruptions on planetary wave propagation

3.1 Introduction

The climate system can be influenced by anthropogenic forcing such as increasing emission of greenhouse gas, aerosols, and CFC_s, which are considered to play a key role on reducing the density of ozone in the stratosphere. Moreover, natural external forcing such as solar variability and volcanic eruption has also impacts on the climate system.

It is well known that violent tropical volcanic eruptions can affect the climate system by injecting huge amounts of aerosols into the atmosphere spreading over the globe (Angell, 1993; Robock, 2001). The aerosols injected into the stratosphere by volcanic eruptions result in warming of the layer where the aerosol resides due to absorption of solar and terrestrial radiation by the volcanic aerosol (Lacis et al., 1992; Angell, 1993). The stratospheric warming will begin in 1 – 3 months after eruptions and last 1 – 2 years after the volcanic eruptions (Robock, 2001). Due to nonlinear response of atmospheric dynamics, warmer winters over the Northern Hemisphere continents following a large tropical eruption are observed, starting few months after the eruptions and lasting 1 to 3 years (Robock, 2001). Volcanic aerosols have the potential to change not only the radiative balance in the stratosphere inducing a dynamical feedback, but also the stratosphere chemistry. The most important chemical changes in the stratosphere are related to ozone, which has a significant effect on ultraviolet and longwave radiative fluxes. The chemical reactions, which produce or destroy ozone, depend on the longwave flux, the atmospheric temperature, and the aerosol surface available for heterogeneous reactions. And all these can be changed by volcanic eruptions (Crutzen, 1976; Tabazadeh and Turco, 1993; tie and Brasseur, 1995; Robock, 2001).

The lower stratospheric warming after violent tropical volcanic eruptions was also observed and studied by many other scholars. By applying the general circulation model ECHAM2 with stratospheric aerosol effects and run in a perpetual-January mode, Graf et al. (1993) investigated the typical volcanic aerosol induced tropical stratospheric heating of the El Chichon (1982) eruption or the 1991 Mt. Pinatubo eruption and simulated continent varying for the first time. Afterwards, Ramachandran et al. (2000) investigated the total stratospheric warming due to aerosols injected by the Pinatubo (1991) eruption using the SKYHI GCM (from Geophysical Fluid Dynamics Laboratory) and aerosol spectral optical properties dataset. Another study of stratospheric warming induced by Pinatubo (1991) eruption has been performed by applying the NASA Goddard Institute for Space Studies ModelE climate model (Oman et al., 2005). Ramaswamy et al. (2006)

applied a coupled atmosphere-ocean model to study the stratospheric temperature trend from 1979 to 2003 and tried to demonstrate that the complex space-time pattern of the lower stratospheric temperature anomalies is a consequence of the combined temporal changes in natural forcing (solar irradiance and volcanic aerosols) and anthropogenic forcing (well-mixed greenhouse gases, stratospheric and tropospheric ozone, troposheric aerosols, and land use). The obvious stratospheric warmings, which were caused by the eruptions of El Chichon (1982) and Pinatubo (1991), were observed for both, observation and model experiments (Ramaswamy et al., 2006). Using a longer time dataset (1958 – 1999), Cordero and Forster (2006) found not only the stratospheric warming induced by El Chichon (1982) eruption and Pinatubo (1991) eruption, they also found another case, Agung, which erupted in 1963.

However, following the violent tropical volcanic eruptions, especially during the Northern Hemisphere (NH) winter, not only the stratospheric warming in the tropics and low latitudes, but also a major stratospheric cooling around the northern polar area has been observed. For the single case of the Pinatubo 1991 eruption, stratospheric cooling at the NH pole during the following NH winter (1991-1992) was observed (Kodera and Yamazaki, 1994). Stechikov et al. (2004) and Oman et al. (2005) found that the polar stratospheric cooling happened during the next 2 winters after the eruption (Stechikov et al., 2004). Moreover, the stratospheric cooling induced by a number of volcanic eruptions from 1958 to 2000 has also been shown by Stechikov et al. (2006).

Combining the lower stratospheric warming at tropics and extratropics, with the cooling of the lower stratosphere at high latitudes, an increased meridional temperature gradient can be induced. The enhanced pole-equator meridional temperature gradient in the lower stratosphere could have a dynamical response with a geostrophically driven strengthened stratospheric polar vortex and stronger zonal mean zonal wind (ZMZW) which can extend down into the troposphere (Graf et al. 1993; Graf et al. 1994; Kodera, 1994; Kodera and Yamazaki, 1994; Robock, 2001; etc.). As discussed in Chapter 2, the variations of the stratospheric polar vortex have influence on propagation and refraction of planetary waves and based on wave-mean flow interactions theorem, these propagated or refracted waves transport eddy momentum, heat fluxes and zonal momentum forcing on mean flow. Hence, the anomalies of wind and temperature induced by violent tropical volcanic eruptions will also affect on the planetary wave propagation and, these propagated or refracted waves will consequently modify the mean flow in both the stratosphere and troposphere. This dynamic feedback mechanism provides a very important contribution to the resulting climate change (Robock and Mao, 1992; Graf et al., 1993; Kirchner and Graf, 1995; Mao and Robock, 1998; etc.).

In this chapter, we will focus on the dynamical influence of violent tropical volcanic eruptions on the climate system. As indicated above, the coupling between the stratosphere and the troposphere by planetary wave–mean flow interaction is an important dynamical mechanism, which can help to improve our understanding of the potential impacts of volcanic eruptions on the anomalies of atmospheric circulation and therefore on the climate change. In short, we will investigate the influences of volcanic eruptions on planetary wave propagation.

3.2 Violent tropical volcanic eruptions of Agung (1963), El Chichon (1982) and Pinatubo (1991)

In the historical record, there were a number of volcanic eruptions, which have been observed and investigated. Most of these eruptions caused observable impacts on the climate system (Robock and Mao, 1992; Graf et al., 1994; Robock and Free, 1995; Robock, 2000). There are three violent tropical volcanic eruptions – Agung (1963), El Chichon (1982) and Pinatubo (1991) and, all these three eruptions showed very strong influences on climate system (Robock and Free, 1995; Robock, 2002).

As indicated before, the large stratospheric warming has been observed after the 3 major tropical volcanic eruptions of Agung (1963), El Chichon (1982) and Pinatubo (1991) (Angell, 1993, 1997; Robock, 2000; Ramaswamy et al., 2006; Cordero and Forster, 2006). With the tropical lower stratospheric warming simultaneously stratospheric cooling around the northern pole area during the NH winters after the eruptions was also observed. The simultaneous warming and cooling will enhance the northern pole-equator temperature gradient. At the same time, an increased polar night jet in the NH and stronger ZMZW extending down to the troposphere can also be observed (Graf et al., 1993).

There are several similarities between the three volcanic eruptions besides the eruption-induced stratospheric temperature anomalies, which can benefit the study of considering the three cases as violent tropical volcanic eruptions and further investigation of their influences on climate system. These similarities are summarized in Table 3.1. Firstly, all these three eruptions happened in the location of tropical area. Therefore the aerosols injected into the atmosphere can spread over the entire globe in relatively short period (Oman et al., 2005). Moreover, all these three eruptions ejected great amount of aerosols into the lower stratosphere in similar magnitudes shown from the values of dust veil index (DVI, Table 3.1). It is reasonable to treat these three eruptions as a group of violent volcanic eruptions.

Table 3.1 Volcanic eruptions considered in this study. DVI was taken from Robock and Mao (1992).

Volcano	Latitude	Longitude	Date of Eruption	DVI (dust veil index)
Agung	8^oS	116^oE	March 17, 1963	800
El Chichon	17^oN	93^oW	April 3, 1982	800
Pinatubo	15^oN	120^oE	June 15, 1991	1000

Therefore, in this chapter, we choose the eruptions of Agung (1963), El Chichon (1982) and Pinatubo (1991) as the representative cases to investigate the impacts of violent tropical volcanic eruptions on anomalies of atmospheric circulation and the planetary wave propagation.

3.3 Data processing

As in Chapter 2, in this chapter we also used the NCEP/NCAR reanalysis data for 45 years (1958-2002) (Kalnay et al., 1996; Kistler et al., 2001). The dataset contains daily averages of geopotential height, wind, and temperature on $2.5^{o} \times 2.5^{o}$ grid at 17 vertical pressure levels extending from 1000 to 10 hPa.

In this study, we are interested in the wind and temperature anomalies occurring in winters following volcanic eruptions, only the two NH boreal winters (DJF) after the eruptions are analyzed. The winters of 1963-1964 and 1964-1965 are selected to for the Agung (1963) eruption; the winters of 1982-1983 and 1983-1984 for El Chichon (1982) eruption; and the winters of 1991-1992 and 1992-1993 for Pinatubo (1991) eruption. We name all these 6 winters as volcanic winters

In order to separate the signals of volcanic eruptions from the general NH boreal winter, we took other 38 winters without the six volcanically affected winters (1963-1964, 1964-1965; 1982-1983, 1983-1984; 1991-1992, 1992-1993), to represent the general Northern Hemisphere winters.

3.4 Influences of volcanic eruptions on atmospheric circulation and on planetary wave propagation

3.4.1 Northern Hemispheric winter wind and temperature anomalies after volcanic eruptions

Fig.3.1 shows the climatological mean of zonal mean zonal wind (ZMZW), wind shear, and temperature and buoyancy frequency in 38 NH winters not disturbed by the three volcanic eruptions. As discussed in Chapter 2, the main patterns of ZMZW show the stratospheric polar vortex and the extratropical jet (Fig.3.1a). The center of negative values of vertical shear of ZMZW, which has been shown in Chapter 2 (Fig.2.3b), is also observed for the general winters excluding the volcanic winters (Fig.3.1b).

Fig.3.2 shows the average of ZMZW, vertical shear of ZMZW, temperature and buoyancy frequency for the influenced winters after the three volcanic eruptions. The Figures of each single winter for each volcanic case are shown in the Appendix B. For the ZMZW, compared to the general winters (Fig.3.1a), a stronger stratospheric polar vortex can be observed in the volcanic winters (Fig.3.2a). Relatively bigger values of vertical shear in the polar and subpolar stratosphere can also be found in the volcanic winters (Fig.3.2b) compared with the general winters (Fig.3.1b). As indicated in Chapter 2, the vertical shear of ZMZW can probably contribute to the more chance for planetary wave propagation in lower stratosphere at high latitudes in the strong polar vortex regime (SVR). However, it is found that the influences of vertical shear of ZMZW on planetary wave propagation in the polar and subpolar lower stratosphere is not significant
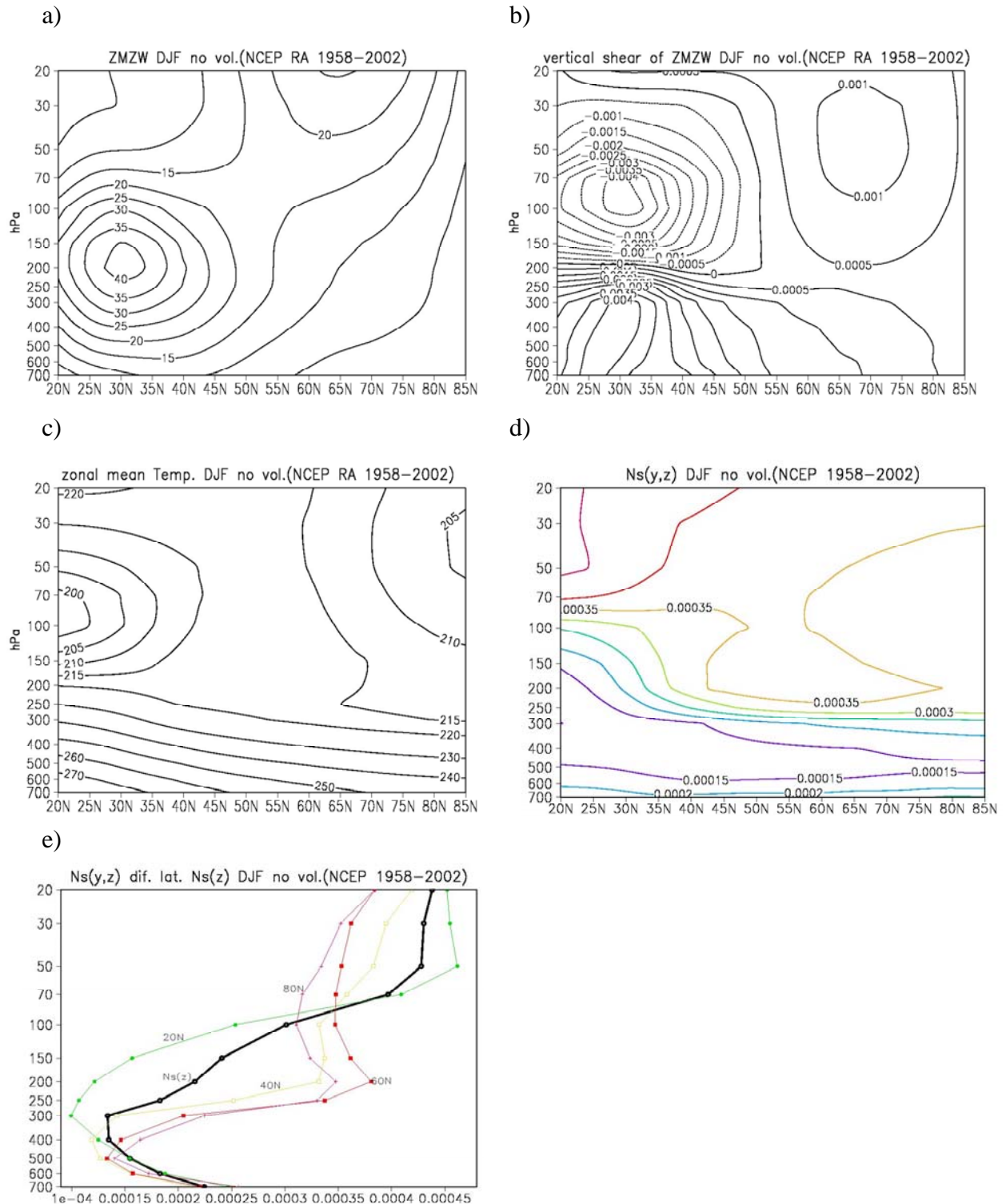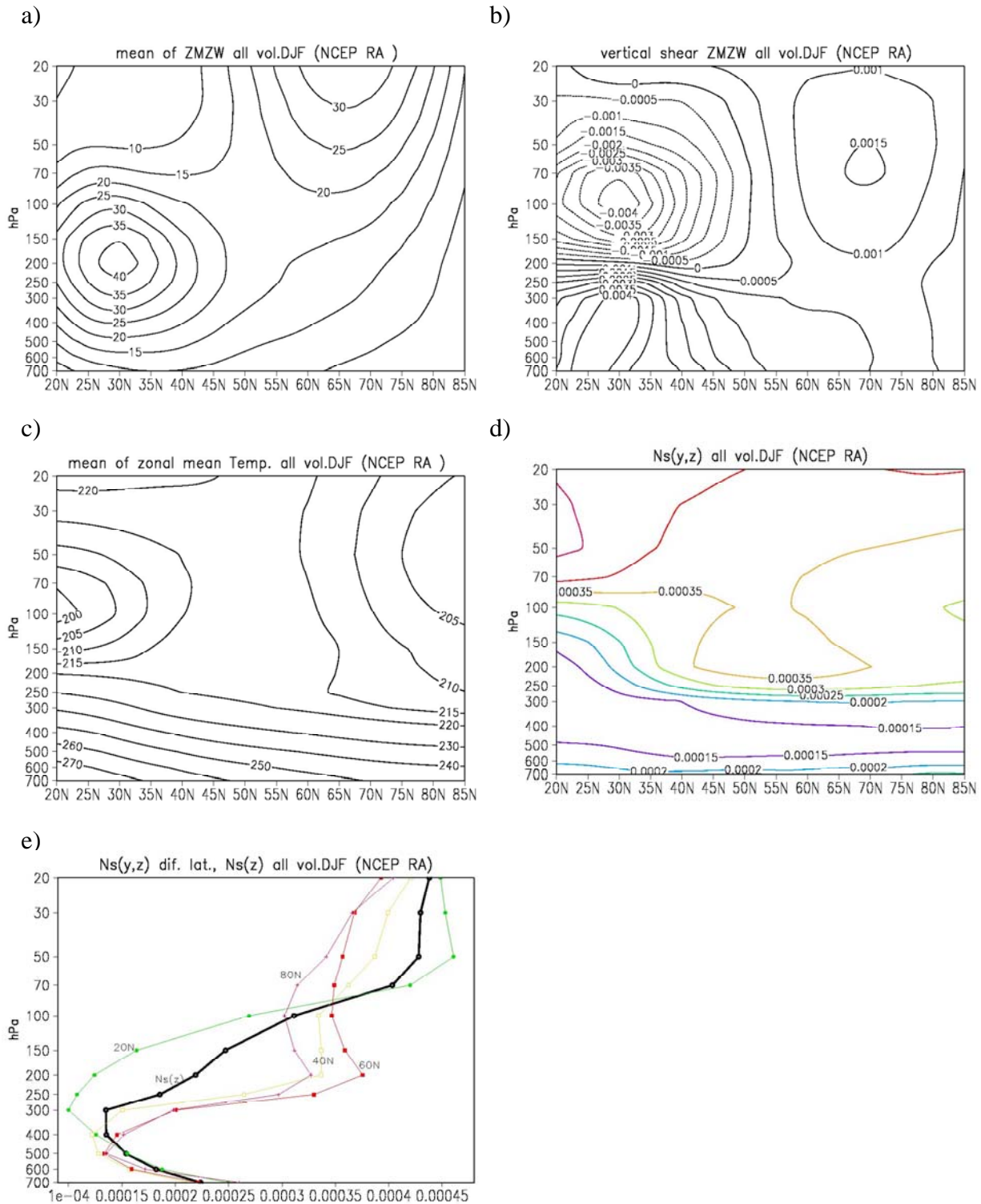
a)

b)

c)

d)

e)

Figure 3.1. Zonal mean zonal wind (m/s) (a), vertical wind shear (s^{-1}) (b), zonal mean temperature (K) (c), $N^2(\phi, z)$ on meridional plane (d), and $N^2(z)$ profile (black line) and $N^2(\phi, z)$ profiles on different latitudes (e) in DJF excluding volcanic winters (NCEP/NCAR RA, 1958-2002). Unit of N^2 is s^{-2}.

a)

b)

c)

d)

e)

Figure 3.2. Zonal mean zonal wind (m/s) (a), vertical wind shear (s^{-1}) (b), zonal mean temperature (K) (c), $N^2(\phi, z)$ on meridional plane (d), and $N^2(z)$ profile (black line) and $N^2(\phi, z)$ profiles on different latitudes (e) in mean of DJF of volcanic winters (NCEP/NCAR RA, 1958-2002). Unit of N^2 is s^{-2}.

compared to the influences at middle latitudes. At the same time, it is found that the stratosphere over the NH pole is colder in volcanic winters (Fig.3.2c) than in general winters (Fig.3.1c). The major patterns of buoyancy frequency (Fig.3.2d) and its distribution with latitudes (Fig.3.2e) for volcanic winters are similar to the general winters (Fig.3.1d and Fig.3.1e).

In order to clearly investigate the influences of violent tropical volcanic eruptions on the NH atmosphere, the differences of ZMZW, vertical shear of ZMZW, temperature and buoyancy frequency between the volcanic winters and the general winters are also analyzed (Fig.3.3). The figures of the differences between each single volcanic winter and general winters are also reproduced in the Appendix B.

In Fig.3.3a, the stronger polar vortex during the winters after volcanic eruptions, which extends into the troposphere as indicated by other scholars (Graf et al., 1993; Graf et al., 1994; Kodera, 1994; etc.), can be observed. Not only a stronger polar vortex, but also relatively weak westerlies can be observed in the tropical and extratropical troposphere (Fig.3.3a). This indicates that the tropical jet is reduced during the winters after volcanic eruptions. Furthermore, it is found that the distribution of the strengthened and extended polar vortex and the weakened tropical jet can compose a "dipole" structure on the meridional plane for wind anomalies. This "dipole" structure has also been indicated in previous studies (Kodera, 1994).

In Fig.3.3b, the differences of vertical shear of ZMZW between the winters after the volcanic eruptions and the general winters show that a stronger wind shear can be found in the lower stratosphere (250hPa to 50hPa) at mid and high latitudes (60°N – 80°N) in the winters after volcanic eruptions, which can help planetary waves propagating from the troposphere to stratosphere.

The differences of zonal mean temperature between volcanic winters and general winters are also analyzed (Fig.3.3c). As ZMZW, clear differences of temperature can also be observed. There are two major centers occur in the lower stratosphere. One is a stronger cooling, which locates in the polar lower stratosphere. The other is a relatively weaker warming, which locates in the tropical and extratropical lower stratosphere. The amplitudes of the tropical and extratropical stratospheric warming are smaller than the polar stratospheric cooling. These two centers can also compose a "dipole" structure on the meridional plane of zonal mean temperature. In this study, we will focus on the distribution of the anomalies on the meridional plane since by the dynamics mechanisms, the induced increased meridional temperature gradient can cause the strengthened stratospheric polar vortex extending down into the troposphere (Graf et al., 1993; Graf et al., 1994; Kodera, 1994; Kodera and Yamazaki, 1994; Robock, 2001; etc.). The dynamical response can be reflected by the properties of planetary wave propagation and refraction between the stratosphere and troposphere as analyzed in Chapter 2. On the other hand, the strong cooling in the polar lower stratosphere can reduce the atmospheric stability in the northern pole. The local convection in NH pole is expected to be reduced during the volcanic winters.
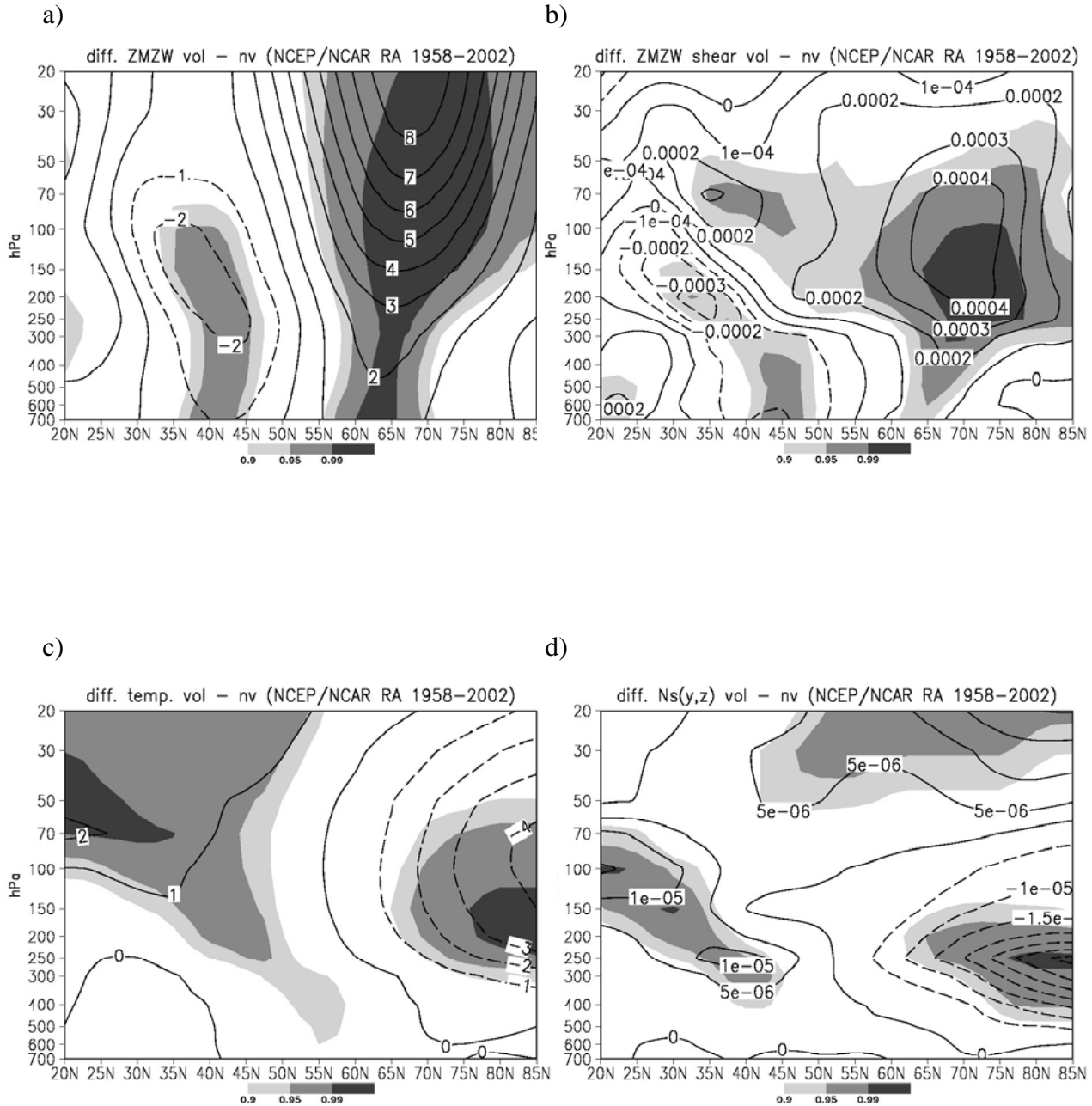
a)

b)

c)

d)

Figure 3.3. The difference of zonal mean zonal wind (m/s) (a), vertical wind shear (s^{-1}) (b), zonal mean temperature (K) (c), $N^2(\phi, z)$ on meridional plane (d), and $N^2(z)$ profile (black line) and $N^2(\phi, z)$ profiles on different latitudes (e) in between the mean of DJF of volcanic winters and the DJFs excluding volcanic winters (NCEP/NCAR RA, 1958-2002). Unit of N^2 is s^{-2}. Area with significant level above 90% is lightly shaded, above 95% is medium shaded and above 99% is heavily shaded.

The differences of buoyancy frequency between volcanic winters and general winters are shown in Fig.3.3d. The reduced atmospheric stability in the northern pole, which mentioned above can be found. Furthermore, there are two other major differences with positive values, which represent the enhanced atmospheric stability, are located in the polar stratosphere (above 50hPa) and around the tropical tropopause (~ 100hPa). The obvious negative values of differences of buoyancy frequency between volcanic winters and general winter around polar tropopause can also be found (Fig.3.3d).

As discussed in Chapter 2, a stronger stratospheric polar vortex occurs in the strong polar vortex regime (SVR) too. Similar analysis as for SVR is also performed in volcanic winters. All SVR regimes have been listed in Table 2.1. In order to illustrate the difference between volcanic winters and SVR, in this chapter, the volcanic winters have been removed from the SVR regimes. Therefore, there are only 8 strong polar vortex regimes left. A similar analysis as in Fig.3.1 (general winters) and Fig.3.2 (volcanic winters) are also done for SVR (Fig.3.4). Fig.3.4a shows clearly the much stronger stratospheric polar vortex and the relatively weaker tropical jet. The latter cannot be found obviously weaker in volcanic winters (Fig.3.2a) compared with general winter (Fig.3.1a). Similarly, relatively bigger values of vertical shear of ZMZW can also be found in SVR (Fig.3.2b) compared with general winters (Fig.3.1b). The stratospheric cooling, which has also been observed in volcanic winters (Fig.3.2c, central contour with 205K), can also be shown in SVR even cooler (Fig.3.4c, central contour with 200K). However, the buoyancy frequency on meridional plane (Fig.3.4d) and distribution with latitudes (Fig.3.4e) do not show much difference in SVR compared with general winter (Fig.3.1d, e).

The differences of ZMZW, vertical shear of ZMZW, temperature and buoyancy frequency between SVR and general winters, as between volcanic winters and general winters (Fig.3.3), are also shown in Fig.3.5. The "dipole" structure of anomalies of ZMZW, composed by a center with the positive values located in the polar stratosphere and the other with negative values located in the extratropical troposphere, can also be found (Fig.3.5a). However, the amplitudes of the "dipole" structure in SVR (Fig.3.3a) are much bigger than in volcanic winters (Fig.3.5a). The biggest values of vertical shear of ZMZW can be found in SVR (Fig.3.5b) with bigger amplitudes than those for volcanic winters (Fig.3.3b). The "dipole" structure of zonal mean temperature in SVR is also shown in Fig.3.5c. Similar as the wind, the magnitudes of the polar stratospheric cooling are also stronger in SVR than in volcanic winters (Fig.3.3c). However, the tropical and extratropical stratospheric warming is of the same amplitudes. Fig.3.5d shows that the great negative values of differences of buoyancy frequency around the polar tropopause between SVR and general winter, which represent the greatly reduced atmospheric stability around this area in SVR. Similar pattern has also been found in the for volcanic winters with relatively smaller amplitudes (Fig.3.3d).

In short, the anomalies of wind and temperature are similar in SVR and in volcanic winters. The "dipole" structures of ZMZW and zonal mean temperature can be observed for both SVR and volcanic winters, but the amplitudes of the anomalies in volcanic winters are smaller than in SVR.
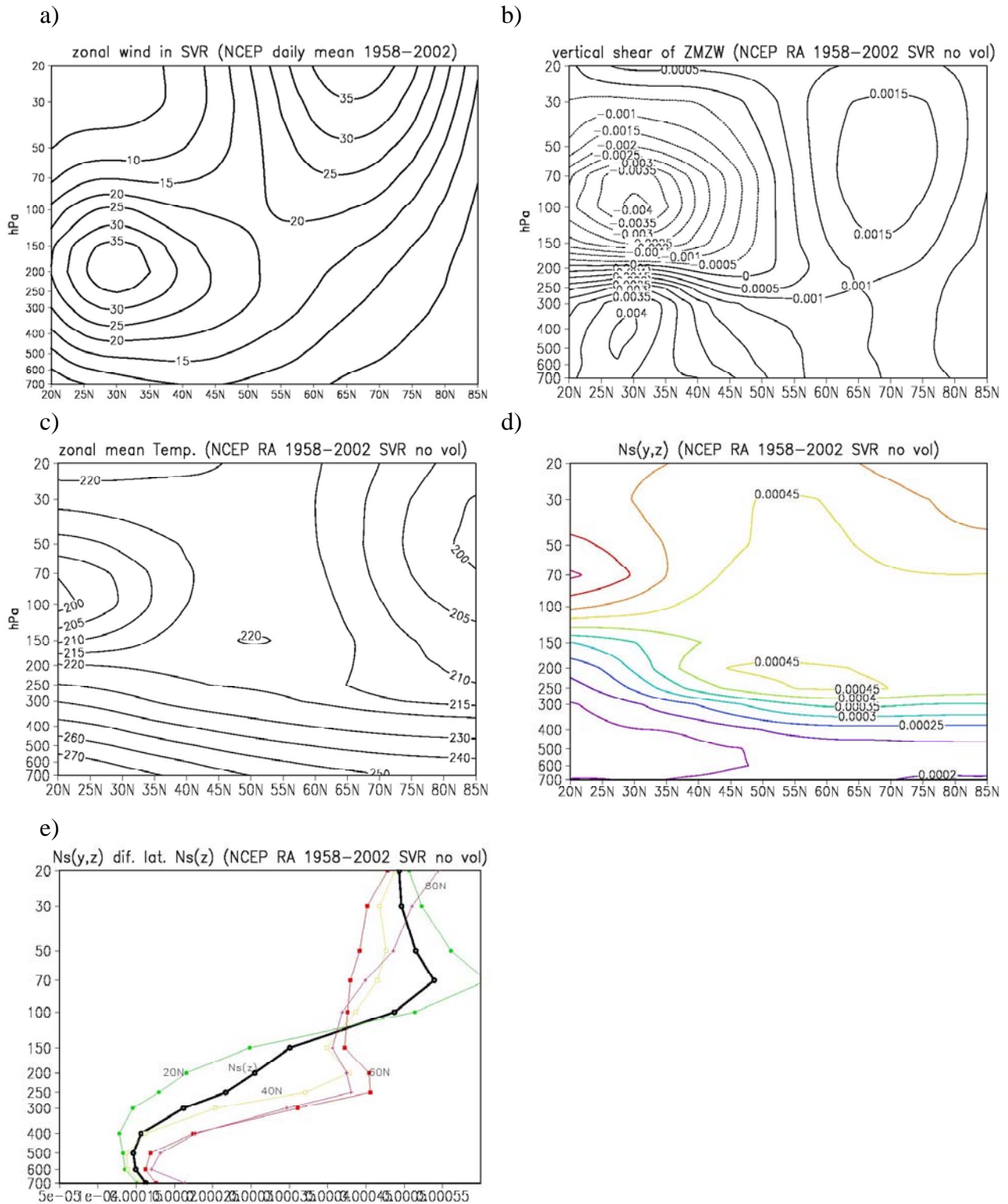
a)

b)

c)

d)

e)

Figure 3.4. Zonal mean zonal wind (m/s) (a), vertical wind shear (s^{-1}) (b), zonal mean temperature (K) (c), $N^2(\phi,z)$ on meridional plane (d), and $N^2(z)$ profile (black line) and $N^2(\phi,z)$ profiles on different latitudes (e) in SVR excluding volcanic winters (NCEP/NCAR RA, 1958-2002). Unit of N^2 is s^{-2}.
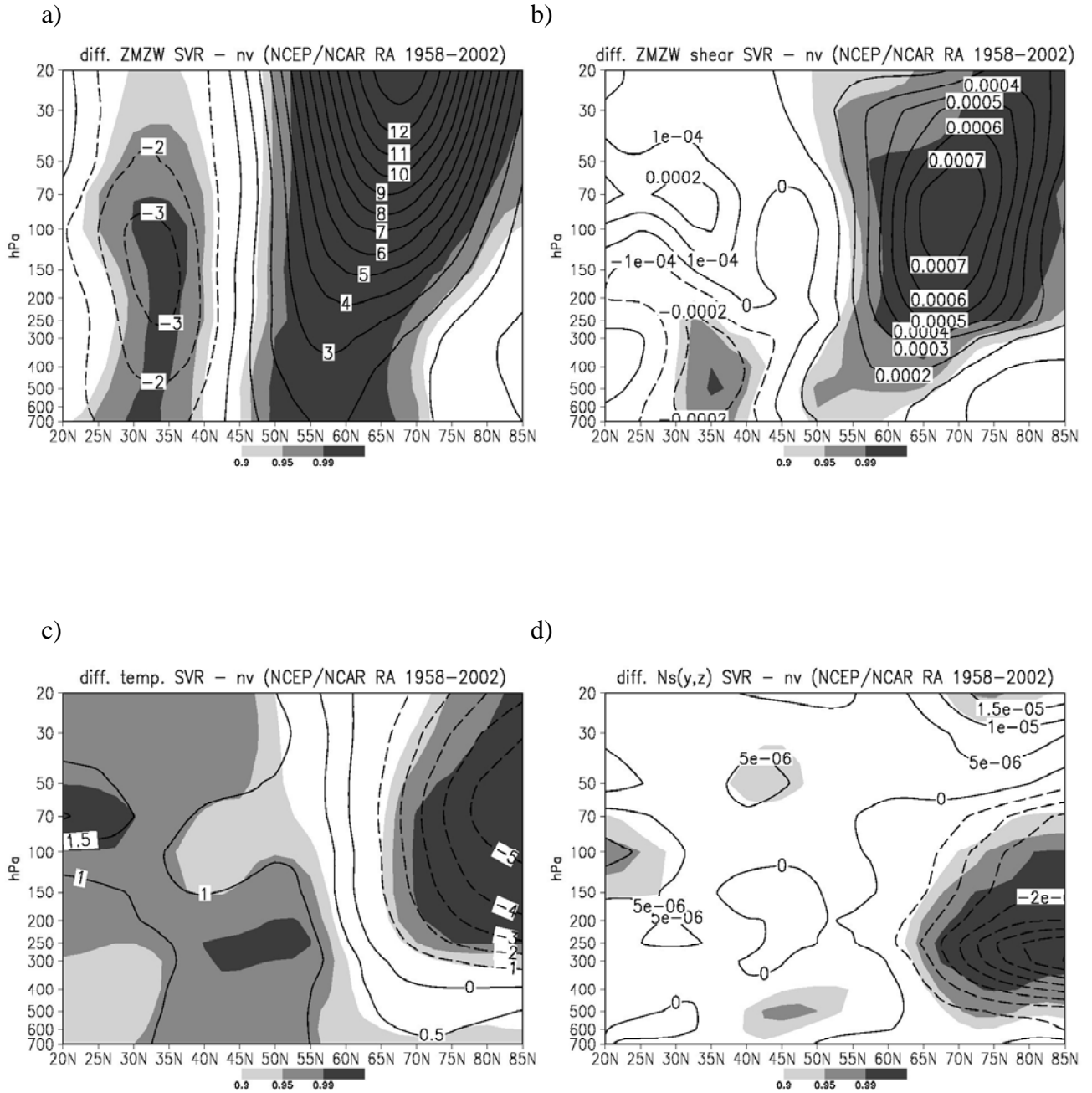
a)

b)

c)

d)

Figure 3.5. The difference of zonal mean zonal wind (m/s) (a), vertical wind shear (s^{-1}) (b), zonal mean temperature (K) (c), $N^2(\phi, z)$ on meridional plane (d), and $N^2(z)$ profile (black line) and $N^2(\phi, z)$ profiles on different latitudes (e) between in SVR excluding volcanic winters and the DJFs excluding volcanic winters (NCEP/NCAR RA, 1958-2002). Unit of N^2 is s^{-2}. Area with significant level above 90% is lightly shaded, above 95% is medium shaded and above 99% is heavily shaded.

3.4.2 Potential influences on planetary wave propagation

3.4.2.1 Control of the atmospheric circulation on planetary wave propagation - analysis of $f(n_k^2<0)$

Fig.3.6 shows the frequency of negative refractive index squared ($f(n_k^2<0)$) for the general winters excluding the volcanic winters for zonal wave number (ZWN) 1, 2 and 3 waves, respectively. The patterns are similar as for all winters including the winters after volcanic eruptions shown in Chapter 2 (Fig.2.2). The "channel", which presents the high possibility of planetary wave propagation from the troposphere to the stratosphere, is reduced to a shallower one when the ZWN of stationary planetary waves increased, implying that only ultra-long stationary planetary waves have more chance to propagate from the troposphere to the stratosphere. On the other hand, the small area with high values of $f(n_k^2<0)$ located above the tropopause around 35°-40°N, which is corresponding with the center of negative values of vertical shear of ZMZW around the same place (Fig.3.1b), can also be found in general winter excluding volcanic winters (Fig.3.6).

In order to investigate clearly the effects of violent tropical volcanic eruptions on planetary wave propagation, the $f(n_k^2<0)$ is also analyzed for the winters after volcanic eruptions (Fig.3.7, left column) for ZWN1, 2 and 3 waves, respectively. The general patterns remain same as in all winters including volcanic winters (Fig.2.2) but some differences still can be found. Although the "channel" representing big chance for planetary wave propagation from the troposphere to stratosphere still can be observed in volcanic winters, for ZWN1 in volcanic winters, the "channel" is wider (Fig. 3.7a), compared with in general winters (Fig.3.6a). This indicates that the ZWN1 wave has more chance to propagate from the troposphere to the stratosphere in the winters after the volcanic eruptions. The "channel" is also more widely open for ZWN2 wave in the winters after volcanic eruptions (Fig. 3.7b). However, it is found that ZWN3 planetary wave has relatively less chance to propagate from the troposphere to the stratosphere in the volcanic winters (Fig.3.7c). In general winters ZWN3 wave still has slight possibility to propagate from the troposphere to the stratosphere although the "channel" is quite shallow (Fig.3.6c) compared with ZWN1 (Fig.3.6a) and ZWN 2 (Fig.3.6b) waves. This shallow "channel" is even more shallow and almost blocked in the volcanic winters (Fig.3.7c).

The differences of $f(n_k^2<0)$ are also drawn between the volcanic winters and general winters (Fig.3.7, right column) for ZWN1, 2 and 3 waves, respectively. The similar conclusion as indicated above can also be drawn. However, it can be found that for ZWN1 and 2, the planetary waves have better chance to propagate from the troposphere to the stratosphere but at high latitudes (65° – 75°N), where less energy is available. This implies that although atmosphere shows better chance for ZWN1 and 2 waves to propagate from the troposphere to the stratosphere, there is no actual energy arriving in the stratosphere through planetary wave propagation.
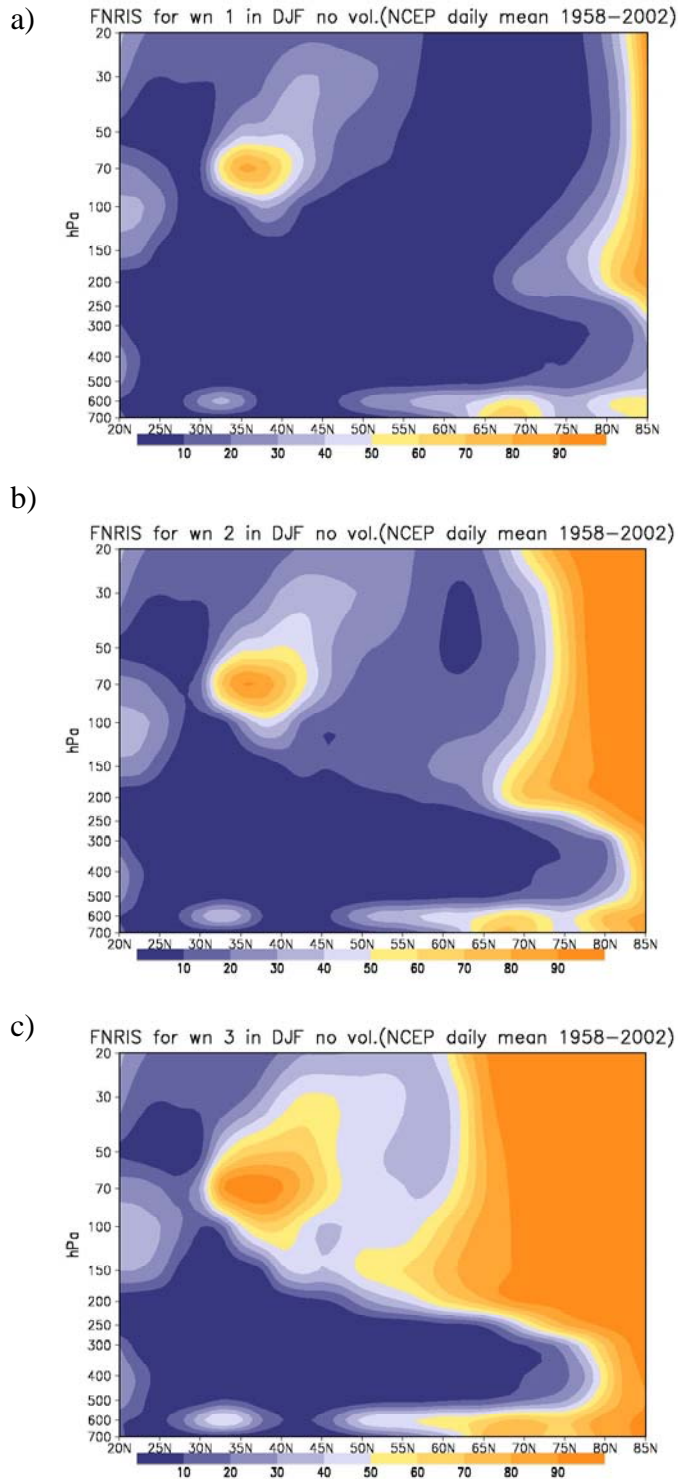
a)

b)

c)

Figure 3.6. f (n_k^2 <0) for stationary planetary waves in DJF (1958-2002) without violent volcanic eruptions (Agung, 1963-1965; El Chichon, 1982-1984; Pinatubo, 1991-1993) (NCEP/NCAR RA) for ZWN1 wave (a), ZWN2 wave (b) and ZWN3 wave (c). Unit of f (n_k^2 <0) is %.
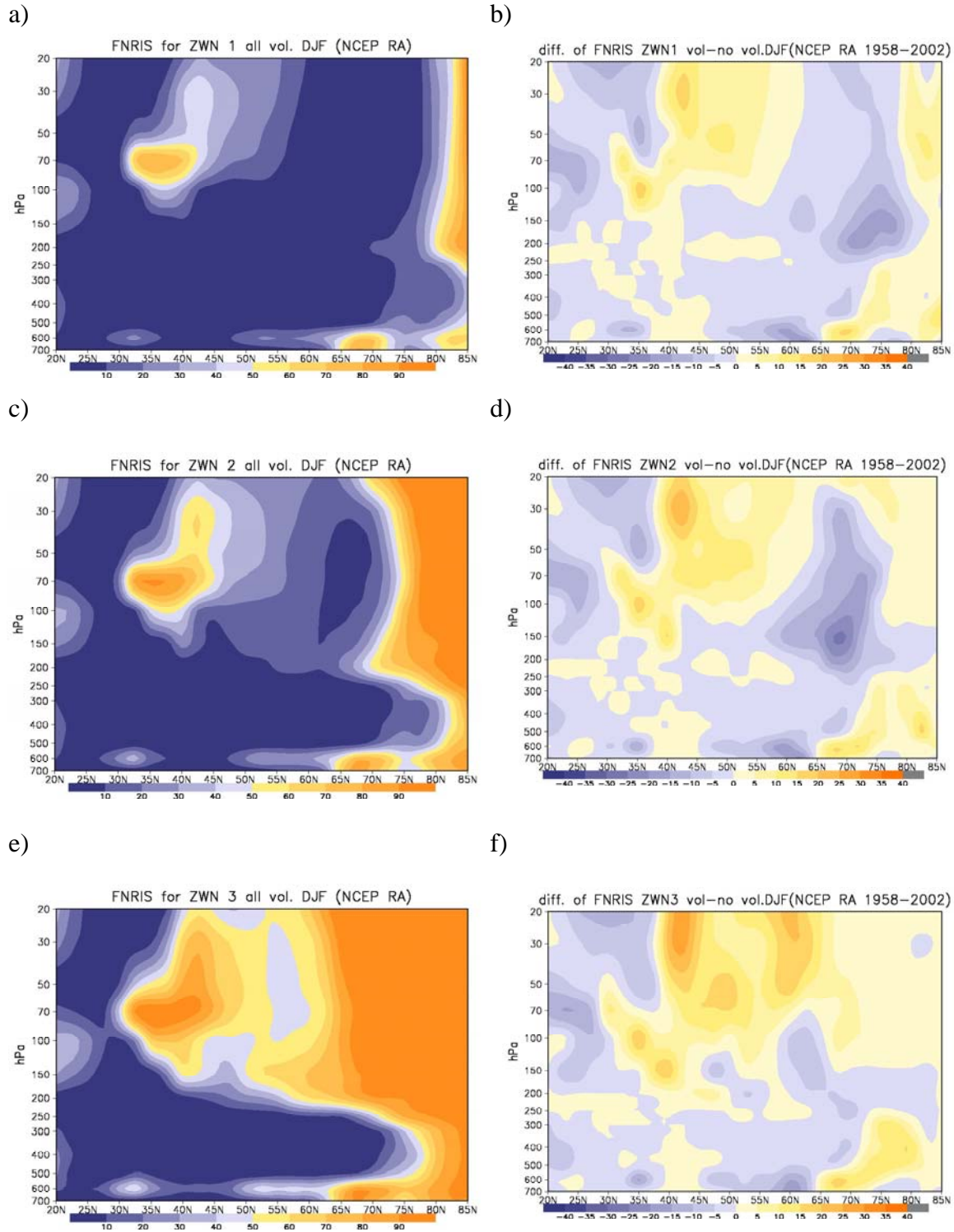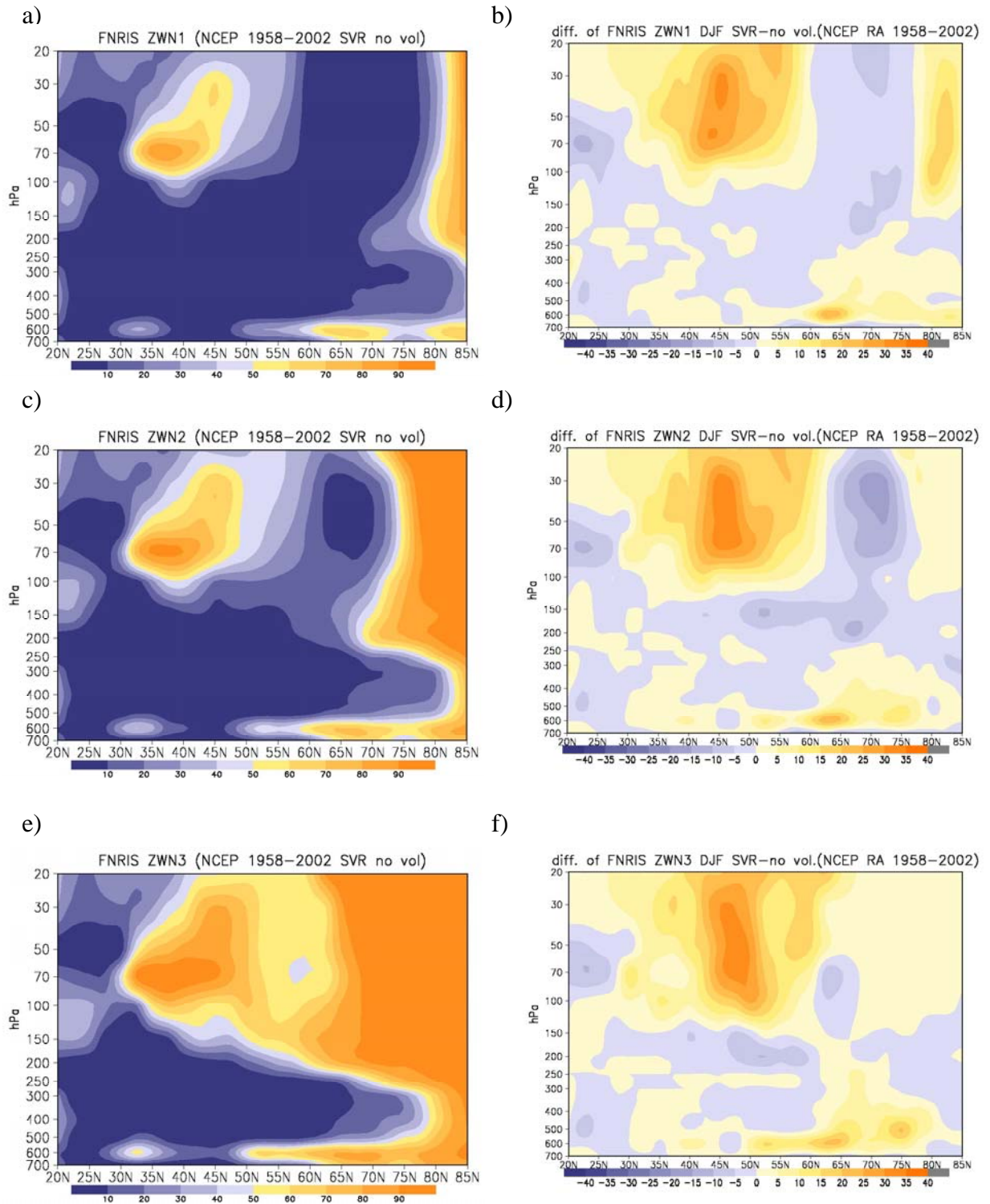
a)

b)

c)

d)

e)

f)

Figure 3.7. f ($n_k^2 < 0$) for stationary planetary waves in DJF (1958-2002) in volcanic winters (left column) and the difference between volcanic winters and the general winter excluding volcanic winters (NCEP/NCAR RA) for ZWN1 wave (first row), ZWN2 wave (second row) and ZWN3 wave (third row). Unit of f ($n_k^2 < 0$) is %.

a)

b)

c)

d)

e)

f)

Figure 3.8. f ($n_k^2 < 0$) for stationary planetary waves in DJF (1958-2002) in SVR excluding volcanic winters (left column) and the difference between SVR and the general winter excluding volcanic winters (NCEP/NCAR RA) for ZWN1 wave (first row), ZWN2 wave (second row) and ZWN3 wave (third row). Unit of f ($n_k^2 < 0$) is %.

Similar analysis of f (n_k^2<0) is also performed for SVR (Fig.3.8). For ZWN1 and 2, as in volcanic winters (Fig.3.7b and d), planetary waves also have more chances to propagate from the troposphere to the stratosphere at high latitudes in SVR (Fig.3.8a, b, c and d) than in general winters (Fig.3.6a, b). However, atmosphere shows even more less possibility for ZWN3 wave in SVR (Fig.3.8e, f) than in volcanic winters (Fig.3.7e, f).

To summarize shortly, in the winters after the violent volcanic eruptions, the atmosphere provides better chance at high latitudes (65° – 75^oN) for ZWN1 and 2 waves to propagate from the troposphere to the stratosphere, but less chance for ZWN3 wave. The more possibilities for ZWN1 and 2 waves can also be found in SVR. Although the stronger polar vortex, observed in both volcanic winters and SVR, can help to prevent the propagation of planetary waves into the stratosphere as concluded in Chapter 2, the stronger vertical shear of ZMZW in stratosphere at high latitudes probably plays a role for the stronger potential of planetary wave propagation in the polar and subpolar lower stratosphere. However, as indicated in Chapter 2, the enhancement of positive values of vertical shear of ZMZW in the lower stratosphere at high latitudes is not significant compared with the impedance of negative values at midlatitudes. Also, there is less energy available at high latitudes, which can propagate into the stratosphere, although the better chance is shown by the atmospheric state.

3.4.2.2 Contribution of planetary waves to the anomalies – analysis of E-P flux and its divergence

Previous studies discussed the potential roles of planetary waves on the anomalies of ZMZW and temperature in the winters after volcanic eruptions (Graf et al., 1993; Graf et al., 1994; Kodera, 1994; Kodera and Yamazaki, 1994). This leads to the conclusion that the stronger winds prevent planetary waves to propagate into the stratosphere, leading to the colder atmosphere in high latitudes and then, in a potential dynamical feedback, strengthening of the polar vortex. In this chapter, the cross sections of E-P flux and its divergence, which present the planetary wave activities and wave momentum forcing on mean flow, are analyzed to study the influences of volcanic eruptions.

Fig.3.9 shows the E-P flux and its divergence of stationary planetary waves for general winters excluding the winters after volcanic eruptions for ZWN1, 2, 3 and 1+2+3 waves, respectively. Two branches of vectors (momentum flux into the subtropical higher troposphere and heat flux into the subpolar stratosphere) and two major convergence areas (one located in the extratropical troposphere and the other located in the subpolar stratosphere) can be found for ZWN1+2+3 wave.

Similar figures of E-P flux and its divergence are also drawn for volcanic winters (Fig.3.10). The major patterns of the two branches of vectors and two major convergences still can be observed, while with some differences. It is found that the upward vectors are stronger for ZWN1 wave in the subpolar stratosphere in volcanic winters (Fig.3.10a) than in general winters (Fig.3.9a). The convergence in the extratropical troposphere shows bigger values (Fig.3.10g) while the convergence in the
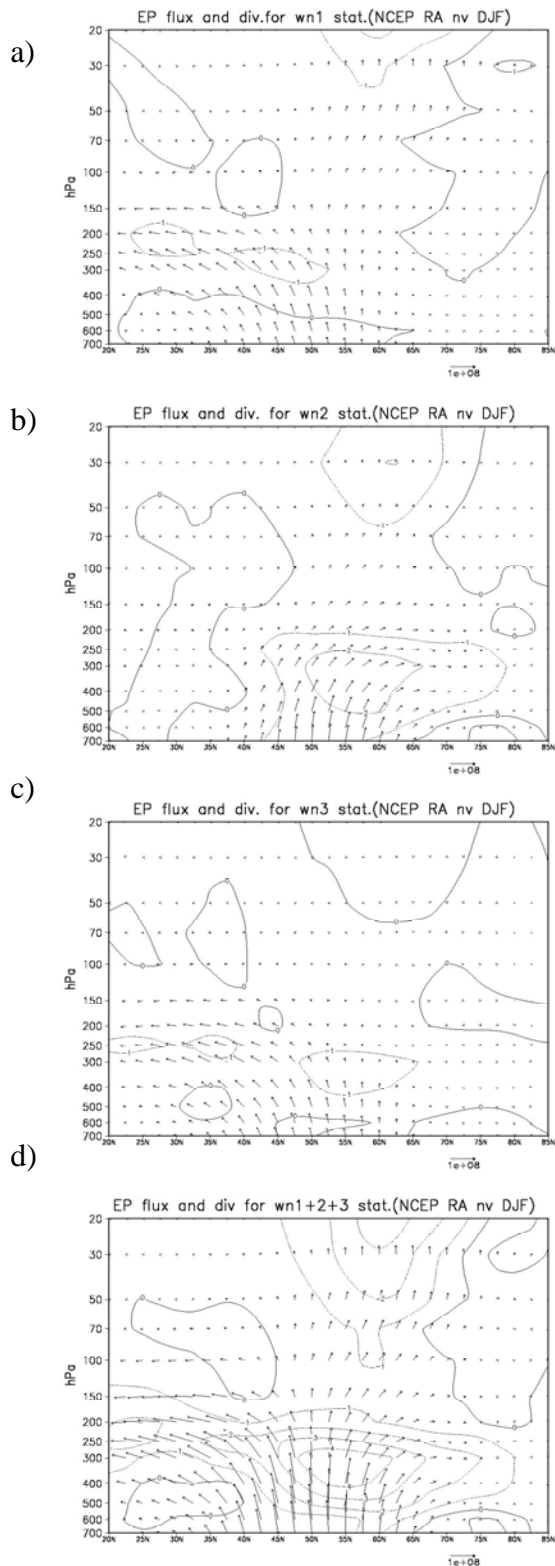
a)

b)

c)

d)

Figure 3.9. E-P flux and divergence for stationary planetary waves in DJF (1958-2002) without violent volcanic eruptions (NCEP/NCAR RA) for ZWN1 wave (a), ZWN2 wave (b), ZWN3 wave (c) and ZWN1+2+3 wave (d). Divergence contour interval is 1ms^{-1}day^{-1}, the unit of vector is kg s^{-2}.

a)

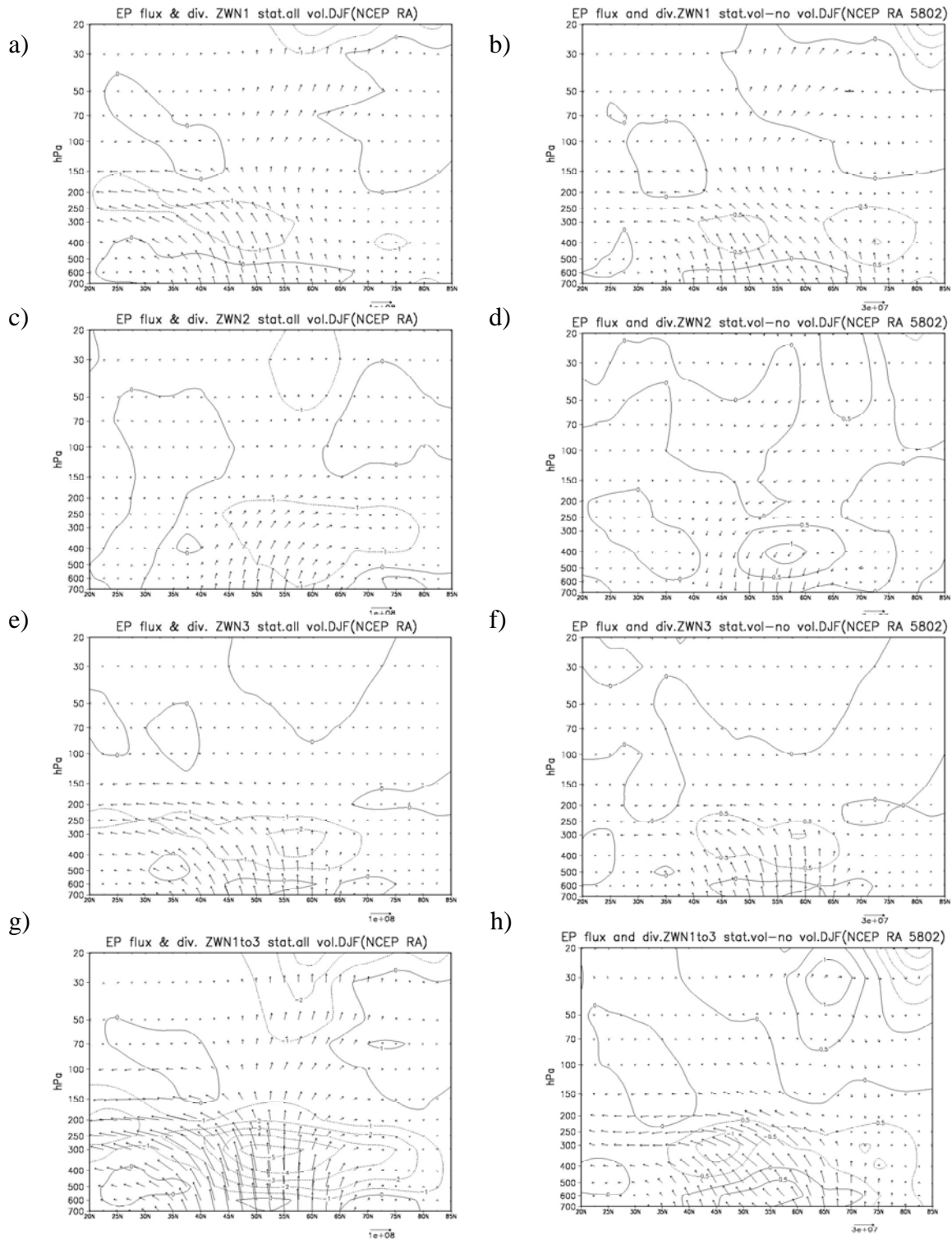*EP flux & div. ZWN1 stat.all vol.DJF(NCEP RA)*

b)

EP flux and div.ZWN1 stat.vol-no vol.DJF(NCEP RA 5802)

c)

EP flux & div. ZWN2 stat.all vol.DJF(NCEP RA)

d)

EP flux and div.ZWN2 stat.vol-no vol.DJF(NCEP RA 5802)

e)

EP flux & div. ZWN3 stat.all vol.DJF(NCEP RA)

f)

EP flux and div.ZWN3 stat.vol-no vol.DJF(NCEP RA 5802)

g)

EP flux & div. ZWN1to3 stat.all vol.DJF(NCEP RA)

h)

EP flux and div.ZWN1to3 stat.vol-no vol.DJF(NCEP RA 5802)

Figure 3.10. E-P flux and divergence for stationary planetary waves in DJF of volcanic winters (left column) and the difference between volcanic winters and the general winter excluding volcanic winters (right column) (NCEP/NCAR RA) for ZWN1 wave (first row), ZWN2 wave (second row), ZWN3 wave (third row) and ZWN1+2+3 wave (bottom row). Divergence contour interval is $1ms^{-1}day^{-1}$ and $0.5ms^{-1}day^{-1}$ for difference, the unit of vector is kg s^{-2}.

subpolar stratosphere extends to the polar stratosphere around 20hPa. The contributions of stationary planetary waves to the anomalies can be shown more clearly in the difference of E-P flux and its divergence between volcanic winters and general winters (Fig.3.10, right column). Clearly ZWN1 wave transports both stronger eddy momentum flux to the tropical troposphere and stronger eddy heat flux to the subpolar stratosphere. At the same time, stronger divergence appears in the subpolar stratosphere, which represents more zonal westerly forcing on mean flow. The major differences of ZWN2 and 3 waves between in volcanic winter and in general winters mostly are located in the troposphere. For ZWN1+2+3 waves, the stronger convergences, which represent more zonal easterly forcing on mean flow, can be found both in the extratropical troposphere and in the polar stratosphere, while the stronger divergence occurs in the subpolar stratosphere. Considering the observation of more heat flux and less easterly momentum forcing induced by stationary planetary waves in the subpolar stratosphere, these results suggest that the stationary wave can propagate into the stratosphere, but these waves do not break and get absorbed in lower stratosphere during the winters after volcanic eruptions. Instead of getting absorbed, these waves probably can propagate even higher upward into the upper stratosphere. These results contrast with some conclusions from previous studies (Graf et al.1993, 1994; Kodera, 1994; Kodera and Yamazaki, 1994).

Similarly, the difference of E-P flux and its divergence between SVR and general winters can be shown in Fig.3.11. The much weaker eddy heat fluxes can be found both in the troposphere and the stratosphere in SVR (Fig.3.11). At the same time, the stronger divergence occurs also in both the extratropical troposphere and the polar and subpolar stratosphere. Although the stronger polar vortex is observed in both of SVR and volcanic winters, the planetary wave propagation is different in these two regimes. These findings confirm the suggestion above that the planetary waves can propagate more from the troposphere to the stratosphere in volcanic winters, but the waves can propagate higher to the upper stratosphere.

This suggestion can be also supported by the analysis of the vertical component of E-P flux - Fz on the levels of 200hPa and 20hPa, respectively. Fig.3.12 shows the comparisons of Fz of ZWN1+2+3 stationary planetary waves on 200hPa in volcanic winters, in general winters, and in SVR regimes. It is found that in all three kinds of winters, planetary waves can transport a certain amount of eddy heat fluxes from the troposphere to the stratosphere at mid latitude ($40^{o} – 60^{o}$N) at 200hPa (Fig.3.12a). The biggest amplitudes of Fz with top value 179000kg/s^{-2}, is contributed by the waves in general winters. The values of Fz are smaller in SVR (maximum ~ 128000kg/s^{-2}) and but bigger values can be observed in volcanic winters (maximum ~ 199000kg/s^{-2}). The standard deviation of Fz in SVR is negligible (maximum 20000kg/s^{-2}) compared with the values of Fz in SVR. Similar, Fz at 20hPa is also draw for volcanic winters, general winters and SVR in Fig.3.12b. It is found that the planetary waves still have chances to propagate higher up in all volcanic winters, general winters and SVR. However, the amplitudes of Fz are changed. In general winters, Fz can transport at most around 52100kg/s^{-2} eddy heat fluxes upward, which is about 29% of the part propagated from the troposphere to the stratosphere at 200hPa. In SVR, the biggest value of Fz is around amplitude of 32400kg/s^{-2} at 20hPa, which is about 25% of those at 200hPa. However, in
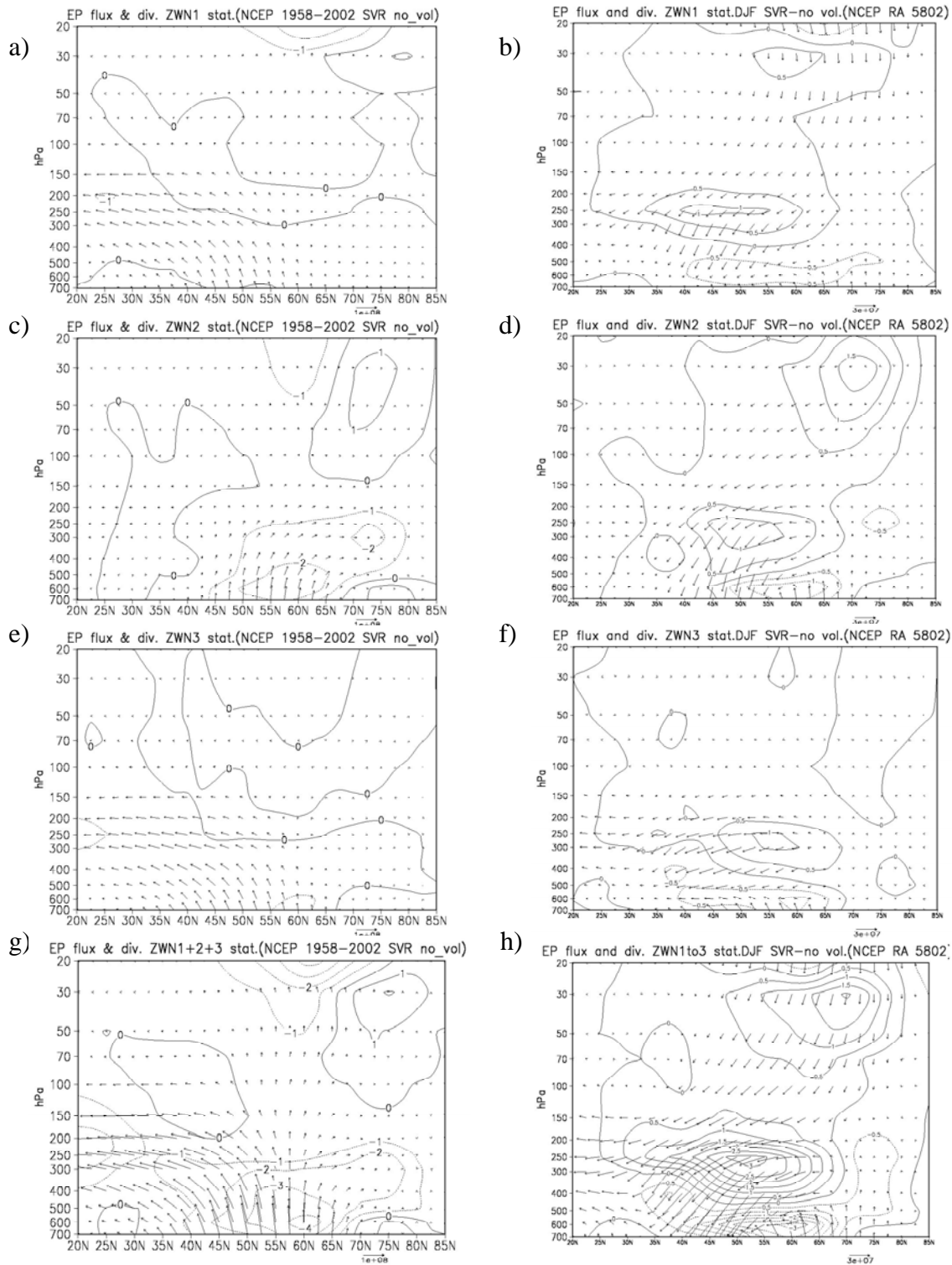
Figure 3.11. E-P flux and divergence for stationary planetary waves in SVR excluding volcanic winters (left column) and the difference between SVR and the general winter excluding volcanic winters (right column) (NCEP/NCAR RA) for ZWN1 wave (first row), ZWN2 wave (second row), ZWN3 wave (third row) and ZWN1+2+3 wave (bottom row). Divergence contour interval is $1ms^{-1}day^{-1}$ and $0.5ms^{-1}day^{-1}$ for difference, the unit of vector is $kg\ s^{-2}$.

a)

Fz for ZWN1to3 on 200hPa (NCEP/NCAR RA 1958-2002)
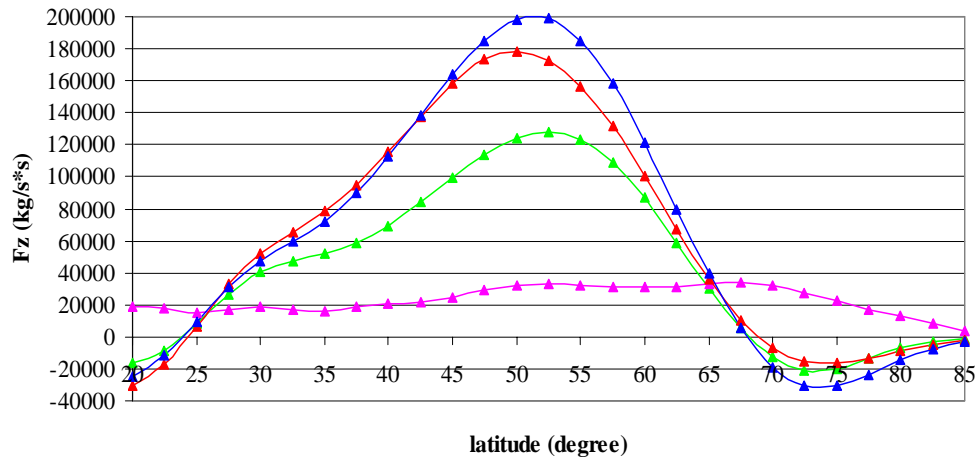
SVR   SVR standard deviation   general winter (no vol.)   volcanic winter

b)

Fz for ZWN1to3 on 20hPa (NCEP/NCAR RA 1958-2002)
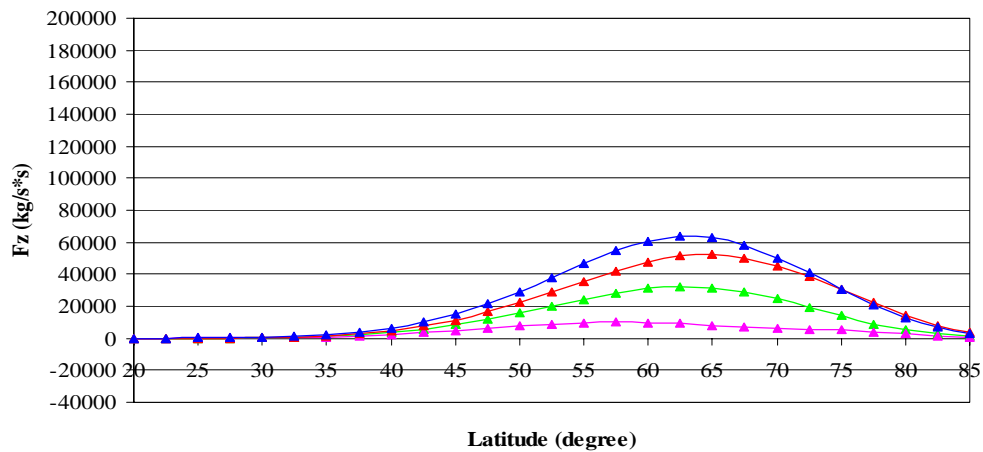
SVR   SVR standart deviation   general winter (no vol.)   vol. winter

Figure 3.12. Vertical component of E-P flux - Fz for ZWN1+2+3 stationary planetary waves on 200hPa in DJF, general winters (red profile) excluding volcanic winters, in SVR (green profile) excluding volcanic winters, the mean of Fz on 20hPa in volcanic DJFs (blue profile), and the standard deviation for SVR (purple profile) excluding volcanic winters. a) at 200hPa from 20N to 80N. b): at 20hPa. The unit of Fz is kg s^{-2}.

volcanic winters, the maximum of Fz is around 63600kg/s^{-2} at 20hPa, which is about 32% of the one at 200hPa. Based on these observations, it can be concluded that the planetary waves can induce more eddy heat fluxes into the stratosphere in volcanic winters than in other winters. Also, these waves can continuously propagate more upward to the upper stratosphere than in other winters. Hence, in volcanic winters planetary waves transport more eddy heat fluxes from the troposphere to the stratosphere and therefore to the upper stratosphere than in other winters.

Compared with the stationary waves, the transient waves show different behavior. After filtering (Blackmon and Lau, 1980), E-P flux and its divergence of the transient waves with all frequencies (Fig.3.13a), low frequency transient waves (Fig.3.13b) and synoptic transient waves (Fig.3.13c) in the general winters are investigated. The low frequency transient waves dominate the propagation of transient planetary waves (Fig.3.14, left column). There is a wider distribution of heat fluxes and stronger convergences in the lower troposphere, weaker heat fluxes in the subpolar stratosphere. These patterns can also be observed in the volcanic winters (Fig.3.14). Figures of each single volcanic winter are produced in the Appendix B. The stronger divergence in the polar or subpolar stratosphere appears in volcanic winters. This strengthened divergence in the polar stratosphere can be also clearly observed in the difference of E-P flux and divergence of transient waves between in volcanic winters and in general winters (Fig.3.14b and d). An area of negative values of difference of divergence, which represents more zonal easterly forcing on the mean flow, is found in the subpolar stratosphere in the difference figures (Fig.3.14b) especially for low frequency transient waves (Fig.3.14d). These observations imply that the transient waves induce less zonal easterly forcing on mean flow in the polar stratosphere and more easterly forcing in the subpolar stratosphere in volcanic winters. This finding is opposite to the results shown by the stationary waves (Fig.3.10). For stationary waves, stronger convergence in the polar stratosphere and the stronger divergence in the subpolar stratosphere are observed in volcanic winters (Fig.3.10h). Another difference between stationary and transient waves is that the eddy momentum fluxes from the extratropical lower troposphere to the tropical upper troposphere are stronger for stationary waves (Fig.3.10h) but weaker for transient waves (Fig.3.14b) in volcanic winters compared with general winters. However, the stronger eddy heat fluxes can be found for both stationary waves (Fig.3.10h) and transient waves (Fig.3.14b) in the subpolar stratosphere in volcanic winters.

Fig.3.15 shows the E-P flux and its divergence for transient waves in SVR and their differences between SVR and general winters. Similar as in volcanic winters, a stronger convergence in the subpolar stratosphere is found. However, unlike in volcanic winters, stronger eddy momentum flux from the extratropical lower troposphere to the tropical upper troposphere, and weaker eddy heat flux in the subpolar stratosphere can be observed. Based on these results, it can be concluded that in volcanic winters, the stationary waves and transient waves have different feedbacks to the impacts of volcanic eruptions in the troposphere and stratosphere, respectively. Although the anomalies of zonal mean zonal wind and temperature show "dipole" structures for both SVR and volcanic winters, planetary wave propagation has different aspects in SVR and in volcanic winters.

a)

EP flux and div.for all wn unfil.tran.(NCEP RA 5802 djf, no vol

b)

EP flux and div.for all wn l-p tran.(NCEP RA 5802 djf, no vol

c)

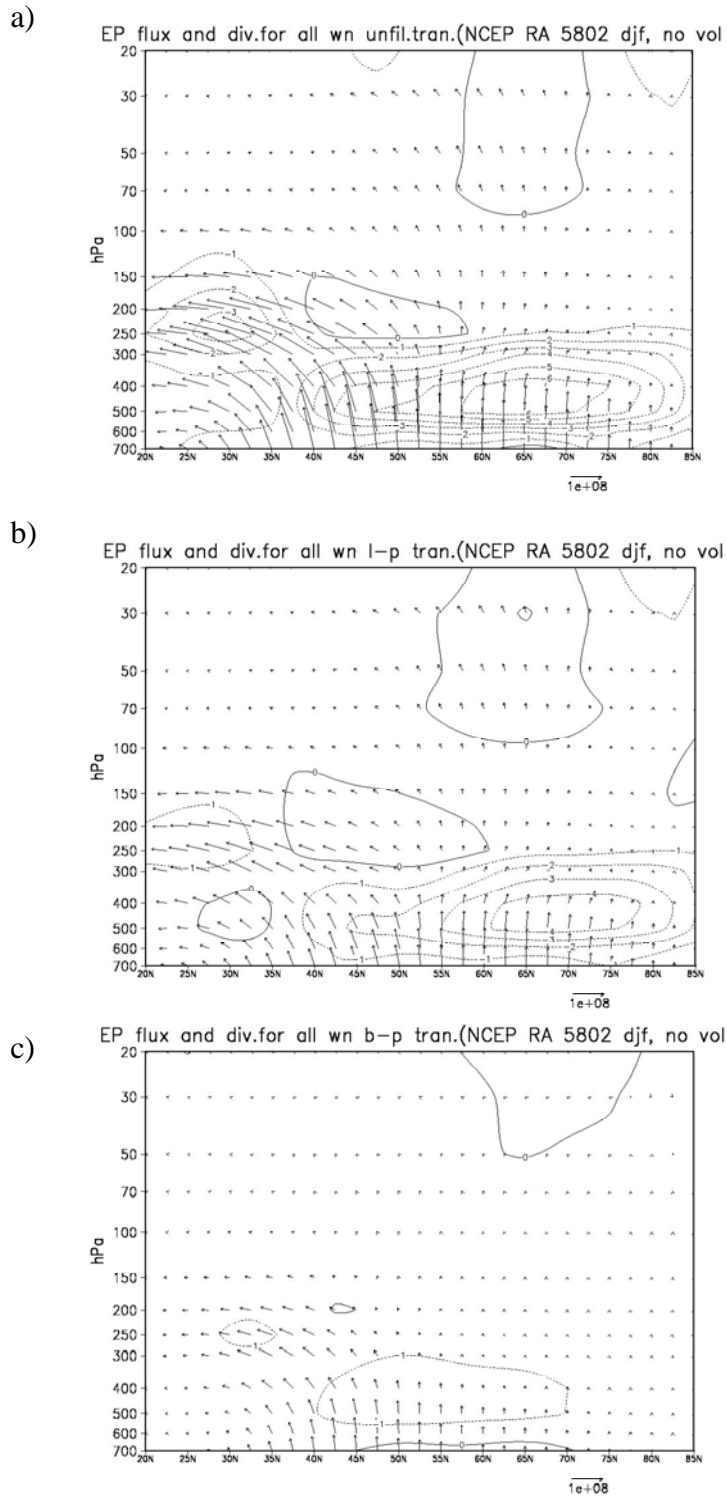EP flux and div.for all wn b-p tran.(NCEP RA 5802 djf, no vol

Figure 3.13. E-P flux and divergence for transient planetary waves in DJF (1958-2002) without violent volcanic eruptions (NCEP/NCAR RA) for unfiltered wave (a), low-pass filtered wave (b) and band-pass filtered wave (c). Divergence contour interval is 1 ms^{-1}day^{-1}, the unit of vector is kg s^{-2}.

a)

EP flux & div. unfil. tr. all vol.DJF(NCEP RA)

$\overrightarrow{1e+08}$

b)

EP flux and div. u-f. tran. vol-no vol.DJF(NCEP RA 5802)

$\overrightarrow{3e+07}$

c)

EP flux & div. l-p. tr. all vol.DJF(NCEP RA)

$\overrightarrow{1e+08}$

d)

EP flux and div. l-p. tran. vol-no vol.DJF(NCEP RA 5802)

$\overrightarrow{3e+07}$

e)

EP flux & div. b-p. tr. all vol.DJF(NCEP RA)

$\overrightarrow{1e+08}$

f)

EP flux and div. b-p. tran. vol-no vol.DJF(NCEP RA 5802)

$\overrightarrow{3e+07}$
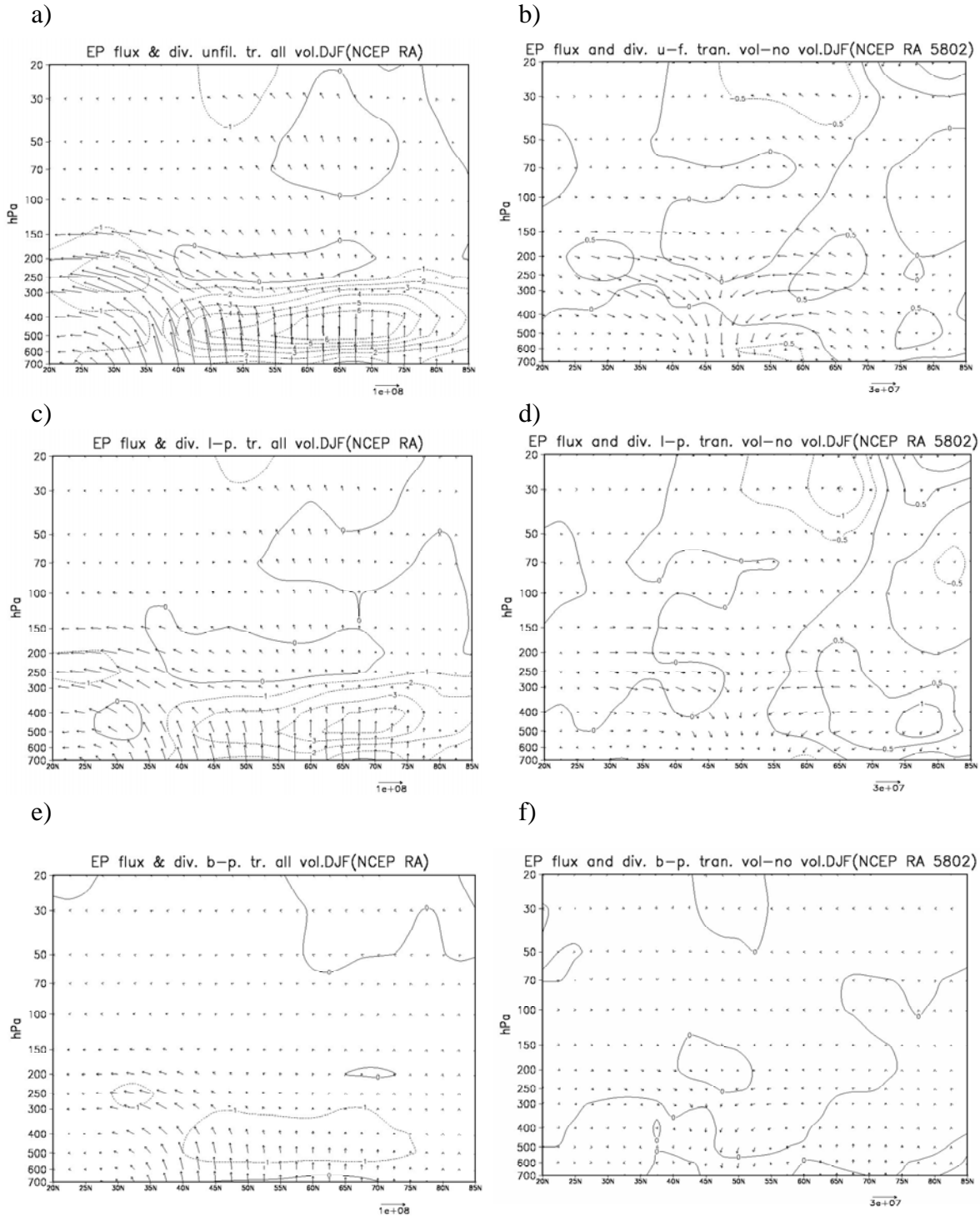
Figure 3.14. E-P flux and divergence for transient planetary waves in DJF of volcanic winters (left column) and difference between volcanic winters and general winters excluding volcanic winters (right column) (NCEP/NCAR RA) for unfiltered wave (first row), low-pass filtered wave (second row) and band-pass filtered wave (third row). Divergence contour interval is $1ms^{-1}day^{-1}$ and $0.5ms^{-1}day^{-1}$ for difference, the unit of vector is kg s^{-2}.

a)

EP flux & div. allZWN unfil.tran.(NCEP 1958-2002 SVR no vol)

b)

EP flux and div. u-f. tran.DJF SVR-no vol.(NCEP RA 5802)

c)

EP flux & div. allZWN l-p tran.(NCEP 1958-2002 SVR no vol)

d)

EP flux and div. l-p. tran.DJF SVR-no vol.(NCEP RA 5802)

e)

EP flux & div. allZWN b-p tran.(NCEP 1958-2002 SVR no vol)

f)

EP flux and div. b-p. tran.DJF SVR-no vol.(NCEP RA 5802)
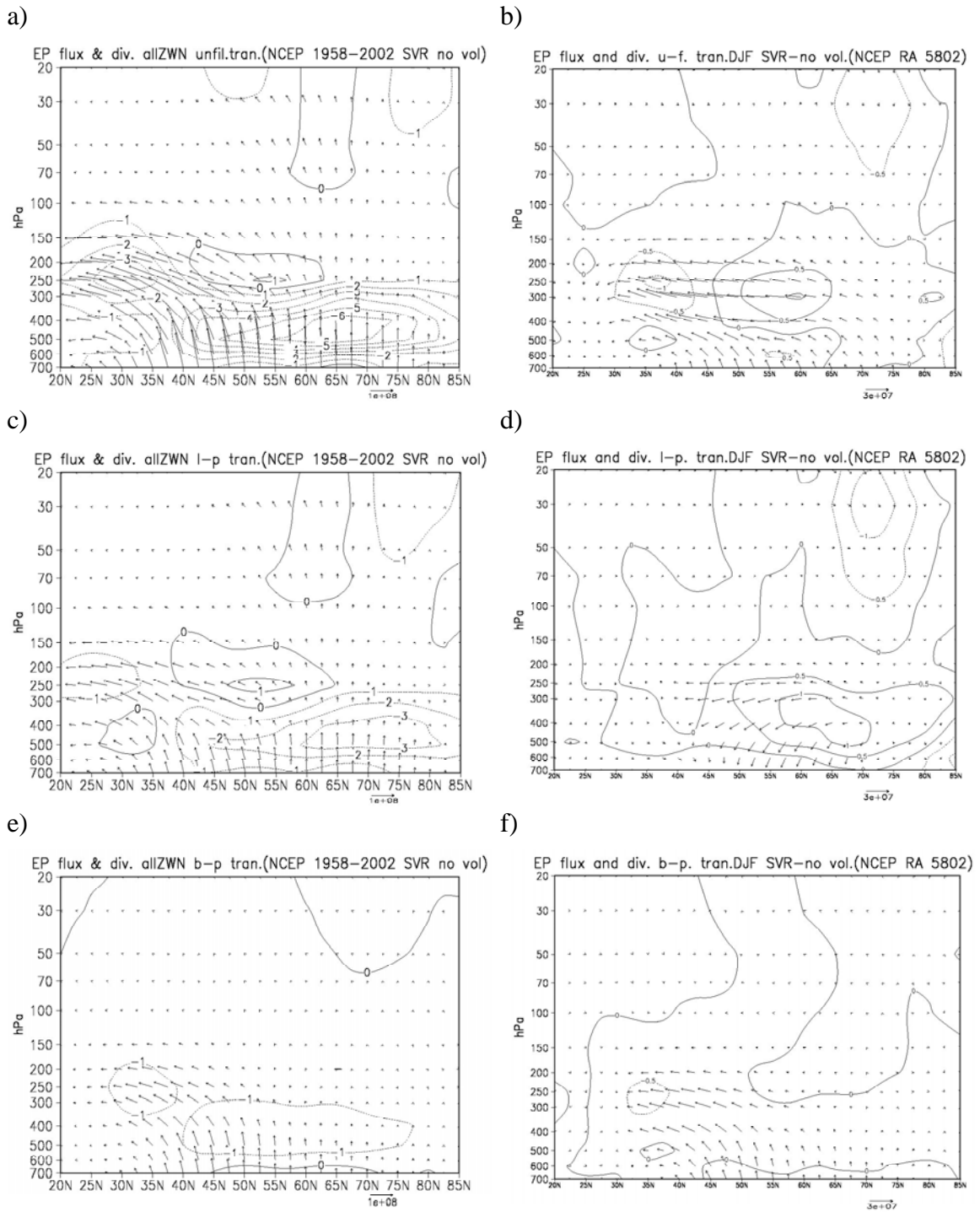
Figure 3.15. E-P flux and divergence for transient planetary waves in SVR excluding volcanic winters (left column) and difference between SVR and general winters excluding volcanic winters (right column) (NCEP/NCAR RA) for unfiltered wave (first row), low-pass filtered wave (second row) and band-pass filtered wave (third row). Divergence contour interval is $1ms^{-1}day^{-1}$ and $0.5ms^{-1}day^{-1}$ for difference, the unit of vector is kg s^{-2}.

3.5 Summary

In this chapter, the anomalies of ZMZW and zonal temperature in NH winter induced by violent tropical volcanic eruptions and their influences on planetary wave propagation have been investigated. Three volcanic eruptions, which all injected huge amounts of aerosols into the lower stratosphere - Agung (1963), El Chichon (1982) and Pinatubo (1991) eruptions, are analyzed. Since the impacts of volcanic eruptions on the climate system can last 1-3 years (Robock, 2001), the two winters after these three volcanic eruptions are studied. The "dipole" structures for the anomalies of both of ZMZW and temperature in NH winter are observed - the "dipole" structure of anomalies of ZMZW composed by a stronger stratospheric polar vortex and a weaker tropical jet, and the "dipole" structure of anomalies of temperature composed by the cooling in the polar stratosphere and the warming in the tropical stratosphere. The similar "dipole" structures can also be observed in strong polar vortex regimes (SVR) excluding the volcanic winters.

Not only the ZMZW and temperature, but also the anomalies of vertical shear of ZMZW and buoyancy frequency in the volcanic winters are found. The relatively smaller values of buoyancy frequency around the polar tropopause in volcanic winters are shown. Therefore it is expected that the atmosphere is more instable around the polar tropopause in the winters after volcanic eruptions.

By analyzing the frequency of negative refractive index squared (f (n_k^2 <0)), it is concluded that the atmosphere shows more possibilities for ZWN1 and 2 but less possibility for ZWN3 stationary planetary waves to propagate from the troposphere to the stratosphere at high latitudes (65° – 75^oN). Similar results can also be drawn in SVR. These better chances for ZWN1 and 2 waves probably correspond with the stronger vertical shear of ZMZW in stratosphere at mid and high latitudes in both volcanic winters and SVR. However, there is very less wave energy available at high latitudes, although the better chance for wave propagation is shown by the atmospheric state.

Moreover, the analysis of E-P flux and its divergence indicate that the stationary waves can propagate easily from the troposphere to the stratosphere in the volcanic winters. Furthermore, these waves can continually propagate higher up to the middle and upper stratosphere and probably induce wave forcing on the upper stratospheric circulation. This can help us understand the mechanism of more planetary waves propagated from the troposphere to the stratosphere and stronger stratospheric polar vortex appearing at the same time in the Northern Hemisphere winters after violent volcanic eruptions. Unlike the stationary waves, the propagation of transient waves shows different aspects in both volcanic winters and SVR.

Finally, it should be indicated that the available observed violent tropical volcanic eruptions are limited although the impacts of the volcanic eruptions on climate system are very strong and significant. It is very important to understand the mechanism of the dynamical mechanism of the influences of the volcanic eruption on atmosphere. The general circulation models (GCMs) considering the forcing of volcanic eruptions can be a very useful tool to investigate the contribution of volcanoes on climate change.

Chapter 4

Climatology of planetary wave propagation in Northern Hemisphere winter: GCM performance

4.1 Introduction

General circulation models (GCMs) are always used to improve our understanding of climate system and the mechanism of climate change. If all relevant physical processes are correctly represented, a GCM should provide a faithful simulation of the three-dimensional circulation. Moreover, externally specified parameters (e.g., orography) can be altered to provide "controlled" experiments that cannot be done on the real atmosphere. Potential feedback of climate system to natural external forcing (e.g., solar cycle, sea surface temperature and sea ice variations, and volcanic eruptions), and anthropogenic forcing (e.g., greenhouse gases, CFCs) can also be investigated by simulations of GCMs.

However, in the modelling of the general circulation, many compromises are necessary for scientific reasons and computational efficiency reasons. Therefore, focusing on one of the physical processes, it is an appropriate attempt to analyze experiments of GCMs under specified conditions. The models are not perfect and we want to know if they produce reasonable results for the right reasons.

As discussed in earlier chapters, the mechanism of planetary wave propagation and planetary wave-mean flow interaction is one of the major current research topics. In order to illuminate the dynamical coupling between the stratosphere and the troposphere, we need to understand planetary wave propagation and refraction and its influences on mean flow. Associated with observational studies, one of the appropriate methods is to investigate the GCM's performance on planetary wave propagation, especially in Northern Hemisphere winter.

In this chapter, numerical simulations carried out with the latest version of the comprehensive GCM from Max Planck Institute for Meteorology – ECHAM5 (Rockner, et al., 2003) is analyzed to investigate the climatology of planetary wave propagation from the troposphere to the stratosphere in Northern Hemisphere boreal winter (DJF). As indicated in Kodera et al. (1990), the anomalies of the zonal mean zonal wind which are created initially in the upper stratosphere or even in the mesosphere, can propagate downward into the lower stratosphere and the troposphere by wave-mean flow interaction and thereby modify the stratospheric and tropospheric circulation. The potential feedback and influences from the stratosphere on the troposphere were also demonstrated by a few observational studies (Baldwin and Dunkerton, 1999; etc.). Previous GCM studies (Giorgetta et al., 2002) indicated that the middle atmospheric GCM – ECHAM5 (MAECHAM5) with extending upper levels, including most part of the stratosphere (up to 0.01hPa) could properly simulate the quasi-biennial oscillation (QBO). In this chapter,

we will address the importance of considering of the stratosphere-troposphere dynamical coupling in climate system. Associated with the observational analysis, it will help to improve our understanding of climate system by investigating the planetary wave propagation in simulations of both ECHAM5 and MAECHAM5. One of the efforts is to check if the planetary wave propagation is properly represented in these GCMs.

It has been demonstrated that variations of the NH stratospheric polar vortex can be influenced by fluctuations of sea surface temperature (SST) (van Loon and Labitzke, 1987; Hamilton 1993a; Baldwin and O'Sullivan, 1995; Kodera et al., 1996). The potential feedback of ocean to atmosphere has been paid considerable attention. With increasing computer efficiency, it becomes possible to perform the complex model systems, e.g., the atmosphere-ocean coupled general circulation models (AOGCMs). In this chapter, the simulation of AOGCM from the Max Planck Institute for Meteorology – MAECHAM5 coupled with MPIOM (MPI Ocean Model) (Jungclaus et al., 2006) – is also analyzed to investigate the influences of ocean on atmospheric circulation and planetary wave propagation.

4.2 GCMs experiments and datasets

A series of experiments of ECHAM5, MAECHAM5, and MAECHAM5 coupled with MPIOM (MAECHAM5_MPIOM hereafter) are analyzed in this chapter, respectively. As indicated in Table 4.1, the horizontal resolution for all three models is T63. The vertical resolution of ECHAM5 is L31 with 10hPa as top boundary. The experiments of MAECHAM5 have vertical resolution L47 with 0.01hPa as top boundary. While vertical resolution (or levels) from surface to 10hPa is distribute in same way for all three models. The detailed descriptions of ECHAM5 have been given in Rockner et al. (2003, 2006). As the middle-atmosphere configuration of the ECHAM5 model, the implementation of MAECHAM5 was described in Manzini et al. (2006) and Giorgetta et al. (2006). In both experiments of the AGCMs, the lower boundary condition is specified by the monthly climatology of SST and sea ice concentration from the Atmospheric Model Intercomparison Project 2 (AMIP2) datasets (Taylor et al., 2000). The details of the coupled atmosphere - ocean model MAECHAM5_MPIOM was illustrated in Jungclaus et al. (2006). The ocean passes the information of not only SST, sea ice concentration, but also sea ice thickness, snow depth, and the ocean surface velocities to the atmosphere. The technical details of the ocean model MPIOM can be found in Marsland et al. (2003).

The daily mean data of geopotential, wind and temperature of 20 NH winters (DJF of 1979-1999) for all three experiments are analyzed to study the climatology of planetary wave propagation in Models. The NCEP/NCAR reanalysis daily data (Kalnay et al., 1996; Kistler et al., 2001) with same time period (DJF of 1979-1999) are used as observational reference in this chapter. The details of NCEP/NCAR reanalysis data have been given in Chapter 2.

Some details of the datasets of GCMs are given in Table 4.1 beneath.

Table 4.1 Description of datasets of GCMs

Model	Horizontal resolution	Vertical resolution	Vertical extent	Period taken
ECHAM5_AMIP	T63	L31	10hPa	DJF of 1979-1999
MAECHAM5_AMIP	T63	L47	0.01hPa	DJF of 1979-1999
MAECHAM5_MPIOM	T63	L47	0.01hPa	DJF of 1979-1999

4.3 GCMs performance on atmospheric circulation and planetary wave propagation in Northern Hemisphere winter

4.3.1 NCEP/NCAR Reanalysis vs. ECHAM5_AMIP2

Fig.4.1 shows the zonal mean zonal wind (ZMZW) and vertical shear of ZMZW on meridional plane in NH boreal winter for NCEP/NCAR reanalysis data and simulation of model ECHAM5_AMIP2, respectively. The simulation of model shows good agreements with the observations. The strength and the position of both the tropospheric subtropical jet and the stratospheric polar vortex are well shown in ECHAM5_AMIP2 (Fig.4.1b). The model also indicates properly the distribution of vertical shear of ZMZW (Fig.4.1d). However, the differences between observation and model can still be observed. Comparing Fig.4.1a and Fig.4.1b, it can be found that the polar vortex is relatively wider and higher in the model. On the other hand, the vertical shear of ZMZW in the subpolar stratosphere is stronger in the model (Fig.4.1d). The differences between the observation and the model mainly distribute in the polar and subpolar stratosphere. By an intercomparison of different GCMs, Pawson et al. (2000) has addressed the "bias" of GCMs on the stratospheric polar vortex. They attributed the "bias" to the some effects including the behavior of the upper levels, the dynamical forcing in the lower stratosphere by medium-scale waves propagating from the troposphere and the impacts of the parameterization of subgrid-scale diffusion. While in this chapter, the vertical resolutions (L31, L47) of GCMs have been increased, compared to those in Pawson et al (2000, Table 4). Therefore, the "bias" of the polar vortex in ECHAM5 analyzed in this chapter is expected to be relatively smaller than those in Pawson et al. (2000, Fig.3). However, it is obvious that the polar vortex extends more highly above 10hPa, therefore, the altitude of the top boundary level of ECHAM5 (10hPa) probably is not good enough to simulate the stratospheric polar vortex in the NH winter. This problem is somewhat expected to be avoided by applying the middle atmospheric GCM – MAGCM. The potential benefits of higher top boundary in GCM and the consequent influence on planetary wave propagation will be discussed in next section.
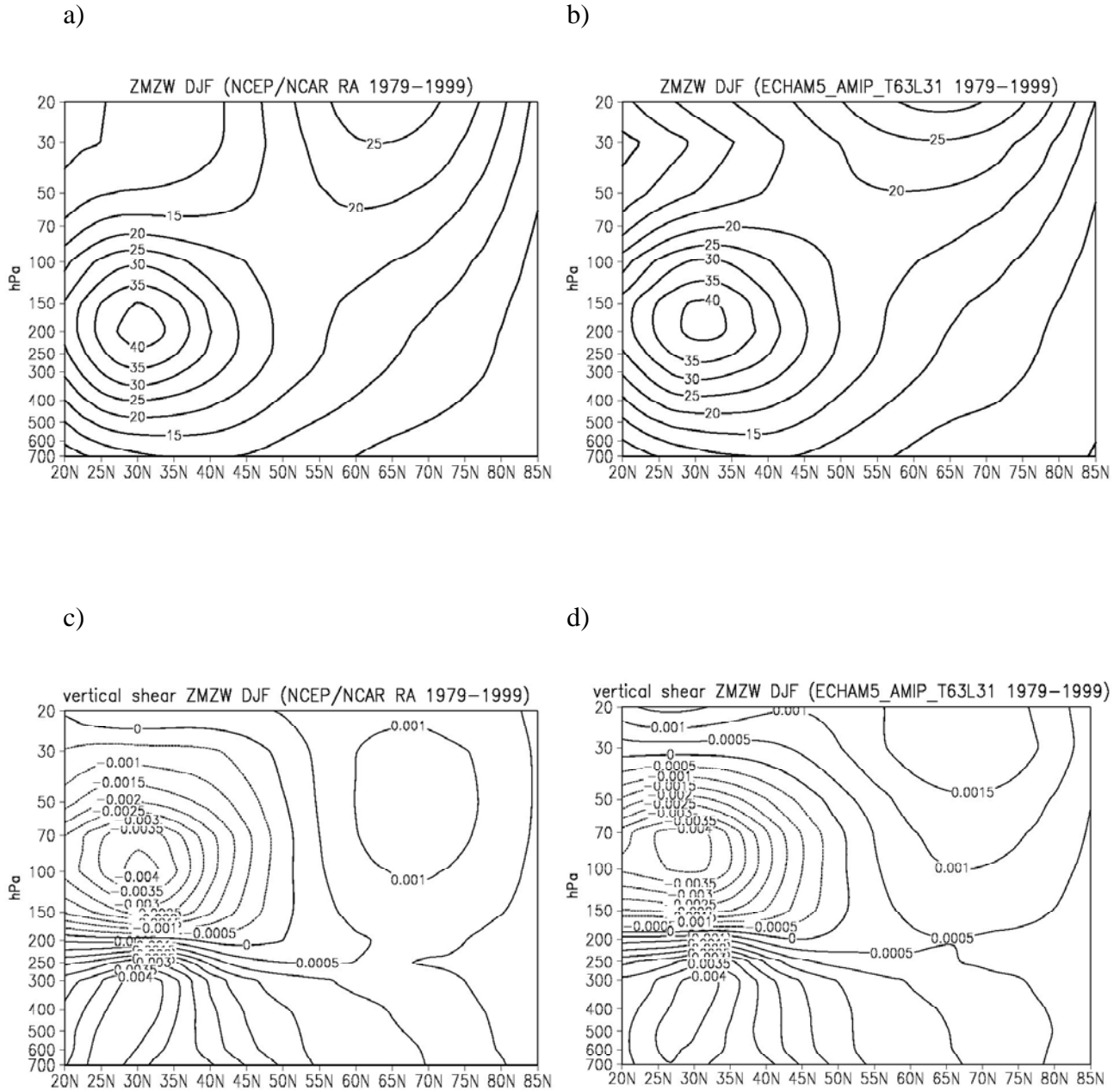
a)

b)

c)

d)

Figure 4.1. Zonal mean zonal wind (m/s) (first row) and vertical shear of zonal mean zonal wind (s^{-1}) (second row) in DJF for 1979-1999 for NCEP/NCAR RA 1979-1999 (left column) and experiment of ECHAM5_AMIP2_T63L31 (right column).
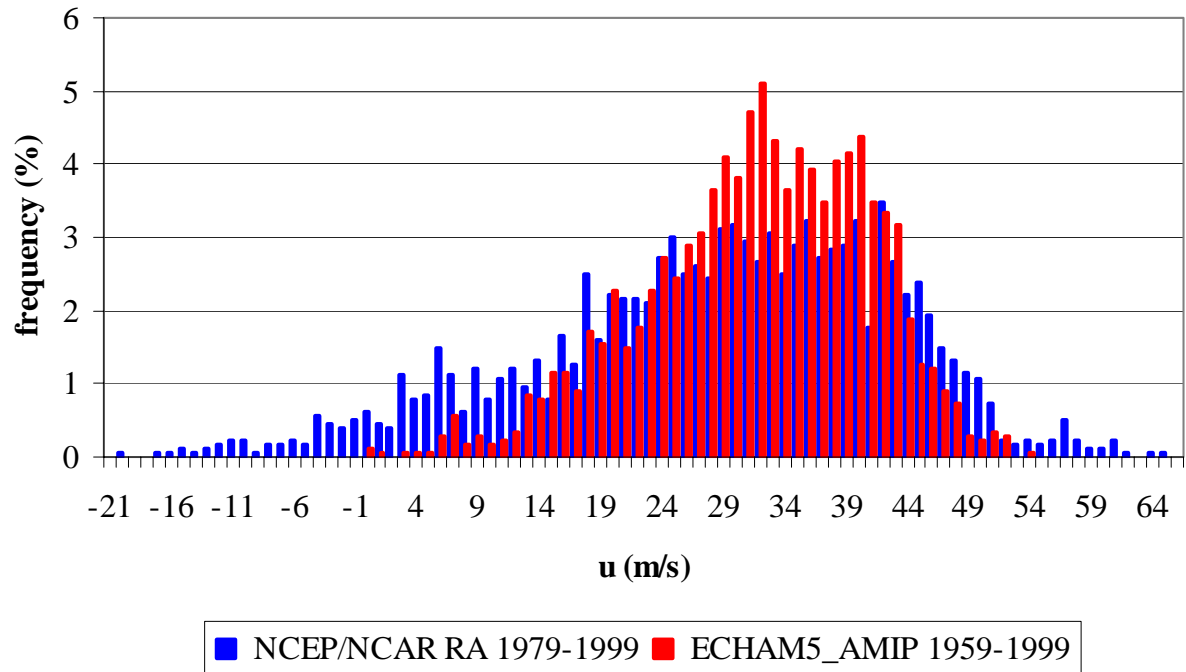
Frequency of ZMZW on 20hPa, 65N in DJF

Figure 4.2. Distributions of frequencies of values of zonal mean zonal wind (ZMZW) on 20hPa, 65N of DJF for data sets: NCEP RA 1958-2002; ECHAM5_AMIP2_T63L31 1979-1999. Unit of ZMZW is m/s. Unit of frequency is %.

As mentioned above, the differences between observation and model are mainly distributed in the polar and subpolar stratosphere. In order to clarify the differences, the frequency distribution of the daily ZMZW on 20hPa, 65°N, which is able to represent the polar vortex, in DJF from 1979 to 1999 for both NCEP/NCAR reanalysis data and simulation of ECHAM5_AMIP2 are analyzed (Fig.4.2). It can be observed that the distributions of the frequencies of ZMZW in simulation of ECHAM5_AMIP2 are concentrating in a shallower area than those of the observations. The values of the higher frequencies mainly distributed near the high values of ZMZW from 30m/s to 40m/s are

much bigger in ECHAM5_AMIP than in NCEP/NCAR reanalysis data (Fig.4.2). This can also be shown in Table 4.2. Table 4.2 shows that the value of median of frequency of ZMZW (U_{median}) on 20hPa, 65°N for model is 31m/s, which is bigger than observation (28m/s). Although the biggest value of ZMZW (U_{max}) on 20hPa, 65°N is relatively smaller in ECHAM5_AMIP2 (54m/s) than in observation (65m/s), the smallest value of ZMZW (U_{min}) in ECHAM5_AMIP2 (0m/s) is much bigger than the one in observation (-20m/s). Moreover, the value of the mean of ZMZW ($\overline{U}$) for 20 NH boreal winters on 20hPa, 65°N is also bigger in ECHAM5_AMIP2 (31.3m/s) than in observation (18.1m/s). These results imply that the NH stratospheric polar vortex in ECHAM5_AMIP2 is relatively stronger than in observation.

Table 4.2 Zonal mean zonal wind on 20hPa, 65°N for different datasets.

Dataset	$\overline{U}$ (m/s)	σ (m/s)	U_{min} (m/s)	U_{max} (m/s)	U_{median} (m/s)
NCEP/NCAR RA 20 DJFs	29.5	14.73	-20	65	28
ECHAM5_AMIP2 (T63L31) 20 DJFs	31.3	9.04	0	54	31
MAECHAM5_AMIP2 (T63L47) 20 DJFs	18.1	11.33	-22	49	18
MAECHAM5_MPIOM (T63L47) 20 DJFs	20.3	12.44	-15	54	21

Furthermore, the climatology of atmospheric temperature and stability in DJF is also analyzed for both NCEP/NCAR reanalysis data and the experiment of ECHAM5_AMIP2 (Fig.4.3), respectively. For the temperature, it can be found that in ECHAM5_AMIP2, the polar and subpolar stratosphere is colder than in observation (Fig4.3a and b). Corresponding to the results of the analysis of ZMZW (Fig.4.2), it can be concluded that the model tends to simulate a stronger and cold NH stratospheric polar vortex. About the buoyancy frequency, it shows ECHAM5_AMIP2 simulated well compared to the observation (Fig.4.3c, d). This finding can also be observed in the mean of $N^2(y,z)$ on meridional plane and its distribution on different latitudes (Fig.4.3e, f).

The frequency of negative refractive index squared f ($n_k^2 < 0$) in DJF of 1979-1999 is also analyzed for both observation and model (Fig.4.4) for ZWN1, 2 and 3 waves, respectively. The similar distributions of f ($n_k^2 < 0$) on meridional plane can be observed for both observation and model (Fig.4.4). The "channel", which implies the high possibility of planetary wave propagation from the troposphere to the stratosphere, can also be observed in analysis of simulation of the ECHAM5_AMIP2. The small area with high value of f ($n_k^2 < 0$) above the subtropical tropopause, which corresponds to the
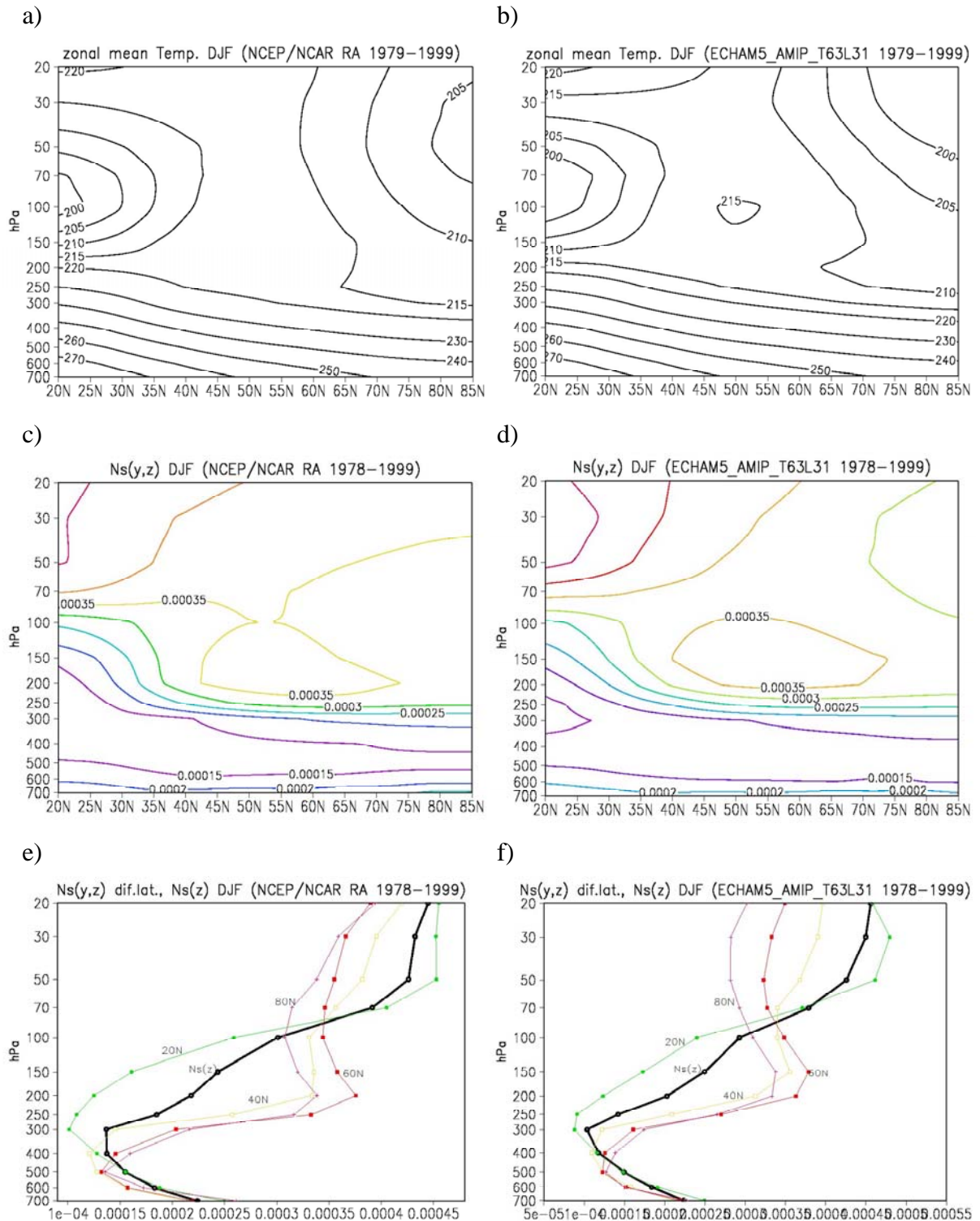
Figure 4.3. Zonal mean of temperature (K) (first row), $N^2(y,z)$ (s^{-2}) on meridiona plane (second row) and $N^2(y,z)$ on different latitude (third row) in DJF for 1979-1999 for NCEP/NCAR RA 1979-1999 (left column) and experiment of ECHAM5_AMIP2_T63L31 (right column).

center of the negative values of vertical shear of ZMZW observed in both observation (Fig.4.1c) and model (Fig.4.1d), is also shown for model. However, the differences between model and observation still can be found. The simulation of ECHAM5_AMIP2 shows that the "channel" for ZWN1 and 2 waves (Fig.4.4b, d) are relatively shallower in model. For ZWN3 wave, it is found that the possibility less than 50% for planetary wave propagation from the troposphere to the stratosphere model (Fig.4.4f). However, in observation, it can be observed that the ZWN3 wave still has more than 50% chance to propagate from the troposphere to the stratosphere by the "channel" indicated above. In short, ECHAM5_AMIP2 shows less chance for planetary wave propagation from the troposphere to the stratosphere than in observation.

Similarly, E-P flux and its divergence are also analyzed for both of observation and simulation of ECHAM5_AMIP2 in Fig.4.5 for ZWN1, 2, 3 and 1+2+3 waves, respectively. It can be concluded that the simulation of model shows good agreement with observation, although for all ZWN waves both of the vectors of E-P flux and its divergence in model (Fig.4.5h) are relatively weaker than in observation (Fig.4.5g). Comparing Fig.4.5g and Fig.4.5h, the two major branches of vectors and the two major convergences, which are observed in observation, can still be found in model. However, the amplitudes for both the vectors and the convergences are relatively smaller in model. For the two branches of vectors, the one located in the extratropical stratosphere, which represent the eddy heat flux from the troposphere to the stratosphere (Fig.4.5g), are much weaker in the model (Fig.4.5h). Another branch of vectors located in the subtropical troposphere, which can induce eddy momentum flux from the extratropical troposphere to the tropical troposphere, are also relatively weaker in the model (Fig.4.5h). About the two major convergences, although the value of the central contour of the one appeared in the troposphere is -6ms^{-1}day^{-1} in both the observation (Fig.4.5g) and the model (Fig.4.5h); the area is greatly reduced in the model. This can also be confirmed by the latitudinal distribution of the contour line with value of 3ms^{-1}day^{-1}. The contour line covers relatively smaller area (40°N – 65°N) in simulation of model than in observation (35°N – 75°N). However, for another convergence located in the subpolar stratosphere, not only the area is smaller, but also the amplitudes are also much smaller in the model (Fig.4.5h). The value of the central contour of the convergence in the subpolar stratosphere is -4ms^{-1}day^{-1} for the observation (Fig.4.5g) but -2ms^{-1}day^{-1} for the model (Fig.4.5h). Since the convergence of E-P flux represents the zonal easterly momentum forcing on zonal mean flow, it can be concluded that planetary waves induce less easterly momentum forcing on the mean flow in the stratosphere in the simulation of model. This finding can correspond to the observed stronger stratospheric polar vortex in the ECHAM5_AMIP2 (Fig.4.1b) since in Chatper 2 it has been concluded that the planetary wave induce less wave activity and eddy forcing under the strong polar vortex regime (SVR). Associated with the analysis of f (n_k^2 <0), it can be concluded that in the simulation of model ECHAM5_AMIP2, the stationary planetary waves show relatively weaker wave activities and zonal easterly forcing on mean flow in both the troposphere and stratosphere. The stronger stratospheric polar vortex (Fig.4.1b, Table 4.2) can correspond to the weaker planetary wave propagation from the troposphere to the stratosphere in model (Fig.4.5h).
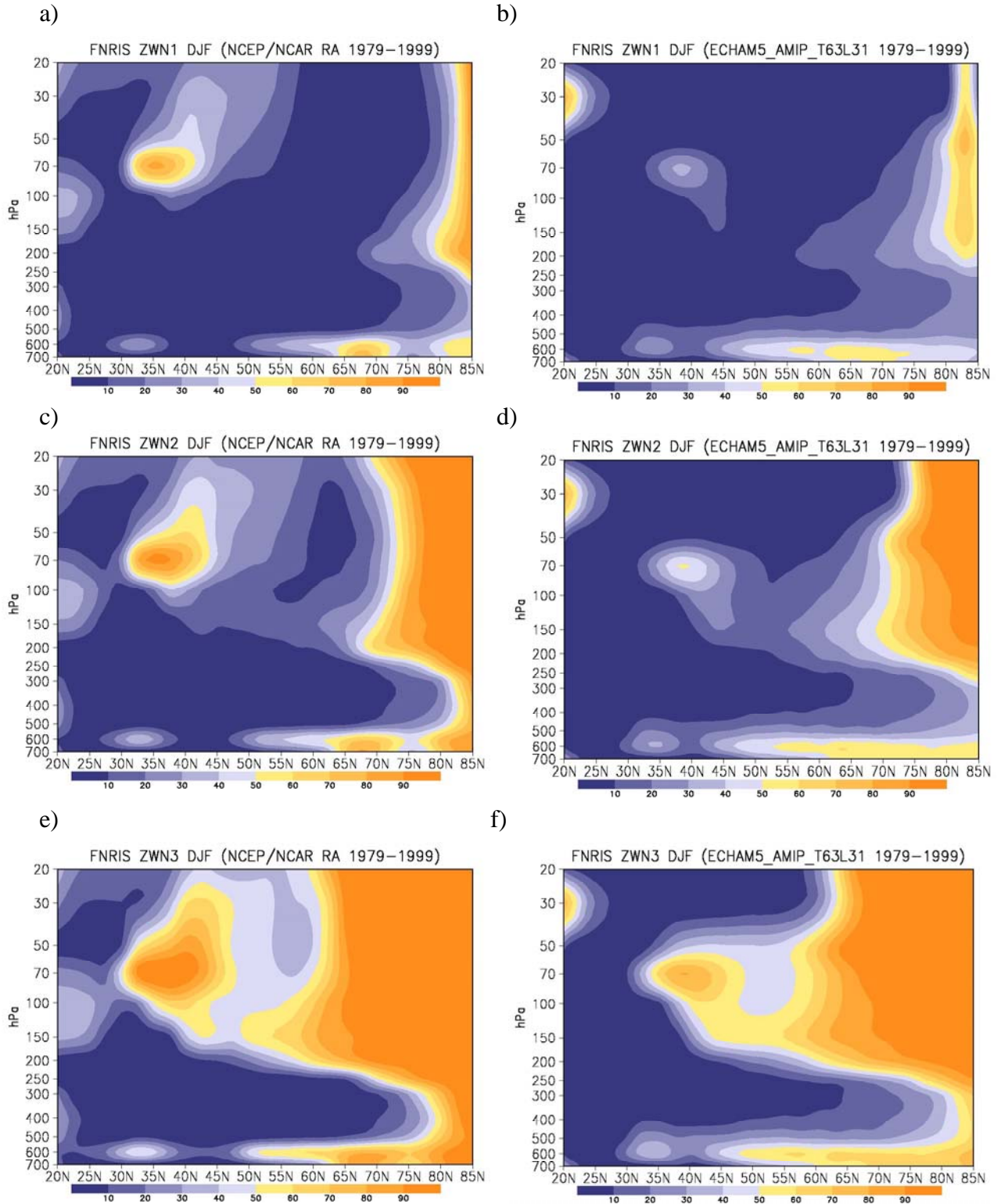
Figure 4.4. f (n_k^2 <0) for stationary planetary waves for ZWN1 (first row), ZWN2 (second row) and ZWN3 (third row) wave in DJF for 1979-1999 for NCEP/NCAR RA 1979-1999 (left column) and experiment of ECHAM5_AMIP2_T63L31 (right column). Unit of f (n_k^2 <0) is %.
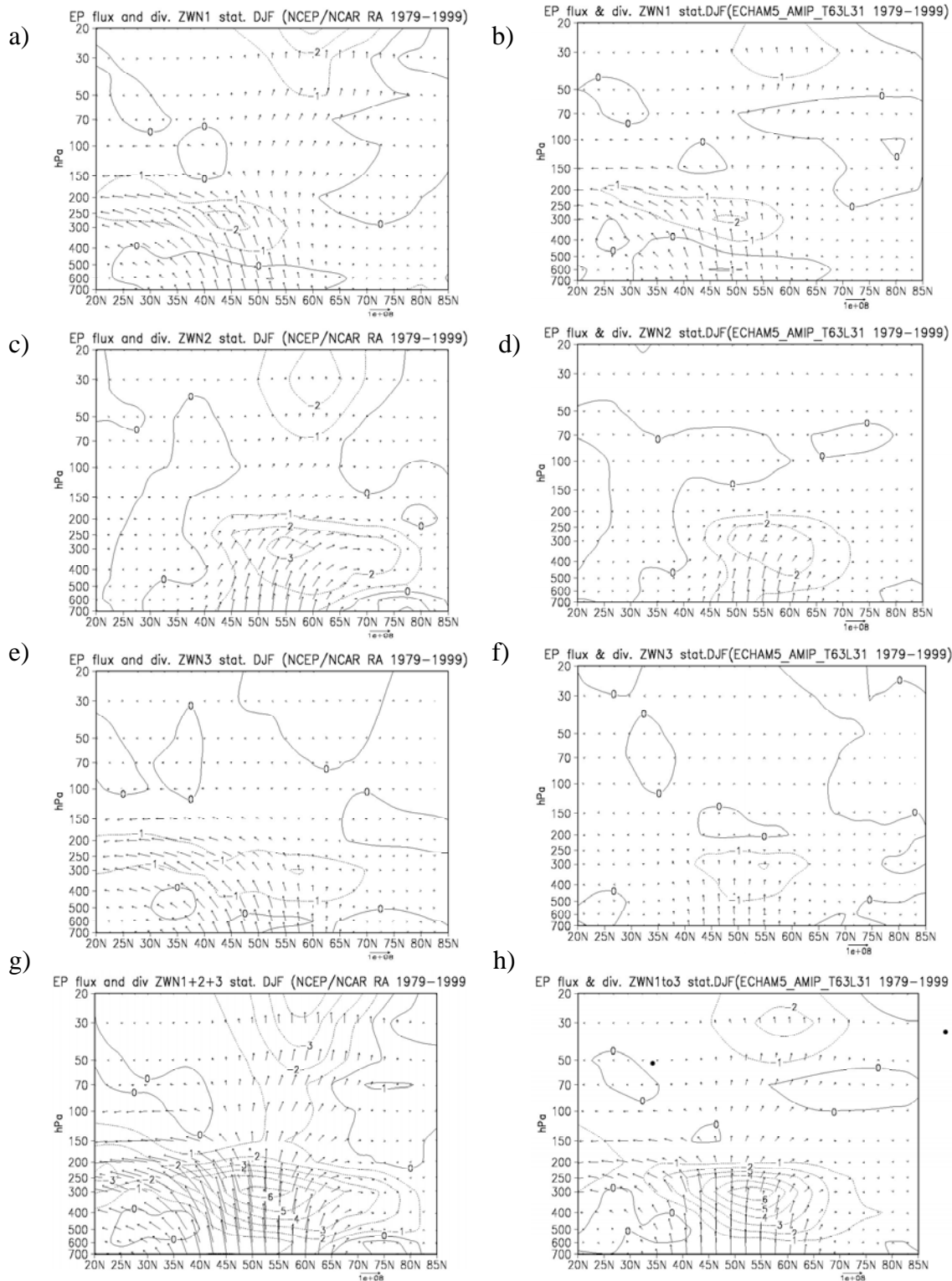
Figure 4.5. E-P flux and divergence for stationary planetary waves for ZWN1 (first row), ZWN2 (second row), ZWN3 (third row) and ZWN1+2+3 (bottom row) wave in DJF for 1979-1999 for NCEP/NCAR RA 1979-1999 (left column) and experiment of ECHAM5_AMIP2_T63L31 (right column). Divergence contour interval is $1ms^{-1}day^{-1}$, the unit of vector is kg s^{-2}.

a)

b)

c)

d)

e)

f)
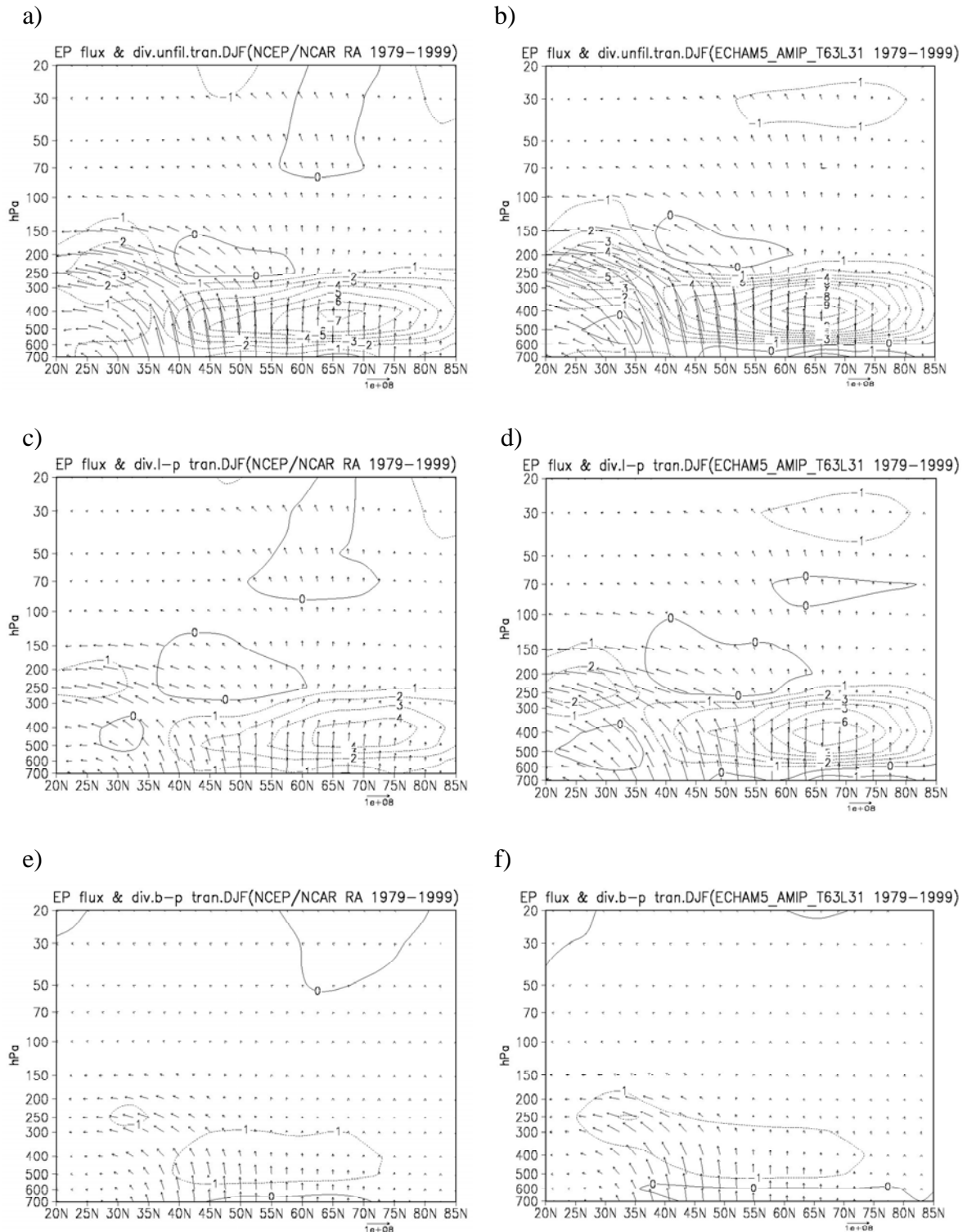
Figure 4.6. E-P flux and divergence for transient planetary waves for unfiltered wave (first row), low-pass filtered wave (second row) and band-pass filtered wave (third row) in DJF for 1979-1999 for NCEP/NCAR RA 1979-1999 (left column) and experiment of ECHAM5_AMIP2_T63L31 (right column). Divergence contour interval is $1\mathrm{ms}^{-1}\mathrm{day}^{-1}$, the unit of vector is kg s^{-2}.

Not only the stationary planetary waves, but also the climatology of transient planetary waves is also analyzed for both observation and model (Fig.4.6). Similar with the observation (Fig.4.6a, c and e), model also shows that the low frequency transient waves dominate the transient wave propagation (Fig.4.6d). However, unlike the stationary waves, transient wave in ECHAM5_AMIP2 shows stronger wave activities and easterly momentum forcing (Fig.4.6b, d) on mean flow, especially in the troposphere. The vectors in the troposphere are stronger in the model (Fig.4.6b) than in the observation (Fig.4.6a). The value of the central contour line of the convergence in the troposphere at mid latitudes is $-7 \text{ms}^{-1}\text{day}^{-1}$ for transient wave of all frequencies in observation (Fig.4.6a) but is $-9 \text{ms}^{-1}\text{day}^{-1}$ in the simulation of ECHAM5_AMIP2 (Fig.4.6b). In the stratosphere, instead of the weak divergence in the subpolar stratosphere observed for observation (Fig.4.6a), a very weak convergence ($-1 \text{ ms}^{-1}\text{day}^{-1}$) can be found for the model (Fig.4.6b). On the other hand, as indicated before, the weaker convergence in the subpolar stratosphere is also observed for stationary waves in model (Fig.4.5). This finding implies that in the simulation of ECHAM5_AMIP2, unlike the stationary waves, the transient planetary waves do not show much contribution to the construction of the stronger stratospheric polar vortex in the model.

On the other hand, the differences of both stationary and transient waves between the observation and the model can be observed not only in the stratosphere but also in the troposphere. As mentioned before, in the experiment of ECHAM5_AMIP2 from 1979-1999, the lower boundary conditions are adopted from the AMIP2 SST and sea ice concentration conditions. It should be indicated that although the AMIP2 boundary condition was preformed based on the monthly of observation of SST and sea ice concentration. Some other feedbacks from the ocean such as sea ice thickness, snow depth, and the ocean surface velocities to the atmosphere have not been considered yet in AMIP2 (Taylor et al. 2000). This approximation of boundary condition may produce some bias of the planetary wave propagation in the troposphere in the model (Fig.4.5, Fig.4.6). Therefore, in next sections, not only the effects of upper boundary level, but also the influences of the lower boundary condition on the planetary wave propagation in simulations of GCMs, will be further investigated in the GCMs.

As discussed above, the analysis of differences between observation and model has already addressed the different performance of planetary wave–mean flow interaction in model. In next sections, it will mainly focus on the model itself. The detailed results of observation will not be indicated repeatedly.

4.3.2 Influence of upper boundary level – ECHAM5_AMIP2 vs. MAECHAM5_AMIP2

It has been discussed that the importance of upper boundary for simulation of GCMs on atmospheric circulation especially on the stratospheric polar vortex (Giorgetta et al., 2002). Therefore, in this section, the similar analysis as for the simulation of ECHAM5_AMIP2 is also performed for the simulation of upper boundary level extended GCM - MAECHAM5_AMIP2. As mentioned in section 4.2, these two models have same horizontal resolutions. The vertical resolutions are also same for both models from the

surface up to 10hPa. However, as shown in Table 4.1, there are 16 additional levels above 10hPa up to 0.01hPa in the middle atmospheric model MAECHAM5_AMIP2. The low boundary conditions are adopted from AMIP2 for both models.

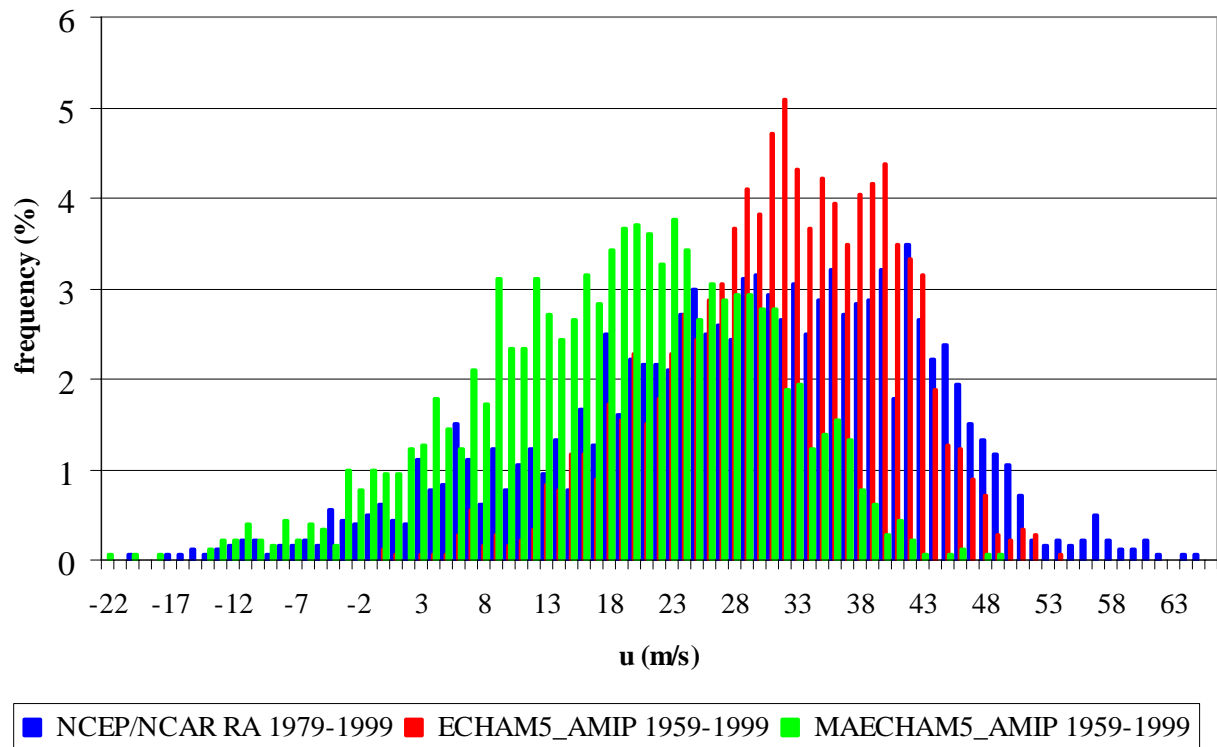## Frequency of ZMZW on 20hPa, 65N in DJF

Figure 4.7. Distribution of frequencies of values of zonal mean zonal wind (ZMZW) on 20hPa, 65N of DJF for data sets: NCEP RA 1958-2002; ECHAM5_AMIP2_T63L31 1979-1999; and MAECHAM5_AMIP2_T63L47 1979-1999Unit of ZMZW is m/s. Unit of frequency is %.

First of all, the distribution of frequencies of ZMZW on 20hPa, 65°N in DJF from 1979-1999 is also shown in Fig.4.7 for simulations of ECHAM5_AMIP2, MAECHAM5_AMIP2 and with the observations reference NCEP/NCAR reanalysis dataset. It can be observed that similar as NCEP/NCAR reanalysis data, the distribution of the frequency of ZMZW for simulation of MAECHAM5_AMIP2 is relatively wider than ECHAM5_AMIP2, although the shift to lower value happened for MAECHAM5_AMIP2. Instead of the high frequencies of high values of ZMZW (30m/s – 40m/s) in ECHAM5_AMIP2, the higher frequencies of ZMZW mostly distribute around relatively smaller values of ZMZW (15/ms – 25m/s) in MAECHAM5_AMIP2 (Fig.4.7). In spite of the shift of the distribution of the frequencies to lower values of ZMZW, this analysis shows that the climatology of stratospheric polar vortex has been more properly illustrated in MAECHAM5_AMIP2. Similar conclusion can also be drawn from Table 4.2. In Table 4.2, $\overline{U}$ on 20hPa, 65°N of DJF from 1979-1999 for MAECHAM5_AMIP2 is much smaller (18.1m/s) than the one for ECHAM5_AMIP2 (31.3m/s). However, this value is also much smaller than the one for NCEP/NCAR reanalysis data (29.5m/s). These results imply that the bias of stronger stratospheric polar vortex in the model with lower upper boundary level (10hPa) - ECHAM5_AMIP2, can be improved in the model with higher upper boundary level (0.01hPa) – MAECHAM5_AMIP2, although the polar vortex is relatively weaker in the middle atmosphere model compared with observation.

The finding drawn above can also be shown by the distribution of ZMZW and its vertical shear on meridional plane. Fig.4.8 shows the ZMZW and vertical shear of ZMZW for MAECHAM5_AMIP2. The differences between ECHAM5_AMIP2 and MAECHAM5_AMIP2 can be observed in Fig.4.8c and Fig.4.8d for ZMZW and its vertical shear, respectively. As indicated before, the polar vortex in MAECHAM5_AMIP2 (Fig.4.8a) is much weaker than in ECHAM5_AMIP2 (Fig.4.1b) and observation (Fig.4.1a). The values of vertical shear of ZMZW in the stratosphere are also relatively smaller in MAECHAM5_AMIP2 (Fig.4.8b) compared with ECHAM5_AMIP2 (Fig.4.8d) and observation (Fig.4.8c). On the other hand, Fig.4.8c and Fig.4.8d show that the significant differences between ECHAM5_AMIP2 and MAECHAM5_AMIP2 are mainly observed in the stratosphere at middle and high latitudes. This finding implies that the major influences of the altitude of the upper boundary level in models on the atmospheric mean flow mainly locate in the middle and high latitudinal stratosphere .

Not only the change of the polar vortex, the distribution of temperature (Fig.4.9a) and the difference of temperature between ECHAM5_AMIP and MAECHAM5_AMIP2 (Fig.4.9c) show that but also the colder bias in the polar stratosphere can be modified with the improved upper boundary. On the other hand, it should be mentioned that the significant differences between ECHAM5_AMIP2 and MAECHAM5_AMIP2 can also be observed in the stratosphere (Fig.4.9c and Fig.4.9d) like the analysis of zonal wind (Fig.4.8c) and wind shear (Fig.4.8d). However, unlike the wind and wind shear, the differences of the temperature and buoyancy frequency mainly located at high latitudes. For buoyancy frequency, significant difference even extends to the polar troposphere.
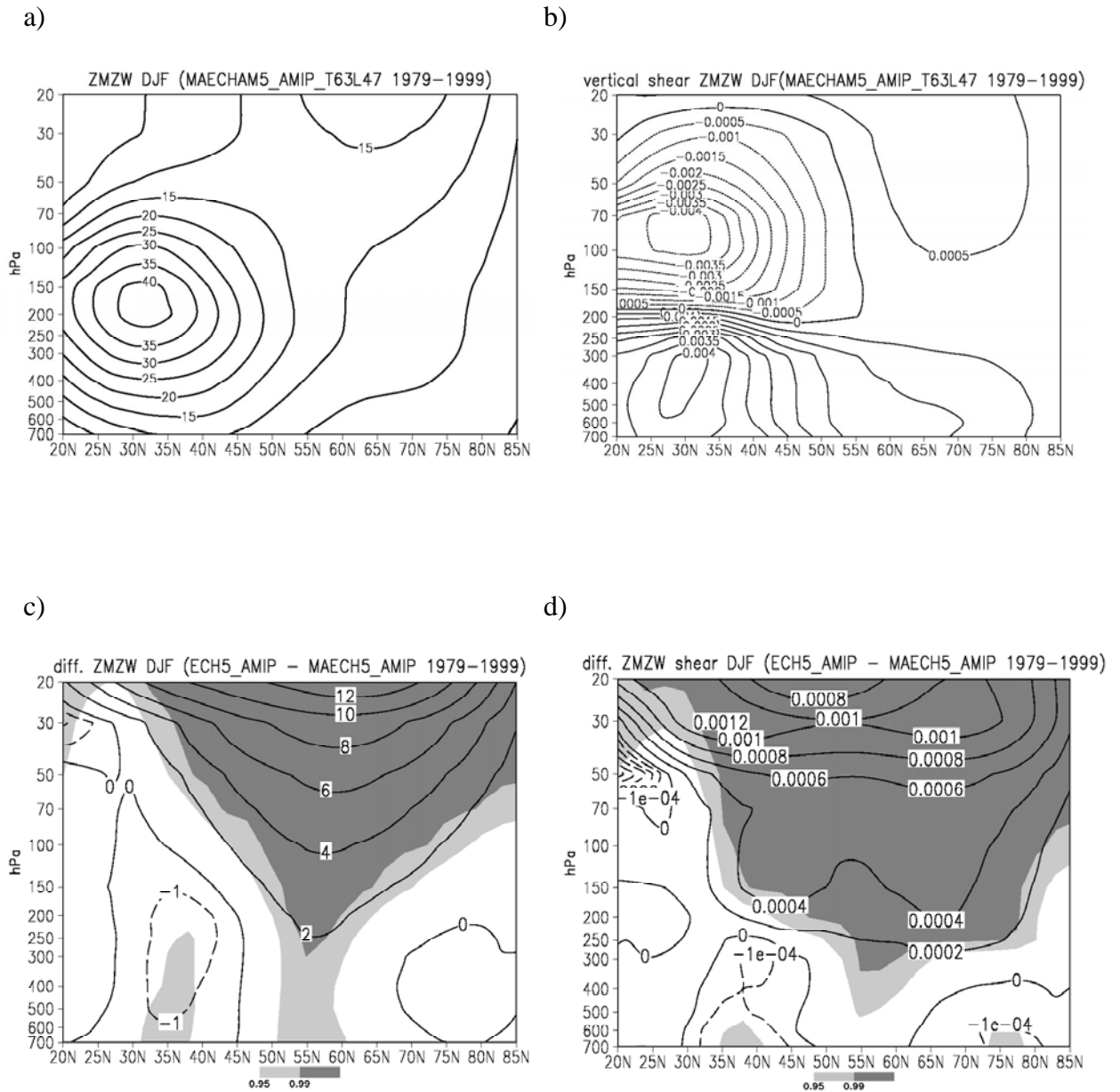
a)

b)

c)

d)

Figure 4.8. Zonal mean zonal wind (m/s) (left column) and vertical shear of zonal mean zonal wind (s^{-1}) (right row) in DJF of 1979-1999 for experiment MAECHAM5_AMIP_T63L47 (first row), and differences with experiment ECHAM5_AMIP2_T63L31 (second row). Area with significant level above 95% is lightly shaded and with significant level above 99% is heavily shaded.
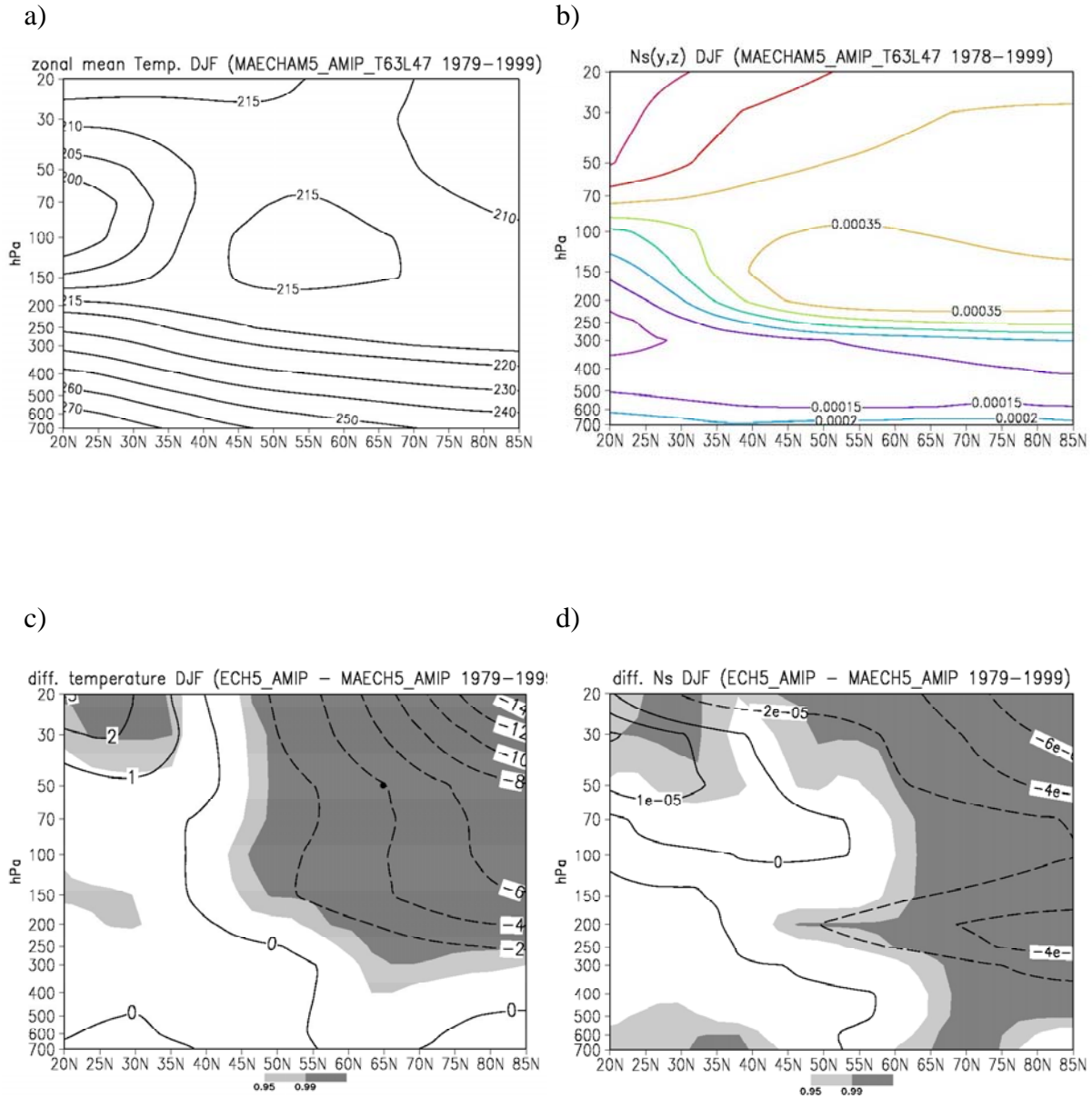
a)

b)

c)

d)

Figure 4.9. Zonal mean of temperature (K) (left column) and buoyancy frequency (s^{-2}) (right column) in DJF of 1979-1999 for experiment MAECHAM5_AMIP2_T63L47 (first row), and differences with experiment ECHAM5_AMIP2_T63L31 (second row). Area with significant level above 95% is lightly shaded and with significant level above 99% is heavily shaded.

The influences of higher upper boundary level in model can also be observed for the analysis of the atmospheric controlling on stationary planetary wave propagation from the troposphere to the stratosphere. Fig.4.10 shows the frequency of negative refractive index squared f (n_k^2<0) for simulation of MAECHAM5_AMIP2 in DJF from 1979-1999 and the difference of f (n_k^2 <0) between simulations of ECHAM5_AMIP2 and MAECHAM5_AMIP2. The relatively bigger chance for ZWN1 and 2 waves propagated from the troposphere to the stratosphere for ECHAM5_AMIP2 compared with MAECHAM5_AMIP2 can be observed in Fig.4.10b and c, respectively. However, similar with ECHAM5_AMIP2, the ZWN3 wave still has less chance to propagate from the troposphere to the stratosphere in MAECHAM5_AMIP2 (Fig.4.10e).

Fig.4.11 shows the E-P flux and divergence for simulation of MAECHAM5_AMIP2 and the differences between ECHAM5_AMIP2 and MAECHAM5_AMIP2. Similar with ECHAM5_AMIP2, although the main patterns of two major branches of vectors and two major convergences can still be observed as shown in the observation (Fig.4.5, left column), the amplitudes of vectors and divergences are still fairly weaker in MAECHAM5_AMIP2 (Fig.4.11, left column). It should be noted that the differences between two models indicate that the wave activities are even weaker in MAECHAM5_AMIP2 than in ECHAM5_AMIP2 (Fig.4.11). The differences of divergence of E-P flux show that in MAECHAM5_AMIP2, planetary waves induce much less easterly momentum forcing in both the subpolar troposphere and the subpolar stratosphere than in the observation (Fig.4.5 left column) and in the simulation of ECHAM5_AMIP2. The stronger divergences in the simulation of ECHAM5_AMIP2 can be found around 150hPa to 70hPa at high latitudes (Fig.4.11h). These findings mean that although the higher upper boundary level can help to modified the bias of stronger polar vortex in the model with relatively lower upper boundary level, the problem of weaker stationary planetary wave propagation in the model still exists.

Similarly, about the transient planetary waves, the stronger vectors and convergence of E-P flux can also be observed in the troposphere for the simulation of MAECHAM5_AMIP2 (Fig.4.12a, c). It is found that instead of the stronger convergence in the subpolar stratosphere in ECHAM5_AMIP2 (Fig.4.6a, c), the weaker convergence is observed in the simulation of MAECHAM5_AMIP2 (Fig.4.12a, c). This finding can be confirmed by the differences of the E-P flux and divergence between ECHAM5_AMIP2 and MAECHAM5_AMIP2 (Fig.4.12b, d). Similarly, the domination of low frequency transient waves is also simulated well by MAECHAM5_AMIP2 (Fig.4.12 left column).

To shortly summarize, the bias of the stronger stratospheric polar vortex in ECHAM5_AMIP2 can be partly modified in MAECHAM5_AMIP2. This implies that the improvement can be induced by extending upper levels of GCMs. However, the weaker stationary wave propagation from the troposphere to the stratosphere, stronger transient wave activities in the troposphere can be observed in the simulations of both ECHAM5_AMIP2 and MAECHAM5_AMIP2. On the other hand, the weaker wave activities for stationary waves and also, stronger wave activities for transient waves, probably are caused by the lower boundary condition adopted from AMIP2, which only
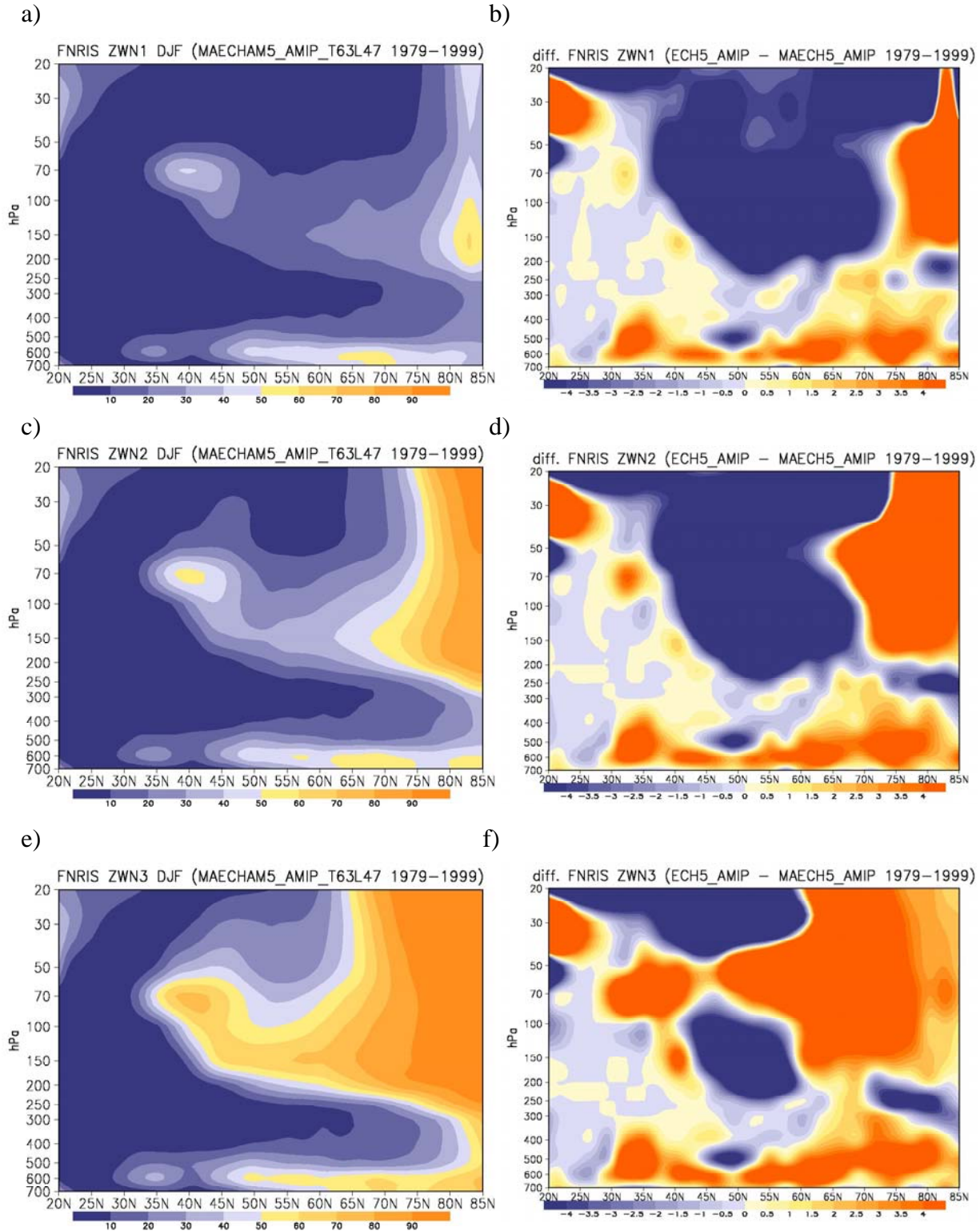
a)

b)

c)

d)

e)

f)

Figure 4.10. f (n_k^2 <0) for stationary planetary waves or ZWN1 wave (first row), ZWN2 wave (second row) and ZWN3 wave (bottom row) in DJF of 1979-1999 for experiment MAECHAM5_AMIP2_T63L47 (left column), and differences with experiment ECHAM5_AMIP2_T63L31 (right column). Unit of f (n_k^2 <0) is %.
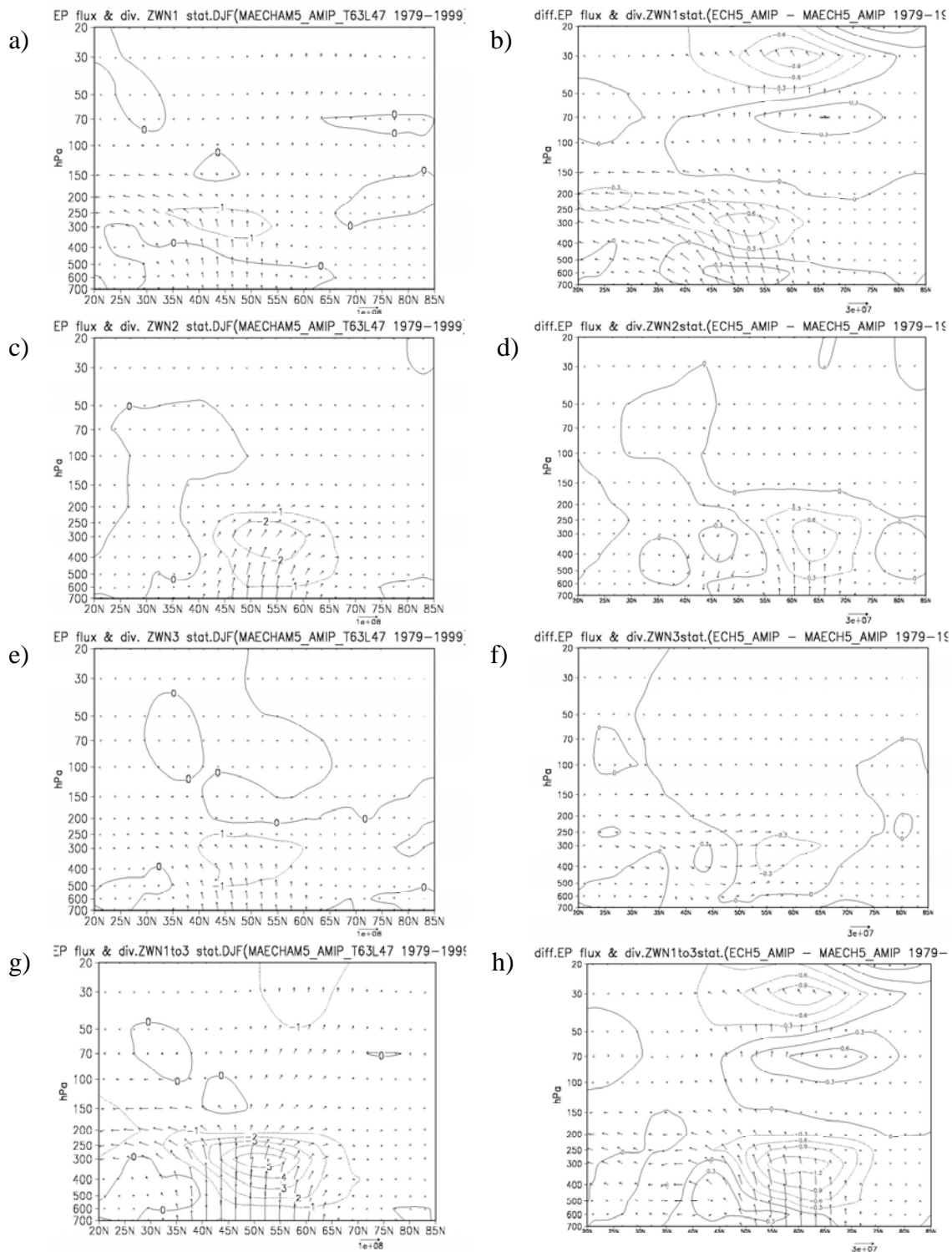
Figure 4.11. E-P flux and divergence for stationary planetary waves for ZWN1 wave (first row), ZWN2 wave (second row), ZWN3 wave (third row) and ZWN1+2+3 wave (bottom row) in DJF of 1979-1999 for experiment MAECHAM5_AMIP2_T63L47 (left column), and differences with experiment ECHAM5_AMIP2_T63L31 (right column). Divergence contour interval is $1ms^{-1}day^{-1}$ and $0.3m^{-1}day^{-1}$ for difference, the unit of vector is kg s^{-2}.

a)

EP flux & div.unfil.tran.DJF(MAECHAM5_AMIP_T63L47 1979-1999)

b)

diff. EP flux & div. u-f. tr.(ECH5_AMIP - MAECH5_AMIP 1979-19

c)

EP flux & div.l-p tran.DJF(MAECHAM5_AMIP_T63L47 1979-1999)

d)

diff. EP flux & div. l-p. tr.(ECH5_AMIP - MAECH5_AMIP 1979-19

e)

EP flux & div.b-p tran.DJF(MAECHAM5_AMIP_T63L47 1979-1999)

f)

diff. EP flux & div. b-p. tr.(ECH5_AMIP - MAECH5_AMIP 1979-19
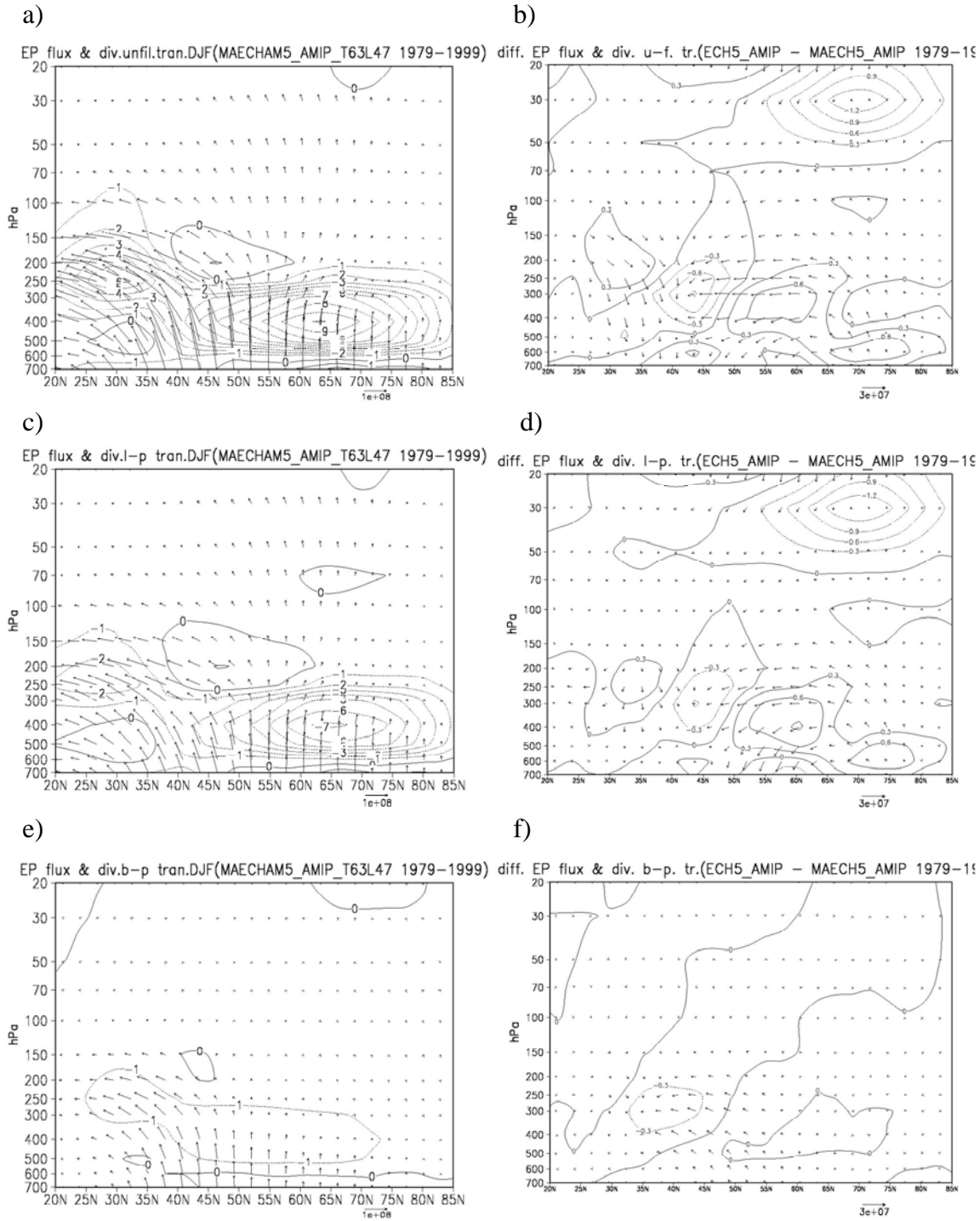
Figure 4.12. E-P flux and divergence for transient planetary waves for unfiltered wave (first row), low-pass filtered wave (second row), and band-pass filtered wave (third row) in DJF of 1979-1999 for experiment MAECHAM5_AMIP2_T63L47 (left column), and differences with experiment ECHAM5_AMIP2_T63L31 (right column). Divergence contour interval is $1 \text{ms}^{-1}\text{day}^{-1}$ and $0.3\text{m}^{-1}\text{day}^{-1}$ for difference, the unit of vector is kg s^{-2}.

considered SST and SIC. The other important feedbacks from ocean such as sea ice thickness, snow depth, and the ocean surface velocities, have not been considered yet (Taylor et al. 2000). In next section, the impacts of feedback from ocean on the simulation of climatology of atmospheric circulation and planetary wave propagation in the model will be investigated further.

4.3.3 Feedback from ocean – MAECHAM5_AMIP2 vs. MAECHAM5_MPIOM

In order to study the influences of boundary condition especially the influences from ocean on atmospheric circulation and planetary wave propagation in models, the simulation of the middle atmospheric model coupled with ocean general circulation model MAECHAM5_MPIOM is investigated in this section.

From the analysis of the distribution of frequencies of ZMZW on 20hPa, 65°N, it is found that the frequencies of ZMZW in MAECHAM5_MPIOM still distribute around lower values of ZMZW than those in NCEP/NCAR reanalysis data. This implies that the stratospheric polar vortex is also weaker in the simulation of this model than in observation. However, the frequencies of higher values of ZMZW (>30m/s) are bigger and of lower values of ZMZW (<19m/s) are smaller in MAECHAM5_MPIOM than in MAECHAM5_AMIP2. From Table 4.2, it is found that U_{max} and U_{min} on 20hPa, 65°N in NH boreal winter from 1979 to 1999 in MAECHAM5_MPIOM are 54m/s and –15m/s, respectively. Both of them are bigger than those in MAECHAM5_AMIP2 (U_{max}=49/ms, U_{min}=-22m/s), although U_{max} and U_{min} in simulations of MAECHAM5_MPIOM and MAECHAM5_AMIP2 are smaller than in NCEP/NCAR reanalysis data. Similar conclusion can also be drawn for the mean value of ZMZW ($\overline{U}$), and the median value of ZMZW for the frequency distribution (U_{median}).

It can be found that the stratospheric polar vortex is relatively weaker in simulation of MAECHAM5_MPIOM (Fig.4.14a) in observation (Fig.4.1a). Similarly, the amplitudes of vertical shear of ZMZW in the subpolar lower stratosphere are also smaller in MAECHAM5_MPIOM (Fig.4.14c) than in observation (Fig.4.1c). However, compared with MAECHAM5_AMIP2, the differences of ZMZW between these two models indicate the stratospheric polar vortex in MAECHAM5_MPIOM is stronger than in MAECHAM5_AMIP2 (Fig.4.14b). The same conclusion can also be drawn for the vertical shear of ZMZW in the subpolar lower stratosphere. On the other hand, Fig.4.15a shows that the polar stratosphere is slightly warmer in MAECHAM5_MPIOM than in observation (Fig.3a). However, the differences of zonal mean temperature between MAECHAM5_AMIP2 and MAECHAM5_MPIOM show that the polar stratosphere is colder in latter. There is no significant difference of buoyancy frequency between the simulation of MAECHAM5_MPIOM (Fig.4.15c) and observation (Fig.4.3c), neither between MAECHAM5_MPIOM and MAECHAM5_AMIP2 (Fig.4.15d) can be found. This implies that the models are able to simulate well the climatology of atmospheric stability in Northern Hemisphere winter.
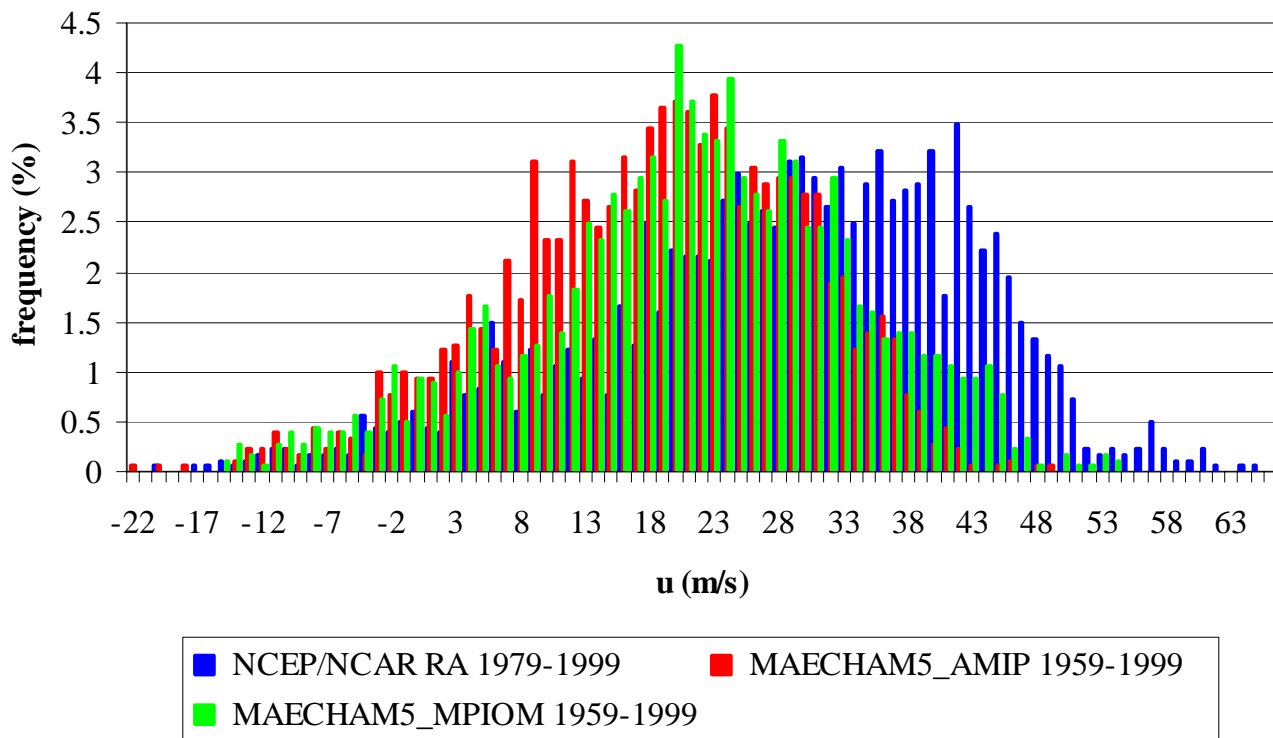
Frequency of ZMZW on 20hPa, 65N in DJF

Figure 4.13. Distribution of frequencies of values of zonal mean zonal wind (ZMZW) on 20hPa, 65N of DJF for data sets: NCEP RA 1958-2002; MAECHAM5_AMIP2_T63L47 1979-1999; and MAECHAM5_MPIOM_T63L47 1979-1999Unit of ZMZW is m/s. Unit of frequency is %.
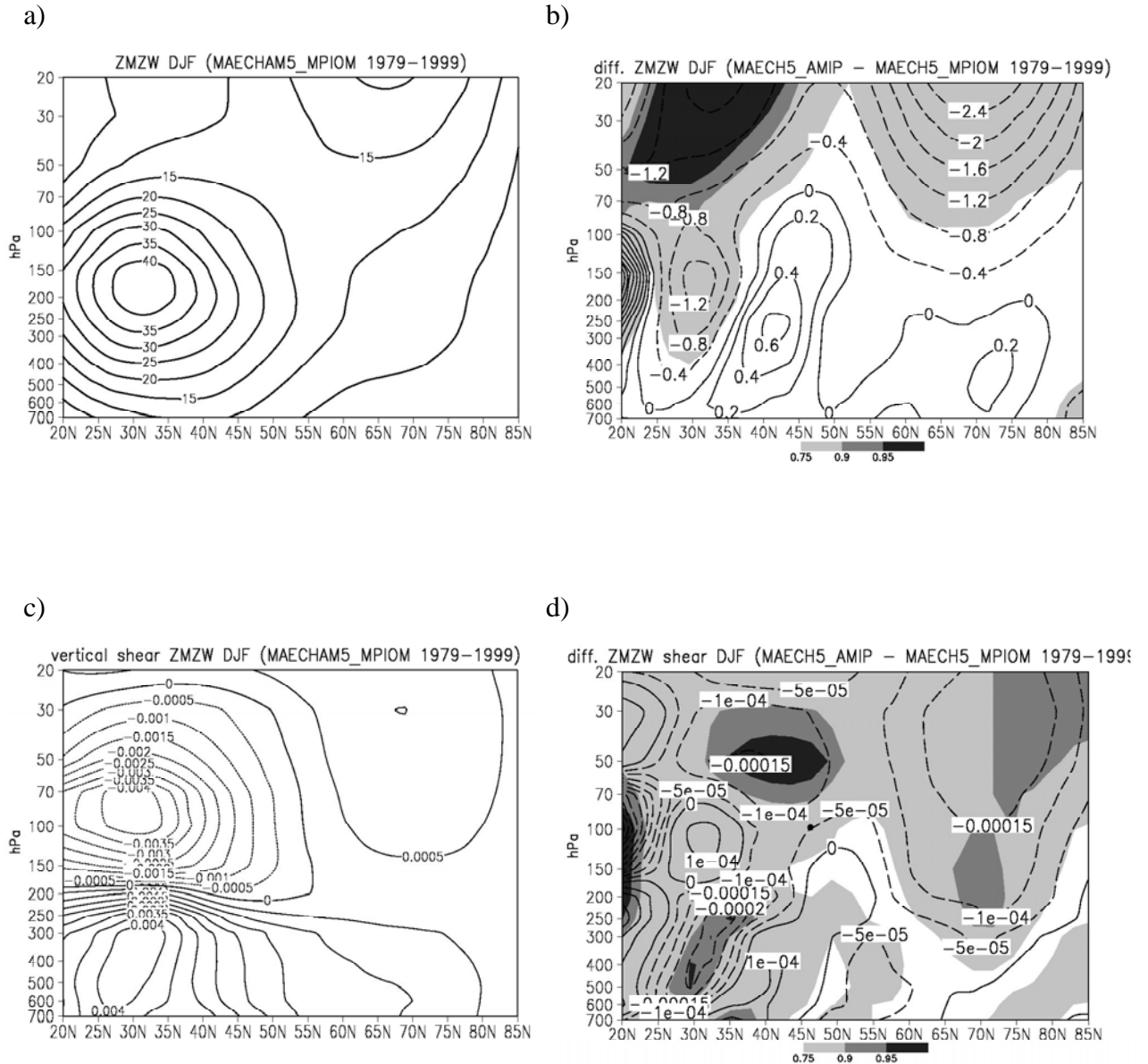
a)

b)

c)

d)

Figure 4.14. Left column: zonal mean zonal wind (m/s) (first row) and vertical shear of zonal mean zonal wind (s^{-1}) (second row) in DJF of 1979-1999 for experiment MAECHAM5_MPIOM_T63L47. Right column: differences between experiments MAECHAM5_AMIP2_T63L47 and MAECHAM5_MPIOM_T63L47. Area with significant level above 75% is lightly shaded, above 90% is medium shaded and above 95% is heavily shaded.

a)

b)

c)

d)
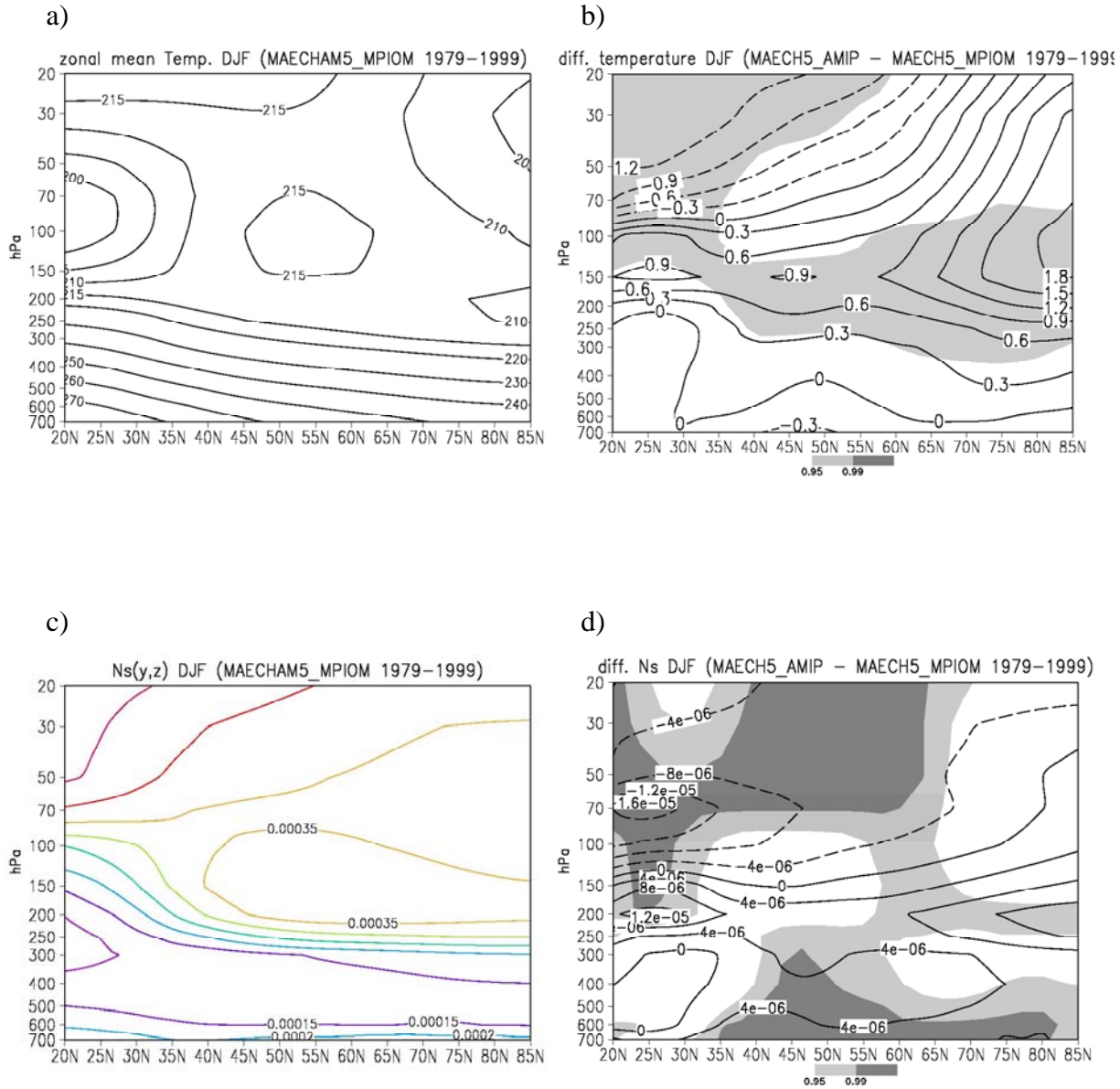
Figure 4.15. Left column: zonal mean of temperature (K) (first row) and buoyancy frequency on meridional plane (s^{-2}) (second row) in DJF of 1979-1999 for experiment MAECHAM5_MPIOM_T63L47. Right column: differences between experiments MAECHAM5_AMIP2_T63L47 and MAECHAM5_MPIOM_T63L47. Area with significant level above 95% is lightly shaded, and with significant level above 99% is heavily shaded.

The analysis of f (n_k^2<0) shows that the atmosphere shows less chance for stationary waves to propagate from the troposphere to the stratosphere in simulation of MAECHAM5_MPIOM for ZWN1, 2 and 3 (Fig.4.16, left column), compared to observation (Fig.4.4, left column). However, there is no significant difference of f (n_k^2<0) between the simulations of MAECHAM5_MPIOM and MAECHAM5_AMIP2 (Fig.4.16, right column). The values of the differences are smaller (-4% to 4%). This finding implies that the influences of ocean on atmospheric state for possibility of stationary wave propagation from the troposphere to the stratosphere can not be observed here.

Fig.4.17 shows E-P flux and its divergence in MAECHAM5_MPIOM and the difference between MAECHAM5_AMIP2 and MAECHAM5_MPIOM. It can be found that the wave activities and eddy forcing on mean flow are weaker in both the troposphere and stratosphere for stationary ZWN1, 2, 3 and 1+2+3 waves in MAECHAM5_MPIOM (Fig.4.17, left column) than in observation (Fig.4.5, left column). On the other hand, the main differences between these two GCMs are located in the troposphere (Fig.4.17, right column). For ZWN1 wave, planetary waves have slightly more eddy heat flux in the troposphere at middle and high latitudes in MAECHAM5_MPIOM (Fig.4.17a). However, for ZWN2 and 3 waves, the stationary waves show stronger eddy heat flux from lower to upper troposphere and more convergence in the troposphere in MAECHAM5_AMIP2 (Fig.4.17d, f). No big difference between these two models can be found in the stratosphere except for a slightly stronger convergence in the polar stratosphere in MAECHAM5_AMIP2 (Fig.4.17h). This relatively stronger convergence, which represents zonal easterly forcing induced by planetary waves on mean flow, can correspond to the weaker stratospheric polar vortex in MAECHAM5_AMIP2 (Fig.4.14b). On the other hand, as indicated before, the main differences between the approaches of the simulations of two GCMs, are the adopted lower boundary conditions. In MAECHAM5_AMIP2, the boundary conditions are adopted from AMIP2 monthly mean observational SST and sea ice concentration. However, in the simulation of MAECHAM5_MPIOM the lower boundary conditions are supplied by the coupled ocean model – MPIOM. The different lower boundary conditions can contribute to the observed major differences of stationary wave activities and eddy forcing in the troposphere.

Moreover, the analysis of E-P flux and its divergence of transient waves also show the major difference in the troposphere between the simulations of MAECHAM5_AMIP2 and MAECHAM5_MPIOM (Fig.4.18, right column). Similar as the stationary waves, the stronger convergence of transient waves in the subpolar and polar stratosphere for transient waves with all frequency (Fig.4.18b), which corresponds with the stronger zonal easterly forcing on mean flow therefore the weaker stratospheric polar vortex, can also be found in MAECHAM5_AMIP2. It should be indicated that the wave activities and eddy forcing in the troposphere are also stronger for transient waves with all frequency (Fig.4.18a), with lower frequency (Fig.4.18c) and with high frequency (Fig.4.18e) in MAECHAM5_MPIOM, than in both observation (Fig.4.6, left column) and MAECHAM5_AMIP2 (Fig.4.12, left column).

Combining the analyses E-P flux for stationary and transient waves in the experiments of MAECHAM5_AMIP2 and MAECHAM5_MPIOM, it can be found that the major
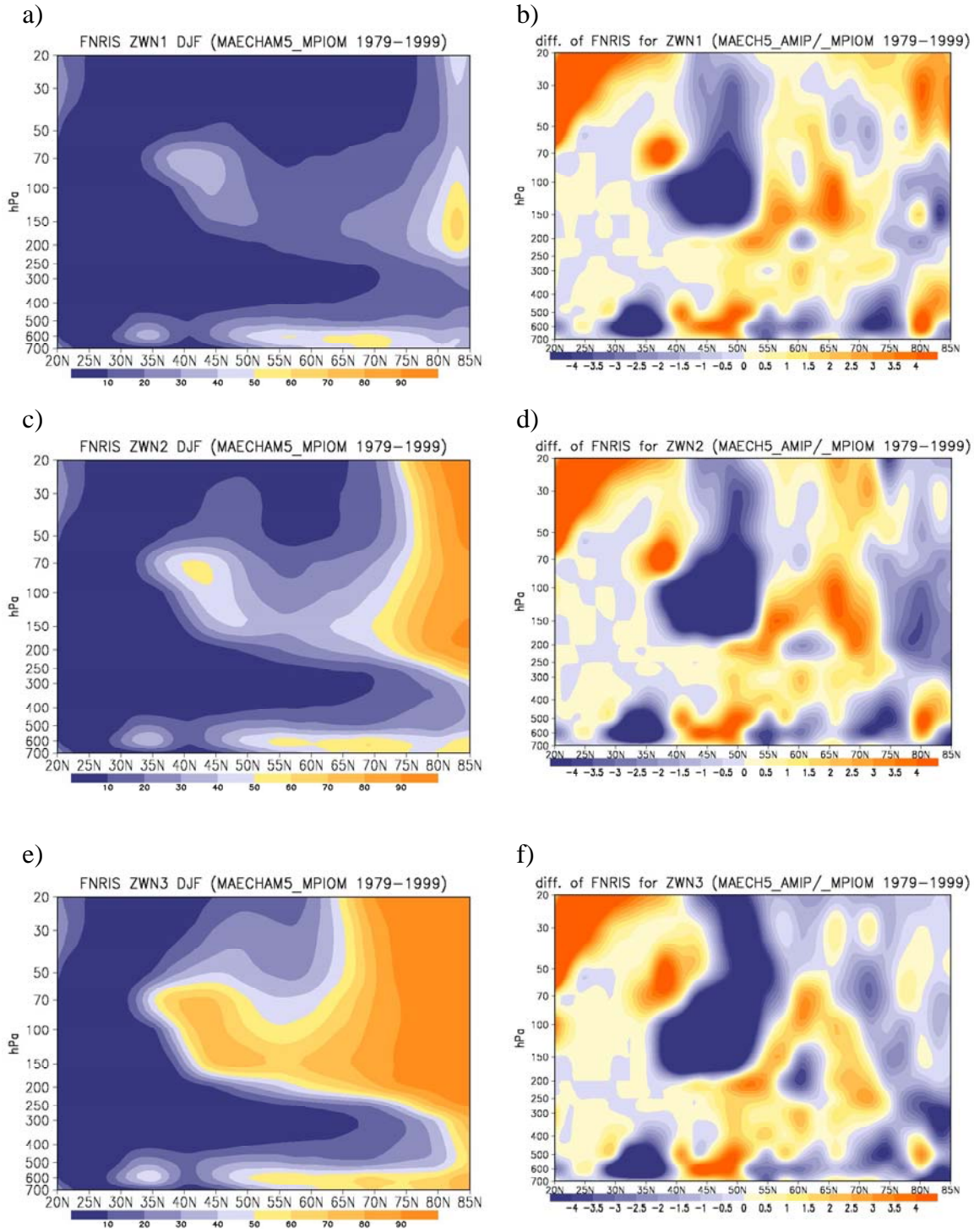
Figure 4.16. Left column: f ($n_k^2 < 0$) for stationary planetary waves in DJF of 1979-1999 for experiment of MAECHAM5_MPIOM for ZWN1 wave (first row), ZWN2 wave (second row), and ZWN3 wave (third row). Right column: differences between experiments of MAECHAM5_AMIP2_T63L47 and MAECHAM5_MPIOM_T63L47. Unit of f ($n_k^2 < 0$) is %.
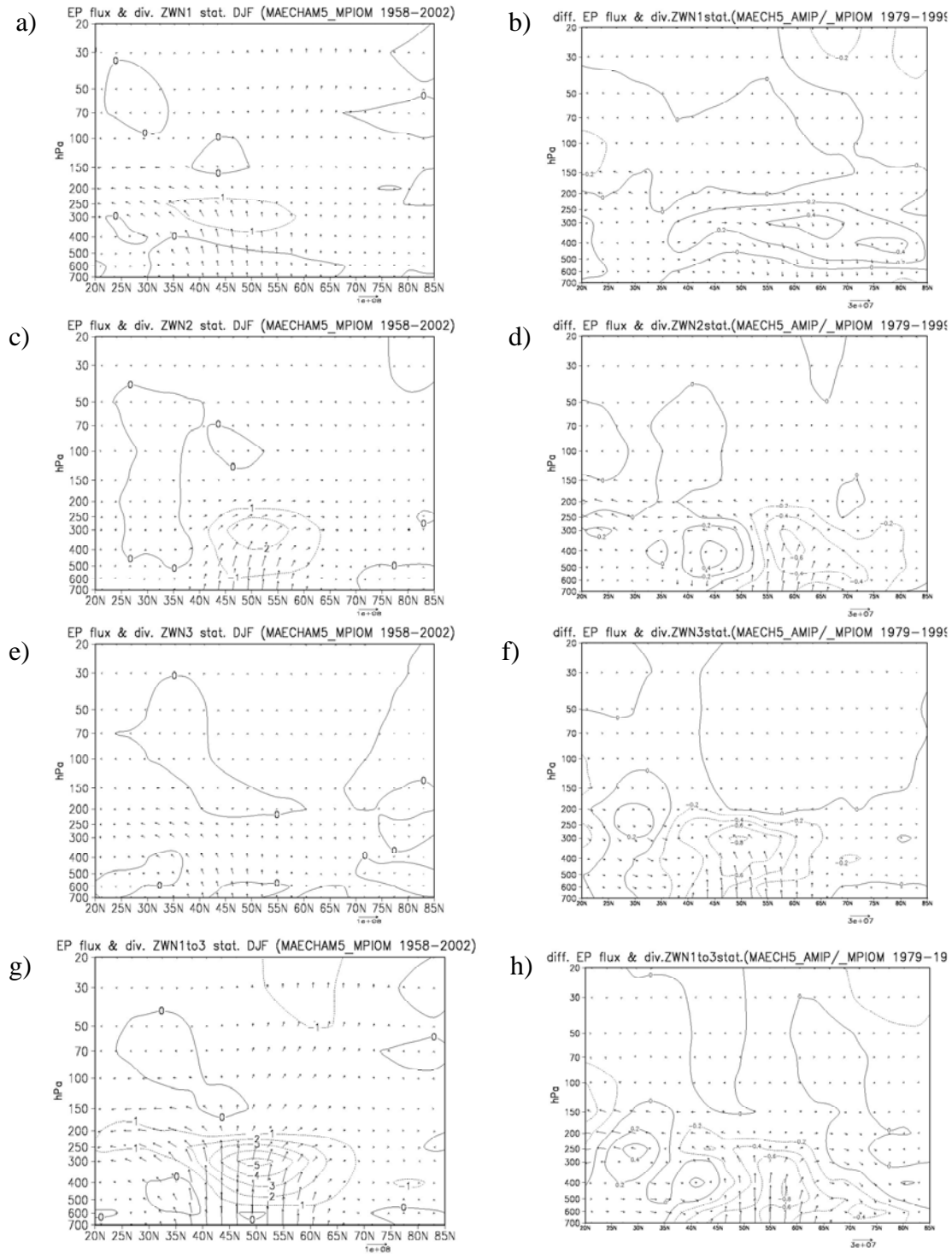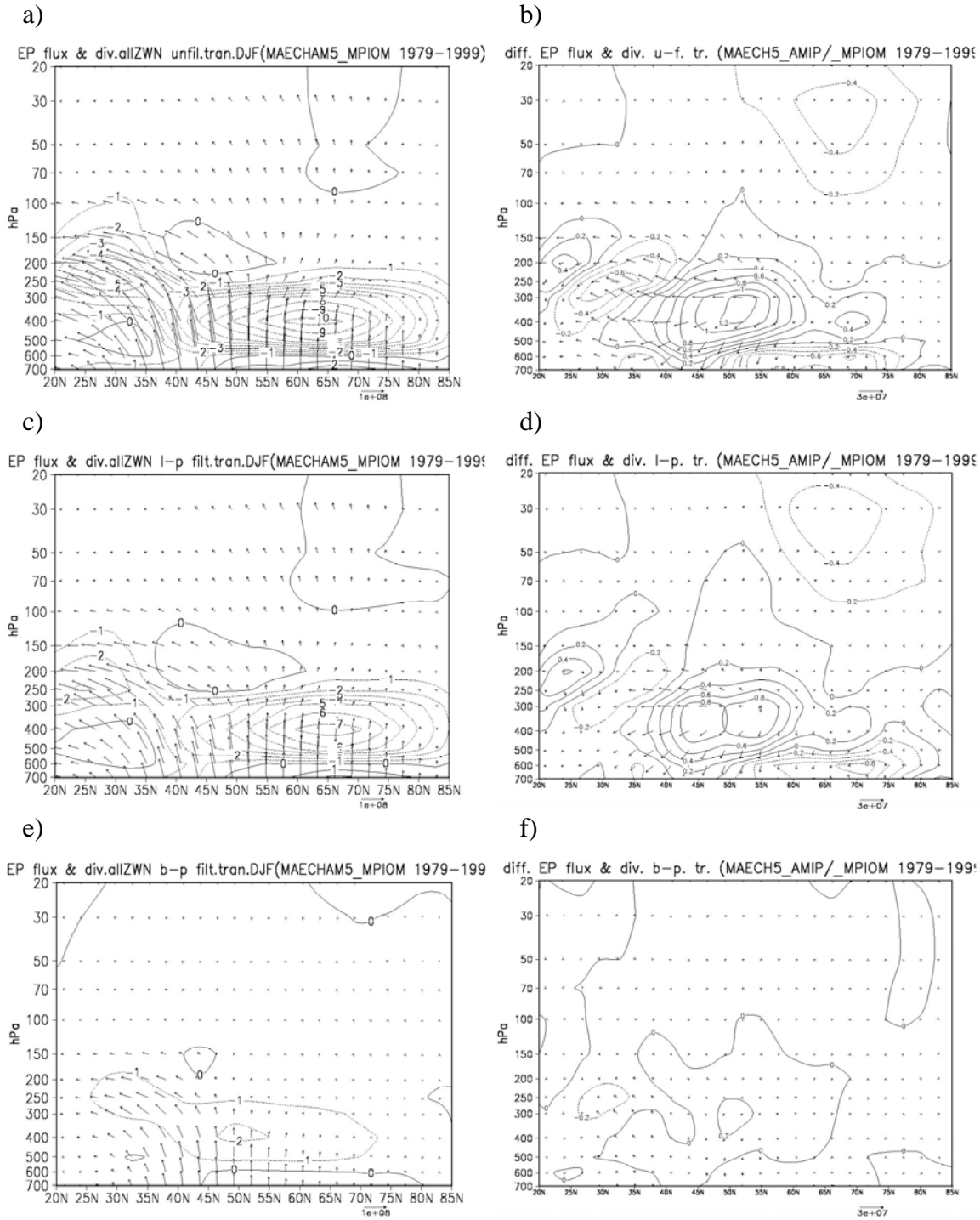
Figure 4.17. Left column: E-P flux and divergence for stationary planetary waves in DJF of 1979-1999 for experiment of MAECHAM5_MPIOM for ZWN1 wave (first row), ZWN2 wave (second row), ZWN3 wave (third row) and ZWN1+2+3 wave (bottom row). Right column: differences between experiments MAECHAM5_AMIP2_T63L47 and MAECHAM5_MPIOM_T63L47. Divergence contour interval is 1ms^{-1}day^{-1} and 0.2m^{-1}day^{-1} for difference, the unit of vector is kg s^{-2}.

a)

EP flux & div.allZWN unfil.tran.DJF(MAECHAM5_MPIOM 1979-1999)

b)

diff. EP flux & div. u-f. tr. (MAECH5_AMIP/_MPIOM 1979-1999)

c)

EP flux & div.allZWN l-p filt.tran.DJF(MAECHAM5_MPIOM 1979-1999)

d)

diff. EP flux & div. l-p. tr. (MAECH5_AMIP/_MPIOM 1979-1999)

e)

EP flux & div.allZWN b-p filt.tran.DJF(MAECHAM5_MPIOM 1979-199)

f)

diff. EP flux & div. b-p. tr. (MAECH5_AMIP/_MPIOM 1979-1999)

Figure 4.18. Left column: E-P flux and divergence for transient planetary waves in DJF of 1979-1999 for experiment of MAECHAM5_MPIOM for unfiltered wave (first row), low-pass filtered wave (second row), and band-pass filtered wave (third row). Right column: differences between experiments MAECHAM5_AMIP2_T63L47 and MAECHAM5_MPIOM_T63L47. Divergence contour interval is 1 ms^{-1}day^{-1} and 0.m^{-1}day^{-1} for difference, the unit of vector is kg s^{-2}.

differences between these two models mainly locate in the troposphere, although there is a relatively stronger convergence in the subpolar and polar stratosphere observed in simulation of MAECHAM5_AMIP2, which corresponds to the slightly weaker polar vortex in this model. These differences in the troposphere probably correspond to the different lower boundary conditions adopted in these two models. The influences of ocean on atmospheric circulation and planetary wave propagation are mainly shown in the troposphere.

4.4 Summary

In this chapter, the performance of three GCMs on atmospheric circulation and planetary wave propagation in Northern Hemisphere winter has been investigated. We analyzed the simulations of ECHAM5_AMIP2, the middle atmospheric GCM – MAECHAM5_AMIP2, and the atmosphere-ocean coupled GCM – MAECHAM5_MPIOM. It should be indicated that the GCMs are not perfect and the experiments were run without considering a number of external facings such as violent volcanic eruptions, anthropogenic greenhouse gas etc. As discussed in Chapter 3, the violent volcanic eruptions can induce a stronger polar vortex in Northern Hemisphere winter. Therefore, it is expected to find the relatively weaker polar vortex in such GCM simulations.

Compared with NCEP/NCAR reanalysis data as the observational reference, the major aspects of these three GCMs experiments on the stratospheric polar vortex, planetary wave propagation, and wave activities and eddy forcing have been illustrated in Table 4.3.

It is found that the simulation of ECHAM5_AMIP2 has fair agreement with observations of the climatology of zonal mean zonal wind and temperature, although some bias still can be observed. It has been found that the model tends to produce a stronger and colder stratospheric polar vortex in Northern Hemisphere winter. The analysis of f (n_k^2 <0) reveals that the atmosphere in the model shows less probability for stationary planetary wave propagation from the troposphere to the stratosphere than in observation. On the other hand, by analysis of E-P flux and its divergence, it is found that the wave activities and eddy zonal easterly forcing are weaker for stationary waves in both, the troposphere and stratosphere, but stronger for transient waves in the troposphere for ECHAM5_AMIP2. An explanation of the stronger transient wave activities and easterly forcing in the model is that the simulation of this model is performed with lower boundary conditions adopted from AMIP2, which only includes the monthly mean SST and sea ice concentration without considering other feedbacks from ocean such as sea ice thickness, snow depth, and the ocean surface velocities.

With higher upper boundary level (0.01hPa), the middle atmospheric GCM MAECHAM5_AMIP2 is also analyzed to study the influences of upper boundary on the atmospheric mean flow and planetary wave propagation. It is found that the bias of the stronger and colder stratospheric polar vortex observed in ECHAM5_AMIP2 is modified in MAECHAM5_AMIP2, but the polar vortex is now becoming too weak. The stationary wave activities and zonal easterly forcing are even weaker than in ECHAM5_AMIP2.

The stronger transient wave activities and zonal easterly forcing in the troposphere are still found in simulation of MAECHAM5_AMIP2.

Table 4.3 Aspects of stratospheric wind, temperature, and planetary wave propagation for different GCMs experiments compared with NCEP/NCAR Reanalysis data in DJF from 1979-1999.

GCMs experiments	ECHAM5_AMIP2	MAECHAM5_AMIP2	MAECHAM5_MIPOM
Strength of stratospheric polar vortex	Stronger	Weaker	Slightly weaker
Stratospheric polar temperature	Colder	Warmer	Slightly warmer
Possibility of stationary planetary wave propagation from Trop. to Strat.	Less	Much less	Much less
Stationary planetary wave activity and eddy forcing in the troposphere	Weaker	Much weaker	The weakest
Stationary planetary wave activity and eddy forcing in the stratosphere	Weaker	Much weaker	Much weaker
Transient planetary wave activity and eddy forcing in the troposphere	Stronger	Stronger	The strongest
Transient planetary wave activity and eddy forcing in the stratosphere	No big difference	Slightly weaker	Slightly weaker

In order to investigate the influences of ocean on atmospheric circulation and planetary wave propagation, the simulation of an atmosphere-ocean coupled model – MAECHAM5_MPIOM is also analyzed. The stratospheric polar vortex, which was observed too weak in MAECHAM5_AMIP2, is now slightly strengthened in MAECHAM5_MPIOM, though the polar vortex is still weaker than in observation. Differences of wave activities for both stationary and transient waves between MAECHAM5_AMIP2 and MAECHAM5_MPIOM are found mainly in the troposphere. This implies influences of ocean on planetary wave propagation mainly distribute in the troposphere. It can be concluded that the influences of ocean on atmosphere have very less chance to reach up to the stratosphere by planetary wave propagation.

Chapter 5

Conclusions and outlook

5.1 Conclusions

The major objective of this thesis is to improve our understanding of the dynamical coupling between the troposphere and stratosphere especially the properties of planetary wave propagation, wave activity and eddy forcing on atmospheric mean flow. The atmospheric state controls planetary wave propagation based on the Charney Drazin Theorem (Charney and Drazin, 1961; Andrews, et al., 1987), and conversely, planetary waves also change atmospheric mean flow through deposition of zonal momentum and heat of waves (Eliassen and Palm, 1961; Andrews, et al., 1985). The different contributions of stationary and transient planetary waves have been analyzed in this study. We found the dynamical links between the stratospheric polar vortex regimes and planetary wave propagation in Northern Hemisphere winter. The anomalies of zonal wind and temperature in the stratosphere induced by the external forcing of violent tropical volcanic eruptions, and their influences on planetary wave propagation, have also been discussed. By analyzing simulations of series of ECHAM5, it showed that this GCM tends to simulate a stronger polar vortex than observed and it can be improved by increasing the height of the upper boundary level. Moreover, the influences of oceanic forcing on planetary wave propagation have been studied in simulation of AOGCM.

5.1.1 Climatology of planetary wave propagation

A new analysis was introduced in this thesis and applied to study the potential influence of the atmospheric mean flow on planetary wave propagation. This new analysis is based on the frequency of negative refractive index squared f ($n_k^2 < 0$) and it avoids several problems in the traditional analysis. Based our analysis, we concluded that not only the zonal mean zonal wind (ZMZW) but also the vertical shear of zonal wind affects the possibility of stationary planetary wave propagation. It is shown that the possibility of upward wave propagation decreases with increased zonal wave number (ZWN). Only ultra-long waves (ZWN1, 2 and 3 waves) have chances to propagate from the troposphere to the stratosphere. In this study, the buoyancy frequency N^2 was treated as a variable of both altitude and latitude on a meridional plane rather than keeping it constant or only altitude-dependent variable as in previous studies. This helps to improve our understanding of influences of atmospheric stability on planetary wave propagation, especially near the extratropical tropopause.

Analysis of the E-P flux and its divergence showed that the stationary planetary waves can transport eddy heat and momentum from the troposphere to the stratosphere in

association with ZWN 1 and 2 waves. Moreover, it has been found that the zonal easterly momentum forcing on mean flow is induced by stationary planetary waves in the extratropical troposphere and in the subpolar stratosphere. The latter corresponds with the stratospheric polar vortex with stronger westerly in the polar stratosphere.

The E-P flux and its divergence of transient waves were also analyzed in this study. After removing the annual mean, annual and semi-annual harmonics, then after time filtering, the transient waves with all frequencies, low frequency (10days to 90days) and high frequency (2.5days to 6days) were isolated. We found that in Northern Hemisphere, the low frequency transient planetary waves dominate the propagation of transient energy, which disagree with the results by Limpasuvan and Hartmann (2000). Rather than transferring much eddy heat flux to the stratosphere as stationary waves, the transient waves have more eddy momentum fluxes propagated from the extratopical lower troposphere to the subtropical upper troposphere and less eddy heat flux to the stratosphere.

The variations of the stratospheric polar vortex are characterized by regime-like properties. We identified two stratospheric polar vortex regimes – 11 strong polar vortex regimes (SVR) and 12 weak polar vortex regimes (WVR) during 1958-2002 based on the zonal wind at 50hPa and 65°N from daily NCEP/NCAR reanalysis data. SVR generally last longer than WVR and they have never been observed occurring both in a single winter. Planetary waves have more possibilities to propagate from the troposphere to the stratosphere in WVR than in SVR. These possibilities also decrease with the increasing ZWNs. Moreover, planetary waves also show stronger propagation in WVR from the troposphere to the stratosphere. The analysis of E-P flux and its divergence showed that, in SVR, the planetary waves lead to strong westerly momentum forcing in the polar stratosphere while in WVR the easterly forcing prevails in both the polar and sub-polar stratosphere. For planetary wave activities, the equatorward eddy momentum fluxes in the upper troposphere around the subtropics are much stronger in SVR, while the eddy heat fluxes from the troposphere to the stratosphere around the northern pole are much stronger in WVR. The stronger propagations of stationary planetary waves to the polar stratosphere in WVR contribute to weaken the polar vortex.

Like stationary planetary waves, transient waves can also contribute to the maintenance of stratospheric polar vortex regimes, but in a different way. The transient waves propagate less eddy heat flux from the troposphere to the subpolar stratosphere in WVR than in SVR. The more propagation of transient planetary waves to the subpolar stratosphere in SVR can break and get absorbed by the mean flow at subpolar latitudes (55°N – 60°N), strengthening the temperature gradient between the subpolar stratosphere and the subpolar stratosphere, and therefore dynamically strengthening the polar. The stronger stratospheric polar vortex located at 65°N can be found in SVR.

The stationary planetary wave activities and the probability of its propagation are not isolated but highly correlated. Strong upward E-P fluxes from the troposphere to the stratosphere occur when and where the frequency of negative refractive index squared is smaller than 50%, for ZWN1 and 2 waves.

5.1.2 Influence of violent volcanic eruptions on planetary waves

It has been observed that tropical violent volcanic eruptions can induce anomalies of zonal mean zonal wind and temperature in Northern Hemisphere winter. By analyzing three violent tropical volcanic eruptions (Agung 1963, El Chichon 1982 and Pinatubo 1991), the anomalies of wind and temperature and their influences on planetary wave propagation, have been investigated in this thesis.

Since the impacts of volcanic eruptions on the climate system can last 1-3 years (Robock, 2001), the two winters after these three volcanic eruptions (volcanic winters) were studied. The "dipole" structures for the anomalies of both, zonal mean zonal wind and temperature in Northern Hemisphere winter, were observed - the "dipole" structure of anomalies of zonal mean zonal wind is composed of a stronger stratospheric polar vortex and a weaker tropical jet, and the "dipole" structure of anomalies of temperature is composed of the cooling in the polar stratosphere and the warming in the tropical stratosphere. On the other hand, the similar "dipole" structures but with stronger amplitudes, were also observed in the anomalies of zonal mean zonal wind and temperature in stronger polar vortex regime (SVR) excluding the volcanic winters.

By analyzing the frequency of negative refractive index squared (f ($n_k^2 < 0$)), it was concluded that the atmosphere shows slightly more possibilities for ZWN1 and 2 but less possibility for ZWN3 stationary planetary waves to propagate from the troposphere to the stratosphere at high latitudes (65° – 75^oN) in volcanic winters compared with the general winters. Similarly, more possibilities at high latitude were also found in SVR. These better chances for ZWN1 and 2 waves probably correspond with the relatively stronger positive vertical shear of the zonal mean zonal wind in the stratosphere at high latitudes in volcanic winters and SVR. However, there is less wave energy available to propagate from the troposphere to the stratosphere at the polar and subpolar area.

Moreover, the analysis of E-P flux and its divergence indicated that although more stationary planetary waves can propagate more from the troposphere to the stratosphere in volcanic winters, instead of breaking and getting absorbed, part (32%) of these waves can continually propagate higher up to the middle and upper stratosphere. This finding can help to improve our understanding of the mechanism by which more planetary wave propagation from the troposphere to the stratosphere and a stronger stratospheric polar vortex were observed at the same time in the Northern Hemisphere winters following violent tropical volcanic eruptions. Unlike the stationary waves, the propagation of transient planetary waves showed different aspects in volcanic winters and SVR.

5.1.3 GCMs performance

Most of current climate general circulation models (GCMs) show the bias of a too strong stratospheric polar vortex. Based on the previous findings of this thesis, this bias can probably have influences on the simulation of planetary wave propagation in GCMs. In this study, the performance of GCMs on the climatology of planetary wave propagation in Northern Hemisphere winter has been investigated by analyzing the simulations of ECHAM5_AMIP2, its middle atmospheric version MAECHAM5_AMIP2, and the coupled ocean model version MAECHAM5_MPIOM. The NCEP/NCAR reanalysis data with same time period (1979-1999) were considered as observational reference.

The comparison between simulations of ECHAM5_AMIP2 and NCEP/NCAR reanalysis data shows that the simulation of ECHAM5_AMIP2 has a fair agreement with observations concerning the climatology of zonal mean zonal wind and temperature. On the other hand, a bias is still observed in the model. It has been found that the ECHAM5_AMIP2 prefers to produce a relatively stronger and colder stratospheric polar vortex. As supposed in previous studies, the bias of stronger polar vortex can be induced by using the lower upper boundary level (10hPa) in model. The analysis of f ($n_k^2 < 0$) revealed that in the model atmosphere shows less permission for stationary planetary wave propagation from the troposphere to the stratosphere. At the same time, by analysis of E-P flux and its divergence, it was found that in ECHAM5_AMIP2 simulation, the wave activities and zonal easterly momentum forcing are relatively weaker for stationary waves in both the troposphere and stratosphere, but stronger for transient waves in the troposphere. One of the possible reasons of improperly represented wave activities in the troposphere in ECHAM5_AMIP2 is that the simulation is performed with lower boundary conditions adopted from AMIP2, which only considers the monthly mean of the sea surface temperature and sea ice concentration. In AMIP2, other feedbacks from the ocean such as sea ice thickness, snow depth, and the ocean surface velocities, have not been considered yet.

With enhanced higher upper boundary level (0.01hPa), the simulation of the middle atmosphere GCM – MAECHAM5_AMIP2 was also analyzed. It was found that the bias of the stronger and colder stratospheric polar vortex observed in ECHAM5_AMIP2 was modified in MAECHAM5_AMIP2, although the polar vortex is shown too weak in MAECHAM5_AMIP2. However, stationary wave activities and zonal easterly forcing are still too weak in MAECHAM5_AMIP2 as in ECHAM5_AMIP2. The stronger transient wave activities and zonal easterly forcing in the troposphere can still be observed in MAECHAM5_AMIP2.

Therefore, in order to understand the importance of proper simulation of feedbacks from the ocean, the simulations of the atmosphere-ocean coupled model – MAECHAM5_MPIOM with the same horizontal and vertical resolution as MAECHAM5_AMIP2 was also analyzed. The too weak stratospheric polar vortex in MAECHAM5_AMIP2 was getting stronger in the atmosphere-ocean coupled GCM, although it is still somewhat weaker than in the observations. Remarkable differences in wave activities for both stationary and transient waves between MAECHAM5_AMIP2

and MAECHAM5_MPIOM were found mainly in the troposphere. This implies that the influences of the lower boundary conditions can only reach up to the troposphere. However, the bias of weaker stationary wave activities and weaker zonal easterly forcing in the troposphere and stratosphere, and stronger transient wave activities and stronger zonal easterly forcing in the troposphere, which has been observed in both ECHAM5_AMIP2 and MAECHAM5_AMIP2 simulations, was still observed in MAECHAM5_MPIOM simulation.

Finally, it should be indicated that in all these three simulations of GCMs, the external forcing of violent volcanic eruptions has not been considered yet. As concluded in Chapter 3, the violent volcanic eruptions can induce stronger polar vortex in Northern Hemisphere winter. Therefore, the simulated relatively weaker polar vortex in the two MAECHAM5 models possibly are expected to be strengthened when the volcanic forcing is considered in the GCMs. Surely, it needs more studies of GCMs and considering complete external forcing to verify this mechanism.

5.2 Outlook

In this thesis, the climatology of planetary wave propagation was investigated in Northern Hemisphere winter. The behavior of stationary planetary waves in the Southern Hemisphere was generally considered rather negligible compared with those in the Northern Hemisphere. The stratospheric polar vortex in the Southern Hemisphere is strong and highly stable and there is no regime-like pattern observed yet. However, stratospheric sudden warming events, which are thought mainly connected with the transient planetary wave propagation from the troposphere to the stratosphere (Andrews, et al., 1987), have been observed in both hemispheres. For example, the Antarctic stratospheric sudden warming event in 2002 has drawn much attention recently. In the future work, it is worth investigating the role of the transient waves during such extreme events not only in the Northern Hemisphere but also in the Southern Hemisphere.

The influences on the stratospheric circulation and therefore on planetary wave propagation can be caused by external forcing including not only the violent tropical volcanic eruptions but also some others, e.g. the 10-12 year oscillation in lower stratospheric temperature and geopotential height is considered in phase with the 11-year solar cycle (Labitzke and van Loon, 1988). Studies of the potential influences of solar cycle on planetary wave propagation will help improve our understanding on the role of stratosphere-troposphere dynamical coupling in the climate system. Moreover, the strengthened polar vortex in past decades is believed partly due to increasing anthropogenic emission of greenhouse gases (Graf, et al., 1995). It is also attractive to study the role of the anthropogenic forcing (emission of greenhouse gases) in climate change especially atmospheric dynamic process.

Considering the external forcing of volcanic eruptions, the available observational cases are limited, although it was found that the influences of eruptions on the climate system are significant. The simulations of GCMs with proper consideration of external forcing of

volcanic eruptions can help to improve understanding of mechanism of planetary wave propagation after violent volcanic eruptions. The stronger polar vortex in simulation of GCMs with lower upper boundary levels shifts to a weaker polar vortex in simulations of MAGCM. This "overdone" shift has been slightly improved in the MAGCM couple with ocean model but it is lack of explanation. Moreover, propagation of the stationary planetary waves from the troposphere to the stratosphere is weaker in simulations of all versions of GCMs. The complete understanding of the mechanism of planetary wave propagation and its influence on mean flow in GCMs is still missing. Regarding this problem, one of the suggestions is to analyze the sensitivity experiments focusing on the dynamical mechanism of constructing and maintaining of the stratospheric polar vortex in GCMs.

Appendix A

A.1 Charney – Drazin Theorem

Charney and Drazin (1961) found that planetary waves can propagate vertically when their phase speeds c are westward relative to the zonal mean flow $\bar{u}$:

$$0 < \bar{u} - c < \bar{u}_c \equiv \beta \left[\left(k^2 + l^2 \right) + f_0^2 \left(4H^2 N^2 \right) \right]^{-1} , \qquad \text{(A.1.1)}$$

with $\beta = 2\Omega \cos \varphi$ and $f_0 = 2\Omega \sin \varphi$. H , N and u are the scale height, the buoyancy frequency and the zonal wind, respectively. $\Omega = 7.292 \times 10^{-5} \text{s}^{-1}$ is the Earth's rotation rate. The zonal and meridional wave lengths are defined by $2\pi k^{-1}$ and $2\pi l^{-1}$, respectively. $\bar{u}_c$ is called the critical Rossby velocity. Equation 1.1.1 reveals that $\bar{u}_c$ decreases with increasing horizontal wave numbers. The waves having the largest amplitudes are stationary with respect to the ground, i.e. c=0. Hence, there is $0 < \bar{u} < \bar{u}_c$.

Andrews et al. (1987) illustrated that for a typical stratospheric stability ($N^2 = 5 \times 10^{-4} s^{-2}$), and choosing $l = \pi /(10,000km)$, $\bar{u}_c$ at 60ºN is given by:

$$\bar{u}_c \approx 110/\left(s^2 + 3 \right) ms^{-1} , \qquad \text{(A.1.2)}$$

where the integer $s = ka \cos \phi$ is the spherical zonal wave number (ZWN). Using this simple model, the critical Rossby velocities for the ZWN 1 and 2 amounts to 28ms^{-1} and 16ms^{-1}, respectively.

The Charney-Drazin Theorem (Equation 1.1.1) gives a theoretical explanation for numerous observational phenomena. The permission of the zonal mean flow for the propagation of tropospheric disturbances becomes less when the zonal wave number s increases. Consequently, the stratosphere and the upper troposphere has a strong filter effect on tropospheric disturbances since zonal west wind normally increases with height. Only ultra-long planetary waves generated by diabatic heating and orography can propagate into the stratosphere.Radiatively caused, the stratospheric zonal mean flow alternates between easterlies in the summer hemisphere and westerlies in the winter hemisphere. This fact is an essential condition for whether a dynamical coupling between both atmospheric layers exists. Only in the winter hemisphere can ultra-long planetary waves propagate into the stratosphere and interact with the mean stratospheric flow. During the summer season ($\bar{u} < 0$), the dynamical coupling between troposphere and stratosphere is strongly reduced because the waves are trapped in the troposphere.

A.2 Theoretical definition of stationary planetary waves

Averaging observational data in various ways is a standard approach for handling the complexity of global scale atmospheric flow. Straightforward average over a set of points

fixed in space or time are known as *Eulerian average*. Given any particular average, one can define the deviations or departure of each atmospheric variable from its mean value. These disturbances are often known as wave quantities. Averaging not only allows compressing of the volume of information but improves the statistical reliability. A suitable framework for the diagnosis and interpretation of atmospheric quantities has also been developed that separates *mean state* and *wave* parts. Owing to the nonlinearity of the equations of motion, there is, in general, a mutual coupling between waves and mean state. Thus, the configuration of the mean flow can strongly influence the propagation of waves, for example through the refraction of the wave, while the disturbances themselves can bring about significant mean flow changes through rectified nonlinear effects (e.g. by breaking of waves).

The theoretical framework providing qualitative physical insight into the two-way process of wave-mean flow interaction has most satisfactorily been constructed for zonal mean average. It is introduced the (Eulerian) zonal average of any quantity for example the geopotential field $\Phi(\lambda, \phi, z, t)$, denoted by an overbar:

$$\overline{\Phi}(\varphi, z, t) = (2\pi)^{-1} \int_0^{2\pi} \Phi(\lambda, \varphi, z, t) d\lambda \,, \tag{A.2.1}$$

and the departure from the average, denoted by a prime:

$$\Phi'(\lambda, \varphi, z, t) = \Phi - \overline{\Phi} \,. \tag{A.2.2}$$

λ, ϕ, z and t are longitude, latitude, height and time, respectively.

A.3 Statistical approach of stationary planetary waves – single wave analysis

The climatological monthly mean flow patterns tend to take a wavy form in the Northern Hemisphere winter: these patterns can, if desired, be separated into zonal mean parts and zonally varying parts. Their zonally varying parts are know as "stationary waves" and can be further separated into zonal Fourier components. The time-dependent departures from the climatological average are often known as "transient eddies". Space-time spectral analysis of these transient components sometimes reveals the presence of large-scale, coherent, zonally propagating "traveling waves". (Andrews et al., 1987)

In order to illustrate the stationary waves, the climatology is first calculated by time mean of 44 years (1958-2002) Northern Hemisphere winter – December, January and February (DJF hereafter) (Andrews et al., 1987), e.g. the mean geopotential field <Φ> (here only the geopotential is used as an example, wind and temperature fields are analyzed in the same way). This climatological mean geopotential field can be furthermore expanded with equation 1.1:

$$\Phi(\lambda, \varphi, z) = \overline{\Phi}(\varphi, z) + \Phi'(\lambda, \varphi, z) \tag{A.3.1}$$

A_s and α_s represent the amplitude and phase of each harmonics respectively, A_0 corresponding to the zonal mean, and λ, φ and z are longitude, latitude and height, respectively, s refers to zonal wave number (ZWN) representing the limit of resolution of the data (Andrews et al., 1987). Since increasing ZWN corresponds to decreasing critical Rossby velocity, at which vertically propagating waves are selectively reflected/refracted (Charney and Drazin, 1961), separate treatment of single wave fields with different ZWNs is a proper approach to study planetary wave propagation and to illustrate the dynamical interaction between troposphere and stratosphere (Perlwitz, 2000).

At a specific latitude, the decomposition of the longitudinal geopotential height fields $z(\lambda)$ in their Fourier harmonics s=1, …, S is given as follows:

$$\Phi'(\lambda) = \sum_{s=1}^{S} \alpha_s \sin s\lambda + \beta_s \cos s\lambda \,. \tag{A.3.2}$$

in which S represents the limit of data resolution. The amplitude A_s and the phase Ψ_s of waves of ZWNs are given by $A_s = \sqrt{\alpha_s^2 + \beta_s^2}$ and $\Psi_s = \arctan(\alpha_s / \beta_s)$. The phase is defined as the longitude of the first maximum eastward of the Greenwich meridian. The recomposed geopotential height field $z_s(\lambda, \phi, t)$ of a single planetary wave with ZWNs is give as

$$\Phi'_s(\lambda, \varphi, t) = \alpha_s(\varphi, t) \cos s\lambda + \beta_s(\varphi, t) \sin s\lambda \,, \tag{A.3.3}$$

in which the total field is received by $\Phi'(\lambda, \varphi, t) = \sum_{s=1}^{S} \Phi'_s(\lambda, \varphi, t)$.

The Charney-Drazin Theorem implies that vertical propagating waves are selectively reflected at levels of critical Rossby velocity, which decreases with increasing ZWN. Clearly, ultra-long planetary waves are primarily involved.

A.4 Time filtering of transient planetary waves

The transient waves are computed by obtaining the seasonal time series of all relevant variables at all grid point, then removing the annual mean and annual and semi-annual harmonics. Furthermore, time-filtering the time series with an appropriate filter is applied on the time series of the variables. Finally calculating the variances from both the filtered and unfiltered series for each season and averaging over equivalent seasons in each data set will be performed (Straus & Shukla, 1988). The 21-point filters introduced by Blackmon and Lau (1980) were applied to isolate fluctuations with low frequency (10days< period <90days) and medium frequency (2.5days< period <6days), which correspond with low frequency eddies and synoptic transient waves, respectively.

In order to isolate eddies from different frequency domains, the 21-point filters introduced by Blanckmon and Lau (1980) is applied in this thesis. The filtering procedures were applied to the October-to-April data. In order to omit spurious fluctuations resulting from jumps in the data between two winters, the months October and April were discarded afterwards.

Two so-called 21-point filters introduced by Blackmon and Lau (1980) to isolate the fluctuations from different frequency are defined as:
1. A band pass filter leaving fluctuations with periods of 2.5 to 6 days (synoptic eddies);
2. A low pass filter leaving fluctuations with periods from 10 to 90 days (low frequency eddies).

It should be mentioned that the filters do not capture fluctuations with periods between 6 and 10 days. This is based on the intention of distinctly separating synoptic and low frequency eddies (Blackmon, 1976; Blackmon and Lau, 1980). Therefore, in this thesis, the low frequency transient waves and the synoptic transient waves are clearly investigated, respectively.

With the 21-point filters, each member of the filtered timeseries of a variable X at a certain grid point is calculated from 21 members of the unfiltered timeseries:

$$\tilde{X}(t_i) = a_0 X(t_i) + \sum_{p=1}^{10} a_p \left[X(t_{i+p}) + X(t_{i-p}) \right], \tag{A.4.1}$$

Where $\tilde{X}(t)$ is the filtered timeseries, and $X(t)$ the unfiltered timeseries. The timestep of the timeseries is 24 hours, corresponding to the use of NCEP/NCAR reanalysis daily mean data. The filter weights a_p are listed in Blackmon and Lau (1980). Values of the coefficients for the low-pass and band-pass 21-point filters are list:

Filtering coefficients	Low-pass filter	Band-pass filter
a_0	0.2119623984	0.4522054510
a_1	0.1974416342	-0.0728693709
a_2	0.1576890490	-0.2885051308
a_3	0.1028784073	0.0973270826
a_4	0.0462514755	0.0395130908
a_5	0.0	0.0283273699
a_6	-0.0281981813	0.0331625327
a_7	-0.0368362395	-0.0708879974
a_8	-0.0300256308	-0.0022652475
a_9	-0.0151817136	0.0030189695
a_{10}	0.0	0.0070759754

Appendix B

Additional Figures for Chapter 3

a)

b)

c)

d)

e)

f)
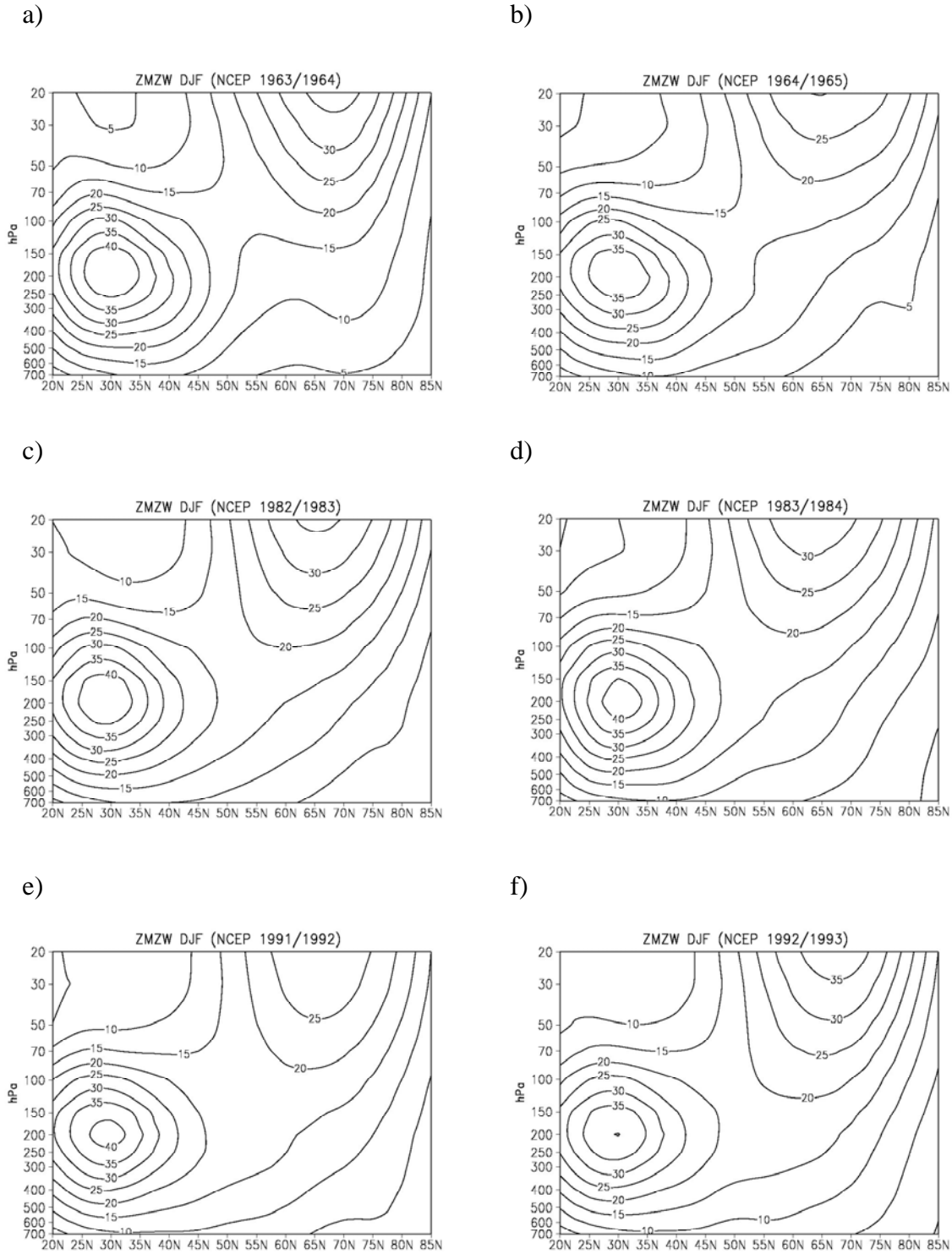
Figure B.1. Zonal mean zonal wind (m/s) in first DJF (left column) and second DJF (right column) after Mt. Agung 1963 eruption (first row), after Mt. El Chichon 1982 eruption (second row) and after Mt. Pinatubo 1991 eruption (third row) (NCEP/NCAR RA).

a)

ZMZW DJF 6364DJF-no vol.(NCEP RA)

b)

ZMZW DJF 6465DJF-no vol.(NCEP RA)

c)

ZMZW DJF 8283DJF-no vol.(NCEP RA)

d)

ZMZW DJF 8384DJF-no vol.(NCEP RA)

e)

ZMZW DJF 9192DJF-no vol.(NCEP RA)

f)

ZMZW DJF 9293DJF-no vol.(NCEP RA)
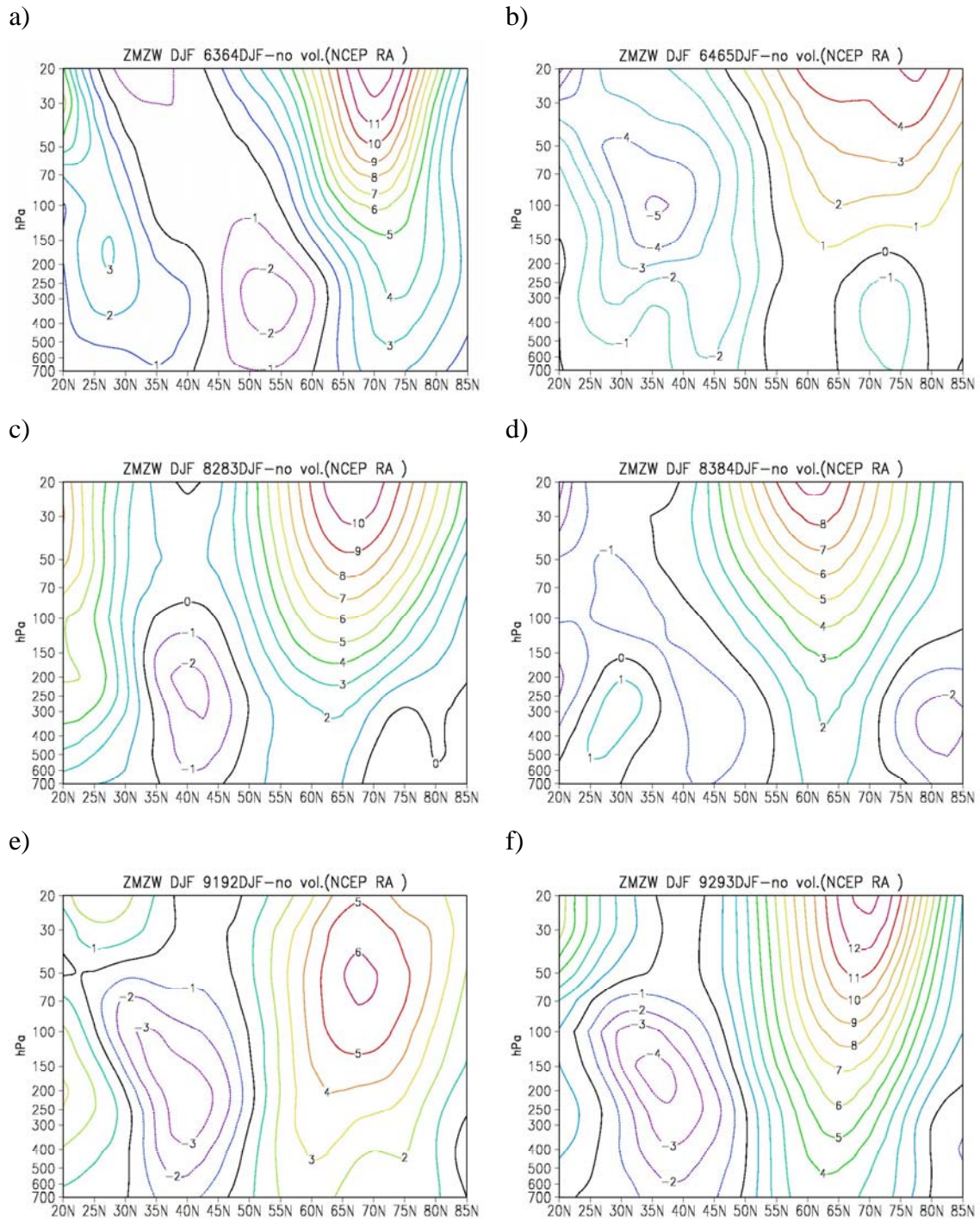
Figure B.2. Difference of zonal mean zonal wind (m/s): the first three rows, the difference between first DJF (left column) and second DJF (right column) after Mt. Agung 1963 eruption (first row), after Mt. El Chichon 1982 eruption (second row), and after Mt. Pinatubo 1991 eruption (third row) with DJFs (1958-2002) without violent volcanic eruptions; the bottom row, the average of the differences for all volcanic winters (NCEP/NCAR RA).

a)

b)

c)

d)

e)

f)
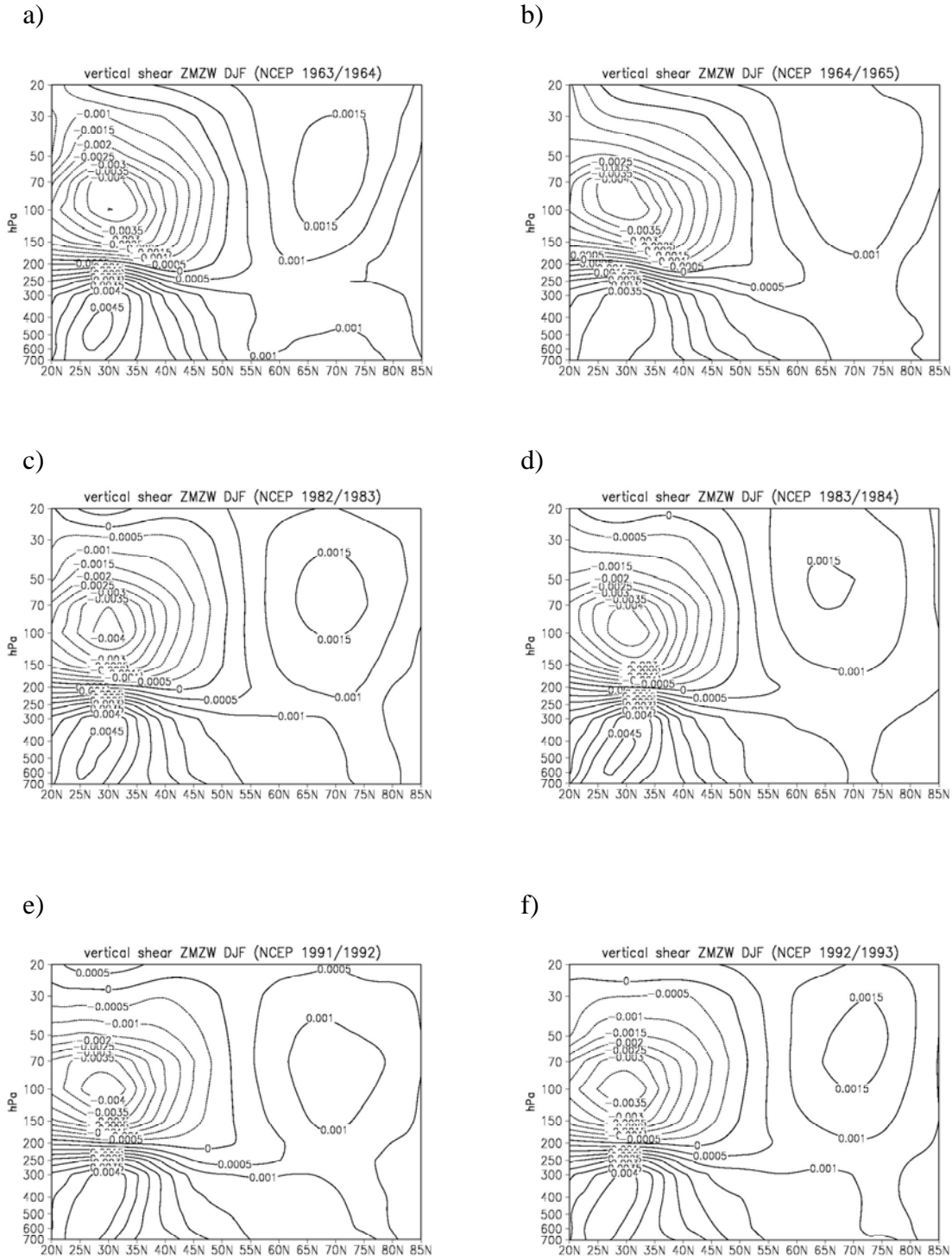
Figure B.3. Vertical shear of zonal mean zonal wind (s^{-1}) in first DJF (left column) and second DJF (right column) after Mt. Agung 1963 eruption (first row), after Mt. El Chichon 1982 eruption (second row) and after Mt. Pinatubo 1991 eruption (third row) (NCEP/NCAR RA).

a)

b)

c)

d)

e)

f)
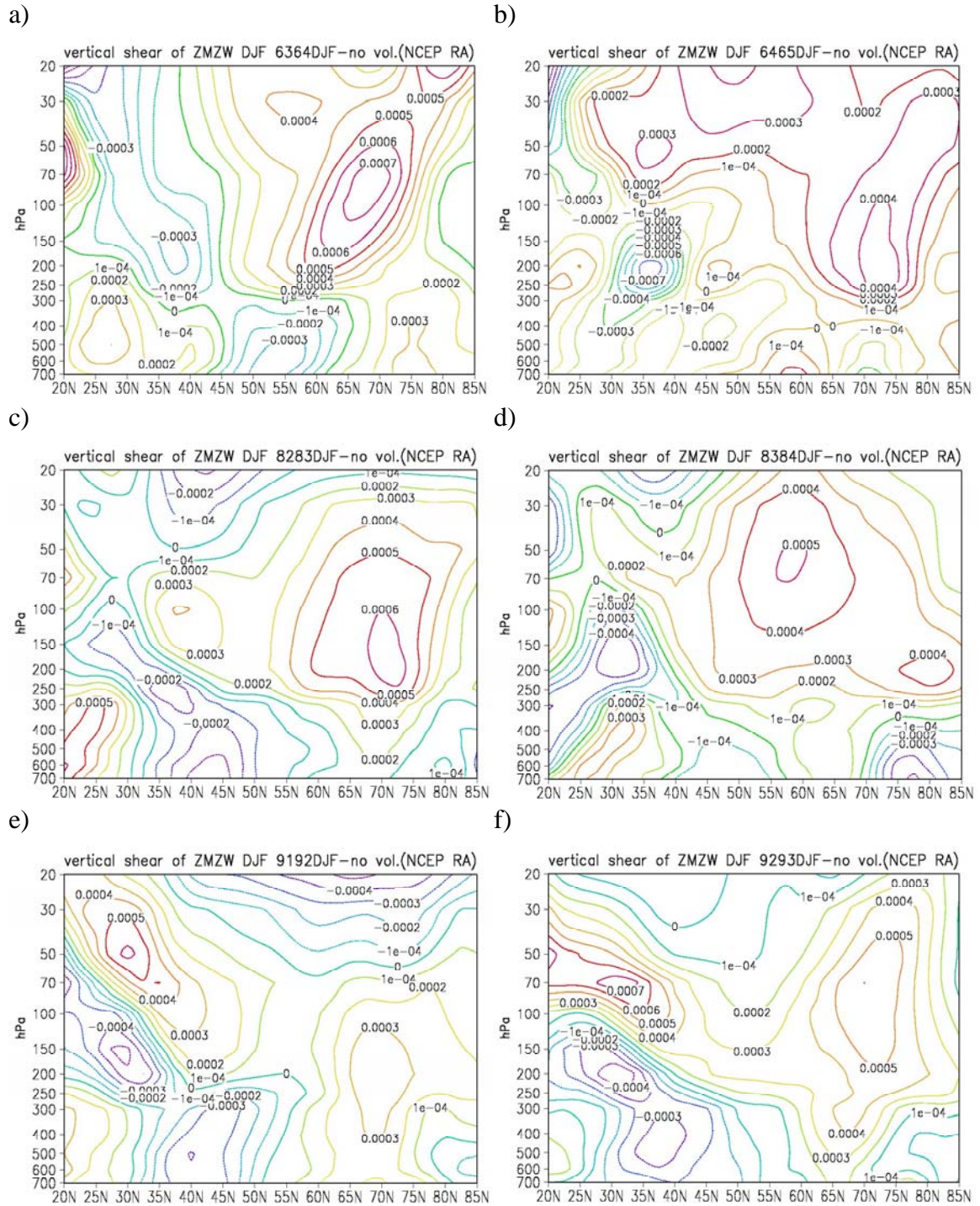
Figure B.4. Difference of vertical shear of zonal mean zonal wind (s^{-1}): the first three rows, the difference between first DJF (left column) and second DJF (right column) after Mt. Agung 1963 eruption (first row), after Mt. El Chichon 1982 eruption (second row), and after Mt. Pinatubo 1991 eruption (third row) with DJFs (1958-2002) without violent volcanic eruptions; the bottom row, the average of the differences for all volcanic winters (NCEP/NCAR RA).

a)

b)

c)

d)

e)

f)
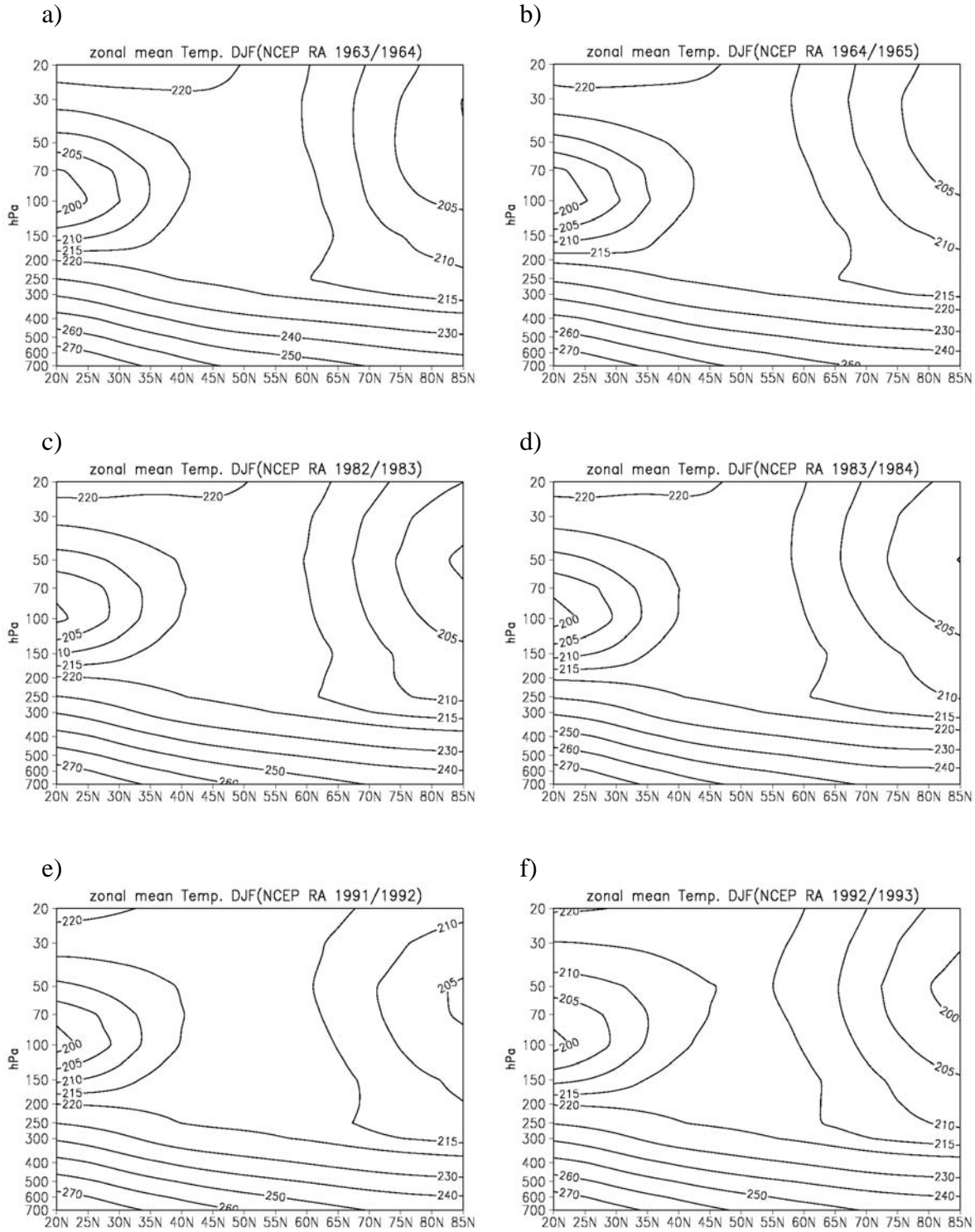
Figure B.5. Zonal mean temperature (K) in first DJF (left column) and second DJF (right column) after Mt. Agung 1963 eruption (first row), after Mt. El Chichon 1982 eruption (second row) and after Mt. Pinatubo 1991 eruption (third row) (NCEP/NCAR RA).

a)   b)

c)   d)

e)   f)
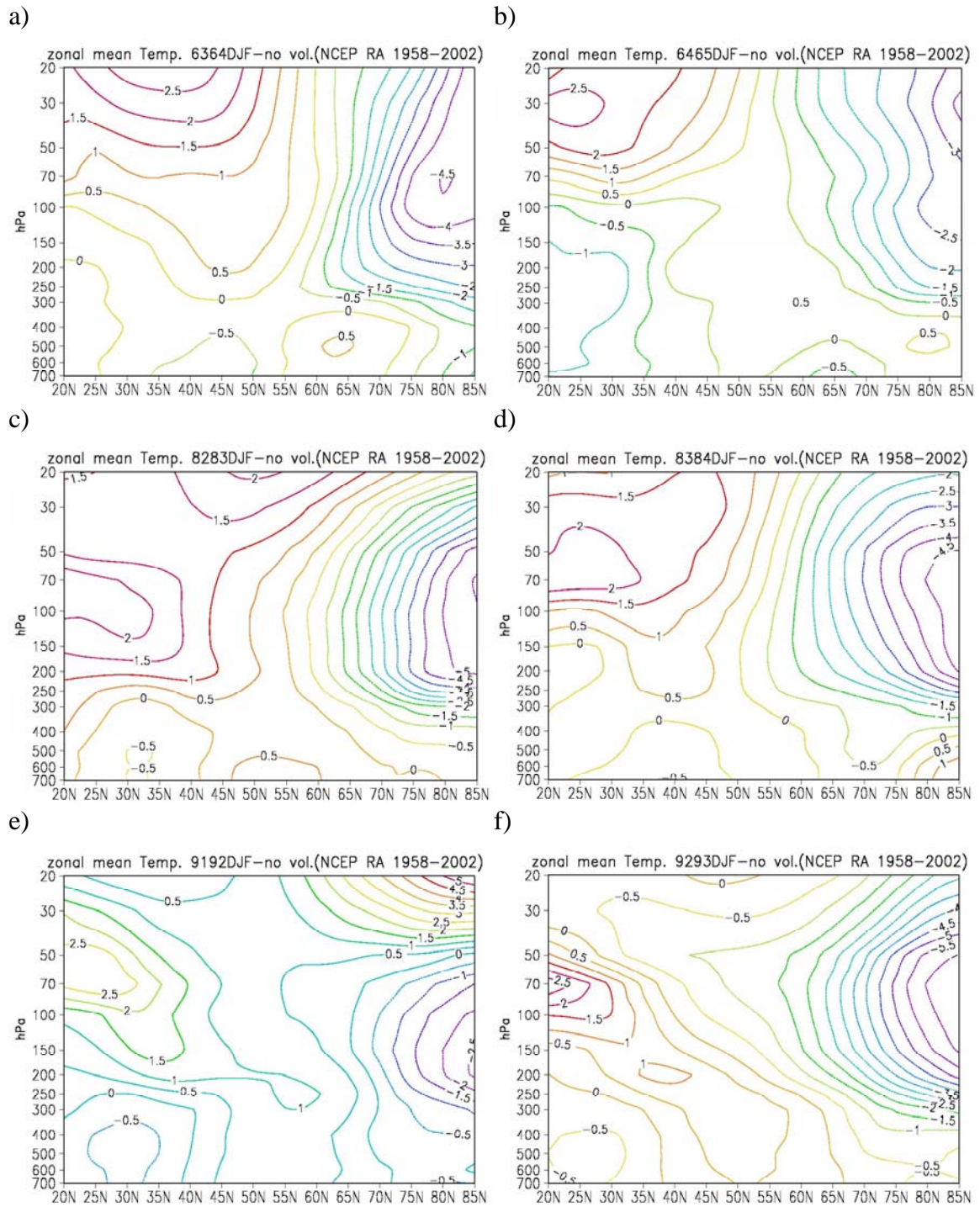
Figure B.6. Difference of zonal mean temperature (K): the first three rows, the difference between first DJF (left column) and second DJF (right column) after Mt. Agung 1963 eruption (first row), after Mt. El Chichon 1982 eruption (second row), and after Mt. Pinatubo 1991 eruption (third row) with DJFs (1958-2002) without violent volcanic eruptions; the bottom row, the average of the differences for all volcanic winters (NCEP/NCAR RA).

a)

b)

c)

d)

e)

f)
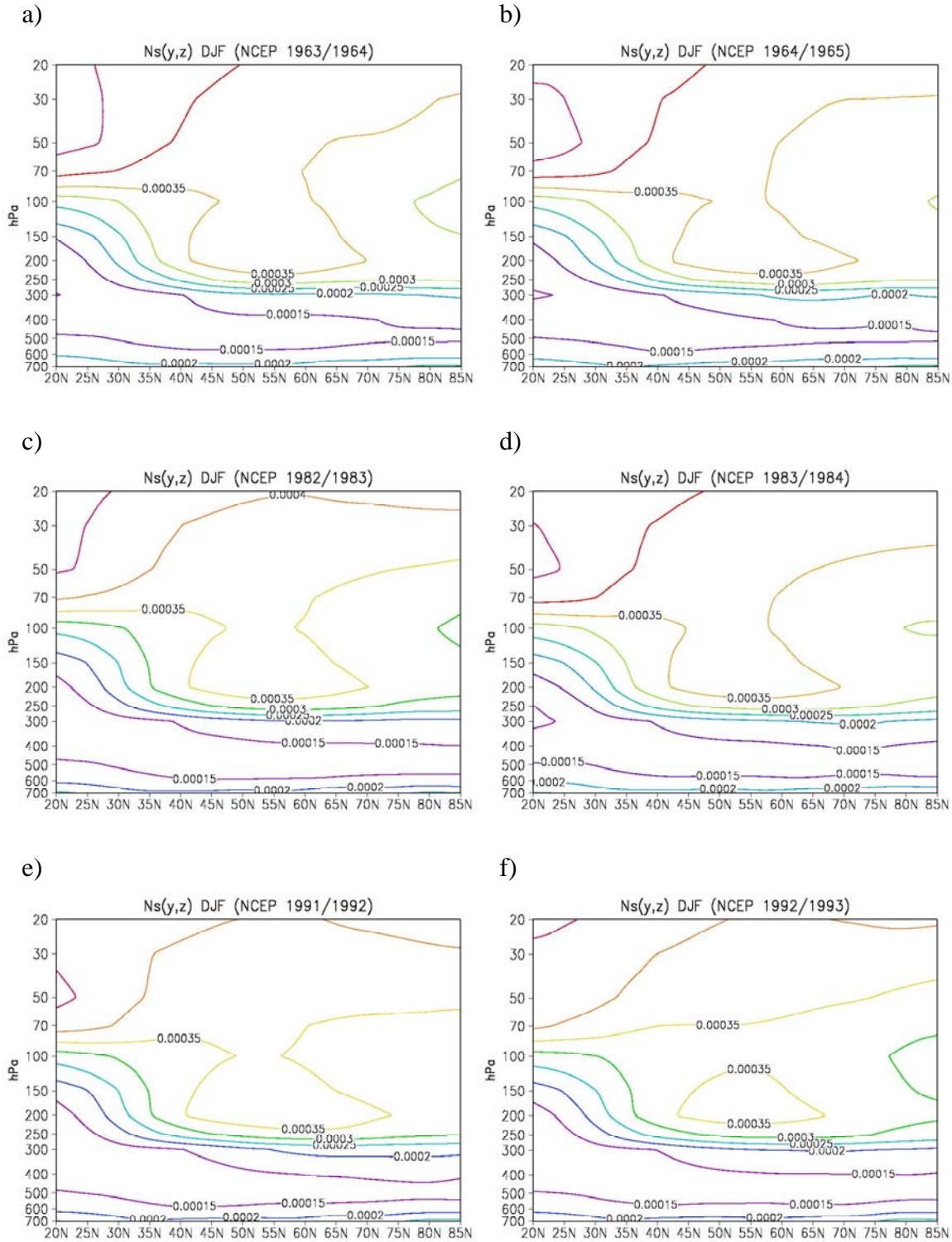
Figure B.7. $N^2(\phi, z)$ (s^{-2}) in first DJF (left column) and second DJF (right column) after Mt. Agung 1963 eruption (first row), after Mt. El Chichon 1982 eruption (second row) and after Mt. Pinatubo 1991 eruption (third row) (NCEP/NCAR RA).

a)

b)

c)

d)

e)

f)
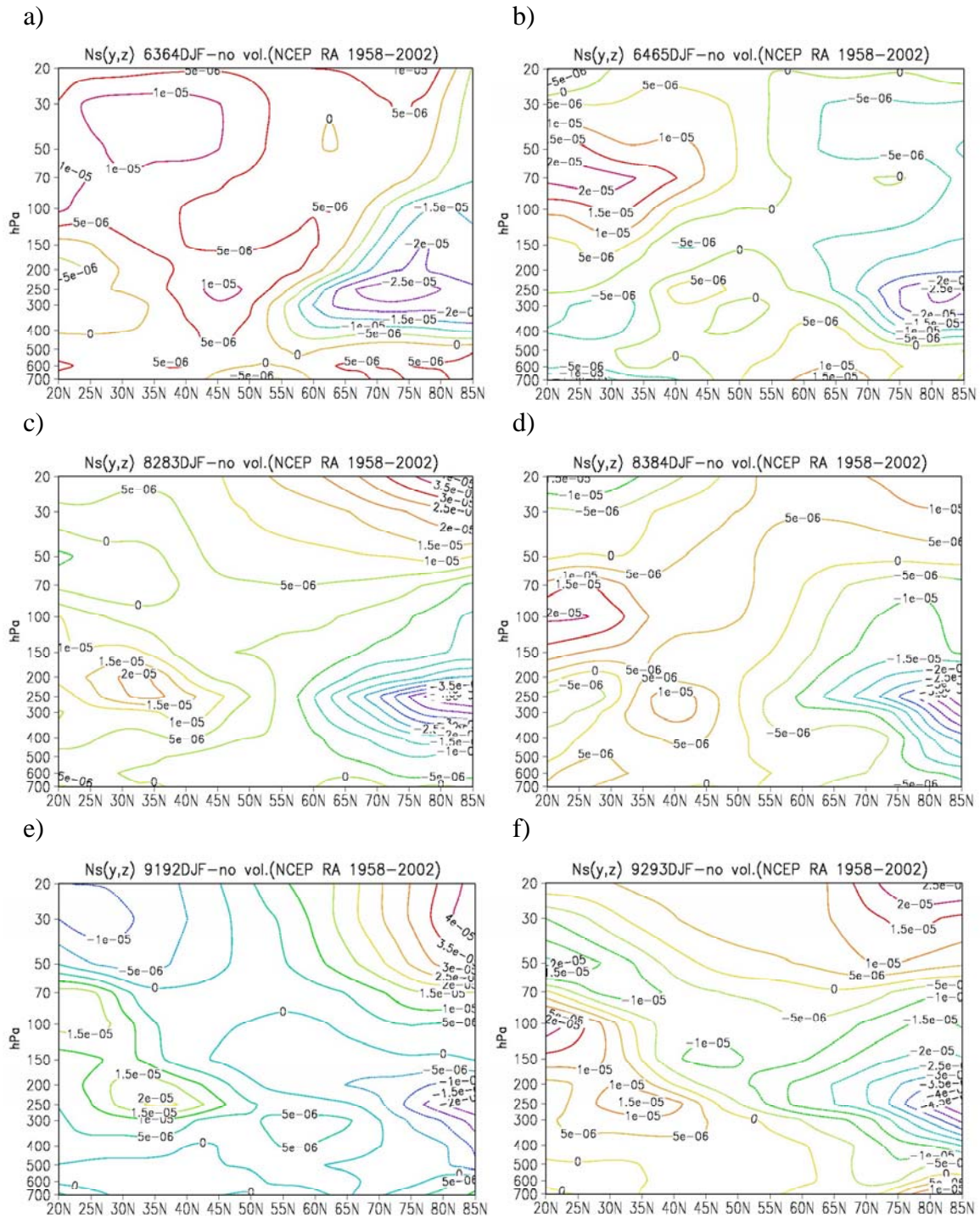
Figure B.8. Difference of $N^2(\phi, z)$ (s^{-2}): the first three rows, the difference between first DJF (left column) and second DJF (right column) after Mt. Agung 1963 eruption (first row), after Mt. El Chichon 1982 eruption (second row), and after Mt. Pinatubo 1991 eruption (third row) with DJFs (1958-2002) without violent volcanic eruptions; the bottom row, the average of the differences for all volcanic winters (NCEP/NCAR RA).
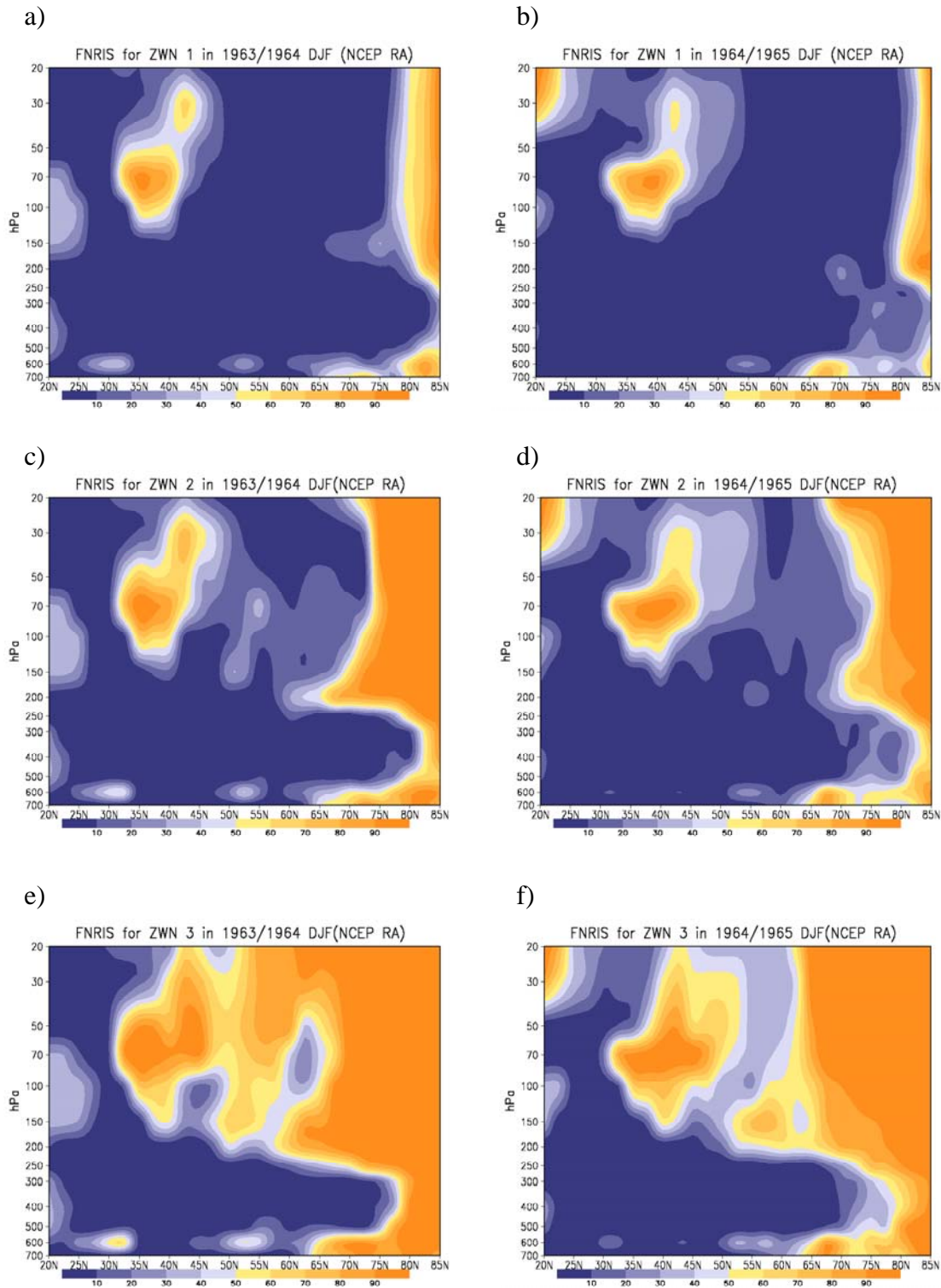
Figure B.9. f (n_k^2 <0) for stationary planetary waves in DJF of 1963-1964 (left column), and1964-1965 (right column) (NCEP/NCAR RA) for ZWN 1 wave (first row), ZWN 2 wave (second row) and ZWN 3 wave (bottom row). Unit of f (n_k^2 <0) is %.

a)

b)

c)

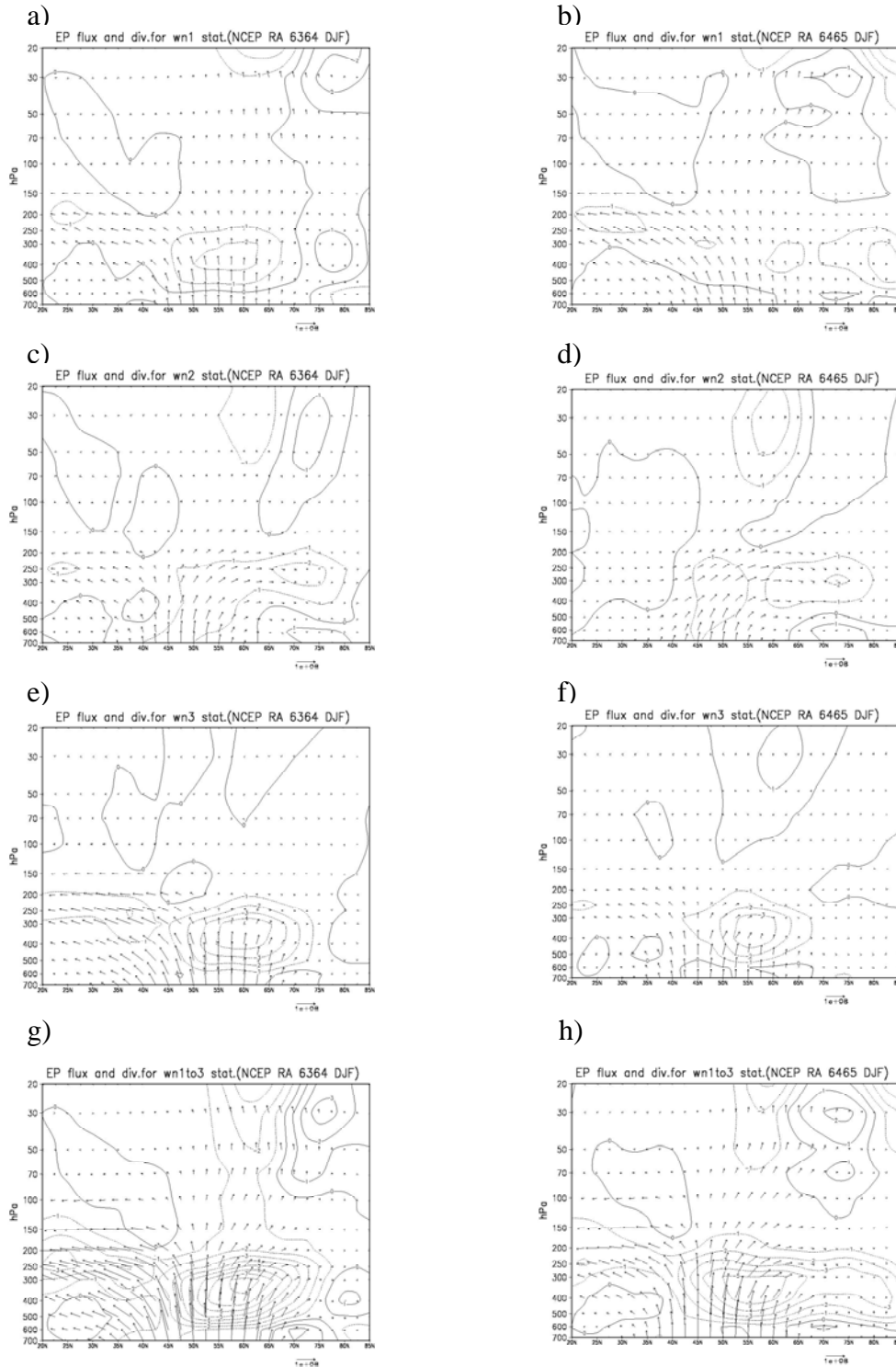d)

e)

f)
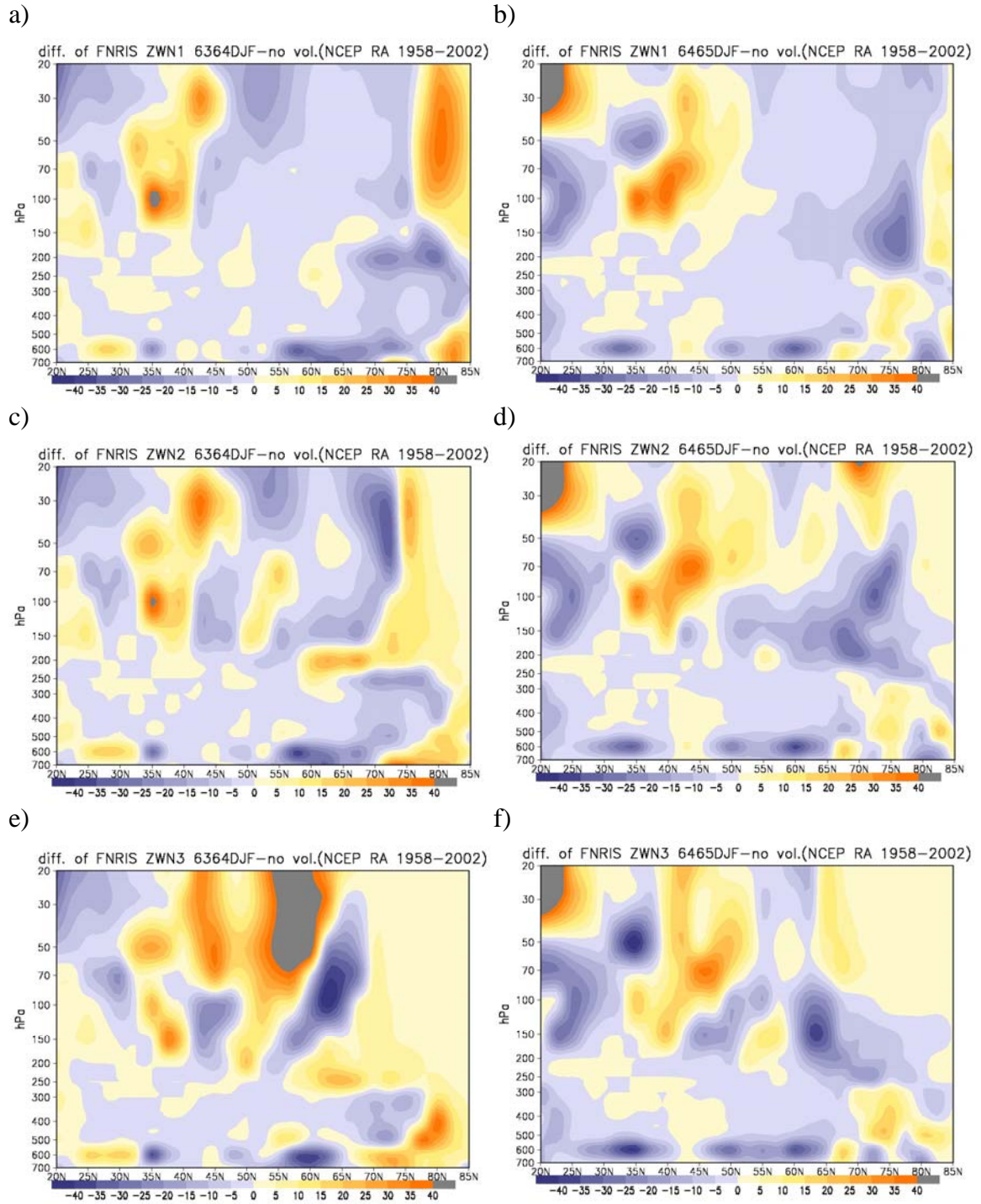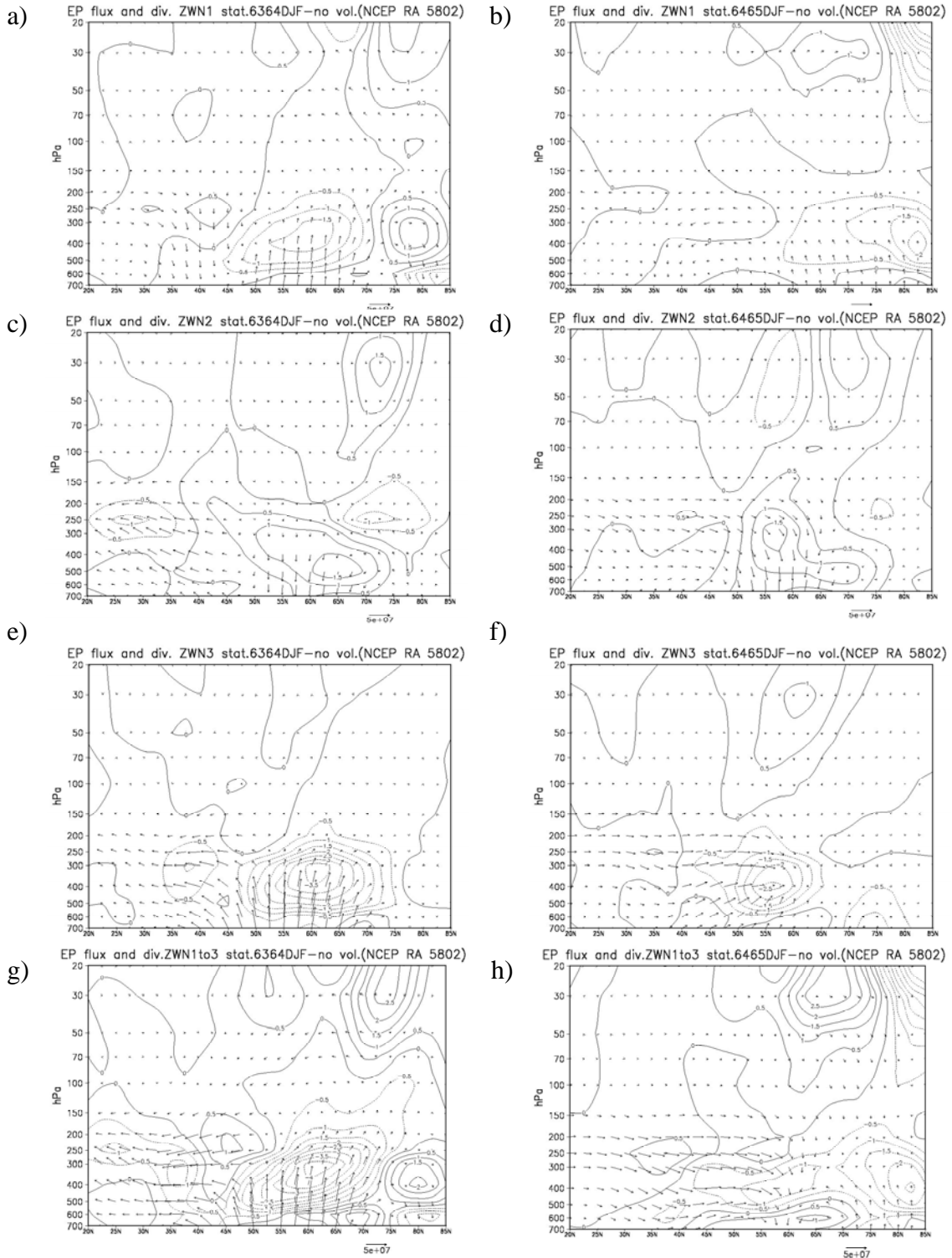

Figure B.10. Difference of f (n_k^2<0) for stationary planetary waves between 1963-1964 DJF (left column), and 1964-1965 DJF (right column) with DJF (1958-2002) without violent volcanic eruptions (Agung, 1963-1965; El Chichon, 1982-1984; Pinatubo, 1991-1993) (NCEP/NCAR RA) for ZWN 1 wave (first row), ZWN 2 wave (second row) and ZWN 3 wave (bottom row). Unit of f (n_k^2<0) is %.
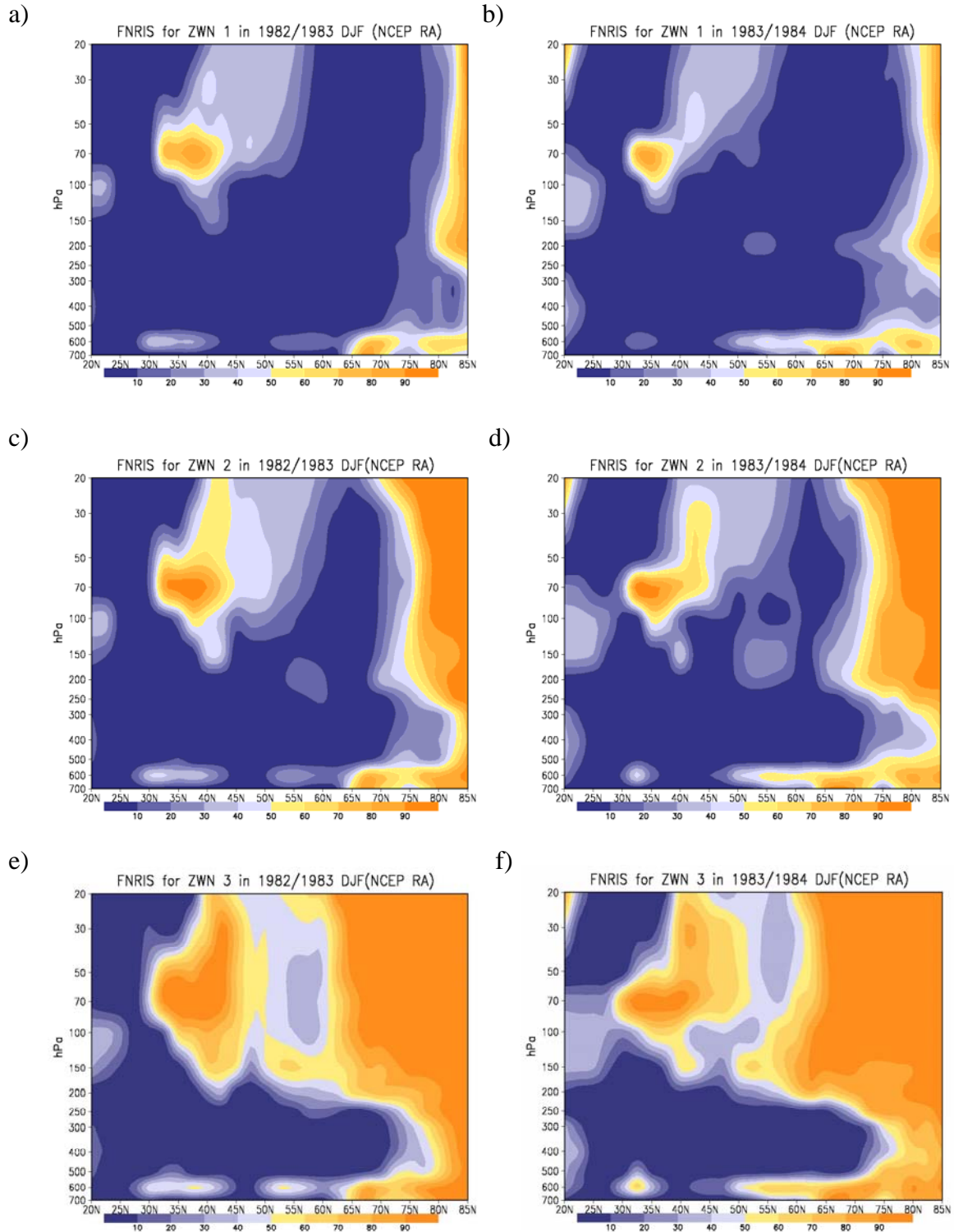
Figure B.11. f ($n_k^2 < 0$) for stationary planetary waves in DJF of 1982-1983 (left column) and 1983-1984 (right column) (NCEP/NCAR RA) for ZWN 1 wave (first row), ZWN 2 wave (second row) and ZWN 3 wave (bottom row). Unit of f ($n_k^2 < 0$) is %.

a)

b)

c)

d)

e)

f)
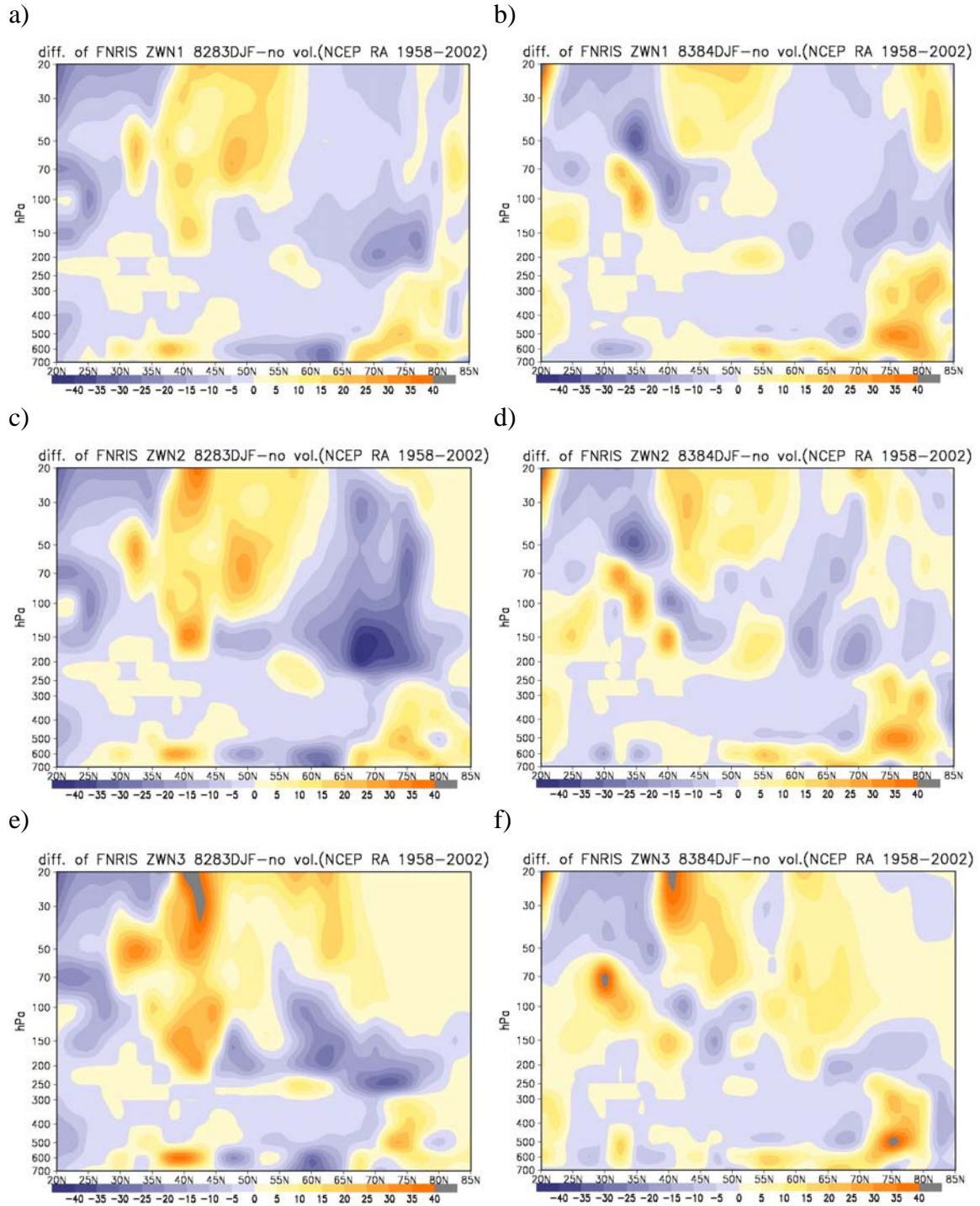
Figure B.12. Difference of f ($n_k^2 < 0$) for stationary planetary waves between 1982-1983 DJF (left column) and 1983-1984 DJF (right column) with DJF (1958-2002) without violent volcanic eruptions (Agung, 1963-1966; El Chichon, 1982-1984; Pinatubo, 1991-1993) (NCEP/NCAR RA) for ZWN 1 wave (first row), ZWN 2 wave (second row) and ZWN 3 wave (bottom row). Unit of f ($n_k^2 < 0$) is %.
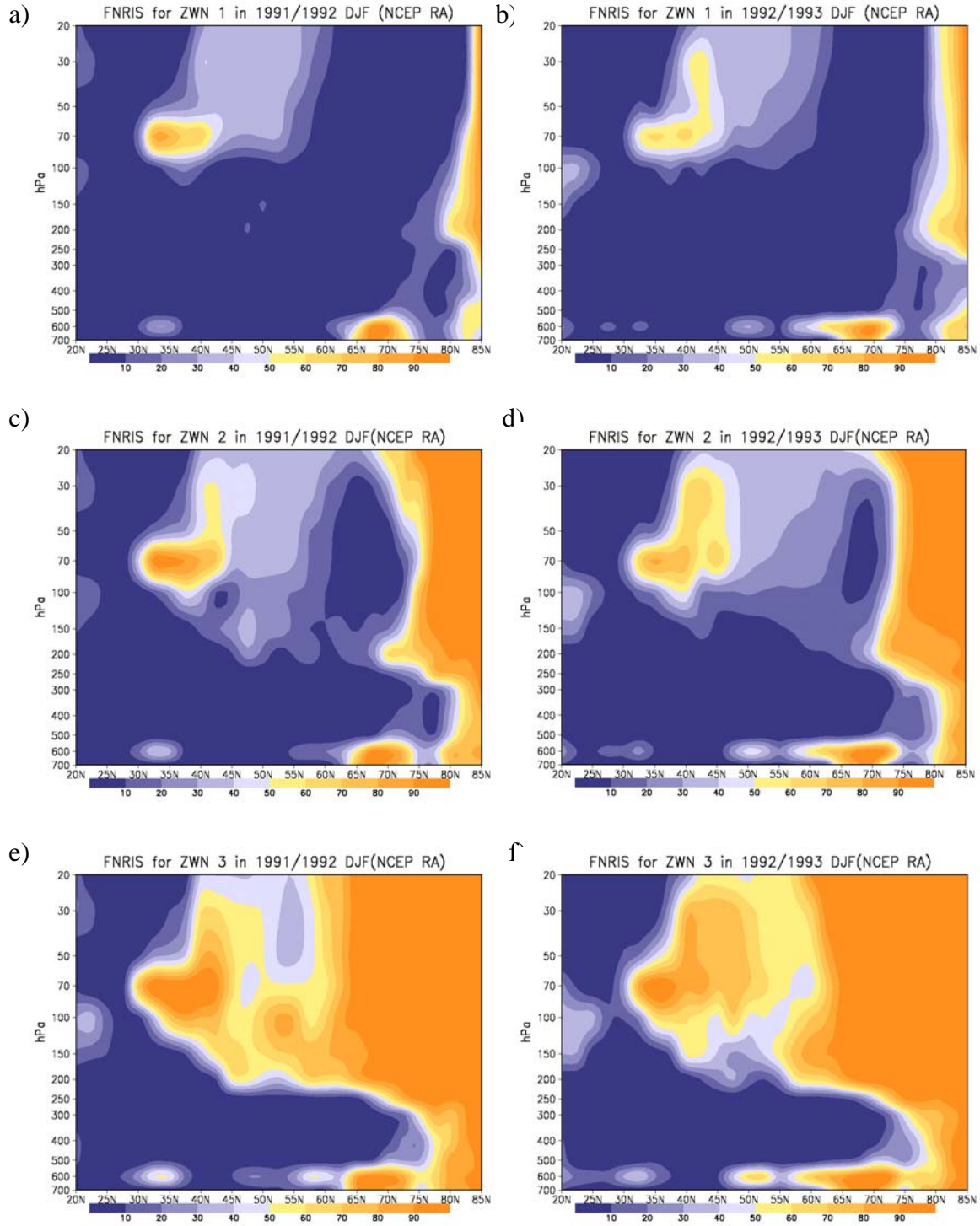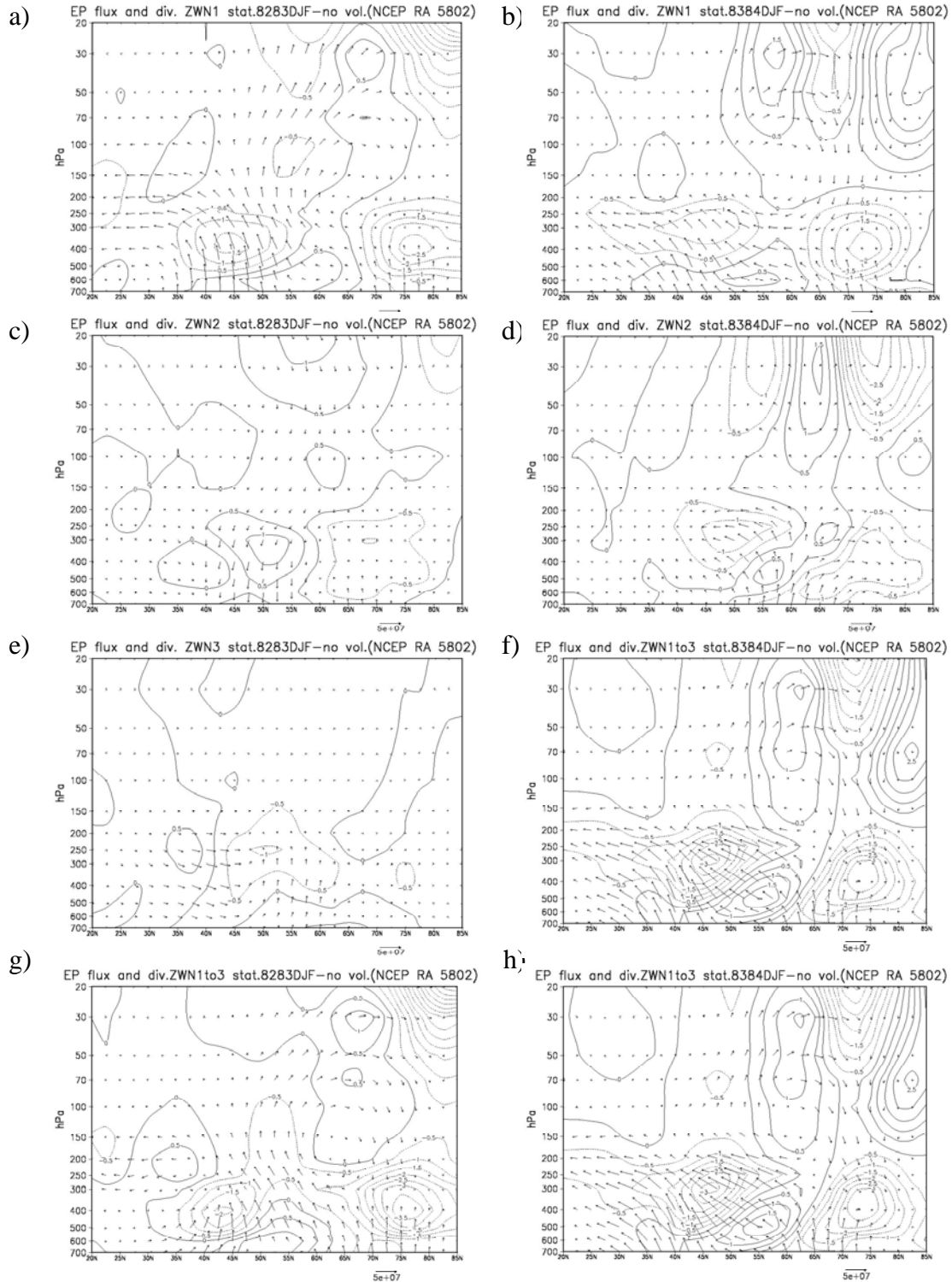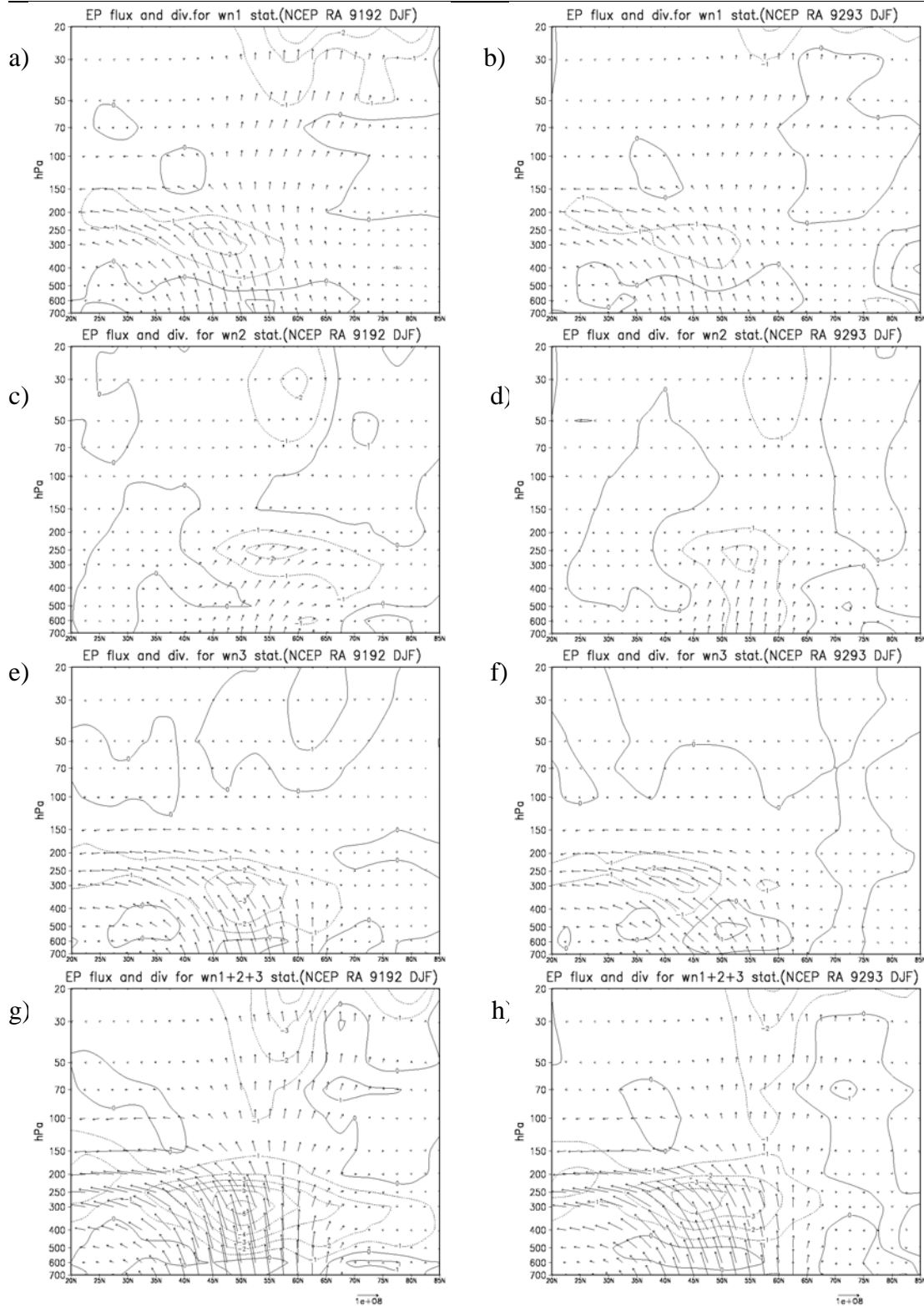
Figure B.13. f (n_k^2 <0) for stationary planetary waves in DJF of 1991-1992 (left column) and 1992-1993 (right column) (NCEP/NCAR RA) for ZWN 1 wave (first row), ZWN 2 wave (second row) and ZWN 3 wave (bottom row). Unit of f (n_k^2 <0) is %.

a)

diff. of FNRIS ZWN1 9192DJF-no vol.(NCEP RA 1958-2002)

b)

diff. of FNRIS ZWN1 9293DJF-no vol.(NCEP RA 1958-2002)

c)

diff. of FNRIS ZWN2 9192DJF-no vol.(NCEP RA 1958-2002)

d)

diff. of FNRIS ZWN2 9293DJF-no vol.(NCEP RA 1958-2002)

e)

diff. of FNRIS ZWN3 9192DJF-no vol.(NCEP RA 1958-2002)

f)

diff. of FNRIS ZWN3 9293DJF-no vol.(NCEP RA 1958-2002)
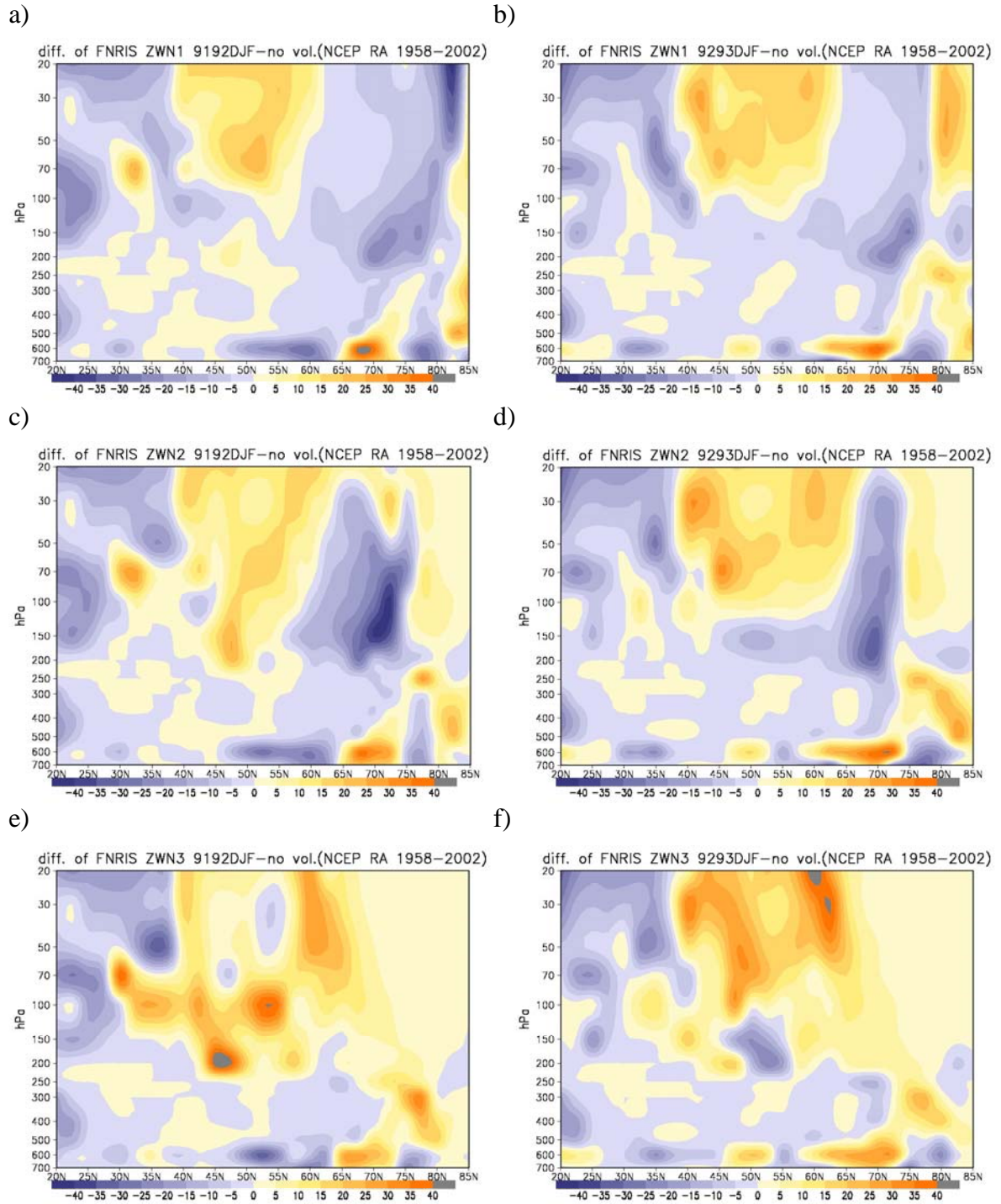
Figure B.14. Difference of f ($n_k^2 < 0$) for stationary planetary waves between 1991-1992 DJF (left column) and 1992-1993 DJF (right column) with DJF (1958-2002) without violent volcanic eruptions (Agung, 1963-1966; El Chichon, 1982-1984; Pinatubo, 1991-1993) (NCEP/NCAR RA) for ZWN 1 wave (first row), ZWN 2 wave (second row) and ZWN 3 wave (bottom row). Unit of f ($n_k^2 < 0$) is %.

a)

EP flux and div.for wn1 stat.(NCEP RA 6364 DJF)

b)

EP flux and div.for wn1 stat.(NCEP RA 6465 DJF)

c)

EP flux and div.for wn2 stat.(NCEP RA 6364 DJF)

d)

EP flux and div.for wn2 stat.(NCEP RA 6465 DJF)

e)

EP flux and div.for wn3 stat.(NCEP RA 6364 DJF)

f)

EP flux and div.for wn3 stat.(NCEP RA 6465 DJF)

g)

EP flux and div.for wn1to3 stat.(NCEP RA 6364 DJF)

h)

EP flux and div.for wn1to3 stat.(NCEP RA 6465 DJF)

Figure B.15. E-P flux and divergence for stationary planetary waves in DJF of 1963-1964 (left column), and1964-1965 (right column) (NCEP/NCAR RA) for ZWN 1 wave (first row), ZWN 2 wave (second row), ZWN 3 wave (third row) and ZWN1+2+3 wave (bottom row). Divergence contour interval is 1 ms^{-1}day^{-1}, the unit of vector is kg s^{-2}.
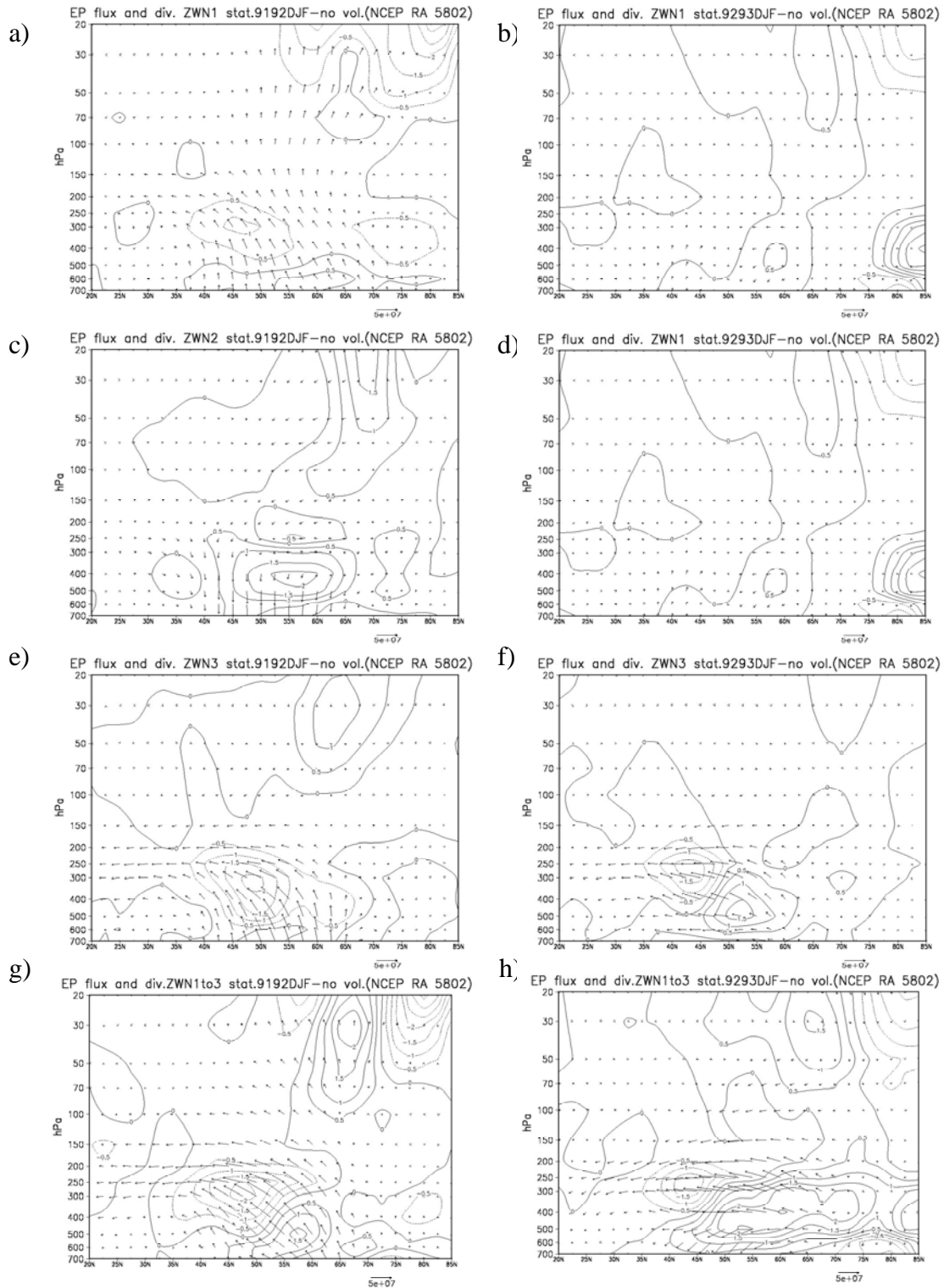
a) EP flux and div. ZWN1 stat.6364DJF—no vol.(NCEP RA 5802)
b) EP flux and div. ZWN1 stat.6465DJF—no vol.(NCEP RA 5802)
c) EP flux and div. ZWN2 stat.6364DJF—no vol.(NCEP RA 5802)
d) EP flux and div. ZWN2 stat.6465DJF—no vol.(NCEP RA 5802)
e) EP flux and div. ZWN3 stat.6364DJF—no vol.(NCEP RA 5802)
f) EP flux and div. ZWN3 stat.6465DJF—no vol.(NCEP RA 5802)
g) EP flux and div.ZWN1to3 stat.6364DJF—no vol.(NCEP RA 5802)
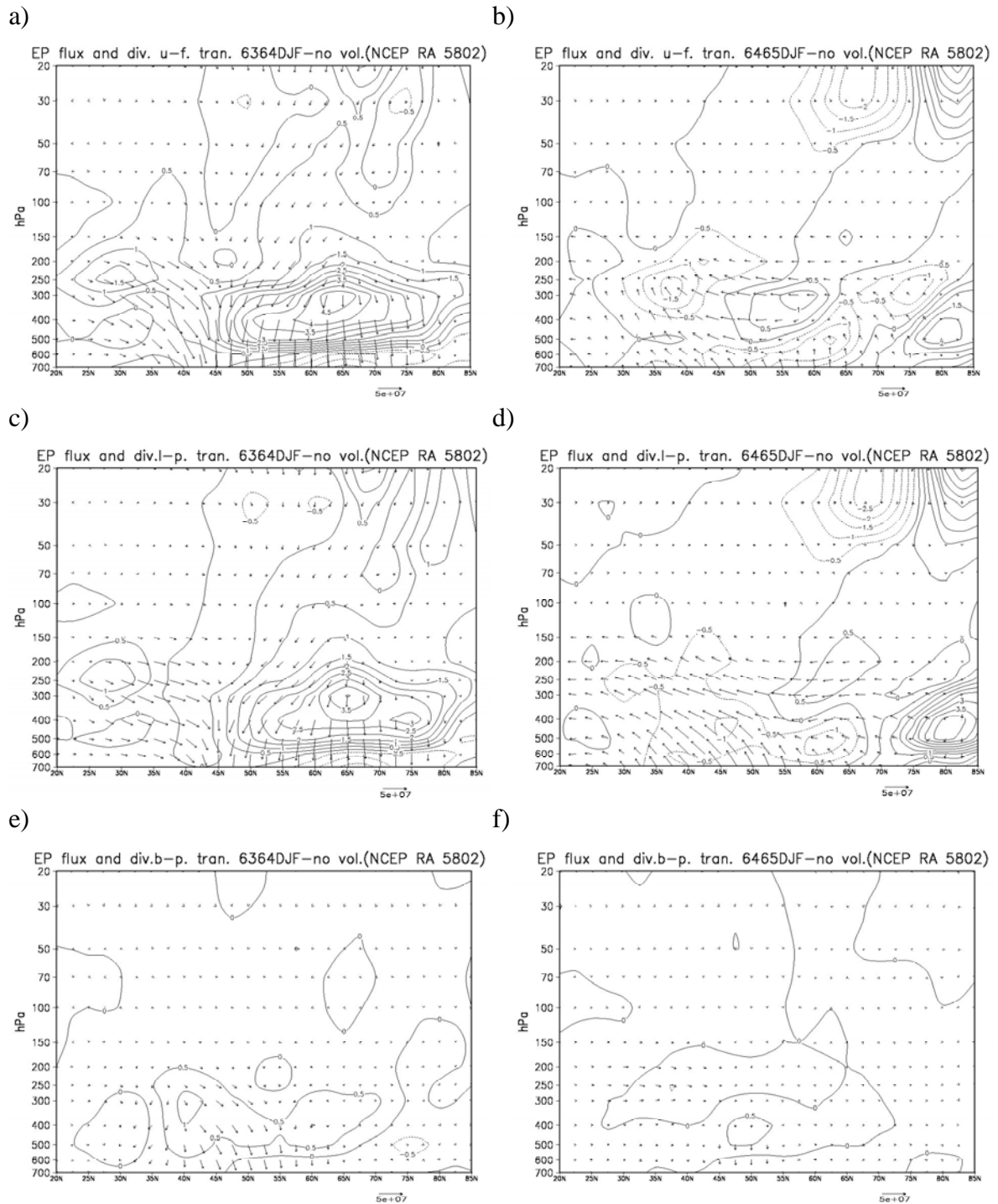h) EP flux and div.ZWN1to3 stat.6465DJF—no vol.(NCEP RA 5802)

Figure B.16. Difference of E-P flux and divergence for stationary planetary waves between 1963-1964 DJF (left column), and 1964-1965 DJF (right column with DJF (1958-2002) without violent volcanic eruptions NCEP/NCAR RA) for ZWN 1 wave (first row), ZWN 2 wave (second row), ZWN 3 wave (third row) and ZWN1+2+3 wave (bottom row). Divergence contour interval is 1 ms^{-1}day^{-1}, the unit of vector is kg s^{-2}.
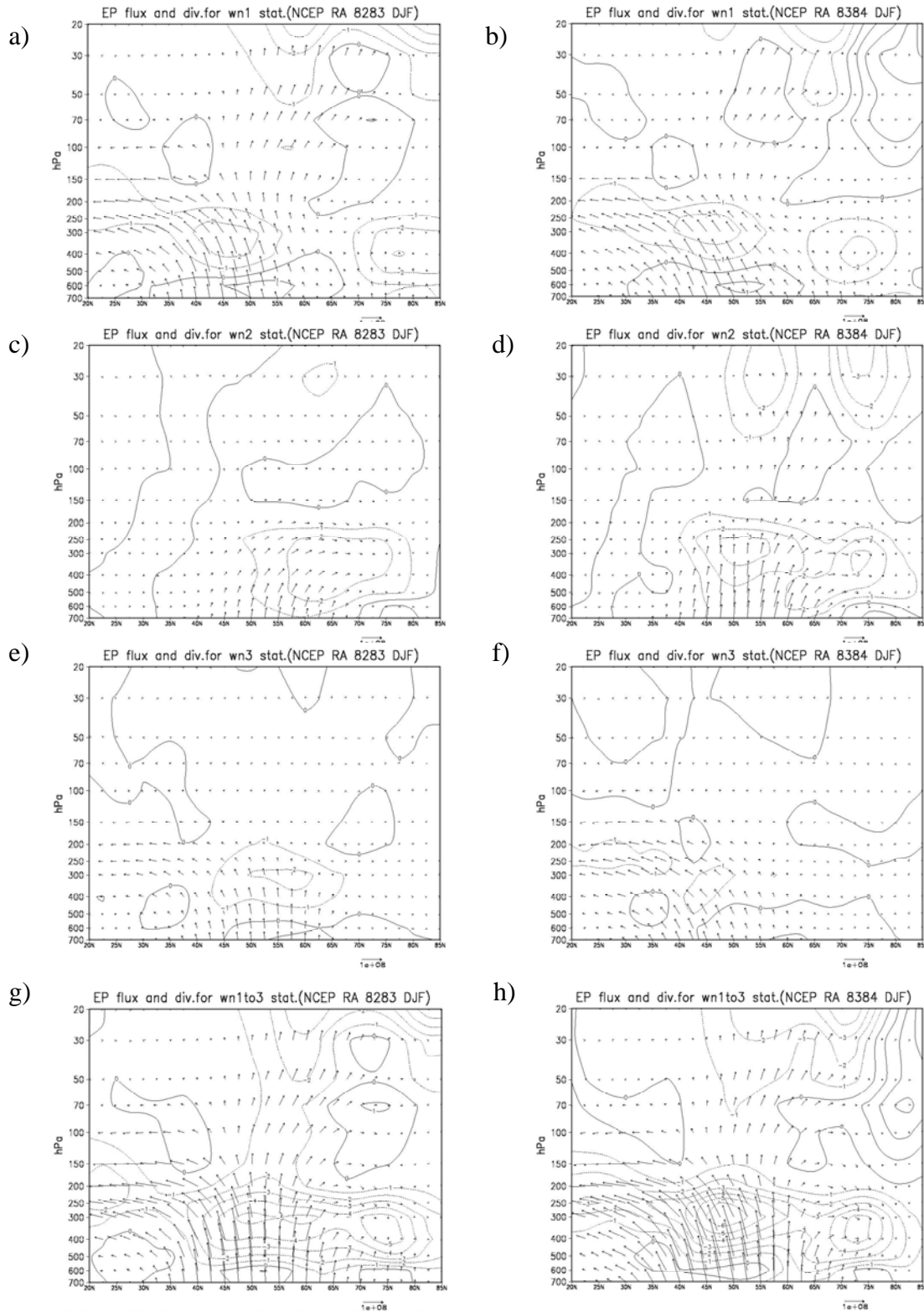
Figure B.17. E-P flux and divergence for stationary planetary waves in DJF of 1982-1983 (left column) and 1983-1984 (right column) (NCEP/NCAR RA) for ZWN 1 wave (first row), ZWN 2 wave (second row), ZWN 3 wave (third row) and ZWN1+2+3 wave (bottom row). Divergence contour interval is 1 ms^{-1}day^{-1}, the unit of vector is kg s^{-2}.
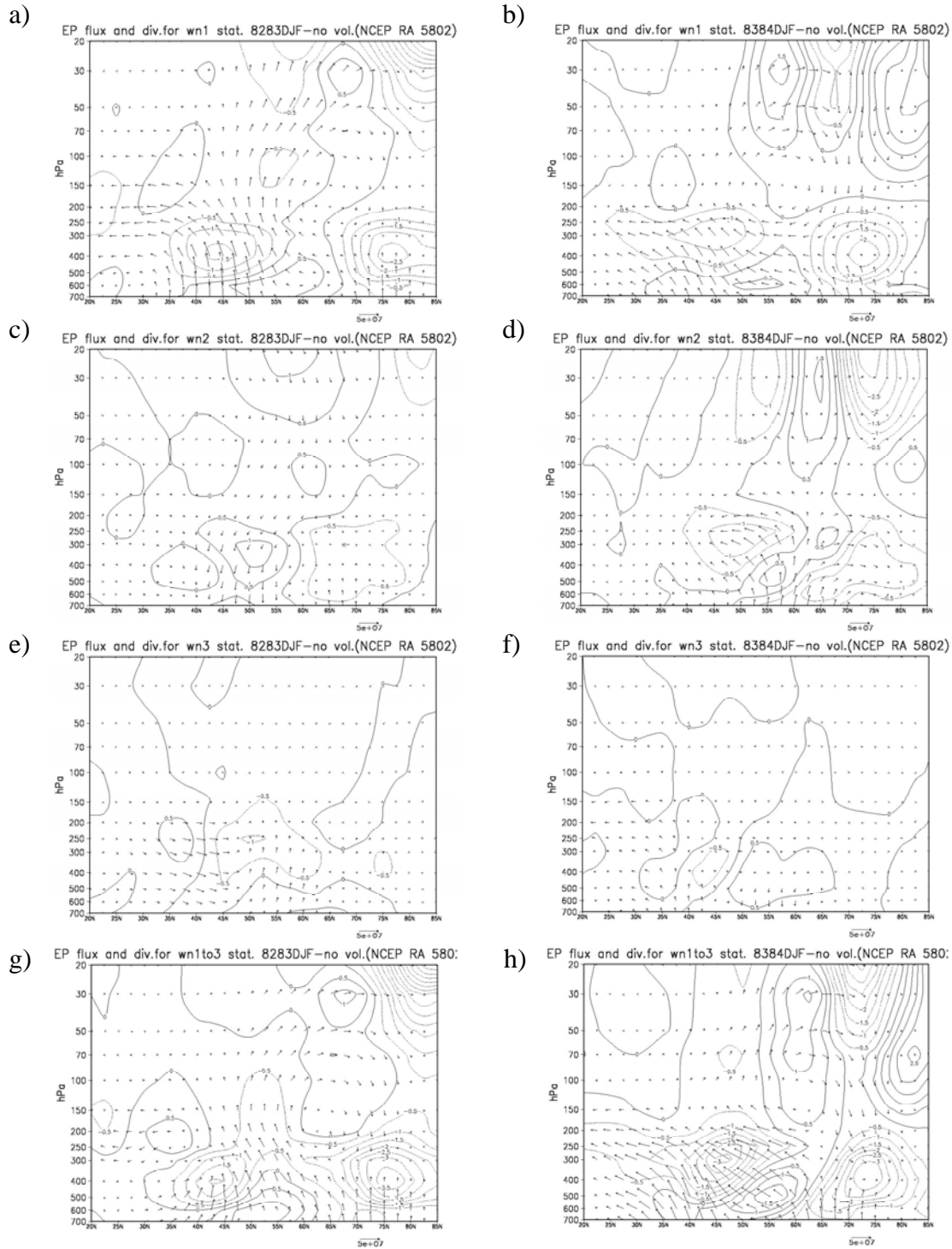
Figure B.18. Difference of E-P flux and divergence for stationary planetary waves between 1982-1983 DJF (left column) and 1983-1984 DJF (right column) with DJF (1958-2002) without violent volcanic (NCEP/NCAR RA) for ZWN 1 wave (first row), ZWN 2 wave (second row), ZWN 3 wave (third row) and ZWN1+2+3 wave (bottom row).
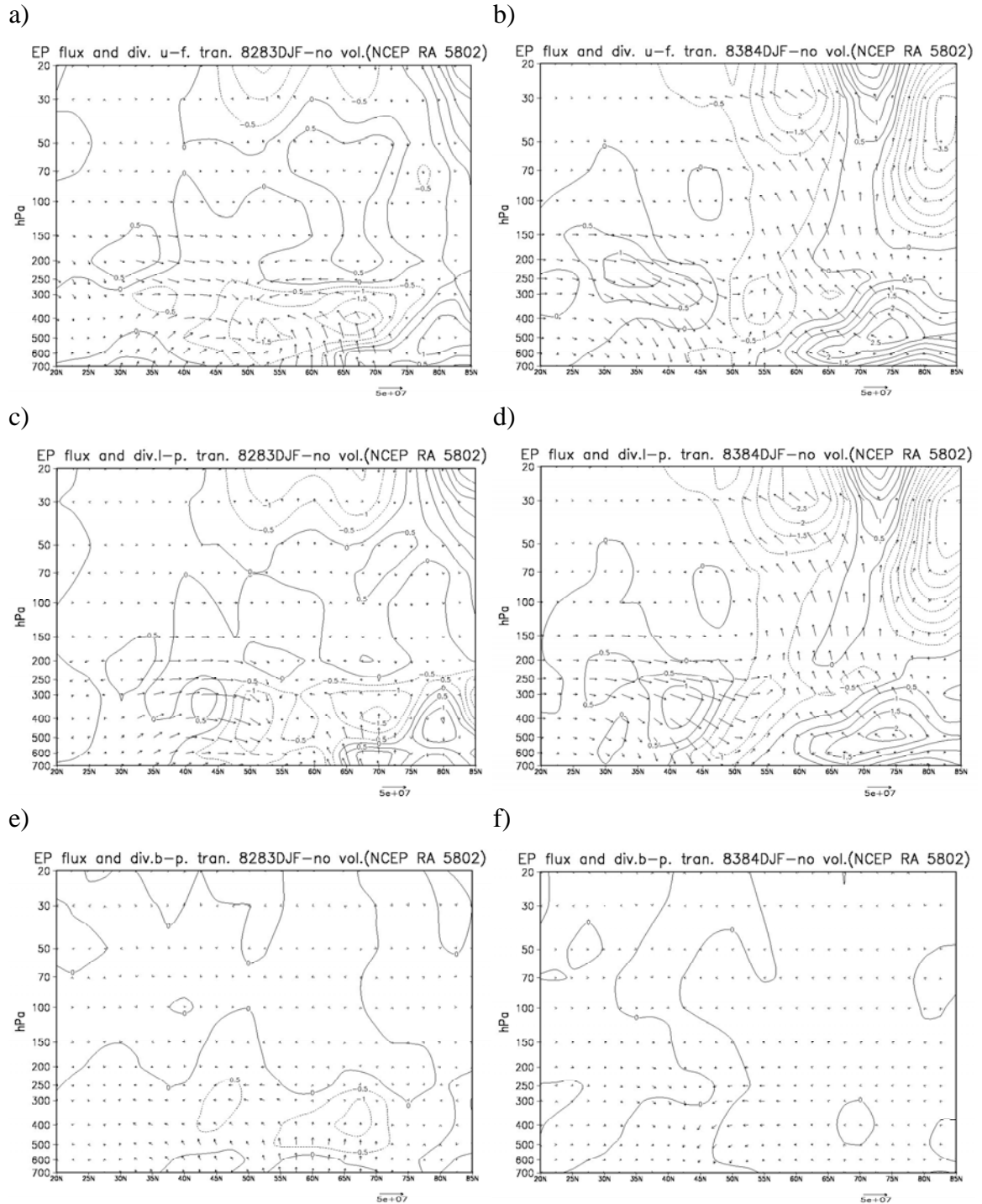
Figure B.19. E-P flux and divergence for stationary planetary waves in DJF of 1991-1992 (left column) and 1992-1993 (right column) (NCEP/NCAR RA) for ZWN 1 wave (first row), ZWN 2 wave (second row), ZWN 3 wave (third row) and ZWN1+2+3 wave (bottom row). Divergence contour interval is 1 ms^{-1}day^{-1}, the unit of vector is kg s^{-2}.

a) EP flux and div. ZWN1 stat.9192DJF—no vol.(NCEP RA 5802)

b) EP flux and div. ZWN1 stat.9293DJF—no vol.(NCEP RA 5802)

c) EP flux and div. ZWN2 stat.9192DJF—no vol.(NCEP RA 5802)

d) EP flux and div. ZWN1 stat.9293DJF—no vol.(NCEP RA 5802)

e) EP flux and div. ZWN3 stat.9192DJF—no vol.(NCEP RA 5802)

f) EP flux and div. ZWN3 stat.9293DJF—no vol.(NCEP RA 5802)

g) EP flux and div.ZWN1to3 stat.9192DJF—no vol.(NCEP RA 5802)

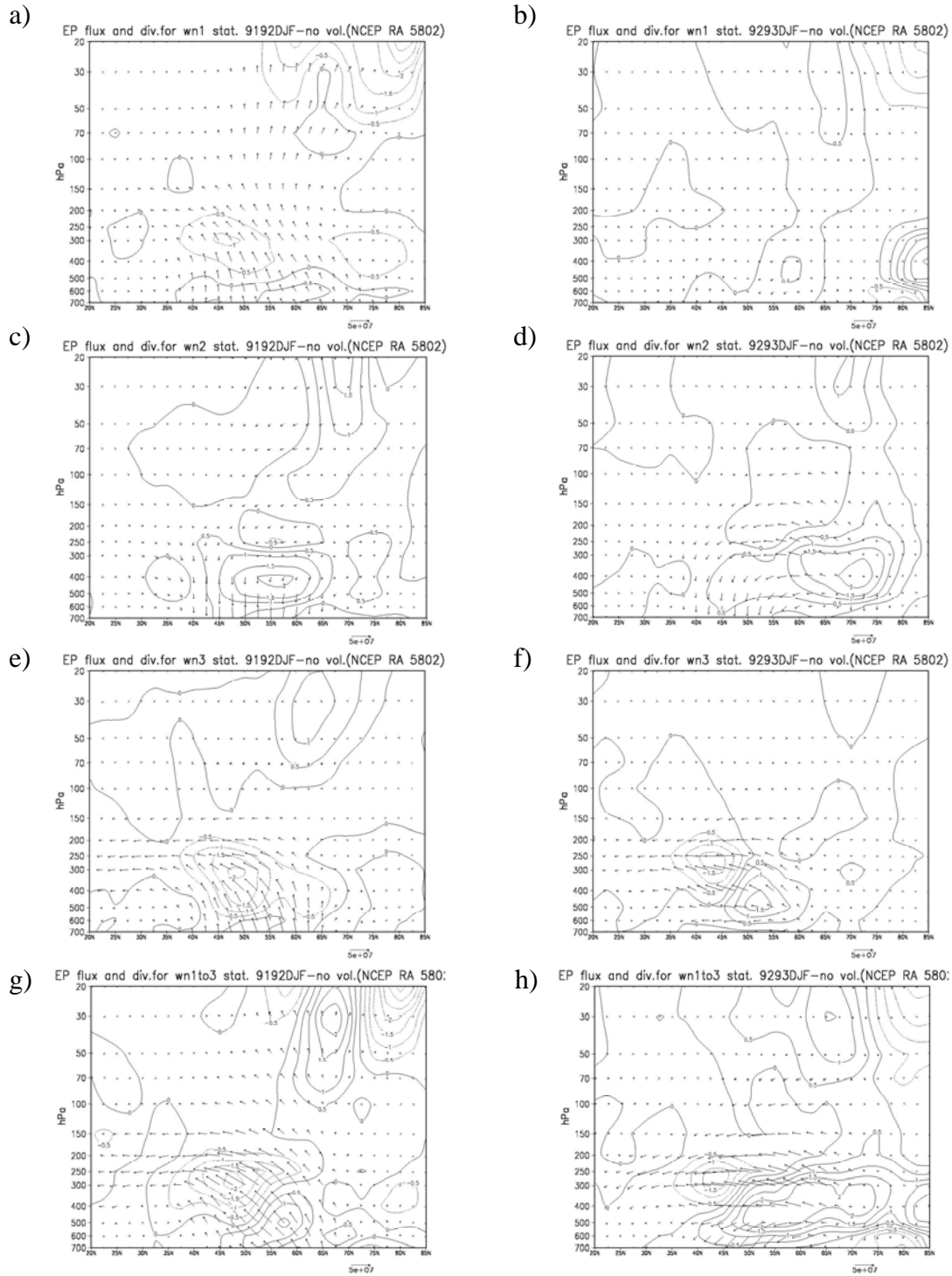h) EP flux and div.ZWN1to3 stat.9293DJF—no vol.(NCEP RA 5802)

Figure B.20. Difference of E-P flux and divergence for stationary planetary waves between 1991-1992 DJF (left column) and 1992-1993 DJF (right column) with DJF (1958-2002) without violent volcanic (NCEP/NCAR RA) for ZWN 1 wave (first row), ZWN 2 wave (second row), ZWN 3 wave (third row) and ZWN1+2+3 wave (bottom row). Divergence contour interval is 1 ms^{-1}day^{-1}, the unit of vector is kg s^{-2}.

a)

b)

c)

d)

e)

f)

g)

h)
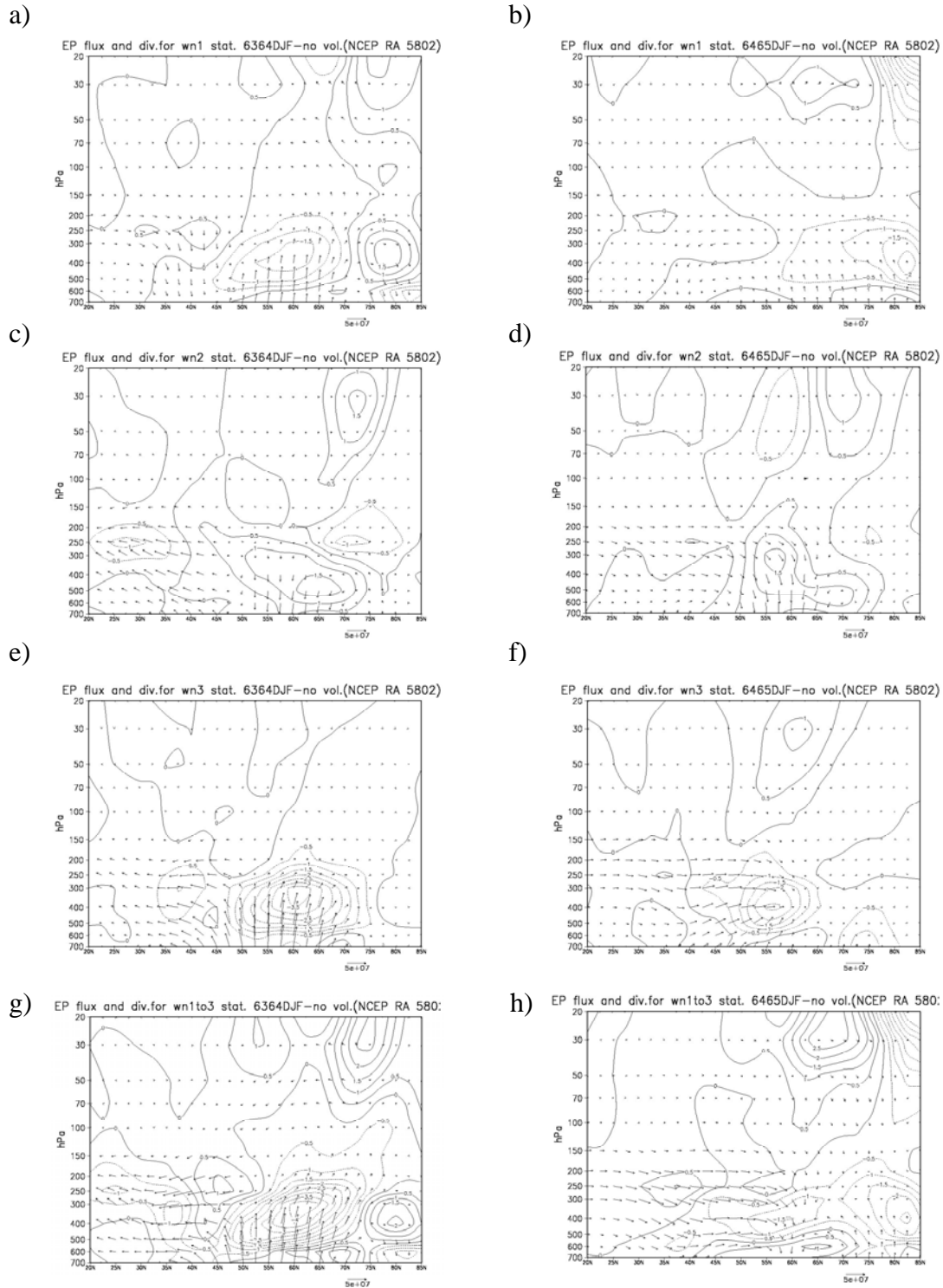
Figure B.21. Difference of E-P flux and divergence for stationary planetary waves between 1963-1964 DJF (left column), and 1964-1965 DJF (right column with DJF (1958-2002) without violent volcanic eruptions NCEP/NCAR RA) for ZWN 1 wave (first row), ZWN 2 wave (second row), ZWN 3 wave (third row) and ZWN1+2+3 wave (bottom row). Divergence contour interval is 1 ms^{-1}day^{-1}, the unit of vector is kg s^{-2}.
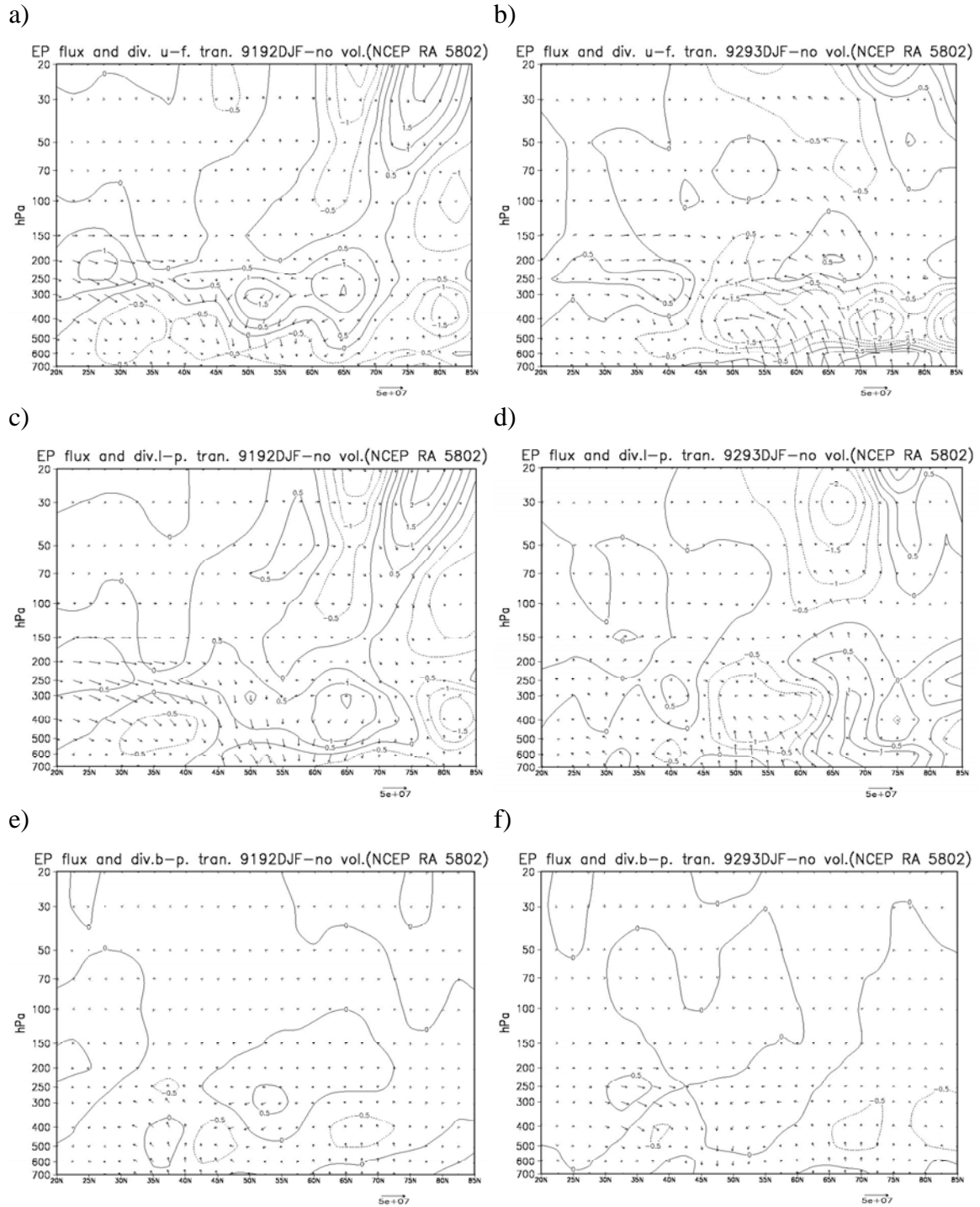
a)

EP flux and div. u-f. tran. 6364DJF-no vol.(NCEP RA 5802)

b)

EP flux and div. u-f. tran. 6465DJF-no vol.(NCEP RA 5802)

c)

EP flux and div.l-p. tran. 6364DJF-no vol.(NCEP RA 5802)

d)

EP flux and div.l-p. tran. 6465DJF-no vol.(NCEP RA 5802)

e)

EP flux and div.b-p. tran. 6364DJF-no vol.(NCEP RA 5802)

f)

EP flux and div.b-p. tran. 6465DJF-no vol.(NCEP RA 5802)

Figure B.22. Difference of E-P flux and divergence for transient planetary waves between 1963-1964 DJF (left column), and 1964-1965 DJF (right column with DJF (1958-2002) without violent volcanic eruptions (Agung, 1963-1965; El Chichon, 1982-1984; Pinatubo, 1991-1993) (NCEP/NCAR RA) for unfiltered wave (first row), low-pass filtered wave (second row) and band-pass filtered wave (third row). Divergence contour interval is 1 ms^{-1}day^{-1}, the unit of vector is kg s^{-2}.

a)
EP flux and div.for wn1 stat. 8283DJF–no vol.(NCEP RA 5802)

b)
EP flux and div.for wn1 stat. 8384DJF–no vol.(NCEP RA 5802)

c)
EP flux and div.for wn2 stat. 8283DJF–no vol.(NCEP RA 5802)

d)
EP flux and div.for wn2 stat. 8384DJF–no vol.(NCEP RA 5802)

e)
EP flux and div.for wn3 stat. 8283DJF–no vol.(NCEP RA 5802)

f)
EP flux and div.for wn3 stat. 8384DJF–no vol.(NCEP RA 5802)

g)
EP flux and div.for wn1to3 stat. 8283DJF–no vol.(NCEP RA 580:

h)
EP flux and div.for wn1to3 stat. 8384DJF–no vol.(NCEP RA 580:

Figure B.23. Difference of E-P flux and divergence for stationary planetary waves between 1982-1983 DJF (left column) and 1983-1984 DJF (right column) with DJF (1958-2002) without violent volcanic (NCEP/NCAR RA) for ZWN 1 wave (first row), ZWN 2 wave (second row), ZWN 3 wave (third row) and ZWN1+2+3 wave (bottom row).

a)

EP flux and div. u−f. tran. 8283DJF−no vol.(NCEP RA 5802)

b)

EP flux and div. u−f. tran. 8384DJF−no vol.(NCEP RA 5802)

c)

EP flux and div.l−p. tran. 8283DJF−no vol.(NCEP RA 5802)

d)

EP flux and div.l−p. tran. 8384DJF−no vol.(NCEP RA 5802)

e)

EP flux and div.b−p. tran. 8283DJF−no vol.(NCEP RA 5802)

f)

EP flux and div.b−p. tran. 8384DJF−no vol.(NCEP RA 5802)

Figure B.24. Difference of E-P flux and divergence for transient planetary waves between 1982-1983 DJF (left column) and 1983-1984 DJF (right column) with DJF (1958-2002) without violent volcanic eruptions (Agung, 1963-1966; El Chichon, 1982-1984; Pinatubo, 1991-1993) (NCEP/NCAR RA) for unfiltered wave (first row), low-pass filtered wave (second row) and band-pass filtered wave (third row). Divergence contour interval is 1 ms^{-1}day^{-1}, the unit of vector is kg s^{-2}.

a)
EP flux and div.for wn1 stat. 9192DJF—no vol.(NCEP RA 5802)

b)
EP flux and div.for wn1 stat. 9293DJF—no vol.(NCEP RA 5802)

c)
EP flux and div.for wn2 stat. 9192DJF—no vol.(NCEP RA 5802)

d)
EP flux and div.for wn2 stat. 9293DJF—no vol.(NCEP RA 5802)

e)
EP flux and div.for wn3 stat. 9192DJF—no vol.(NCEP RA 5802)

f)
EP flux and div.for wn3 stat. 9293DJF—no vol.(NCEP RA 5802)

g)
EP flux and div.for wn1to3 stat. 9192DJF—no vol.(NCEP RA 580:

h)
EP flux and div.for wn1to3 stat. 9293DJF—no vol.(NCEP RA 580:

Figure B.25. Difference of E-P flux and divergence for stationary planetary waves between 1991-1992 DJF (left column) and 1992-1993 DJF (right column) with DJF (1958-2002) without violent volcanic (NCEP/NCAR RA) for ZWN 1 wave (first row), ZWN 2 wave (second row), ZWN 3 wave (third row) and ZWN1+2+3 wave (bottom row). Divergence contour interval is 1 ms^{-1}day^{-1}, the unit of vector is kg s^{-2}.

a)

EP flux and div. u-f. tran. 9192DJF-no vol.(NCEP RA 5802)

b)

EP flux and div. u-f. tran. 9293DJF-no vol.(NCEP RA 5802)

c)

EP flux and div.l-p. tran. 9192DJF-no vol.(NCEP RA 5802)

d)

EP flux and div.l-p. tran. 9293DJF-no vol.(NCEP RA 5802)

e)

EP flux and div.b-p. tran. 9192DJF-no vol.(NCEP RA 5802)

f)

EP flux and div.b-p. tran. 9293DJF-no vol.(NCEP RA 5802)

Figure B.26. Difference of E-P flux and divergence for transient planetary waves between 1991-1992 DJF (left column) and 1992-1993 DJF (right column) with DJF (1958-2002) without violent volcanic eruptions (NCEP/NCAR RA) for unfiltered wave (first row), low-pass filtered wave (second row) and band-pass filtered wave (third row). Divergence contour interval is 1 ms^{-1}day^{-1}, the unit of vector is kg s^{-2}.

Bibliography:

1.   AchutaRao, K., K. R. Sperber, 2006: ENSO simulation in coupled ocean-atmosphere models: are the current model better. Climate Dyn., 27, 1-15.
2.   Andrews, D. G., 1985: Wave, mean-flow interaction in the middle atmosphere. Adv. Geophys., 28A, 249-275.
3.   Andrews, D. G., J.R. Holton, and C. B. Leovy, 1987: Middle Atmosphere Dynamics. Academic Press Inc., 489 pp.
4.   Angell, J. K. and J. Korshover, 1983: Comparison of stratospheric warming following Agung and Chichon. Mon. Weather Rev., 111, 2129-2135.
5.   Angell, J. K., 1993: Comparision of stratospheric warming following Agung, El Chichon and Pinatubo volcanic eruptions. Geo. Res. Lett., 20, 715-718.
6.   Angell, J. K., 1997a: Stratospheric warming due to Agung, El Chichon, and Pinatubo taking into account the quasi-biennial of oscillation. J. Geophys. Res., 102, 9479-9485.
7.   Angell, J. K., 1997b: Estimated impact of Agung, El Chichon and Pinatubo volcanic eruptions on global and regional total ozone after adjustment for the QBO. Geophys. Res. Lett., 24, 647-650.
8.   Antuña, Juan Carlos, Alan Robock, Georgiy Stenchikov, Jun Zhou, Christine David, John Barnes, and Larry Thomason, 2003: Spatial and temporal variability of the stratospheric aerosol cloud produced by the 1991 Mount Pinatubo eruption. J. Geophys. Res., 108 (D20), 4624, doi:10.1029/2003JD003722.
9.   Austin, J., N. Butchart, and R. S. Swinbank, 1997: Sensitivity of ozone and temperature to vertical resolution in a GCM with coupled stratospheric chemistry. Q. J. R. Meteorol. Soc., 123, 1405-1431.
10.   Baldwin, M. P., D. O'Sullivan, 1995: Stratospheric effects of ENSO-related tropospheric circulation anomalies. J. Climate, 8, 649-667.
11.   Baldwin, M. P., and T. J. Dunkerton, 1999: Propagation of the Arctic Oscillation from the stratosphere to the troposphere. J. Geophys. Res., 104, 30937-30946.
12.   Baldwin, M. P., and T. J. Dunkerton, 2001: Stratospheric harbingers of anomalous weather regimes. Science, 294, 581-584.
13.   Blackmon, M. L., 1976: A climatological spectral study of the 500mb geopotential height of the Northern Hemisphere. J. Atmos. Sci., 33, 1607-1623.
14.   Blackmon, M. L., and N. –C. Lau, 1980: Regional characteristics of the Northern Hemisphere wintertime circulation: A comparison of the simulation of a GFDL general circulation model with observations. J. Atmos. Sci., 37, 497-514.
15.   Boville, B. A., 1984: The influence of the polar night jet on the tropospheric circulation in a GCM. J. Atmos. Sci., 41, 1132-1142.
16.   Boville, B. A., 1986: Wave-mean flow interaction in a general circulation model of the troposphere and stratosphere. J. Atmos. Sci., 43, 1711-1725.
17.   Boville, B., and X. Cheng, 1988: Upper boundary effects in a General Circulation Model. J. Atmos. Sci., 45, 2591-2608.
18.   Boville, B. A., 1995: Middle atmosphere version of the CCM2 (MACCM2): Annual cycle and interannual variability. J. Geophys. Res., 100, 9017-9039.

19.   Butchart, N., S. A. Clough, T. N. Palmer, and P. J. Trevelyan, 1982: Simulations of an observed stratospheric warming with quasigeostrophic refractive index as a model diagnostic. Q. J. R. Meteorol. Soc., 108, 475-502.

20.   Calvo, N., et al, 2004: Analysis of the ENSO signal in tropospheric and stratospheric temperature observed by MSU, 1979-2000. J. Climate, 17, 3934-3946.

21.   Castanheira, J. M., and H. F.-Graf, 2003: North Pacific-North Atlantic relationships under stratospheric control?. J. Geophys. Res., 108, 11.

22.   Charney, J. G., and P. G. Drazin, 1961: Propagation of planetary-scale disturbances from the lower into the upper atmosphere. J. Geophys. Res., 66, 83-109.

23.   Chen, P., and W. A. Robinson, 1992: Propagation of planetary waves between the troposphere and stratosphere. J. Atmos. Sci., 49, 2533-2345.

24.   Chen, W., H. -F. Graf, and M. Takahashi, 2002: Observed interannual oscillation of planetary wave forcing in the Northern Hemisphere winter. Geophys. Res. Lett., 29, 2037, doi: 10.1029/2002Gl016062, 2002.

25.   Christiansen, B., 2003: Evidence of nonlinear climate change: Two stratospheric regimes and a regime shift. J. Climate, 16, 3681-3690.

26.   Christiansen, B., 2005: Bimodality of the planetary-scale atmospheric wave amplitude index. J. Climate, 62, 2528-2541.

27.   Cohen, J., A. Frei, and R. D., Rosen, 2005: The role of boundary conditions in AMIP-2 simulations of the NAO. J. Clim., 18, 973-981.

28.   Cordero, E. C., and P. M. de F. Forster, 2006: Stratospheric variability and trends in IPCC model simulations. Atmos. Chem. Phys. Discuss., 6, 7657-7695.

29.   Covey, C. et al., 2004: Coupled ocean-atmosphere climate simulations compared with simulations using prescribed sea surface temperature effect of a "perfect ocean". Global and Planetary Change, 41, 1-14.

30.   Dameris, et al., 2005: Long-term changes and variability in a transient simulation with a chemistry-climate model employing realistic forcing. Atmos. Che. Phys., 5, 2121-2145.

31.   Dickinson, R. E., 1968: Planetary Rossby waves propagating vertically through weak westerly wind wave guides. J. Atmos. Sci., 25, 984-1002.

32.   Eliassen, A., and E. Palm, 1961: On the transfer of energy in stationary mountain waves. Geofys. Publ., 22-3, 1-23.

33.   Eyring, V., et al., 2004: Brief report on the Workshop on Process-Oriented Validation of Coupled Chemistry-Climate Models. SPARC Newsletter, No. 22, 27-28.

34.   Garcia-Herrera, R., N. Calvo, R. R. Garcia, and M. A. Giorgetta, Propagation of ENSO temperature signals into the middle atmosphere: A comparison of two general circulation models and ERA-40 reanalysis data, J. Geophys. Res., 111, D06101, doi:10.1029/2005JD006061, 2006.

35.   Gates, W. L., et al., 1998: An overview of the results of the atmospheric model intercomparison project (AMIP). PCMDI Report No.45, 33pp.

36.   Geller, M. A., and J. C. Alpert, 1980: Planetary wave coupling between the troposphere and the middle atmosphere as a possible sun-weather mechanism. J. Atmos. Sci., 37, 1197-1214.

37.   Ghil, M, 2001: Natural Climate Variability. in Encyclopedia of Global Environmental Change, vol. 1, Ted Munn, Ed., (John Wiley and Sons, London), 544-549.

38.   Gillett, N. P., M. R. Allen, R. E. Mcdonald, C. A. Senior, D. T. Shindell, and G. A. Schmidt, 2002: How linear is the Arctic Oscillation response to greenhouse gases? J. Geophys. Res., 107, D3, 10.1029/2001JD000589, 2002b.

39.   Giorgetta, M., et al, 2006: Climatology and forcing of the quasi-biennial oscillation in the MAECHAM5 model. J. Climate, 19, 3882-3901.

40.   Graf, H. -F, 1992: Arctic radiation deficit and climate variability. Climate Dyn., 7, 19-28.

41.   Graf, H. –F., I. Kirchner, Q. Robock, and I. Schult, 1993: Pinatubo eruption winter climate effects: model versus observations. Clim. Dyn., 9, 81-93.

42.   Graf, H. –F., J. Perlwitz, and I. Kirchner, 1994: Northern Hemisphere tropospheric mid-latitude circulation after violent volcanic eruptions. Contrib. Atmos. Phys., 67, 3-13.

43.   Graf, H. –F., J. Feichter, and B. Langmann, 1997: Volcanic sulfur emission: Estimate of source strength and its contributiuon to the global sulfate distribution. J. Geophys. Res., 102, 10727-10738.

44.   Hamilton, K., 1993a: An examination of observed Southern Oscillation effects in the Northern Hemisphere stratosphere. J. Atmos. Sci., 50, 3468-3473.

45.   Hamilton, K., 1993b: A general circulation model simulation of El Nino effects in the extratropical Northern Hemisphere stratosphere. Geophys. Res. Lett., 20, 1803-1806.

46.   Hamilton, K., 1995: Interannual variability in the Northern Hemisphere winter middle atmosphere in control and perturbed experiments with the GFDL SKYHI general circulation model. J. Atmos. Sci., 52, 44-66.

47.   Hamilton, K., R. J. Wilson, J. D. Mahlman, and L. J. Umscheid, 1995: Climatology of the SKYHI troposphere-stratosphere-mesosphere general circulation model. J. Atmos. Sci., 52, 5-43.

48.   Hansen, J. E., W.-C., Wang, and A. A. Lacis, 1978: Mount Agung eruption provides test of a global climatic perturbation. Science, 199, 1065-1068.

49.   Hansen, J., A. Lacis, R. Ruedy, and M. Sato, 1992: Potential climate impact of Mount Pinatubo eruption, *Geophys. Res. Lett.*, *19*(2), 215–218.

50.   Hartmann, D. L., and F. Lo, 1998: Wave-driven zonal flow vacillation in the Southern Hemisphere. J. Atmos. Sci., 55, 1303-1315.

51.   Hein, R., M. Dameris, C. Schnadt, C. Land, V. Grewe, I. Koehler, M. Ponater, R. Sausen, B. Steil, J. Landgraf, and C. Bruehl, 2001: Results of an interactively coupled atmospheric chemistry-general circulation model: Comparison with observations. Ann. Geophys., 19, 435-457.

52.   Hitoshi, M., and T. Hirooka, 2004: Predictability of stratospheric sudden warming: A case study for 1998/99 winter. Monthly Weather Review, 132, 1764-1776.

53.   Hoerling, M. P., and A. Kumar, 1997: Origins of extreme climate states during the 1982-83 ENSO winter. J. Climate, 10, 2859-2870.

54.   Hoerling, M. P., A. Kumar, and M. Zhong, 1997: El Nino, La Nina, and the nonlinearity of their teleconnections. J. Climate, 10, 1769-1786.

55.   Hofmann, D. J., 1987: Perturbations to the global atmosphere associated with the El Chichon volcanic eruption of 1982. Rev. Geophys., 25, 743-759.

56.   Hu, Y., and K. K. Tung, 2002: Interannual and decadal variations of planetary wave activity, stratospheric cooling, and northern hemisphere annular mode. J. Climate, 15, 1659-1673.

57.   Hu, Y., and K. K. Tung, 2002: Tropospheric and equatorial influences on planetary-wave amplitude in the stratosphere. Geophysical Research Letter, 29, 6-1 – 6-4.

58.   Huang, R., and K. Gambo, 1982: The response of a Hemispheric Multi-Level Model Atmosphere to Forcing by Topography and Stationary Heat Sources (I) Foring by Topography. J. Meteorol. Soc. Japan, 60, 78-92.

59.   Huang, R., 1984: The characteristics of the forced stationary planetary wave propagations in summer northern hemisphere. Advances in Atmospheric Sciences, 1, 84-94.

60.   Hurrel, J. W., M.P. Hoerling, A. S. Phillips, and T. Xu, 2004: Twentieth century North Atlantic climate change. Part I: Assessing determinism. Climate Dyn., 23, 371-389.

61.   Jacqmin, D., and R. S. Lindzen, 1985: The causation and sensitivity of the Northern winter planetary waves. J. Atmos. Sci., 42, 724-745.

62.   Jungclaus, J. H., et al., 2006: Ocean circulation and tropical variability in the coupled model ECHAM5/MPI-OM. J. Climate, 19, 3952-3972.

63.   Kalnay, E., M. Kanamitsu, R. Kistler, W. Collins, D. Deaven, L. Gandin, M. Iredell, S. Saha, G. White, J. Woollen, Y. Zhu, M. Chelliah, W. Ebisuzaki, W. Higgins, J. Janowiak, K. C. Mo, C. Ropelewski, J. Wang, A. Leetmaa, R. Reynolds, R. Jenne, and D. Joseph, 1996: The NCEP/NCAR 40-year reanalysis project. Bull. Amer. Meteor. Soc., 77, 437-472.

64.   Kanamitzu, M., S. Hwang, 2006: The role of sea surface temperature in reanalysis. Monthly Weather Review, 134, 532-552.

65.   Kanzawa, H., 1982: Eliassen-Palm flux diagnostics and the effect of the mean wind on planetary wave propagation for an observed sudden stratospheric warming. J. Meteor. Soc. Japan, 60, 1063-1073.

66.   Kanzawa, H., 1984: Four observed sudden warmings diagnosed by the Eliassen-Palm flux and refractive index. In "Dynamics of the Middle Atmosphere" (J. R. Holton and T. Matzuno, eds.), 307-331. Terrapub, Tokyo.

67.   Kerr, R. A., 1983: El Chichon climate effect estimated. Science, 219, 157.

68.   Kirchner, I., and H. – F. Graf, 1995: Volcanoes and El Nino: Signal separation in Northern Hemisphere winter. Clim. Dyn., 11, 341-358.

69.   Kirchner, I., G. Stenchikov, H. –F. Graf, A. Robock, and J. Antuna, 1998: Cli,ate model simulation of winter warming and summer cooling following the 1991 Mount Pinatubo volcanic eruption. MPI report, 261, 35pp.

70.   Kistler, R., E. Kalnay, W. Collins, S. Saha, G. White, J. Woollen, M. Chelliah, W. Ebisuzaki, M. Kanamitsu, V. Kousky, H. van den Dool, R. Jenne, M. Fiorino, 2001: The NCEP-NCAR 50-year reanalysis: Monthly means CD-ROM and documentation. Bull. Amer. Meteor. Soc., 82, 247-268.

71.   Kodera, K., K. Yamazaki, M. Chiba, and K. Shibata, 1990: Downward propagation of upper stratospheric mean zonal wind perturbation to the troposphere. Geophys. Res. Lett., 17, 1263-1266.

72.   Kodera, K., 1994: Influence of volcanic eruptions on the troposphere through stratospheric dynamical processes in the northern hemisphere winter. J. Geophys. Res., 99, 1273-1282.

73.   Kodera, K., K. Yamazaki, 1994: A possible influence of recent polar stratospheric cooling on the troposphere in the northern hemisphere winter. Geophys. Res. Lett., 21, 809.

74.   Kodera, K., M. Chiba, H. Koide, A. Kitoh, and Y. Nikaidou, 1996: Interannual variability of the winter stratosphere and troposphere in the Northern Hemisphere. J. Meteor. Soc. Japan, 74, 365-382.

75.   Kodera, K., and Y. Kuroda, 2000: a mechanistic model study of slowly propagating coupled stratosphere-troposphere variability. J. Geophys. Res., 105, 12365-12370.

76.   Kumar, A., and M. P. Hoerling, 1997: Interpretation and implications of the observed inter-El Nino variability. J. Climate, 10, 83-91.

77.   Lacis, A., J. Hansen, M. Sato, 1992: Climate forcing by stratospheric aerosols. Geophys. Res. Lett, 19, 1607-1610.

78.   Li, Q., H.-F. Graf, and M. Giorgetta, 2006: Stationary planetary wave propagation in Northern Hemisphere winter – climatological analysis of the refractive index. Amos. Chem. Phy. Dis., 6, 9033-9067.

79.   Li, Q., H.-F. Graf, and M. Giorgetta, 2006: Different contribution of stationary and transient planetary waves propagation in maintaining of stratospheric polar vortex regimes in Northern Hemisphere winter. (submitted to GRL)

80.   Liess, S., L. Bengtsson, and K. Arpe, 2004: The intraseasonal oscillation in ECHAM4 Part I: Coupled to a comprehensive ocean model. Climate Dyn., 22, 653-669

81.   Liess, S., and L. Bengtsson, 2004: The intraseasonal oscillation in ECHAM4 Part II: Sensitivity studies. Climate Dyn., 22, 671-688.

82.   Limpasuvan, V., and D. L. Hartmann, 2000: Wave-maintained annular modes of climate variability. J. Climate, 13, 4414-4429.

83.   Limpasuvan, V., D. W. J. Thompson, and D. L. Hartmann, 2004: The life cycle of Northern Hemisphere Sudden Stratospheric Warming. J. Climate, 17, 2584-2597.

84.   Limpasuvan, V., D. L. Hartmann, D. W. J. Thompson, K. Jeev, and Y. L. Yung, 2005: Stratosphere-Troposphere evolution during polar vortex intensification. J. Geophy. Res., 110, D24101.

85.   Lin, B., 1982 : The behavior of winter stationary planetary waves forced by topagraphy and diabatic heating. J. Atmos. Sci., 39, 1206-1226.

86.   Manzini, E., and L. Bengtsson, 1996: Stratospheric climate and variability fro a general circulation model and observations. Climate Dyn., 12, 615-639.

87.   Manzini, E., M. A. Giorgetta, M. Esch, L. Kornblueh, and E. Roeckner, 2006: The influence of sea surface temperatures on the Northern winter stratosphere: Ensemble simulations with the MAEHCAM5 model. J. Climate, 19, 3863-3881.

88.   Mao, J., and A. Robock, 1998: Surface air temperature simulations y AMIP general circulation models: Volcanic and ENSO signals and systematic errors. J. Clim., 11, 1538-1552.

89.   Marsland, S. J., H. Haak, J. H. Jungclaus, M. Latif, and F. Röske, 2003: The Max Planck Institute global ocean/sea ice model with orthogonal curvilinear coordinates. Ocean Modell., 5, 91-127.

90.   Matsuno, 1970: Vertical propagation of stationary planetary waves in the winter Northern Hemisphere. J. Atmos. Sci., 27, 871-883.

91.   Matsuno, T., 1971: A dynamical model of the stratospheric sudden warming. J. Atmos. Sci., 28, 1479-1494.

92.   McInturff, R. M., A. J. Miller, J. K. Angell, and J. Korshover, 1971: Possible effects on the stratosphere of the 1963 Mt. Agung volcanic eruption. J. Atmos. Sci., 28, 1304-1307.

93.   Mcintyre, M. E., and T. N. Palmer, 1984: The 'surf zone' in the stratosphere. J. Atmos. Terr. Phys., 46, 825-849.

94.   Minnis, P., E. F. Harrison, L. L. Stowe, G. G. Gibson, F. M. Denn, D. R. Doelling Jr., and W. L. Smith, 1993: Radiative climate foring by the Mount Pinatubo eruption. Science, 259, 1411-1415.

95.   Mukougawa, H., and T. Hirooka, 2004: Predictability of stratospheric sudden warming: A case study for 1998/99 winter. Mon. Wea. Rev., 132, 1764-1776.

96.   Newell, R. E., 1970: Stratospheric temperature change from the Mt. Agung volcanic eruption of 1963. J. Atmos. Sci., 27, 977-978.

97.   Oman, L., A. Robock, and G. Stenchikov, 2005: Climatic response to high-latitude volcanic eruptions. J. Geophys. Res., 110, D13103(1-13).

98.   O'Neill, A., and C. E. Youngblut, 1982: Stratospheric warming diagnosed using the Transformed Eulerian-Mean equations and the effect of the mean state on wave propagation. J. Atmos. Sci., 39, 1370-1386.

99.   Palmer, T. N., 1981(a): Diagnostic study of a wavenumber-2 stratospheric sudden warming in a transformed Eulerian-mean formalism. J. Atmos. Sci., 28, 844-855.

100. Palmer, T. N., 1981(b): Aspects of Stratospheric Warmings studied from a Transformed Eulerian-Mean viewpoint. J. Geophys. Res., 86, 9679-9687.

101. Palmer, T. N., 1993: A nonlinear dynamical perspective on climate change. Weather, 48, 314-326.

102. Parker, D. E., and J. L. Barnscombe, 1983: Stratospheric warming following the El Chichon volcanic eruption. Nature, 301, 406-408.

103. Pawson, S., K. Labitzke, R. Lenschow, B. Naujokat, B. Bajewski, M. Wiesner, and R. –C. Wohlfart, 1993: Climatology of the Northern Hemisphere stratosphere derived from Berlin analyses. Part 1: Monthly means. Dietrich-Reimer-Verlag, 299 pp.

104. Pawson, S., K. Lodera, et al., 2000: The GCM-Reality Intercomparison Project for SPARC (GRIPS): Scientific Issues and Initial Results. Bull. Amer. Meteor. Soc., 81, 781-796.

105. Peng, S., W. A. Robinson., and M. P. Hoerling, 1997: The modeled atmospheric response to midlatitude SST anomalies and its dependence on background circulation states. J. Climate, 10, 971-987.

106. Perlwitz, J., and H. –F. Graf, 1995: The statistical connection between tropospheric and stratospheric circulation of the Northern Hemisphere in winter. J. Climate, 8, 2281-2295.

107. Perlwitz, J., 2000: The Dynamical Link Between the Troposphere and Stratosphere and its Potential to Affect Climate (Ph. D. dissertation). Max-Planck-Institut fuer Meteorologie, Hamburg, 145 pp.

108. Perlwitz, J., and H. –F. Graf, 2001a: Troposphere-stratosphere dynamic coupling under strong and weak polar vortex conditions. Geophys. Res. Lett., 28,271-274.

109. Perlwitz, J., and H. –F. Graf, 2001b: The variability of the horizontal circulation in the troposphere and stratosphere – a comparison. Theor. Appl. Climatol., 69, 149-161.

110. Perlwitz, J., and N. Harnik, 2003: Observational evidence of a stratospheric influence on the troposphere by planetary wave reflection. J. Climate, 16, 3011-3026.

111. Perlwitz, J., and N. Harnik, 2004: Downward coupling between the Stratosphere and Troposphere: The relative roles of wave and zonal mean process. J. Climate, 17, 4902-4909.

112. Pittock, A. B., 1974: Stratospheric temperature anomalies in 1963 and 1966. Q. J. R. Meteorol. Soc., 100, 39-45.

113. Quadrelli, R., and J. M. Wallace, 2002: Dependence of the structure of the Northern Hemisphere annular mode on the polarity of ENSO. Geophys. Res. Lett., 29, 2132, doi:10.1029/2002GL015807.

114. Quiroz, R. A., 1983: The isolation of stratospheric temperature change due to the El Chichon volcanic eruption from nonvolcanic signals. J. Geophys. Res., 88, 6773-6780.

115. Ramachandran, S., V. Ramaswamy, Georgiy L. Stenchikov, and Alan Robock, 2000: Radiative impacts of the Mt. Pinatubo volcanic eruption: Lower stratospheric response. J. Geophys. Res., 105, 24,409-24,429.

116. Ramaswamy, V., M. D. Schwarzkopf, W. J. Randel, B. D. Santer, B. J. Soden, G. L. Stenchikov, 2006: Anthropogenic and natural influences in the evolution of lower stratospheric cooling. Science, 311, 1138-1141.

117. Randel, W. J., 1987: Study of planetary waves in the southern winter Troposphere and Stratosphere. part I: wave structure and vertical propagation. J. Atmos. Sci., 44, 917-935.

118. Randel, W. J., F. Wu, J. M. Russell III, J. W. Waters, and L. Froidevaux, 1995: Ozone and temperature changes in the stratospheric following the eruption of Mount Pinatubo. J. Geophys. Res., 100, 16753-16764.

119. Randel, W., et al., 2004: The SPARC intercomparison of middle-atmosphere climatologies. Rev. Geophys., 39, 71-122.

120. Rind, D., N. Balachandran, R. Suozzo, 1992: Climate change and the middle atmosphere. Part II: the impact of volcanic aerosols. J. Clim., 5, 189-208.

121. Rind, D., D. T. Shindell, P. Lonergan, and N. K. Balachandran, 1998: Climate change of the middle atmosphere. Part III: The doubled CO_2 climate revisited. J. Climate, Vol, 15.

122. Robock, A., and J. Mao, 1992: Winter warming from large volcanic eruption. Geophys. Res. Lett., 19, 2405-2408.

123.   Robock, A., and M. Free, 1995: Ice cores as an index of global volcanism from 1850 to the present. J. Geophys. Res., 100, 11549-11567.
124.   Robock, A., 2000: Volcanic eruptions and climate. Rev. Geophys., 38, 191-219.
125.   Robock, A., 2001a: Stratospheric forcing needed for dynamical seasonal prediction. Bull. Amer. Met. Soc., 82, 2189-2192.
126.   Robock, A., 2001b: Volcanic eruptions. in Encyclopedia of Global Environmental Change, vol. 1, Ted Munn, Ed., (John Wiley and Sons, London), 738-744.
127.   Robock, A., 2001c: Volcanic eruption, Mt. Pinatubo. in Encyclopedia of Global Environmental Change, vol. 1, Ted Munn, Ed., (John Wiley and Sons, London), 737.
128.   Robock, A., 2001d: Volcanic eruption, El Chichón. in Encyclopedia of Global Environmental Change, vol. 1, Ted Munn, Ed., (John Wiley and Sons, London), 736.
129.   Robock, A., 2002: Pinatubo eruption: The climatic aftermath, *Science*, 295, 1242-1244.
130.   Robock, A., 2003a: Volcanoes: Role in climate. in Encyclopedia of Atmospheric Sciences, J. Holton, J. A. Curry, and J. Pyle, Eds., (Academic Press, London), 10.1006/rwas.2002.0169, 2494-2500.
131.   Robock, A., 2003b: Introduction: Mount Pinatubo as a test of climate feedback mechanisms, in *Volcanism and the Earth's Atmosphere*, Alan Robock and Clive Oppenheimer, Eds. (American Geophysical Union, Washington, DC), 1-8.
132.   Robock, A., and Clive Oppenheimer, Eds., 2003: Volcanism and the Earth's Atmosphere, Geophysical Monograph 139, American Geophysical Union, Washington, DC, 360 pp.
133.   Roeckner, E., et al., 1996: ENSO variability and atmospheric response in a global coupled atmosphere-ocean GCM. Climate Dyn., 12, 737-754.
134.   Roeckner, E., et al., 2003: The atmospheric general circulation model ECHAM5. Part I. Model description. MPI Rep. 349, Max Planck Institute for Meteorology, Hamburg, Germany, 127pp.
135.   Roeckner, E., et al., 2003: The atmospheric general circulation model ECHAM5. Part II. Sensitivity of simulated climate to horizontal and vertical resolution. MPI Rep. 354, Max Planck Institute for Meteorology, Hamburg, Germany, 56pp.
136.   Roeckner, E., et al., 2006: Sensitivity of simulated climate to horizontal and vertical resolution in the ECHAM5 atmosphere model. J. Climate, 19, 3771-3791.
137.   Salby, M., P. R. Garcia, 1987: Vacillations induced by interference of stationary and traveling planetary waves. J. Atmos. Sci., 44, 2679-2711.
138.   Salby, M. L., and P. F. Callaghan, 2003: Systematic changes of stratospheric temperature: Relationship between the tropics and extratropics. J. Geophys. Res., 108, 4101, doi:10.1029/2001JD002034.
139.   Sasamori, T., and J. Chen, 1982: The interaction of zonal mean temperature, forced stationary waves and transient waves in the high-latitude troposphere. J. Meteor. Soc. Japan, 60, 197-205.
140.   Sassi, F., D. Kinnison, B. A. Boville, R. R. Garcia, and R. Roble, 2004: Effect of El Nino-Southern Oscillation on the dynamical, thermal, and chemical structure of the middle atmosphere. J. Geophys. Res, 109, 17108-17119.

141.   Schlosser, C. A., and B. P. Kirtman, 2005: Predictable skill and its association to sea-surface temperature variations in an ensemble climate simulation. J. Geophy. Res., 110, D19107, doi:10.1029/2005JD005835, 2005.

142.   Schmitz, G., and N. Grieger, 1980: Model calculations on the structure of planetary waves in the upper troposphere and lower stratosphere as a function of the wind field in the upper stratosphere. Tellus, 32, 207-214.

143.   Shindell, D. T., R. L. Miller, G. A. Schmidt, and L. Pandolfo, 1999: Simulation of recent northern winter climate trends by greenhouse-gas forcing. Nature, 399, 452-455.

144.   Shindell, D. T., G. A. Schmidt, R. L. Miller, and D. Rind, 2001: Northern Hemisphere winter climate response to greenhouse gas, ozone, solar, and volcanic forcing. J. Geophys. Res., 106, 7193-7210.

145.   Shiotani, M., and I. Hirota, 1985: Planetary wave-mean flow interaction in the Stratosphere: a comparison between Northern and Southern Hemisphere. Quart. J. R. Met. Soc., 111, 309-334.

146.   Shiotani, M., 1986: Planetary wave activity in the troposphere and stratosphere during the Northern Hemisphere winter. J. Atmos. Sci., 43, 3200-3209.

147.   Soden, B., R. Wetherald, G. Stenchikov, A. Robock, 2002: Global cooling after the eruption of Mount Pinatubo: A test of climate feedback by water vapor. Science, 296, 727-730.

148.   Steinbrecht, W., B. Hassler, C. Bruehl, M. Dameris, M. A. Giorgetta, V. Grewe, E. Manzini, S. Matthes, C. Schnadt, B. Steil, and P. Winkler, 2006: Interannual variation patterns of total ozone and lower stratospheric temperature in observations and model simulations. Atmos. Chem. Phys., 6, 349-374.

149.   Stenchikov, Georgiy L., Ingo Kirchner, Alan Robock, Hans-F. Graf, Juan Carlos Antuña, R. G. Grainger, Alyn Lambert, and Larry Thomason, 1998: Radiative forcing from the 1991 Mount Pinatubo volcanic eruption. J. Geophys. Res., 103, 13,837-13,857

150.   Stenchikov, G., A. Robock, V. Ramaswamy, M. Schwarzkopf, K. Hamilton, and S. Ramachamdran, 2002: Arctic Oscillation response to the 1991 Mount Pinatubo eruption: Effectis of volcanic aerosols and ozone depletion. J. Geophy. Res., 107, (D24), 4803, doi:10.1029/2002JD002090.

151.   Stenchikov, Georgiy, Kevin Hamilton, Alan Robock, V. Ramaswamy, and M. Daniel Schwarzkopf, 2004: Arctic Oscillation response to the 1991 Pinatubo eruption in the SKYHI GCM with a realistic Quasi-Biennial Oscillation. J. Geophys. Res., 109, D03112, doi:10.1029/2003JD003699.

152.   Stenchikov, Georgiy, Kevin Hamilton, Ronald J. Stouffer, Alan Robock, V. Ramaswamy, Ben Santer, and Hans-F. Graf, 2006: Climate impacts of volcanic eruptions in the IPCC AR4 climate models. J. Geophys. Res., 111, D07107, doi:10.1029/2005JD006286.

153.   Straus, D. M. and J. Shukla, 1988: A comparison of a GCM simulation of the seasonal cycle and of the atmosphere with observations. Part II: Stationary waves and transient fluctuations. Atmosphere_Ocean, 26(4), 575-607.

154.   Straus, D. M., and J. Shukla, 2000: Distinguishing between the SST-forced and internal variability in mid latitudes: Analysis of observations and GCM simulations. Quart. J. Roy. Meteor. Soc., 126, 2323-2350.

155. Taylor, K. E., D. Williamson, and F. Zwiers, 2000: The sea surface temperature and sea-ice concentration boundary conditions for AMIP II simulations. PCMDI Report No.60, 24pp.

156. Timmreck, C., H. –F. Graf, and J. Feichter, 1999: Simulation of Mt. Pinatubo Volcanic aerosol with the Hamburg climate model ECHAM4. Theor. Appl. Climatol., 62, 85-108.

157. Timmreck, C., H. –F. Graf, and I. Kirchner, 1999: A one and half year interaction MA/ECHAM4 simulation of Mount Pinatubo aerosol. J. Geophy. Res., 104, 9337-9359.

158. Walter, K, 2003: Changing patterns of tropospheric variability in the north Atlantic region (Ph.D dissertation). Max Planck Institute for Meteorology, 157pp.

159. Walter, K. and H. –F. Graf, 2004: The North Atlantic variability structure, storm tracks, and precipitation depending on the polar vortex strength. Atmos. Chem. Phys. Discuss., 4, 6127-6148.

Acknowledgements

I would like to express my appreciation to my supervisor, Prof. Hans-F. Graf, providing me the opportunity to work in Max Planck Institute for Meteorology and continuous support and expert advice. His open-minded attitude and refreshing enthusiasm in the discussion of scientific subjects have been particularly motivated and stimulated me.

I am also very grateful to my supervisor, Dr. Marco Giorgetta, for his open-mind discussion and continuous support. His timely and valuable guidance helped a lot in the completion of this thesis.

I greatly appreciate the supervision from my advisor panel chair, Prof. Guy Brasseur, for his expert advices in the process. I am also grateful for his strong interest in my work and for examining this dissertation.

I am glad to be enrolled in the International Max Planck Research School on Earth System Modelling (IMPRS-ESM) and benefited a lot from it. I am grateful to the support from the school, including Prof. Hartmut Grassl, Prof. Jochem Marotzke, Prof. Martin Claussen, Dr. Antje Weitz, Ms. Cornelia Kampmann, and Ms. Hanna Stadelhofer.

I want to thank all my colleagues at MPI for Meteorology and friends in IMPRS, who helped me during my PhD in several aspects, in particular. Especially, I thank Dr. Claudia Timmreck for her useful discussion. I would like to thank my colleagues, Manu Anna Thomas, Rene Hommel, Heinz Juergen Punge, Hui Wan, Anglika Heil, Elina Marmer, Mellisa pfeffer, Dr. Baerbel Langmann for their help both in working and living.

I also would like to thank Prof. Wen Chen (Institute of Atmospheric Physics, CAS, China), Dr. Jose Castanheira (University of Aveiro, Portugal), Dr. Jian Yan (University of Cambridge, UK), Prof. Klaus Fraedrich (University of Hamburg), Toben Kurz (University of Hamburg) and Dr. William Randel for their inspiring discussion and generous help.

Especially, I would like to thank my parents and my brother for their always confidence in me. Finally and most importantly, I thank my husband, Dr. Xuefeng Cui, for his love, accompany and support all these years. Without him, I cannot imagine the completion of this thesis.

Publikationsreihe des MPI-M
„Berichte zur Erdsystemforschung" , *„Reports on Earth System Science*", ISSN 1614-1199
Sie enthält wissenschaftliche und technische Beiträge, inklusive Dissertationen.